Energy

FOSSIL

20001-15
DOE/BC/~~103452~~
(DE85000112)

TERTIARY OIL RECOVERY PROCESSES RESEARCH AT THE UNIVERSITY OF TEXAS

Annual Report for the Period October 1981—September 1982

By
R. S. Schechter
W. H. Wade

January 1985
Date Published

Work Performed Under Contract Nos. AS19-80BC10345
AC19-79BC20001

University of Texas
Austin, Texas

Technical Information Center
Office of Scientific and Technical Information
United States Department of Energy

DISCLAIMER

This report was prepared as an account of work sponsored by an agency of the United States Government. Neither the United States Government nor any agency thereof, nor any of their employees, makes any warranty, express or implied, or assumes any legal liability or responsibility for the accuracy, completeness, or usefulness of any information, apparatus, product, or process disclosed, or represents that its use would not infringe privately owned rights. Reference herein to any specific commercial product, process, or service by trade name, trademark, manufacturer, or otherwise does not necessarily constitute or imply its endorsement, recommendation, or favoring by the United States Government or any agency thereof. The views and opinions of authors expressed herein do not necessarily state or reflect those of the United States Government or any agency thereof.

This report has been reproduced directly from the best available copy.

Available from the National Technical Information Service, U. S. Department of Commerce, Springfield, Virginia 22161.

Price: Printed Copy A09
Microfiche A01

Codes are used for pricing all publications. The code is determined by the number of pages in the publication. Information pertaining to the pricing codes can be found in the current issues of the following publications, which are generally available in most libraries: *Energy Research Abstracts (ERA); Government Reports Announcements* and Index *(GRA* and I); *Scientific and Technical Abstract Reports (STAR);* and publication NTIS-PR-360 available from NTIS at the above address.

DOE/BC/10345-2
(DE85000112)
Distribution Category UC-92a

TERTIARY OIL RECOVERY PROCESSES RESEARCH AT THE UNIVERSITY OF TEXAS--ANNUAL REPORT

October 1981-September 1982

R. S. Schechter, Principal Investigator
W. H. Wade, Principal Investigator

and

I. Carmona
L. Fortney
J. Harwell
R. Hazlett
J. Hoskins
A. Lam
I. Lee
R. Truchetet
U. Weerasooriya
V. Weerasooriya
S. Yiv

University of Texas
Department of Chemistry and Petroleum Engineering
Austin, Texas 78712

Work Performed for the Department of Energy
Under Contract Nos. DE-AC19-78BC20001 &
DE-AC19-80BC10345

Fred W. Burtch, Technical Project Officer
Bartlesville Project Office
P.O. Box 1398
Bartlesville, Oklahoma 74005

Date Published -- January 1985

FOREWORD

The work summarized here is fully documented by publications of the research group. These are referenced and available in the technical and scientific literature. Work that is in pre-print form or contained in a thesis may be obtained by writing Dr. R.S. Schechter or Dr. W.H. Wade.

This research has been carried out as a part of the educational program of The University of Texas at Austin and has involved many undergraduate, graduate and postgraduate students. This past year the following degrees were awarded to students who worked on oil recovery research:

Master's Degrees: Remy Truchetet

Ph.D.: Jeffrey Harwell

TABLE OF CONTENTS

	Page
Foreword	ii
List of Figures	iv
List of Tables	viii
Summary	1
I. Surfactant Adsorption	2
II. Chromatographic Movement	60
III. Surfactant Synthesis and Phase Behavior	96
A. Synthesis and Performance of Isomer-free Secondary Alkane Sulfonate Surfactants	98
B. Synthesis and Performance of Linear Monoisomeric Ethylene Oxide Sulfonate Surfactants	113
C. Alpha-Olefin Sulfonates for Enhanced Oil Recovery	126
D. Ethoxylated Oleyl Sulfonates as Model Compounds for Enhanced Oil Recovery	147
E. The Phase Behavior of Simple Salt Tolerant Sulfonates	165
Publications of last year's work	184
Invited lectures, papers and speeches by	
William H. Wade	185
Robert S. Schechter	185

LIST OF FIGURES

Figure		Page
	I. Surfactant Adsorption	
I-1	Surfactants, names, and abbreviations used in this study	16
I-2	Experimental and theoretical adsorption of $3\phi C_9ABS$ on α-alumina	17
I-3	Experimental and theoretical adsorption of $3\phi C_{10}ABS$ on α-alumina	18
I-4	Pure component CMC data used to obtain phase separation model constants for monomer/micelle equilibrium for $3\phi C_9ABS$ and $3\phi C_{10}ABS$	19
I-5	Plateau adsorption as a function of pH for $3\phi C_9ABS$ on α-alumina	20
I-6	Cumulative distribution function used to fit isotherms in this study. Note that $F_A(\sigma S)$ is the fraction of the surface having a charge density of σS or greater	21
I-7	$3\phi C_9$ adsorption versus $3\phi C_9$ and $3\phi C_{10}$ concentrations	25
I-8	$3\phi C_{10}$ adsorption versus $3\phi C_9$ and $3\phi C_{10}$ concentrations	26
I-9	Total surfactant adsorption versus $3\phi C_9$ and $3\phi C_{10}$ concentrations	27
I-10	$3\phi C_9$ adsorption above the CMC as a function of $3\phi C_9$ and $3\phi C_{10}$ concentrations	28
I-11	$3\phi C_{10}$ adsorption above the CMC as a function of $3\phi C_9$ and $3\phi C_{10}$ concentrations.	29
I-12	Total surfactant adsorption a ove the CMC as a function of $3\phi C_9$ and $3\phi C_{10}$ concentrations.	33
I-13	Variation of monomer concentration with phase composition for mixtures of decyl benzene sulfonate with dodecyl benzene sulfonate	37
I-14	Variation of micellar phase composition with the monomer phase composition for mixtures of decyl benzene sulfonate with dodecyl benzene sulfonate	38
I-15	Variation of monomer concentration with phase composition for mixtures of decyl benzene sulfonate with IGEPAL CO 660	40
I-16	Variation of micellar phase composition with the monomer phase composition for mixtures of decyl benzene sulfonate with IGEPAL CO 660	41
I-17	Variation of monomer concentration with phase composition for mixtures of undecyl benzene sulfonate with IGEPAL CO 660	42
I-18	Variation of micellar phase composition with the monomer phase composition for mixtures of undecyl benzene sulfonate with IGEPAL CO 660.	43

List of Figures (continued)

Figure		Page
I-19	Variation of monomer concentration with phase composition for mixtures of dodecyl benzene sulfonate with IGEPAL CO 660	44
I-20	Variation of micellar phase composition with the monomer phase composition for mixtures of dodecyl benzene sulfonate with IGEPAL CO 660	45
I-21	Variation of monomer concentration with phase composition for mixtures of decyl benzene sulfonate with IGEPAL CO 850 . . .	46
I-22	Variation of micellar phase composition with the monomer phase composition for mixtures of decyl benzene sulfonate with IGEPAL CO 850	47
I-23	Variation of monomer concentration with phase composition for mixtures of undecyl benzene sulfonate with IGEPAL CO 850	48
I-24	Variation of micellar phase composition with the monomer phase composition for mixtures of undecyl benzene sulfonate with IGEPAL CO 850	49
I-25	Variation of monomer concentration with phase composition for mixtures of dodecyl benzene sulfonate with IGEPAL CO 850.	50
I-26	Variation of micellar phase composition with the monomer phase composition for mixtures of dodecyl benzene sulfonate with IGEPAL CO 850	51
I-27	Variation of monomer concentration with phase composition for mixtures of dodecyl benzene sulfonate with IGEPAL CO 970	52
I-28	Variation of micellar phase composition with the monomer phase composition for mixtures of dodecyl benzene sulfonate with IGEPAL CO 970.	53
I-29	Values obtained for the interaction parameter for different ethylene oxide chain lengths, plotted versus the weight fraction of ethylene oxide in the surfactant molecule . .	54
I-30	Heat of adsorption apparatus	57
	II. Chromatographic Movement in Real Systems	
II-1	Composition path grid for $3\phi C_9ABS/3\phi C_{10}ABS$ on α-alumina in 0.2 M NaCl, pH 8, T = 30°C. . .	61
II-2	Composition path grid for higher concentrations .	62
II-3a	Composition route for case 1.	67
II-3b	Distance-time diagram for case 1.	68
II-3c	Observed and predicted composition routes for case 1.	68
II-3d	Observed and predicted effluent profiles for case 1.	70
II-4a	Composition route for case 2.	73

List of Figures (continued)

Figure		Page
II-4b	Distance-time diagram for case 2.	74
II-4c	Composition route for case 2.	74
II-4d	Observed and predicted effluent profiles for case 2.	75
II-5a	Schematic of composition route for case 3.	77
II-5b	Distance-time diagram for case 3.	78
II-5c	Observed and predicted effluent histories for case 3.	80
II-5d	Observed and predicted composition routes for case 3.	81
II-6a	Schematic of composition route for case 4.	83
II-6b	Observed and predicted composition routes for case 4.	84
II-6c	Distance-time diagram for case 4.	85
II-6d	Observed and predicted effluent history for case 4.	86
II-7a	Schematic of composition route for case 5.	88
II-7b	Observed and predicted composition route for case 5.	89
II-7c	Distance-time diagram for case 5.	90
II-7d	Observed and predicted effluent profiles for case 5.	92
II-8	Effect of dispersion on observed compositions.	93
	III-A Synthesis and Performance of Isomer-free Secondary Alkane Sulfonate Surfactants	
III-A-1	Minimal sec butanol concentration for microemulsion formation as a function of attachment point of sulfonate to a linear octadecane chain (I.N.)	110
III-A-2	Optimum Phase Behavior lines in salinity/ EACN space	111
III-A-3	Optimum Solubilization Parameters taken on the lines in Figure 2.	112
	III-B Synthesis and Performance of Linear Monoisomeric Ethylene Oxide Sulfonate Surfactants	
III-B-1	LQXTAL/μE transition temperatures as a function of EON for system conditions as noted	123
III-B-2	Electrolyte concentrations requirements for optimum for conditions as noted	124
III-B-3	Solubilization parameters versus EON for conditions as noted	125

Figure | Page

III-C Alpha-olefin Sulfonates for Enhanced Oil Recovery

III-C-1 Phase behavior for the systems as noted. Lines with data points are the optimum lines and the other lines are the extreme of the three phase regions 143
III-C-2 Optimum phase behavior lines for the system as noted 143
III-C-3 Phase map showing transition line between liquid crystal state (below line) and microemulsion state (above line). Numbers by data points are the optimum ACNs for the system conditions as noted 144
III-C-4 Phase map showing transition lines between liquid crystal state (below lines) and microemulsion state (above lines). Numbers by data points are the optimum ACNs for the system conditions as noted 144
III-C-5 Solubilization parameter as a function of alcohol concentration for system conditions as noted 145
III-C-6 Optimum solubilization parameter versus concentration of NaCl for a variety of sec butanol concentration 145
III-C-7 Optimum solubilization parameter versus NaCl concentration for two isopentanol concentrations 145
III-C-8 Solubilization parameter versus reciprocal width of the three phase regime for various salinities 145
III-C-9 Solubilization parameter versus $CaCl_2$ concentration for the C_{18} α-olefin sulfonate and its components for the conditions as noted 146
III-C-10 Optimum interfacial tension versus salinity for C_{18} alkene sulfonate for the conditions noted 146
III-C-11 Optimum interfacial tension versus concentration of alcohol for C_{18} α-olefin sulfonate for the conditions as noted 146

III-D Ethoxylated Oleyl Sulfonates as Model Compounds for Enhanced Oil Recovery

III-D-1 Temperature coefficient of optimum ACN for the three ethoxylated species. For comparison, data is also reproduced for an ethoxylated nonylphenol 162
III-D-2 Phase boundary separating the liquid crystal and microemulsion regimes for the n=1 species . 162

Figure		Page
III-D-3	Phase boundary separating the liquid crystal and microemulsion regimes for the n=3 species .	162
III-D-4	Optimum phase behavior lines for the n=1 species in S*/ACN* spaces for four isopentanol concentrations	162
III-D-5	Optimum solubilization parameters vs. S* for the n=1 species at three isopentanol concentrations. Dashed lines indicate constant ACN	163
III-D-6	LnS*/ACN* for the n=1,2, and 3 species at two isopentanol concentrations	163
III-D-7	The linear S* plot of Figure 6	163
III-D-8	Optimum solubilization parameters for the data presented in Figure 7	163
III-D-9	Additional solubilization parameters for the n=3 species for conditions as noted	164
III-D-10	The relationship between optimum solubilization parameter and reciprocal width of the 3-phase regime (ΔACN) for the n=1 and n=2 species	164
III-D-11	The influence of $CaCl_2$ on optimum solubilization parameter for the n=1 species at 3 alcohol concentrations	164
III-D-12	Optimum ACN with concentration of $CaCl_2$ as the variable	164

III-E The Phase Behavior of Simple Salt Tolerant Sulfonates

III-E-1	Synthesis scheme for alkane sulfonates	176
III-E-2	Optimum phase behavior for primary sulfonates . .	176
III-E-3	Phase maps for secondary alkane sulfonates	176
III-E-4	Phase map for three isomers of octadecyl sulfonate	176
III-E-5	Solubilization parameters for the systems of Figure 2	177
III-E-6	Solubilization parameters for the systems of Figure 3 at a function of NaCl concentration . .	177
III-E-7	σ* vs (2-C_4OH) f r conditions as noted by the data points	177
III-E-8	σ* vs (NaCl) for different alcohol concentrations	177
III-E-9	Solubilization parameter, σ* vs reciprocal ΔEACN .	178
III-E-10	Influence of ($CaCl_2$) on σ* for surfactants as shown	178

LIST OF TABLES

Table		
I-1	Values of Constants in Equation 6 for 3ϕC_9 and 3ϕC_{10}	22
I-2	Experimental Constants for Fit of Figures 4 and 5	24
III-D-1	Transition Temperatures	160
III-D-2	NaCl increment related to EON	161

SUMMARY

During the past year we have continued three major projects: I) further delineation of surfactant adsorption mechanisms, II) the systematics of chromatographic separation processes, and III) the design and evaluation of surfactants.

In I we have: (A) explored surface condensed structures and plateau adsorption levels; and (B)expanded adsorption theory to encompass heterogeneities, studied the critical admicelle concentration and multicomponent adsorption.

In II we have traced the composition path for several pure alkyl benzene sulfonates in the grid diagram and examined surfactant wave fronts.

In III we have developed two and quantitative surfactant synthesis schemes and finished studies on α-olefin suflonates, ethoxylated oleyl sulfonates and alkane sulfonates.

I. SURFACTANT ADSORPTION

A. MECHANISM OF SURFACTANT ADSORPTION FROM AQUEOUS SOLUTIONS

The University of Texas research group has, over the years, developed a theory of surfactant adsorption which is detailed in recent publications by Scamehorn et al.[1,2] This theory includes the following mechanisms which we believe are central to understanding how surfactant adsorption can be reduced:

(1) The existence of an interaction between the surfactant's hydrocarbon tail and the substrate even though that substrate may be a mineral oxide covered with a layer of chemically adsorped water[3] has been found and is fundamental to the theory. The force thought to be responsible for this interaction is the hydrophobic effect.[4] It becomes important because increasing the surfactant tail length increases adsorption even in the region whose coverage is sparse.

(2) The surface is heterogeneous. It is not possible to understand adsorption isotherms without understanding and taking into account this fundamental principle. During the adsorptive process, the density of adsorbed molecules varies from patch to patch on the surface.

(3) Lateral interactions between the adsorbed surfactant molecules become significant as the density of adsorbed molecules increases. These interactions then promote the further adsorption of surfactant thus accounting for the typical S-shaped isotherm. At a critical concentration surface aggregates form spontaneously. If the surface and surfactant have opposite charges, then bilayers may form. In other cases, when the interaction between the hydrophilic moiety of the surfactant and the substrate is weak,

monolayers are expected. These surface aggregates form because of the hydrophobic effect.

(4) Adsorption is a function of the surfactant monomer concentration. This remains true even though micelles may form. This concept is especially useful in understanding adsorption from aqueous solutions of surfactant mixtures. In this regard mixed micelles have been shown to be an important feature of surfactant behavior which affects both microemulsion phase behavior and adsorption.

In view of these advances which have been made in the past, it seems reasonable to try to summarize the goals which we believe remain to be attained and the work which has been accomplished this year in striving to accomplish these goals. Actually, the use of the word goal is somewhat misleading, more precisely there are aspects of the adsorptive process not yet fully understood and our aim is to explain them. The premise being that with better understanding will come the ability to reduce surfactant adsorptive losses.

A.1. Adsorption from Dilute Solutions (Region I[1])

In our work and those of others (see, for example, Wakamatsu and Fuersteneau[5]) adsorption in this region has been modeled by Henry's law which has also been called the Stern-Grahame equation. They are equivalent; adsorption is predicted to vary linearly with concentration. It is certainly true that in many cases studied, the adsorption does vary linearly with concentration; however, it is not always true. Adsorption of some nonionic surfactants have shown deviations.[6] It is of importance (we believe) to know under what circumstances Henry's law will apply and since the observed deviations from Henry's law are generally negative; that is, the actual adsorption

is less than that calculated by extrapolating Henry's law, an understanding of the mechanisms may lead to methods for reducing adsorption.

This year we have not specifically set out to ascertain the necessary conditions for the existence of a regime in which adsorption is linear with solution concentration; however, we have developed a new model, extending the work of Scamehorn et al.,[1,2] to elucidate the influence of both the pH and added salts on the Henry's law constant and in the course of its development have seen circumstances in which Henry's law will fail. These are the subject of an ongoing study. A new apparatus designed to provide accurate measurements of small levels of surfactant adsorption has been constructed and is now being tested. A brief description of this apparatus is given in this report and by next year we hope to have studied the adsorption of many different surfactant species.

In this report only the main features of our new theory is described and supporting experimental evidence provided.

A.2. Surfactant Surface Aggregates

The shape of the isotherm in region II, which is distinguished from region I by a sharp increase in adsorption, clearly indicates that adsorption in this region is a collective phenomenon. We now believe that it is important to distinguish between the type of surface structures which do form. The model presented in this report considers the case in which bilayered structures form.

The influence of added electrolyte and solution pH also affect the concentration at which these aggregates form and the model presented here takes these factors into account. We have not had time to verify its predictions with respect to changes in these variables, but the model also predicts the

adsorption of individual surfactant species from a mixture of surfactants in solution. It is this aspect which is considered in this report since we are also concerned with the chromatographic separation of surfactant mixtures and the adsorption of each individual molecule must be known to determine the degree of separation which will be observed.

A.3. The Adsorption Plateau

Surfactant adsorption at solution concentrations above the surfactant CMC is determined by monomer concentrations which for mixtures vary even for concentrations above the mixture CMC. Thus, the surfactant plateau is a result of the monomer concentration attaining a constant value even though the total solution concentration may change between wide limits.

In the past we have shown[7] that these monomer concentrations can, for mixtures of alkyl benzene sulfonates, be accurately calculated by assuming that the micelles can be represented as a separate phase (pseudophase) which consists of an ideal solution of surfactant molecules. Mixtures of nonionic and anionic surfactants do not, however, form an ideal psuedo-phase.[8] It is this problem which we have studied this past year using ultrafiltration methods to separate monomer molecules from micelles. Typical results are presented in this report.

B. A NEW THEORY OF SURFACTANT ADSORPTION

B.1. Effects of Surface Heterogeneity

Our approach is to assume a phase transition to bilayer coverage occurs on a given patch of a heterogeneous surface at a critical solution concentration characteristic of that surface patch. If conditions are the same everywhere on the surface, the whole surface will go to bilayer coverage at

the same concentration; i.e., if we assume the mineral oxide surface to be homogeneous, then the entire surface will go from region I to plateau adsorption at a single surfactant concentration. To describe an experimental surfactant adsorption isotherm, we must account for the heterogeneity of the surface onto which the surfactant is adsorbing. Experimental evidence for assuming surface heterogeneity on α-alumina has been presented.[1] All that needs be said here is that surface studies have shown heterogeneity is the rule, not the exception; and, further, that if we allow our distribution function for the surface charge or amphoteric site density to be arbitrary, the homogeneous case becomes a subset of the heterogeneous.

In the expression below, we will assume that there is a critical site or charge density at which the admicelle will form. All regions of the surface with higher charge or amphoteric site density are assumed to also be covered by a local bilayer. The total adsorption of surfactant at a given surfactant and counterion concentration is, therefore, given by

$$\Gamma_{S^-} = \Gamma_{bilayer} \int_{\sigma_S^*}^{(\sigma_S)_{max}} f_{\sigma_S} d\sigma_S + \int_{(\sigma_S)_{min}}^{\sigma_S^*} f_{\sigma_S} \Gamma_I (C_{S^-}, C_{Na^+}, \sigma_S) d\sigma_S \qquad (1)$$

where Γ_{S^-} is the Gibb's adsorption, $\Gamma_{bilayer}$ the experimentally determined bilayer adsorption density, σ_S^* the charge density on the mineral oxide surface below the bilayered structure (called here admicelle, that is adsorbed micelle) that just formed at the solution monomer and counterion concentration, $(\sigma_S)_{max}$ and $(\sigma_S)_{min}$ the minimum and maximum charge densities on the

mineral oxide, $\Gamma_I(C_{S^-}, C_{Na^+}, \sigma_S)$ an isotherm appropriate for low surface coverages, such as the Stern-Grahame-Gouy equation, the site binding model[9] or, for small variations of salt concentration at high total electrolyte concentration, a Henry's law model, and f_{σ_S} is the distribution function for the surface charge. The distribution function is defined so that $f_{\sigma_S} d\sigma_S$ is the fraction of the surface having a charge density between σ_S and $\sigma_S + d\sigma_S$. Introducing the cumulative distribution function $F_{\sigma_S}(\sigma_S)$, where $F_{\sigma_S}(\sigma_S)$ is that fraction of the surface having a charge density greater than or equal to σ_S, and assuming Henry's law to be adequate for region I adsorption, we obtain

$$\Gamma_{S^-} = \Gamma_{bilayer} F_{\sigma_S}(\sigma_S^*) + HC_{S^-}[1 - F_{\sigma_S}(\sigma_S^*)] \tag{2}$$

Equation 2 is the model that will be applied. However, since the surface charge is a function of pH (and of added electrolyte concentration at low added electrolyte), equations 1 and 2 are valid only at a single pH and at counterion concentrations high enough to electrostatically shield new molecules which are adsorbing from the influence of the field created by these molecules already adsorbed. In such a case, Henry's law applies.

A more general expression can be derived if the amphoteric surface site model is adapted to explain the origin of the surface charge.[9] We then obtain

$$\Gamma_{S^-} = \Gamma_{bilayer} \int_{n_S^*}^{(n_S)_{max}} f_{n_S}(n_S) dn_S + \int_{(n_S)_{min}}^{n_S^*} \Gamma_I(C_{S^-}, C_{Na^+}, \sigma_S) f_{n_S}(n_S) dn_S \tag{3}$$

where $(n_S)_{max}$ and $(n_S)_{min}$ are the maximum and minimum densities of amphoteric sites and n_S^* the critical site density for an admicelle to form at the solution pH, surfactant monomer, and counterion concentrations. The surface charge is obtained from the site density from the expressions[9]

$$\sigma_S = n_S(\theta_+ - \theta_-)$$

$$K_+(1 - \theta_+ - \theta_-)[H^+]_S = \theta_+$$

$$K_-(1 - \theta_+ - \theta_-) = \theta_-[H^+]_S \qquad (4)$$

where K_+ and K_- are equilibrium constants, σ_S is the surface charge, θ_+ is the fraction of the surface sites which are positive, θ_- is the fraction of the surface sites which are negative, n_S is the number of sites, and $[H^+]_S$ is the hydrogen ion concentration near the surface. The latter quantity can be greater than or less than the solution hydrogen ion concentration depending on the sign of the net surface charge. Equation 4 neglects the possibility that there is a distribution in equilibrium constants for the different types of amphoteric groups. When the region I adsorption can be adequately described by Henry's law, equation 3 becomes

$$\Gamma_{S^-} = \Gamma_{bilayer}F_{n_S}(n_S^*) + HC_{S^-}[1 - F_{n_S}(n_S^*)] \qquad (5)$$

where $F_{n_S}(n_S)$ is the cumulative distribution function for the amphoteric surface site density defined so that $F_{n_S}(n_S)$ is the fraction of the mineral oxide surface having a site density greater than or equal to n_S. In equation 5 n_S^* is a function of pH.

Since the Henry's law constant should vary from patch to patch if the surface charge density varies from patch to patch, the constant in equations 2 and 5 is an average integrated over the surface, as indicated by equations 1 and 3. At low admicelle coverage, this integrated average changes little

with increasing coverage because only a small fraction of the surface is removed from the integration by bilayer coverage. As the fraction of local bilayer coverage increases, the region I contribution quickly becomes insignificant because of the term $(1 - F_{n_S})$ and because $\Gamma_{bilayer} F_{n_S}(n_S^*)$ is orders of magnitude larger than HC_S-.

Equations 2 and 5 are deceptively simple. To solve for Γ_S- at given surfactant and salt concentrations requires not only an expression for the surface distribution function, $F_{n_S}(n_S)$ or $F_{\sigma_S}(\sigma_S)$, but also an expression for the surfactant and salt concentration as a function of surface charge density at which an admicelle will form. Derivation of this latter expression requires derivation of general expressions for the chemical potential of surfactant ions in the bulk on the surface, an evaluation of the electrostatic work of adding one surfactant molecule to an admicelle, and some consideration of the counterion binding to an admicelle. The details of this analysis are reported elsewhere.[7]

B.2. The Critical Admicelle Concentration

By considering the electrostatic contributions to the chemical potential of a surfactant in an admicelle, the following equations can be derived for the critical surfactant solution concentration, ρ_i, at which admicelles form. Note that ρ is used to denote the solution concentration when it is expressed in molecules per unit volume rather than moles. The parameters A, B, C, and E given in Table 1 are expressed in molecular units.

$$\exp\left(C - \frac{B\sigma_S}{e}\right) = \left(y + \sqrt{y^2 - 1}\right)\rho_i \tag{6}$$

$$y = \frac{1 + (\sigma_S + A)^2}{E\rho_0} \tag{7}$$

where $\rho_0 = \rho_i + \rho_{Na^+}$, and ρ_{Na^+} is the concentration of added monovalent counterions. The constants A, B, C, and E have the following physical interpretations: A is the residual charge on the admicelle. B is the inverse of the capacitance of admicelle. C is the adsorption potential not due to the mineral oxide charge. E is related to the capacitance of the Gouy-layer. In the remainder of this report we shall regard A, B, C, and E as adjustable parameters; however, we wish to stress that B, C, and E can be estimated from molecular parameters based on equations reported elsewhere[12] and A is accessible from counterion binding measurements. Note also that ρ_i, ρ_0, and ρ_{Na^+} have units of molecules/nm^3. As stated before, ρ_i is the CAC of the patch of charge density ρ_S in units of molecules of i/nm^3.

Equation 6 gives the CAC of a patch as a function of the charge density on that patch on the mineral oxide surface. Recall that the purpose of deriving this expression was to be able to construct an adsorption isotherm using the concept of local admicelle formation for use in equation 2. We do not know $F_{\rho_S}(\rho_S)$, nor is there an accepted method of determining $F_{\rho_S}(\rho_S)$. For application here, $F_{\rho_S}(\rho_S)$ will be an adjustable function. The procedure for determining $F_{\rho_S}(\rho_S)$ from equations 6 and 7 and the experimental isotherm is discussed in the results and discussion section. Though it is outside the purview of this work, this model, if properly verified, might actually be a means of determining surface distribution functions. But for the purpose of studying surfactant in practical cases, equations 2, 6, and 7 must be extended to include mixtures.

B.3. Extension to Multicomponent Adsorption

Equations 6 and 7 are easily extended to multicomponent adsorption for ideal systems (all ionic surfactants). Following Mysels and Otter,[10]

Scamehorn et al.,[2] and Osborne-Lee et al.,[11] we assume that an admicelle is an ideal solution of surfactant monomers (note that this will not be true, for example, if nonionic and anionic surfactants are mixed together)

$$\bar{\mu}_i = \mu_i^0 + kT\ln Z_i \tag{8}$$

and the chemical potential of bulk monomers can be written as

$$\mu_i = \mu_i^0 + kT\ln C_i \tag{9}$$

In these expressions Z_i is the mole fraction of the monomers in an admicelle which are component i, μ_i is the chemical potential of the i monomer in the admicelle, $\bar{\mu}_i^0$ and μ_i^0 the standard state chemical potential of an i-monomer in an admicelle and in bulk solution, respectively, μ_i the chemical potential of monomers in the bulk and, C_i the concentration of i-monomers in the bulk in units of moles/m^3. At equilibrium $\mu_i = \bar{\mu}_i$ the expression

$$\frac{Z_i}{X_i CAC_m} = \exp\left(\frac{\mu_i^0 - \bar{\mu}_i^0}{kT}\right) \tag{10}$$

where we have made the substitution $C_i = X_i CAC_m$, X_i being the mole fraction of the total bulk monomer which is component i and CAC_m being the total concentration of monomer in the bulk in units of moles/m^3. The symbol CAC_m indicates the Critical Admicelle Concentration of the surfactant mixture (subscript m) for a particular local patch. In order to evaluate $\exp[(\mu_i^0 - \bar{\mu}_i^0)/kT]$ we imagine ourselves on a local patch on which an admicelle has just formed. Keeping the charge density below the admicelle and the total counterion concentration constant, we change Z_i and observe the change in X_i. In the limit as $Z_i \to 1$, $X_i \to 1$, and the bulk monomer concentration must go to the concentration of i-monomer necessary to form an admicelle on the local patch in question at the same surface charge density as the original mixed admicelle and at the same mixture counterion concentration. We designate this concentration of i-monomer as CAC_i. Thus,

$$\exp\left(\frac{\mu_i^0 - \bar{\mu}_i^0}{kT}\right) = \frac{1}{CAC_i} \tag{11}$$

and

$$\frac{Z_i}{X_i} = \frac{CAC_m}{CAC_i}, \quad i = 1,2,\ldots,m \tag{12}$$

The value of CAC_i is obtained from

$$CAC_i = N\rho_i \times 10^{27} \tag{13}$$

where N is Avagadros number, the factor 10^{27} converts from nm^3 to m^3 and ρ_i is given by equations 6 and 7 and may correspond to a hypothetical standard state. The final multicomponent isotherm used in this work is given by

$$\Gamma_i = Z_i F_{\sigma_S}(\sigma_S^*)\Gamma_{bilayer} + H_i C_i[1 - F_{\sigma_S}(\sigma_S^*)] \tag{14}$$

To solve equation 14 at given values of the monomer concentrations for a m-component system, equation 12 is solved simultaneously with two equations of the form (6 and 7) for each component to find the Z_i and σ_S^*. Given the distribution function, $F_{\sigma_S}(\sigma_S)$, equation 14 can then be solved. Note that in this procedure σ_S^* is the charge density of the local patch on which an admicelle has just formed; patches with higher charge densities are assumed to also be covered with admicelles of the same composition.

B.4. Region I Adsorption

The number density in molecules/nm^2 of adsorbed surfactant ions at low local surface concentrations is given in this new model of surfactant adsorption by

$$\sigma_i = \frac{\Lambda_i \rho_i}{2\pi(q_i/\bar{q}_i)} \exp\left(-\frac{\bar{W}_i - W_i}{kT}\right) \tag{15}$$

where σ_i is the number density in the bulk, Λ_i the translational partition function, and q_i and $\bar{q}_i$ the partition functions for the internal degrees of freedom in the bulk and at the surface and $\bar{W}_i - W_i$ the work of bringing the ion to the surface. The factor 2π arises from the ion having a preferred orientation at the interface, in this case flat on the surface. As a first approximation $\bar{W}_i - W_i$ is given by the expression

$$\bar{W}_i - W_i = - E^{el} + m\bar{\omega}_I \tag{16}$$

where E^{el} is the electrical work of bringing the charged head group to the surface and $m\bar{\omega}_I$ the free energy change from partially removing the hydrocarbon chain from solution by bringing it into contact with the surface, whether the surface is hydrophobic or hydrophilic. The electrical work can be approximated by the Gouy-Chapman equation:

$$E^{el} = - e\psi_0 = - kT \cosh^{-1}\left(1 + \frac{\sigma_S^2}{4kT\hat{\varepsilon}_D\rho_0}\right) \tag{17}$$

where we assume the adsorbing ion has negligibly changed the surface charge density and the head group has been treated as a point charge. The term ψ_0 is the electrical potential at the surface relative to the bulk, $\hat{\varepsilon}_D$ is the effective dielectric constant over the Gouy-layer, σ_S is the surface charge density in charges/nm^2 and ρ_0 is the number density of counterions in the bulk (all assumed to have a single unit charge, e). To properly evaluate the value of $m\bar{\omega}_I$, we need a combination of zeta potential and low concentration (region I) adsorption densities. Wakamatsu and Fuerstenau[5] report such data but show no dependence of region I adsorption on tail length. On the other hand, Scamehorn et al.[1] report low concentration adsorptions which show significant effects of tail length. We can obtain

(17) in more convenient units by making the substitutions $\rho_0 = NC_0$ where N is Avagadro's number and C_0 the bulk electrolyte concentration, $C_{S^-} = N\rho_{S^-}$, where C_{S^-} is the molar concentration of surfactant in the bulk and N is again Avagadro's number, and $\sigma_i = \overline{C}_{S^-}N/a_S$ where $\overline{C}_{S^-}$ is the adsorption of surfactant in moles/g and a_S the specific surface area of the solid in nm^2/g. Thus, we obtain

$$\overline{C}_{S^-} = \frac{\Lambda_{S^-}C_{S^-}a_S}{2\pi} \exp[- m\overline{\omega}_I + \cosh^{-1}(1 + \frac{\sigma_S^2}{4kT\hat{\varepsilon}_D C_0})] \tag{18}$$

This gives a Henry's law coefficient of

$$H_{S^-} = \frac{\Lambda_{S^-}a_S}{2\pi} \exp[- m\overline{\omega}_I + \cosh^{-1}(1 + \frac{\sigma_S^2}{4kT\hat{\varepsilon}_D C_0})] \tag{19}$$

for oppositely charge surfactant and surface. This Henry's law relationship has been shown to give a reasonable comparison with experimental data, but the details are presented elsewhere.[12]

C. COMPARISON WITH EXPERIMENT

In the course of this work aspects of the behavior of two alkyl benzene sulfonates were studied. The model presented in the previous section contains various parameters which are adjustable within a certain range. In order to find the proper values of these parameters, two experimental isotherms for the pure components were obtained. As a preliminary check of the validity of the multicomponent adsorption isotherm, a few measurements were made of adsorption from mixtures of the two components, which were then compared to the model predictions. The adsorption measurements are not extensive enough to confirm the efficacy of the model. Data are still being gathered for this purpose.

Two pure component isotherms and one binary (two surfactant components) isotherm were determined. The adsorbents were the two alkyl benzene sulfonates $3\phi C_9$ABS and $3\phi C_{10}$ABS (see Figure 1), and adsorption was from dilute aqueous solution onto α-alumina. The procedures used are described elsewhere.[12]

C.1. Pure Component Isotherms

The weakest link in the model is the absence of an independent expression for the distribution function for either the surface charge density or the distribution of surface sites. Nor, indeed, are there any accepted, much less standard, means of determining such a distribution. We adopt, then, a heuristic approach, which is as follows:

(1) Make best estimates of the adjustable parameters A, B_i, C_i, and E for one surfactant (in this case $3\phi C_{10}$).

(2) Determine from the data a distribution function which will describe the isotherm for the best estimates of A, B_i, C_i, and E.

(3) Do a least squares fit of a second adsorption isotherm at the same salt and pH, beginning from best estimates of A, B_i, C_i, and E for second surfactant (in this case $3\phi C_9$) but using the distribution function developed in step 2.

(4) Determine if the parameters for the second surfactant are reasonably related to those for the first surfactant.

The final results appear in Figures 2 and 3 using the values of the constants given in Table 1. Data used to determine bilayer coverage appear in Figures 4 and 5. It can be seen from the solid line in Figures 2 and 3 that the model reproduces the data very well. The cumulative distribution function for the system appears in Figure 6. This function is defined so

1.

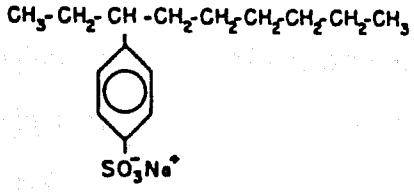

Sodium P(1-butyl heptyl) Benzene Sulfonate
(3-ϕ-C_9 ABS)

2.

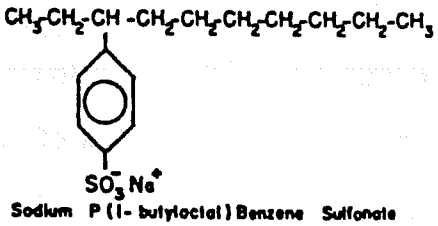

Sodium P (1- butyloctal) Benzene Sulfonate
(3-ϕ-C_{10} ABS)

Figure 1. Surfactants, names, and abbreviations used in this study.

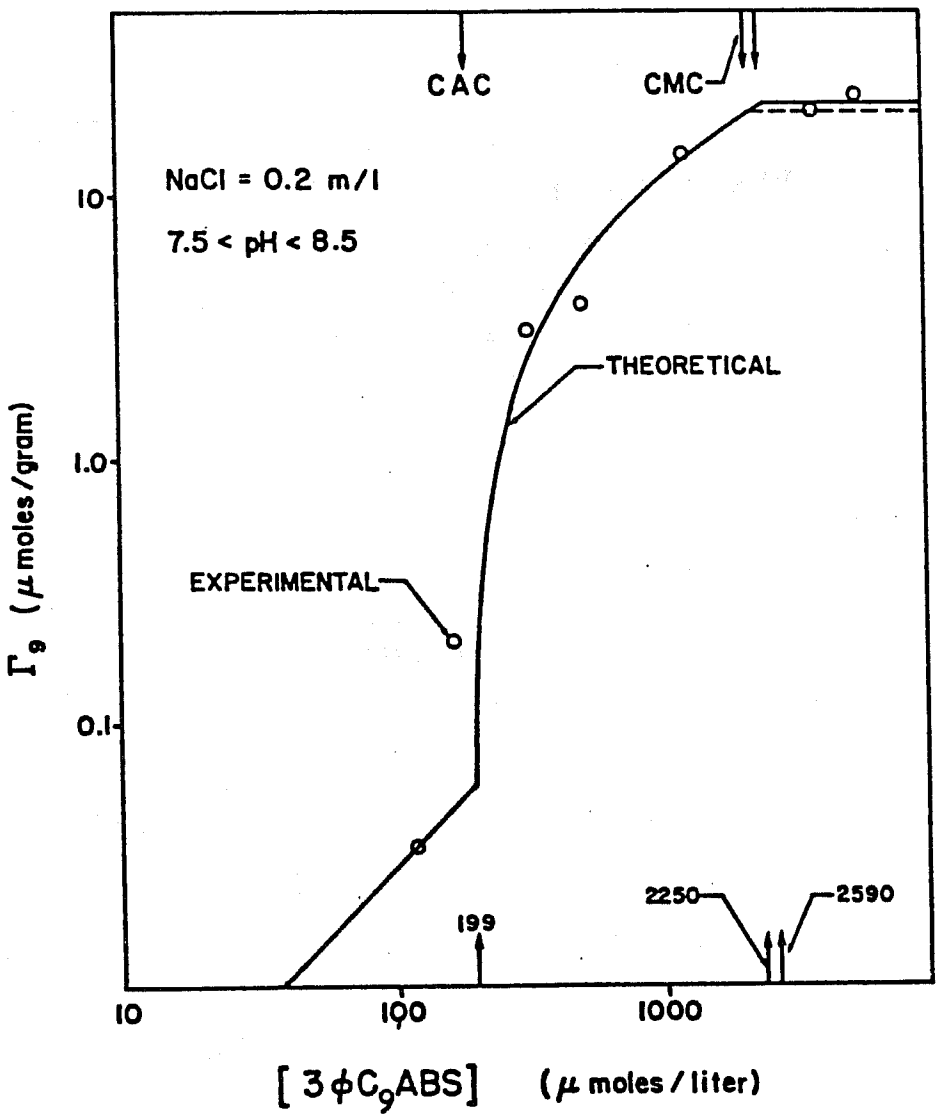

Figure 2. Experimental and theoretical adsorption of 3ϕC$_9$ABS on α-alumina.

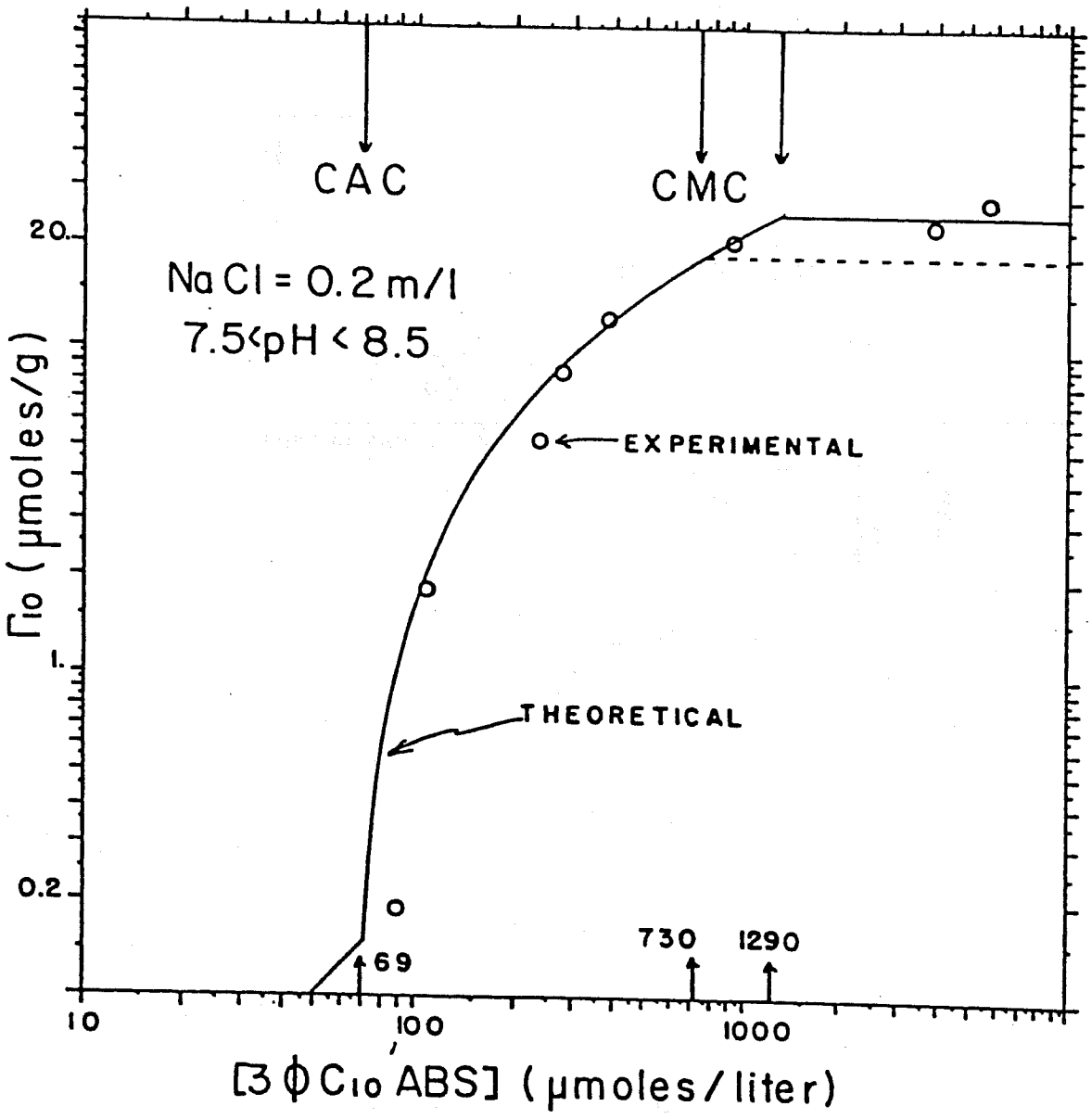

Figure 3. Experimental and theoretical adsorption of $3\phi C_{10}ABS$ on α-alumina.

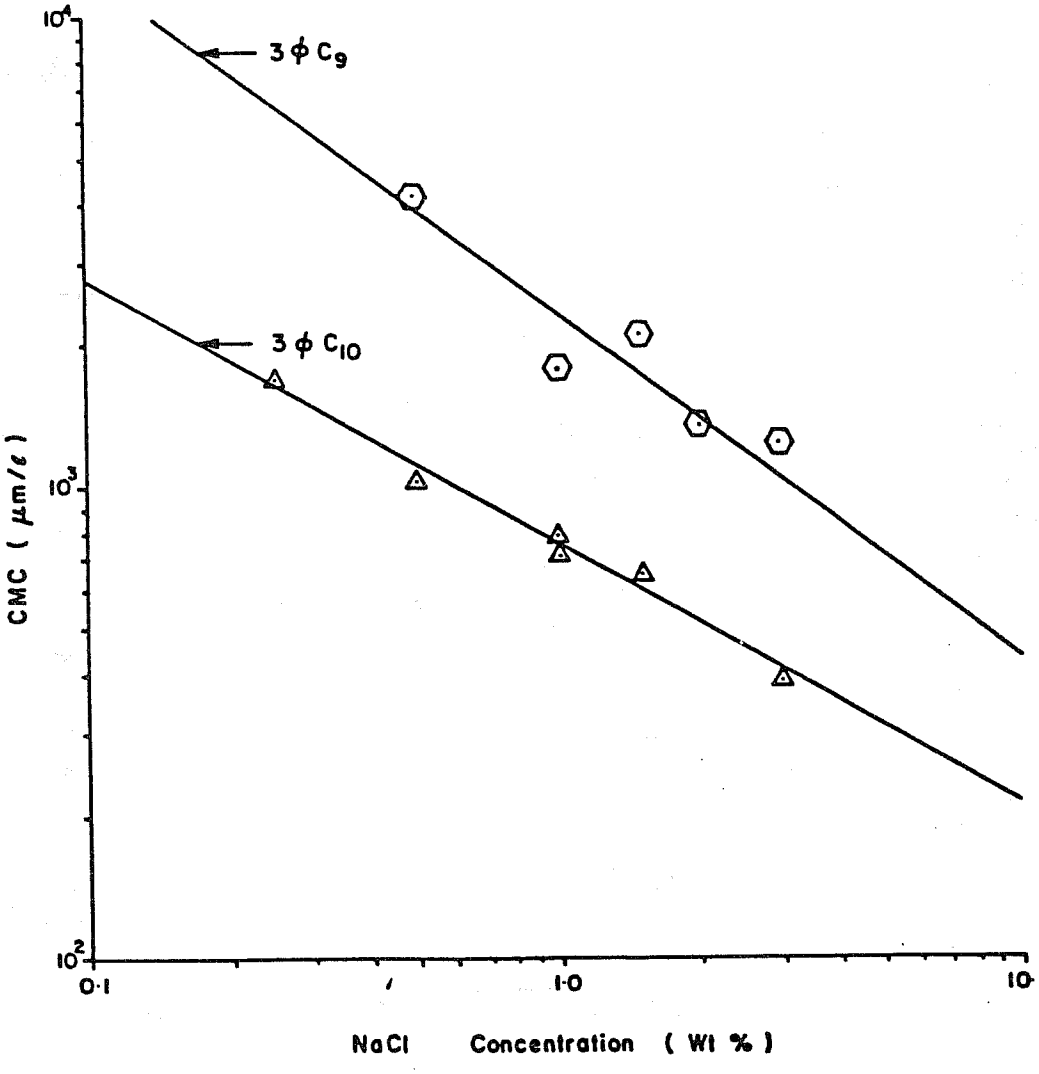

Figure 4. Pure component CMC data used to obtain phase separation model constants for monomer/micelle equilibrium for $3\phi C_9$ABS and $3\phi C_{10}$ABS.

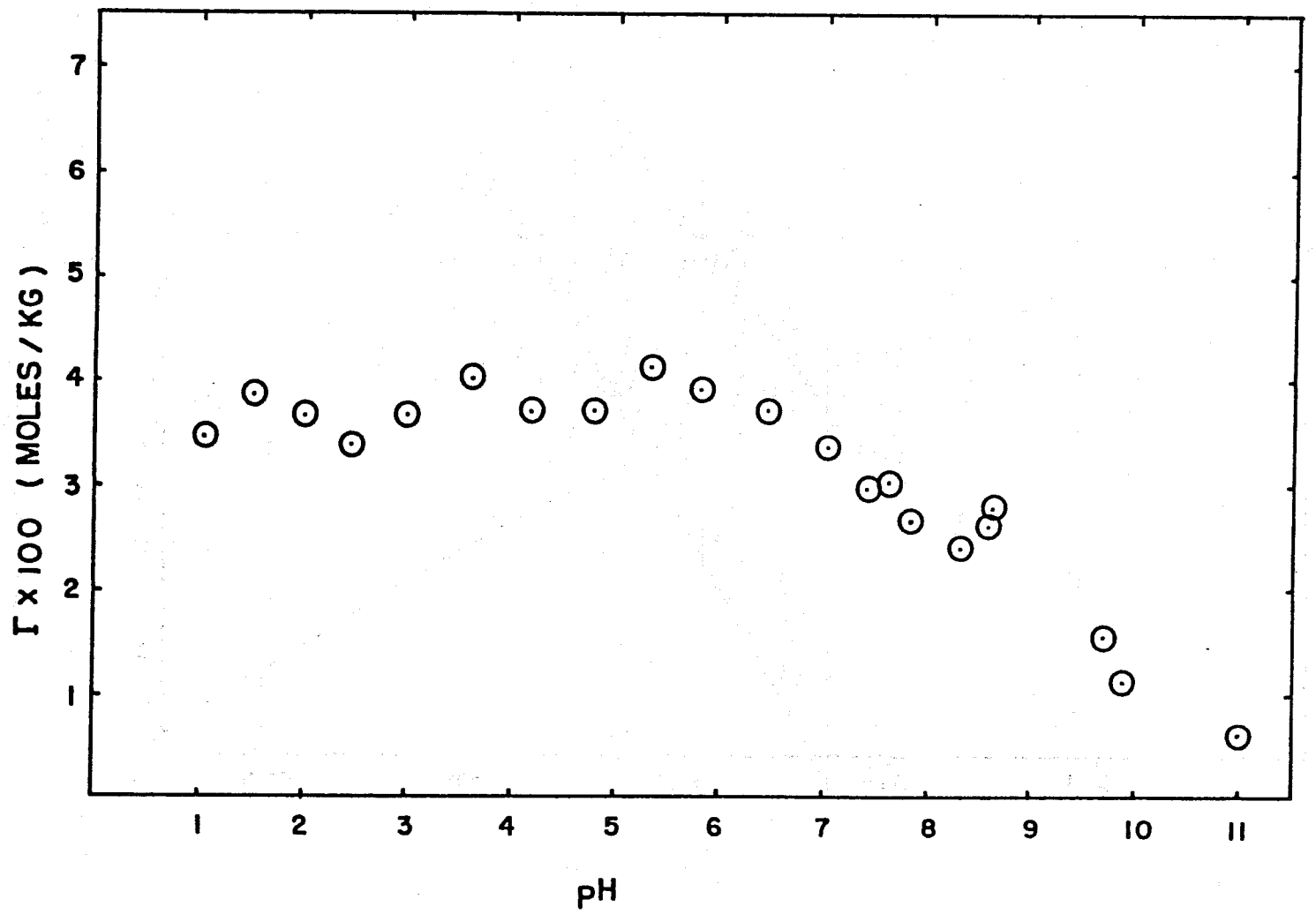

Figure 5. Plateau adsorption as a function of pH for $3\phi C_9ABS$ on α-alumina.

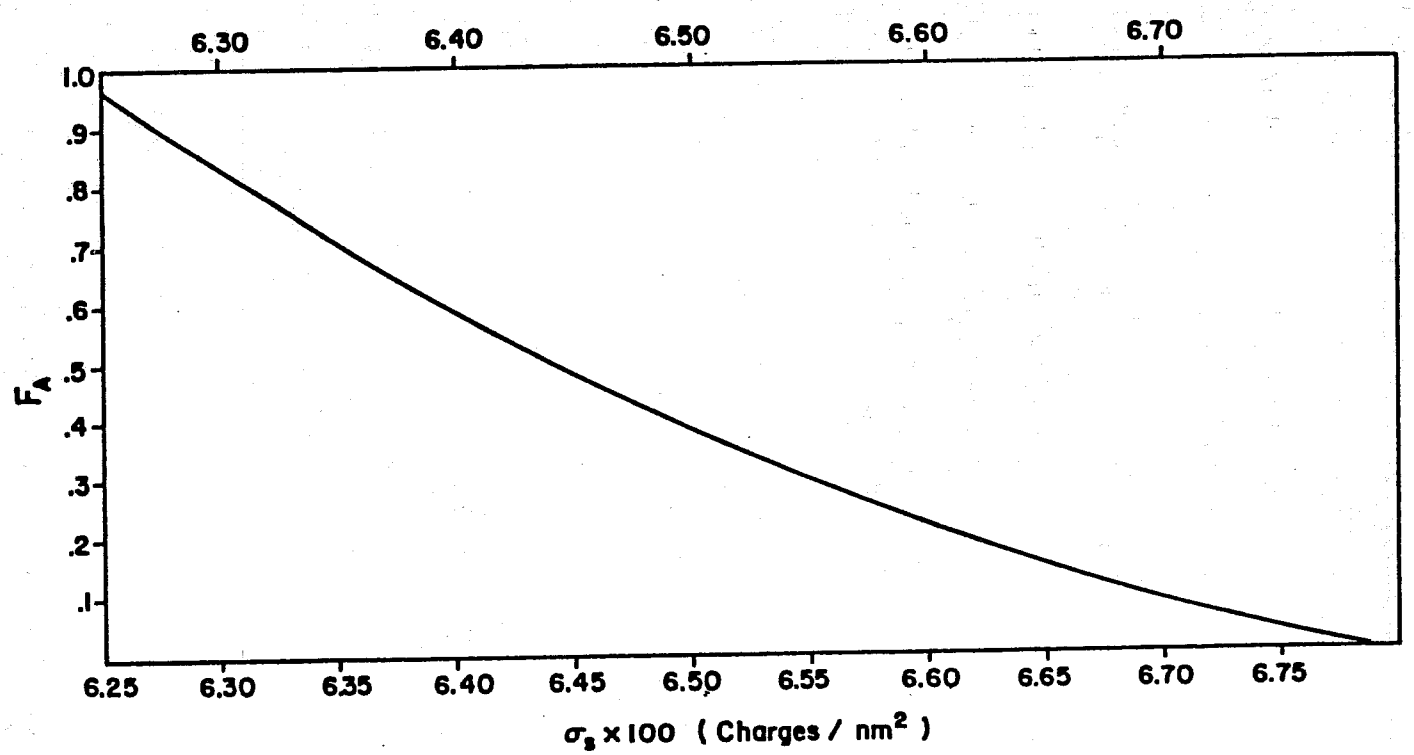

Figure 6. Cumulative distribution function used to fit isotherms in this study. Note that $F_A(\sigma_S)$ is the fraction of the surface having a charge density of σ_S or greater.

Table 1. Constants Used to Fit Data in Figures 2 and 3.

Values of Constants in Equation 6 for $3\phi C_9$ and $3\phi C_{10}$		
	$3\phi C_9$	$3\phi C_{10}$
A =	$-0.458 \frac{e}{nm^2}$	$-0.458 \frac{e}{nm^2}$
B_i =	$503 \frac{nm^2}{e}$	$505 \frac{nm^2}{e}$
C_i =	27.8	26.9
E =	0.200	0.200

that $F_A(\sigma_S)$ is the fraction of the surface having a surface charge density greater than or equal to σ_S. It must be recalled that this is the surface charge below the admicelles, where changes in the electrical potential probably modify the local concentration of potential determining ions; and, thus, the fraction of surface sites protonated or deprotonated. This does not mean the charge below the admicelle is experimentally inaccessible. At least the mean of the distribution is potentially accessible through a combination of counterion activity, zeta potential, and adsorption density measurements.

The adsorption at bilayer coverage, the Henry's law constants, and other parameters needed for adsorption calculations which have been derived from Figures 4 and 5 are presented in Table 2.

In concluding this brief discussion of the pure component isotherms, it seems appropriate to reiterate that only two things have been demonstrated: (1) the proposed model can fit the experimental data and (2) the model is based on reasonable values of the corresponding molecular parameters and gives reasonable estimates of important thermodynamic quantities. To establish the general validity of the model, much more data are required. This task is now underway.

C.2. Binary Surfactant Adsorption

To predict binary surfactant adsorption isotherms, our new model requires only pure component data. Using the pure component data and parameters from the previous section, contour plots of the predicted 2-component adsorption surface for the $3\phi C_9ABS/3\phi C_{10}ABS$ system in 0.2 m NaCℓ at pH = 8 are presented in Figures 7 through 11 along with some experimental data. Figures 7 through 9 show results for equilibrium surfactant concentrations between the CAC and the CMC. It should be emphasized that the

Table 2. Experimental Constants for Fit of Figures 4 and 5

Γ_{max} = 0.041 moles/kg

$H_{3\phi C_9}$ = 2.82×10^{-4} m^3/kg

$H_{3\phi C_{10}}$ = 2.06×10^{-3} m^3/kg

	$3\phi C_9ABS$	$3\phi C_{10}ABS$
CMC_i^0 ($\frac{moles}{m^3}$)	17.04	4.986
Kg_i	0.819	0.519

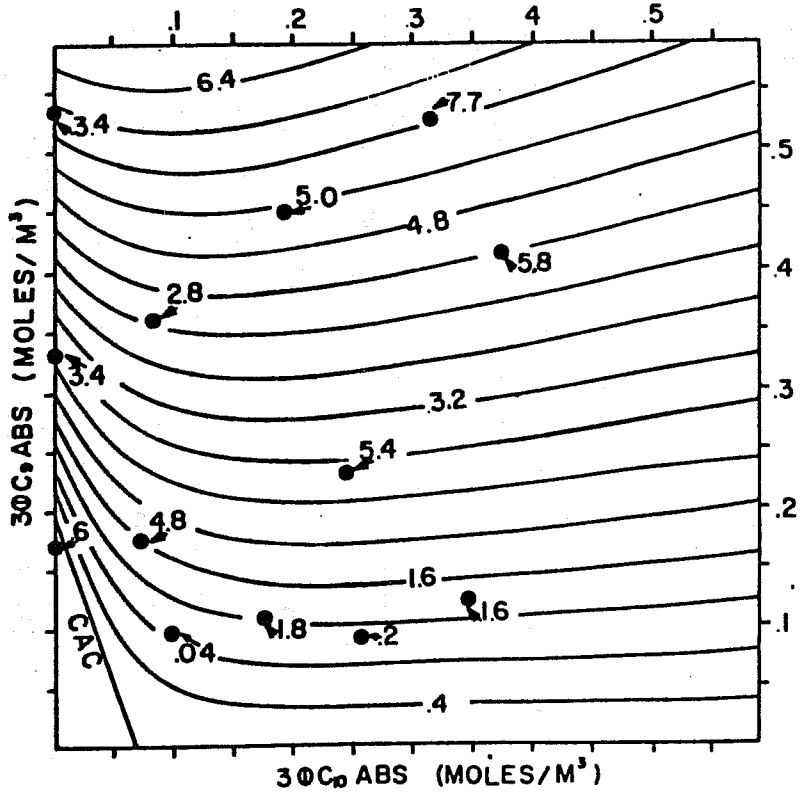

Figure 7. $3\phi C_9$ adsorption versus $3\phi C_9$ and $3\phi C_{10}$ concentrations.

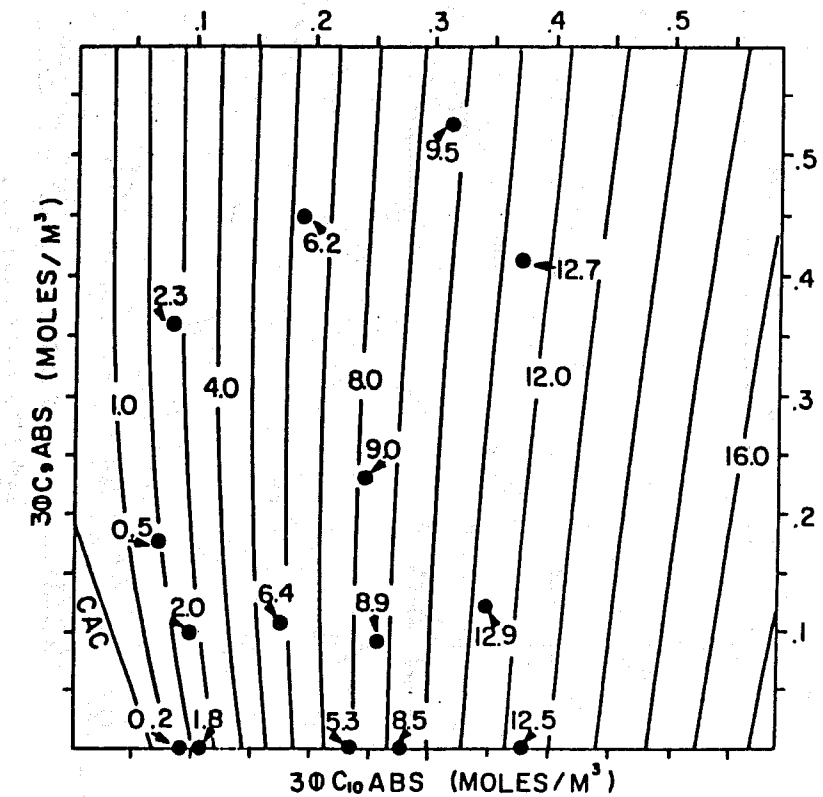

Figure 8. 3ϕC10 adsorption versus 3ϕC9 and 3ϕC10 concentrations.

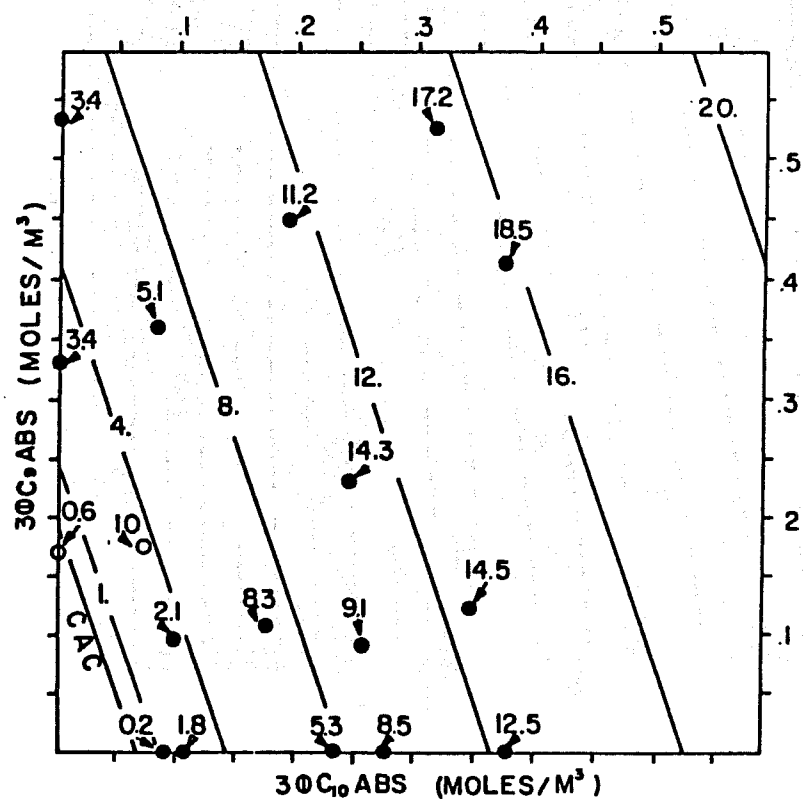

Figure 9. Total surfactant adsorption versus $3\phi C_9$ and $3\phi C_{10}$ concentrations.

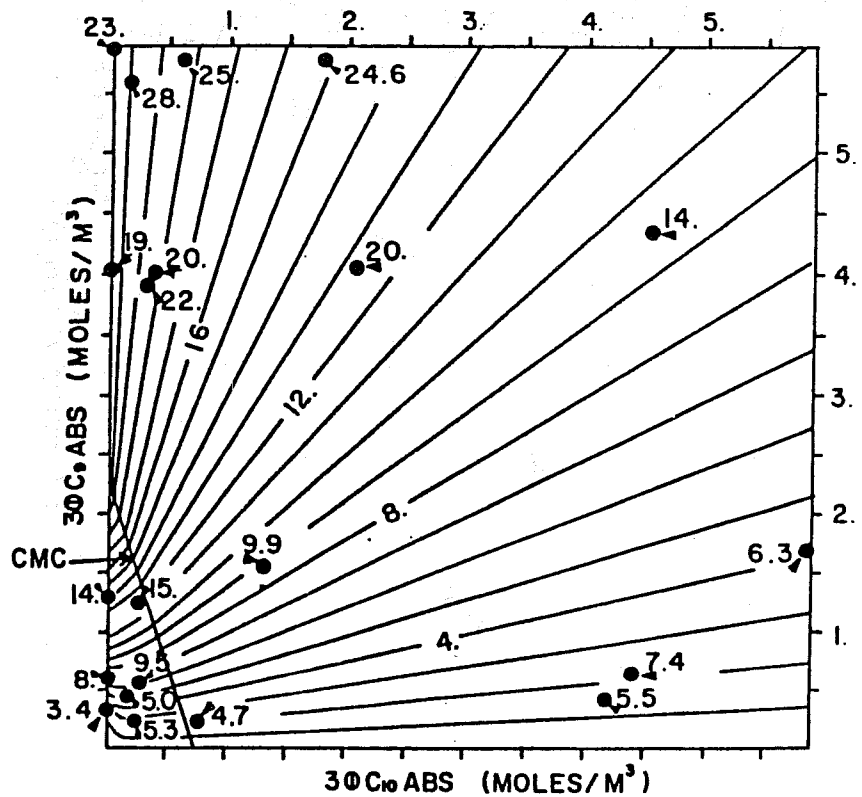

Figure 10. $3\phi C_9$ adsorption above the CMC as a function of $3\phi C_9$ and $3\phi C_{10}$ concentrations.

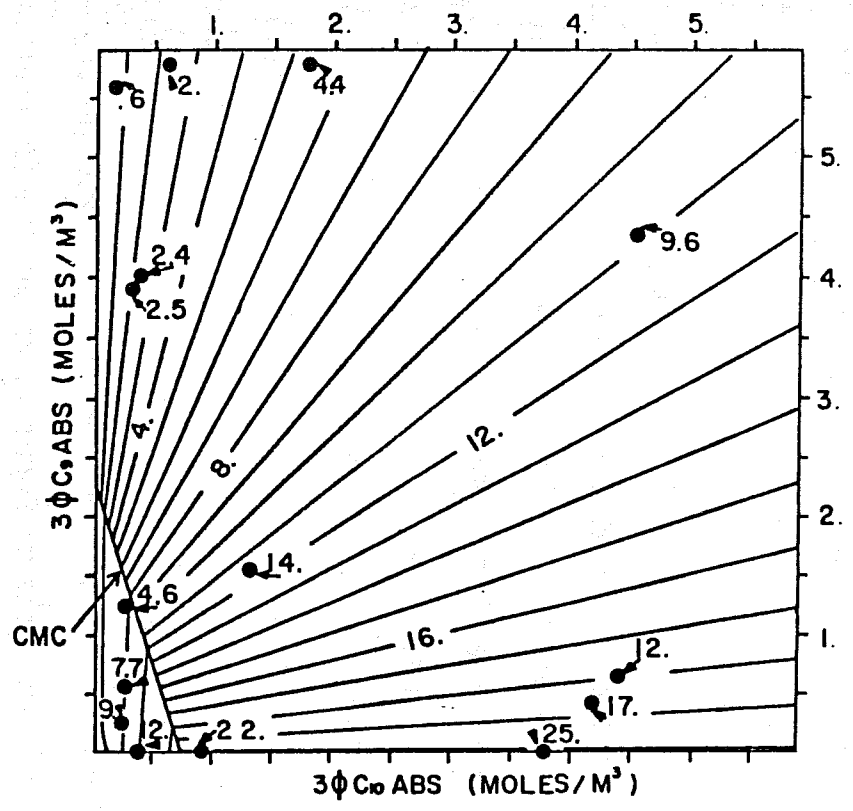

Figure 11. 3ϕC10 adsorption above the CMC as a function of 3ϕC9 and 3ϕC10 concentrations.

contours are not curve fit to the experimental data but are predicted from the pure component isotherms alone. The data compare adequately with prediction, especially the $3\phi C_{10}$ data. Much of the variation between prediction and experimental results is probably attributable to inadequate pH control. Though the pH of the feed solutions was carefully adjusted, surfactant adsorption and equilibration of the solid and the solution produces a pH change. Though high added electrolyte concentrations damps out the variation of equilibrium pH with surfactant adsorption, it does not eliminate it. Even better results should be obtained if the final pH of the solid/solution system were adjusted after equilibration.

In Figure 7 note the effects of $3\phi C_{10}$ concentration on $3\phi C_9$ adsorption. Following a path of constant $3\phi C_9$ concentration, observe that at low $3\phi C_{10}$ concentrations the $3\phi C_9$ adsorption <u>increases</u> very rapidly with increasing $3\phi C_{10}$ concentration. The reason for this is that the larger hydrophobic moiety of the $3\phi C_{10}$ makes it a better aggregate former. As the $3\phi C_{10}$ concentration increases, admicelles appear on a larger fraction of the surface and $3\phi C_9$ is incorporated into these aggregates, causing a very sharp rise in $3\phi C_9$ adsorption. In contrast, in Figure 8, now following a line of constant $3\phi C_{10}$ concentration, near the CAC increasing the $3\phi C_9$ concentration has little effect on the $3\phi C_{10}$ adsorption, since new aggregates do not form as readily. Returning to Figure 7, as the line of constant $3\phi C_9$ concentration goes further from the CAC, $3\phi C_9$ adsorption begins to decrease slowly with increasing $3\phi C_{10}$ concentration. Here, $3\phi C_{10}$ monomers are displacing $3\phi C_9$ from existing admicelles more rapidly than new admicelles are forming so that net $3\phi C_9$ adsorption is decreasing. The same behavior appears in Figure 8 for $3\phi C_{10}$ adsorption but is less noticeable since $3\phi C_{10}$ is preferentially incorporated into the aggregates because of its larger hydrophobic moiety.

The total surfactant adsorption as a function of $3\phi C_{10}$ and $3\phi C_9$ concentration below the CMC is shown in Figure 8. This function is of interest for two reasons. One is that maxima in surfactant adsorption have been observed in a variety of systems. This is explained by the plateau adsorption model and mixed micelle formation. Maxima should not, then, be present below the CMC in the absence of admicelles. This is obviously the case in Figure 9. A second reason for plotting total adsorption is to compare prediction to experimental results. If the $3\phi C_9$ and $3\phi C_{10}$ surfaces of Figures 7 and 8 are compared, the contour lines run nearly perpendicular to each other. The predicted contour lines for the total adsorption, as shown in Figures 9, are practically parallel to the CAC. When compared to the experimental results, it can be seen that this does, indeed, seem to be the direction of the contours.

A dramatic change occurs in the adsorption behavior above the CMC (Figures 10 and 11). The most striking topological feature of the surfaces are the lines of constant adsorption radiating out from the CMC in both figures. The reason for the existence of these lines is the phenomenon of mixed micelle formation. At any point just above the CMC, micelles exist in equilibrium with monomers. If a new micelle is added to the system and this micelle is the same composition of $3\phi C_9$ and $3\phi C_{10}$ as the micelles already in the system, then it will be in equilibrium with the monomer already present and total surfactant concentration will increase at constant monomer concentration. Since the chemical potential of the monomers determines the adsorption, as long as the monomer composition remains unchanged, adsorption is unchanged; hence, total surfactant concentration can be increased at constant adsorption. This is the mechanism

for the existence of lines of constant adsorption radiating out from the mixture CMC in Figures 10 and 11.

As for the surfaces below the CMC, comparison of the pure component adsorption surfaces with the total surfactant adsorption isotherm shows a striking difference. Figure 12 shows the theoretical and experimental total adsorption. There are no contour lines in Figure 12 because the predicted surface is practically flat above the CMC, going from an adsorption of 2.0×10^{-2} moles/kilogram along the CMC to a maximum of 2.07×10^{-2} moles/kilogram just above the CMC, then back down to 2.02×10^{-2} moles/kilogram. There is, then, a very slight maximum predicted for the surface above the CMC; it is, however, less than the accuracy of the data, so that no contours are shown. The observed plateau adsorption in Figure 12 is $24 \pm 3 \times 10^{-2}$ moles/kilogram. The predicted value is 20×10^{-2} moles/kilogram. The principal reason for this discrepancy is most evident in Figures 2 and 3, the pure component isotherms; there is some additional adsorption above the CMC. The plateau adsorption model says that, to good approximation, monomer concentration and adsorption become constant at the CMC of a pure component. This is, however, only an approximation. Micelle formation is only approximately a phase separation phenomenon. Micelle aggregation numbers and morphologies change above the CMC with accompanying small changes in surfactant chemical potential and, hence, surfactant monomer concentrations. These slight changes in monomer concentration are accompanied by slight but measurable changes in the adsorption.

This theory of surfactant adsorption makes clear the need to understand the relationship between the monomer composition and that of the micelles. The following section summarizes the work that we have accomplished this past year on this important subject.

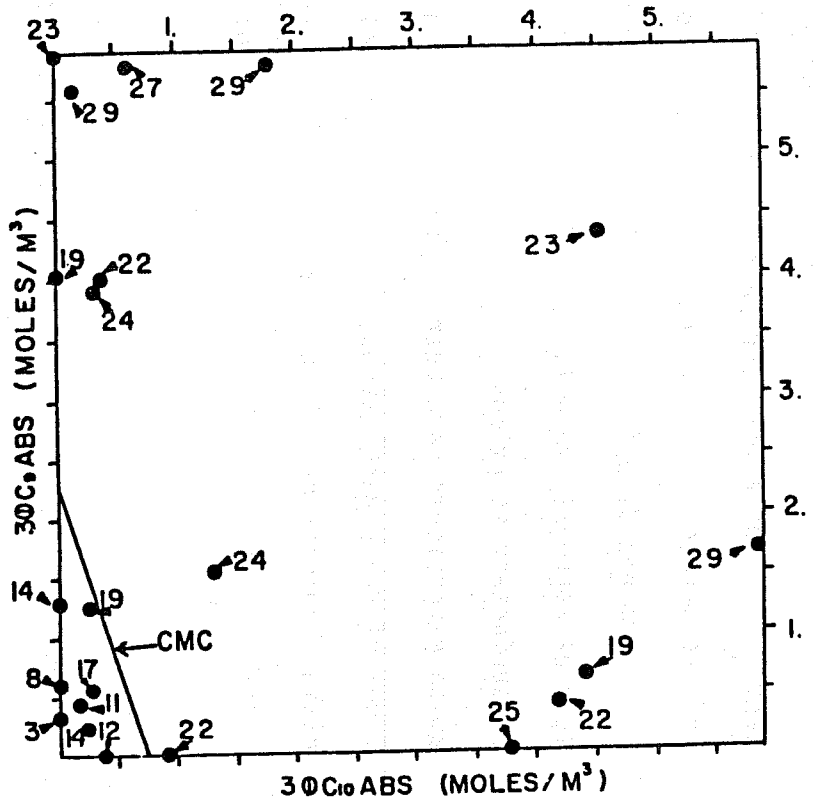

Figure 12. Total surfactant adsorption above the CMC as a function of 3ϕC9 and 3ϕC10 concentrations.

D. MONOMER-MICELLAR EQUILIBRIUM: THE STUDY OF MIXED MICELLAR BEHAVIOR THROUGH THE USE OF ULTRAFILTRATION

D.1. Introduction

It has been demonstrated, in the previous annual report, that an ultrafiltration technique designed to separate monomer from micelles is applicable to aqueous surfactant solutions, both for nonionic surfactant and for anionic surfactant systems. Through the use of an appropriate membrane, under the appropriate conditions of ultrafiltration rate and added electrolyte concentration, for a given surfactant and rate of stirring, the composition of the monomeric surfactant as well as that of micellar surfactant may be determined directly. This makes ultrafiltration very useful in the study of aggregate formation, including the formation of micelles in mixed surfactant solutions.

Ultrafiltration experiments have been performed with binary mixed surfactant solutions of two general types, including mixtures exhibiting ideal micellar mixing behavior as well as some mixtures showing gross deviations from ideal behavior. In both cases, the pseudophase separation model[10] was used to approximate the micellization process.

D.2. Ideal Behavior

The critical micelle concentration (CMC) and the compositions of the two pseudophases in a mixed micellar solution may be predicted when the assumption of ideal mixing is made for both pseudophases. For a binary surfactant mixture, the CMC is given as a function of monomer composition by

$$CMC_M = \frac{CMC_1 CMC_2}{X_1 CMC_2 + X_2 CMC_1}$$

$$= \frac{(CMC_1^o)^{k_{g_1}+1} (CMC_2^o)^{k_{g_2}+1}}{X_1 (CMC_2^o)^{k_{g_2}+1} (CMC_M + C_S)^{k_{g_1}} + X_2 (CMC_1^o)^{k_{g_1}+1} (CMC_M + C_S)^{k_{g_2}}} \quad (20)$$

where CMC_1 and CMC_2 are the pure component CMC of components 1 and 2, respectively, X_1 and X_2 are the monomer compositions, C_S is the added electrolyte concentration, and k_{g_1} and k_{g_2} are the counterion binding of components 1 and 2, respectively. The latter are experimentally determined.

The composition in the micelles is given as a function of the monomer composition by

$$Y_i = X_i \frac{CMC_M}{CMC_i} , \quad i = 1,2 \tag{21}$$

Hence, the formation and composition of mixed surfactant micelles can be predicted easily for the ideal case.

D.3. Nonideal Behavior

The behavior of mixed micellar solutions which exhibit serious deviations from ideality may be adequately described with the use of the pseudophase separation model through the incorporation of an activity coefficient. The equations predicting the CMC and the micellar composition as a function of the monomer composition are then given by

$$CMC_M = \frac{CMC_1 CMC_2}{X_1\gamma_1 CMC_2 + X_2\gamma_2 CMC_1} \tag{22}$$

$$Y_i = X_i\gamma_i \frac{CMC_M}{CMC_i} , \quad i = 1,2 \tag{23}$$

where γ_1 and γ_2 are the activity coefficients of the two surfactant components in the micellar pseudophase. A dilute solution has been assumed for the monomer pseudophase.

The activity coefficient has been predicted with the use of a regular solution type approach such as that used by Scamehorn[9] and Rubingh.[13] In this approach, both activity coefficients are expressed as a function of

the micellar composition and a single parameter, W, as follows:

$$\ln\gamma_1 = Y_2^2 \frac{W}{RT} \tag{24}$$

$$\ln\gamma_2 = Y_1^2 \frac{W}{RT} \tag{25}$$

Values for the parameter, W, were determined experimentally.

Thus, the CMC as well as the micellar composition of nonideal mixed micellar solutions may be predicted through the use of equations 22 through 25.

D.4. Experimental

The apparatus and procedure have been described elsewhere.[11] The ideal mixing surfactant solutions consisted of binary mixtures of alkyl benzene sulfonates (ABS) of monoisomeric purity. In particular, mixtures of decyl benzene sulfonates and dodecyl benzene sulfonates were studied. The mixtures exhibiting nonideal mixing behavior were composed of an alkyl benzene sulfonate and a polyethoxylated nonyl phenol of the IGEPAL CO series. In particular, the ABS used were decyl, undecyl, and dodecyl benzene sulfonates, while the IGEPAL's used were the CO 660, 850, and 970, with 10, 20, and 50 ethylene oxide units on the average, respectively.

All experiments have been performed using aqueous solutions, with 0.171 M NaCℓ as the added electrolyte, at room temperature.

D.5. Results

Experimental determinations of the CMC and micellar composition as a function of the monomer composition have been made for binary mixtures of decyl benzene sulfonate with dodecyl benzene sulfonate. These results are presented in Figures 13 and 14, in which the theoretical predictions of the behavior of the corresponding ideal solution (solid lines) are shown for

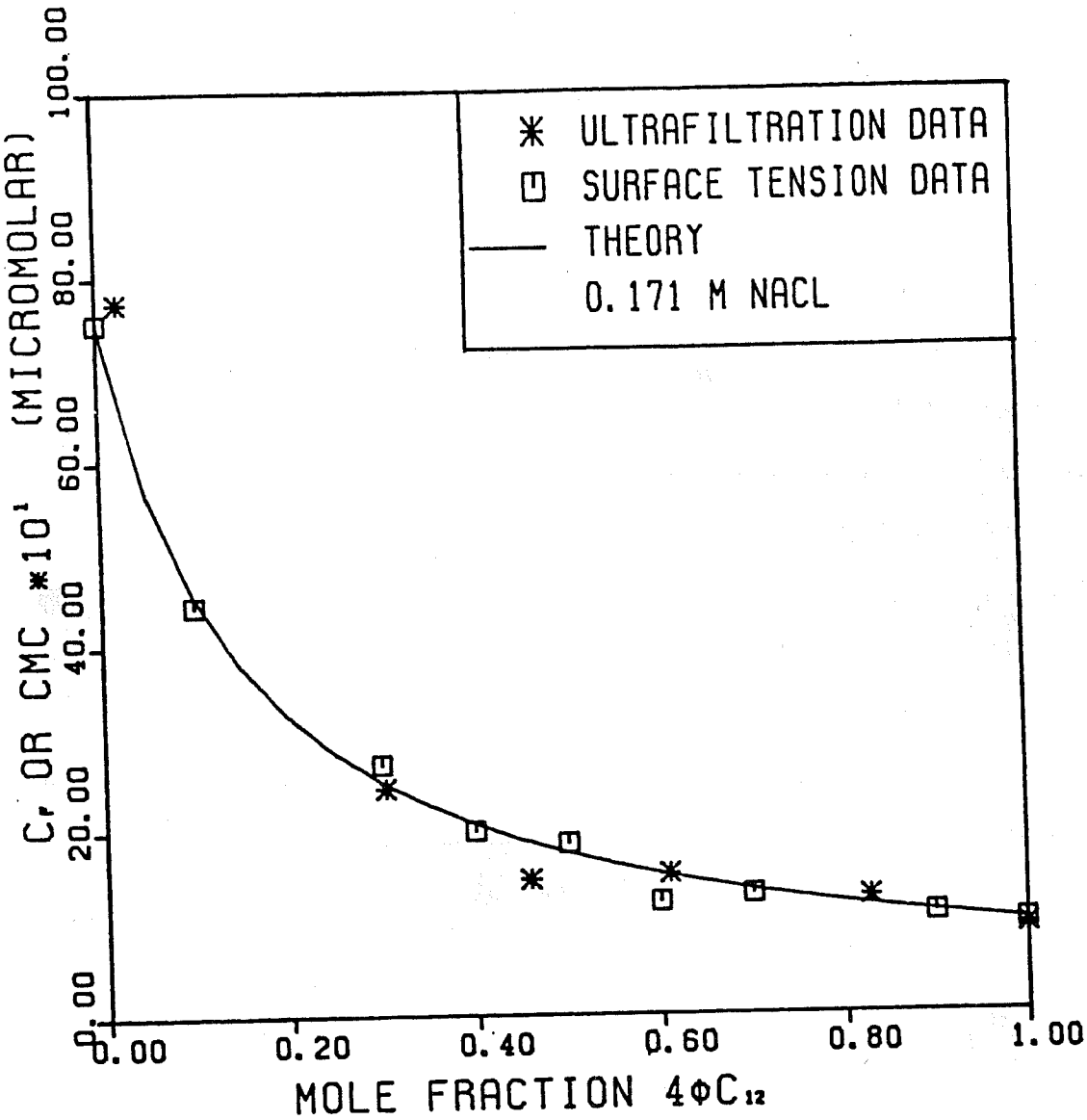

Figure 13. Variation of monomer concentration with phase composition for mixtures of decyl benzene sulfonate with dodecyl benzene sulfonate.

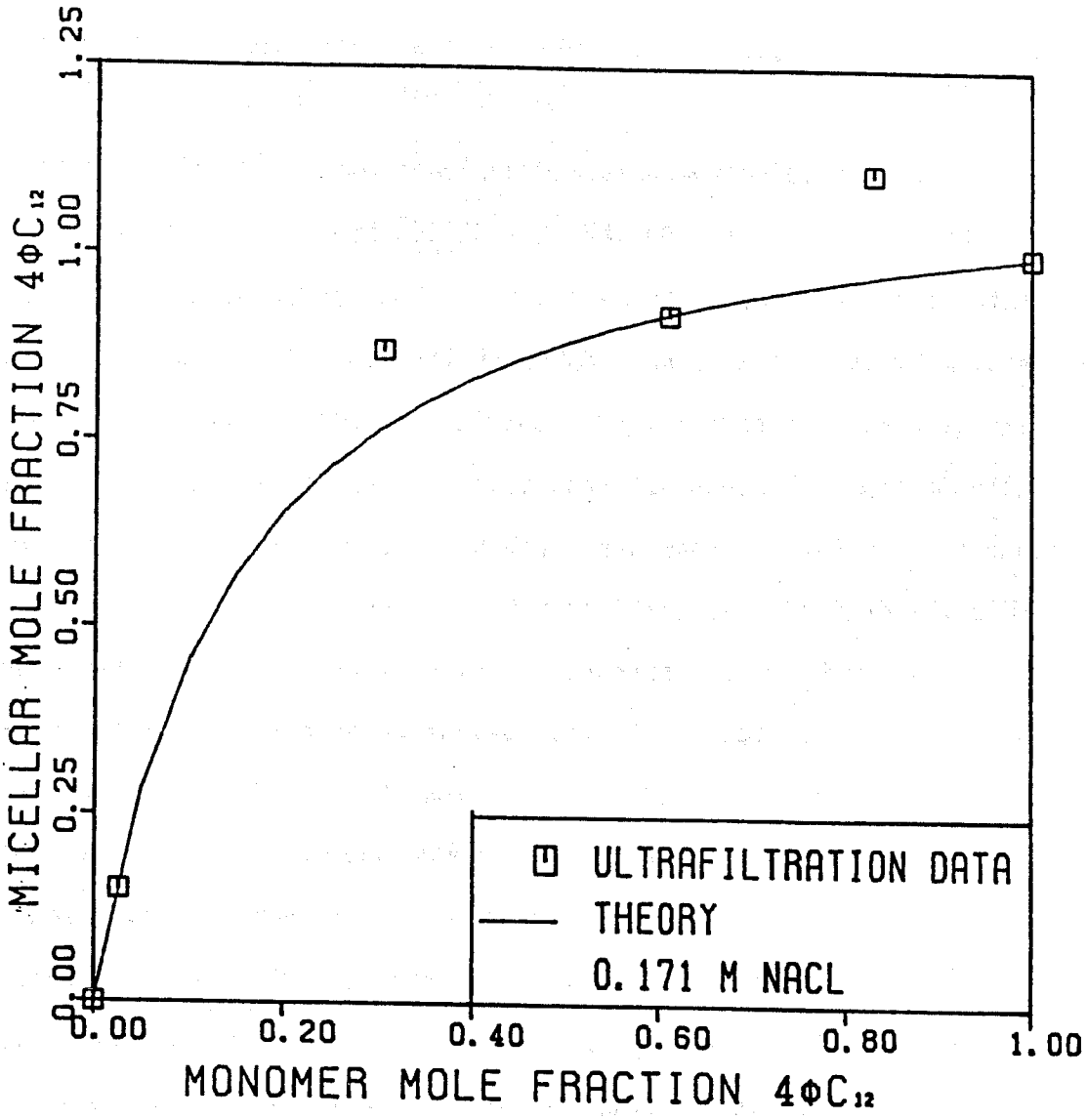

Figure 14. Variation of micellar phase composition with the monomer phase composition for mixtures of decyl benzene sulfonate with dodecyl benzene sulfonate.

comparison. The k_g values which are required by equation 20 were determined by surface tension measurements to be 0.58 and 0.75 for the decyl and undecyl ABS, respectively. The agreement between the experimental results and the theoretical results is good. This indicates that the two assumptions made, namely that pseudophase approximation and that of ideal mixing, were justified. This conclusion is supported by previous works.[14,15]

The mixtures studied which formed nonideal mixed micelles were mixtures of the decyl ABS with the IEGPAL's CO 660 and 850. Also studied were mixtures of the undecyl ABS with the IGEPAL's CO 660 and 850. In addition, mixtures of the dodecyl ABS with the IGEPAL's CO 660, 850, and 970 were studied. The experimental results, as well as the model predictions of equations 22 through 25 (solid lines), are presented in Figures 15 through 28. Figure 29 shows the values selected for the parameter W which were determined by a best fit of the CMC data.

The behavior observed was that of a significant deviation from ideal behavior, as was expected.[8,13] This deviation showed a definite increase with the average length of the ethylene oxide chain. This could be attributed to the increasing ability of the longer polymer chains to shield the charges of the anionic surfactant head groups in the micelle from each other. The model is observed to have described the CMC data quite well. On the other hand, the micellar compositional data is correct only qualitatively. There is a significant discrepancy between the experimental and predicted micellar compositions for high mole fractions of the nonionic in the monomer. This discrepancy is observed to increase as the length of the ethylene oxide chain increases. This behavior could possibly be explained as an effect of the space requirements of the bulky polyethyleneoxide

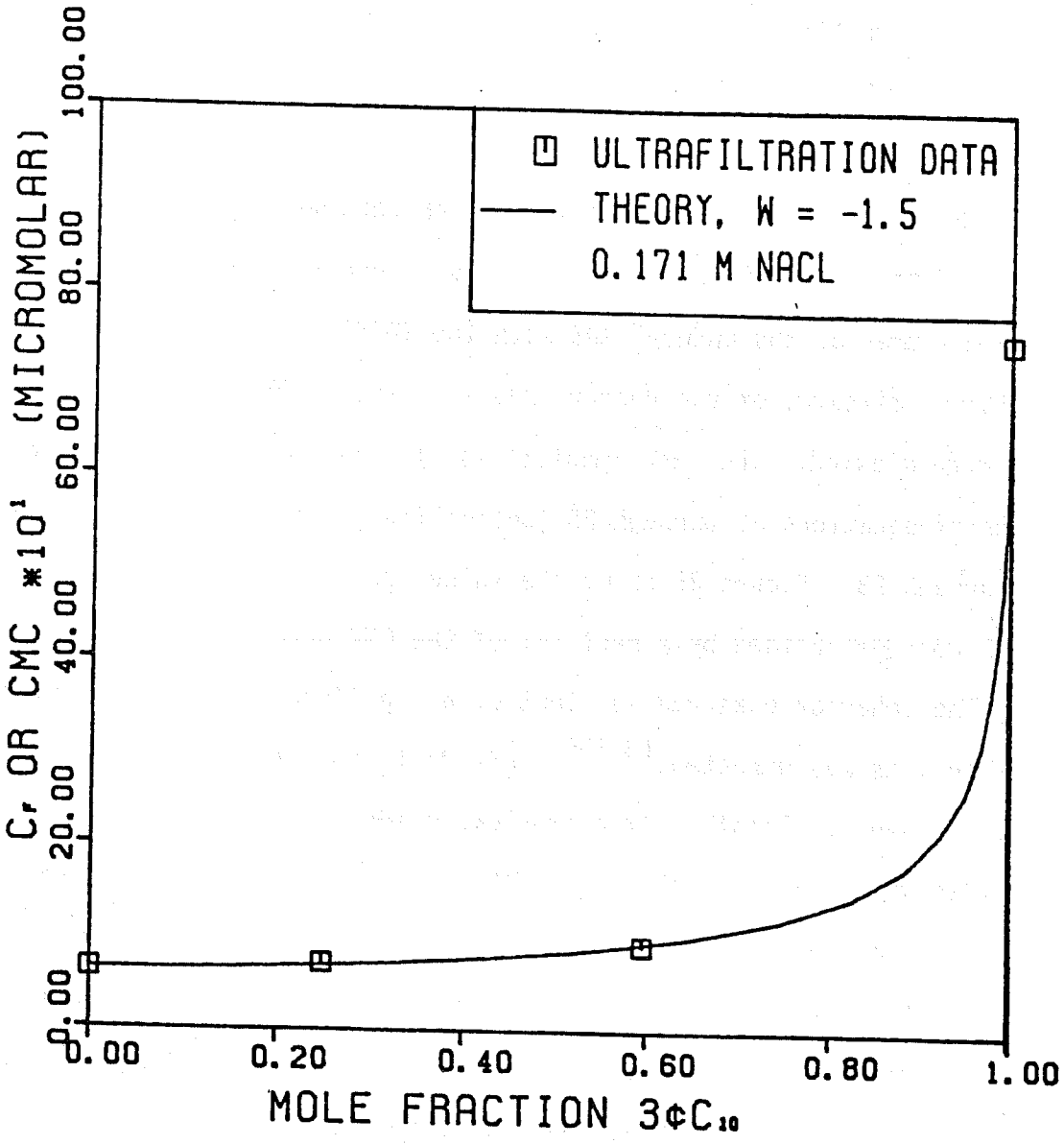

Figure 15. Variation of monomer concentration with phase composition for mixtures of decyl benzene sulfonate with IGEPAL CO 660.

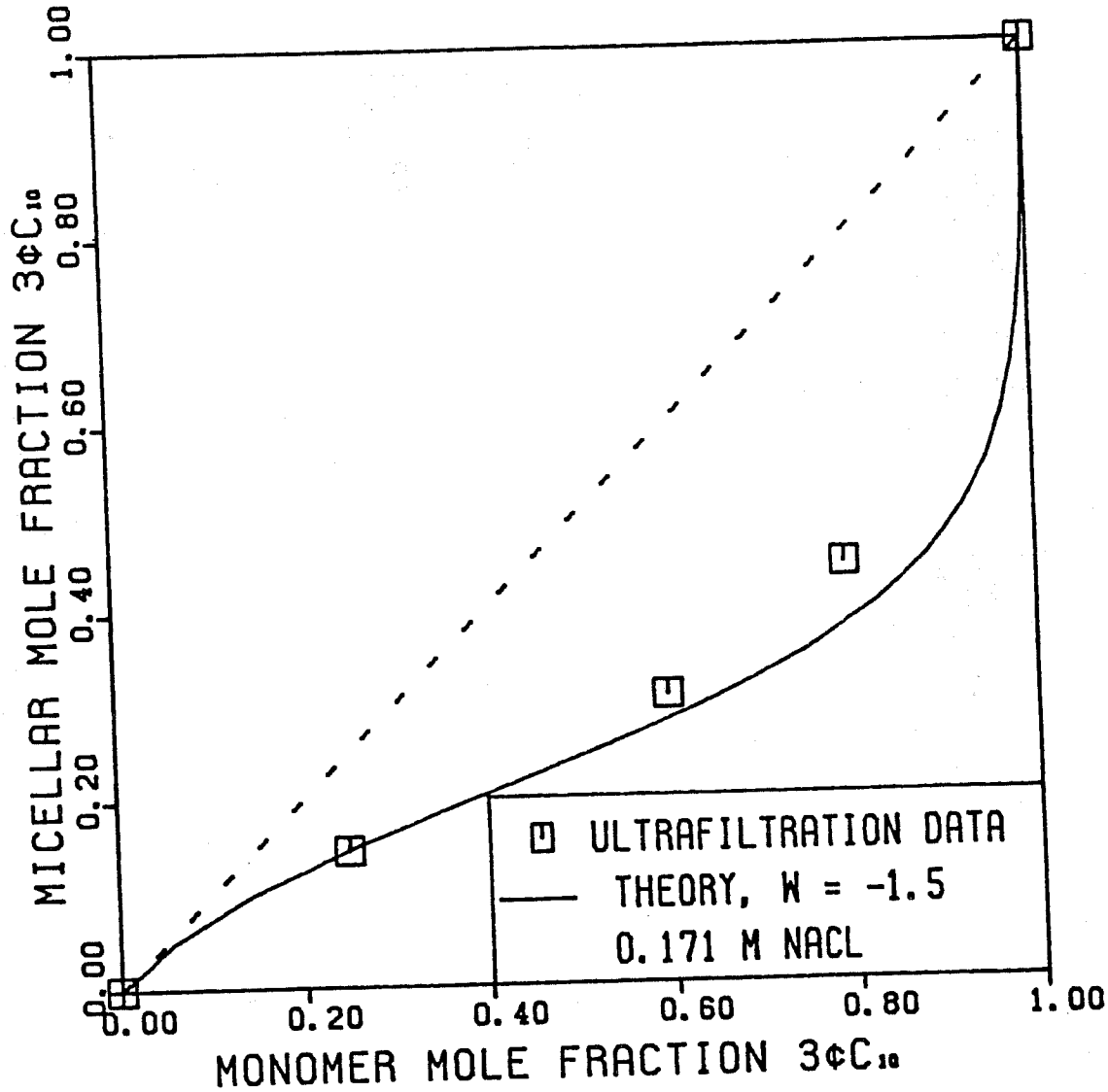

Figure 16. Variation of micellar phase composition with the monomer phase composition for mixtures of decyl benzene sulfonate with IGEPAL CO 660.

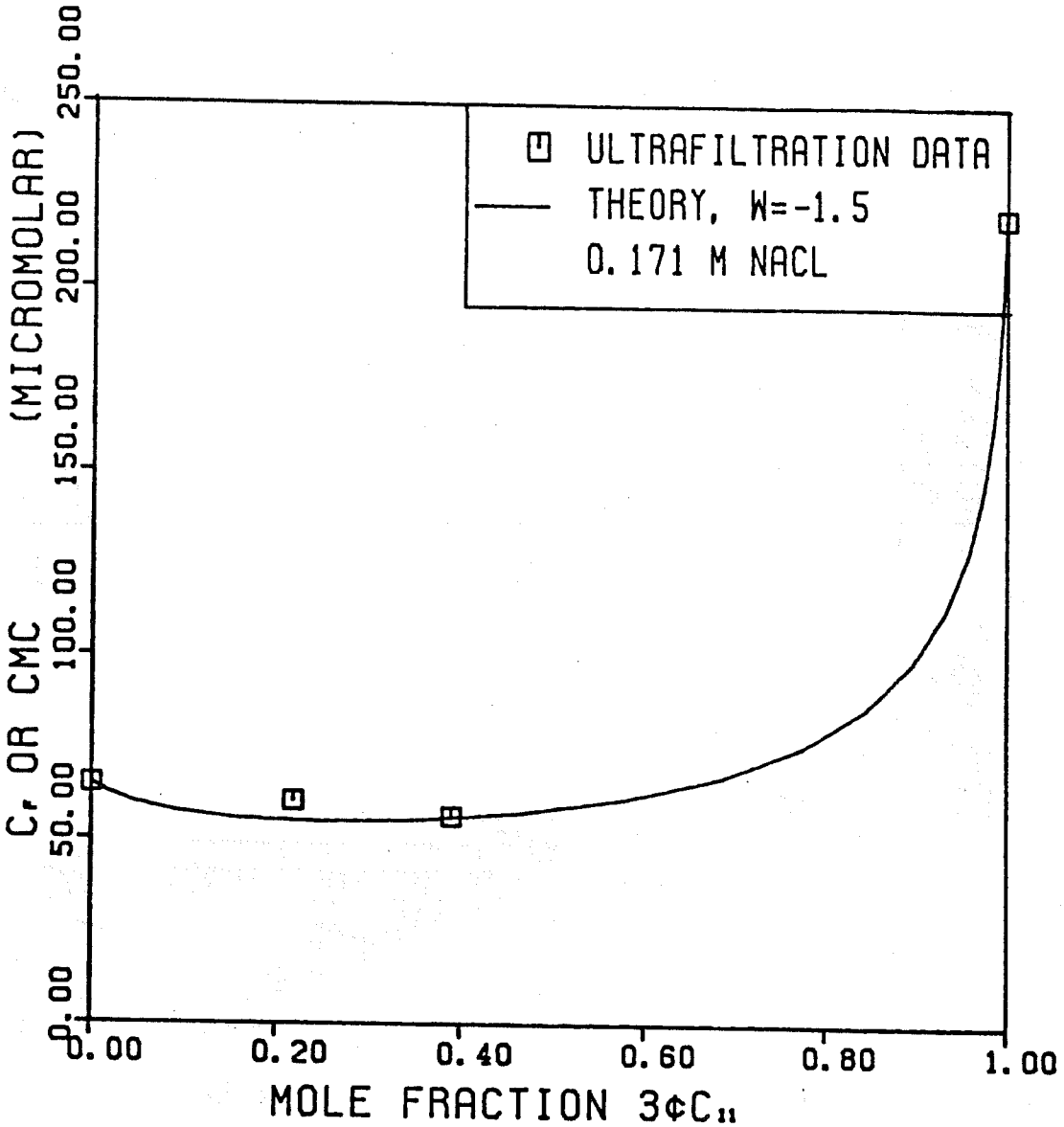

Figure 17. Variation of monomer concentration with phase composition for mixtures of undecyl benzene sulfonate with IGEPAL CO 660.

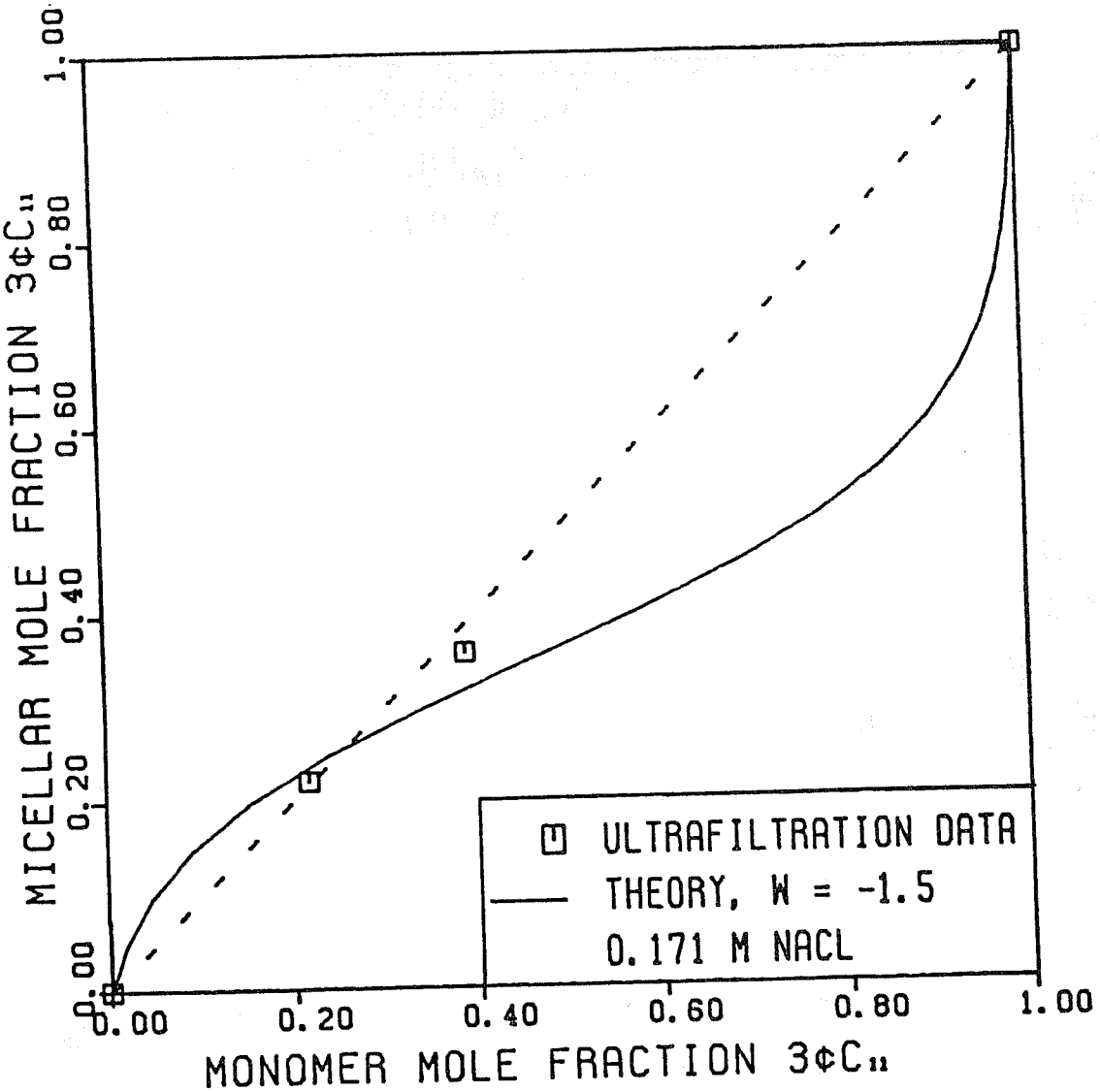

Figure 18. Variation of micellar phase composition with the monomer phase composition for mixtures of undecyl benzene sulfonate with IGEPAL CO 660.

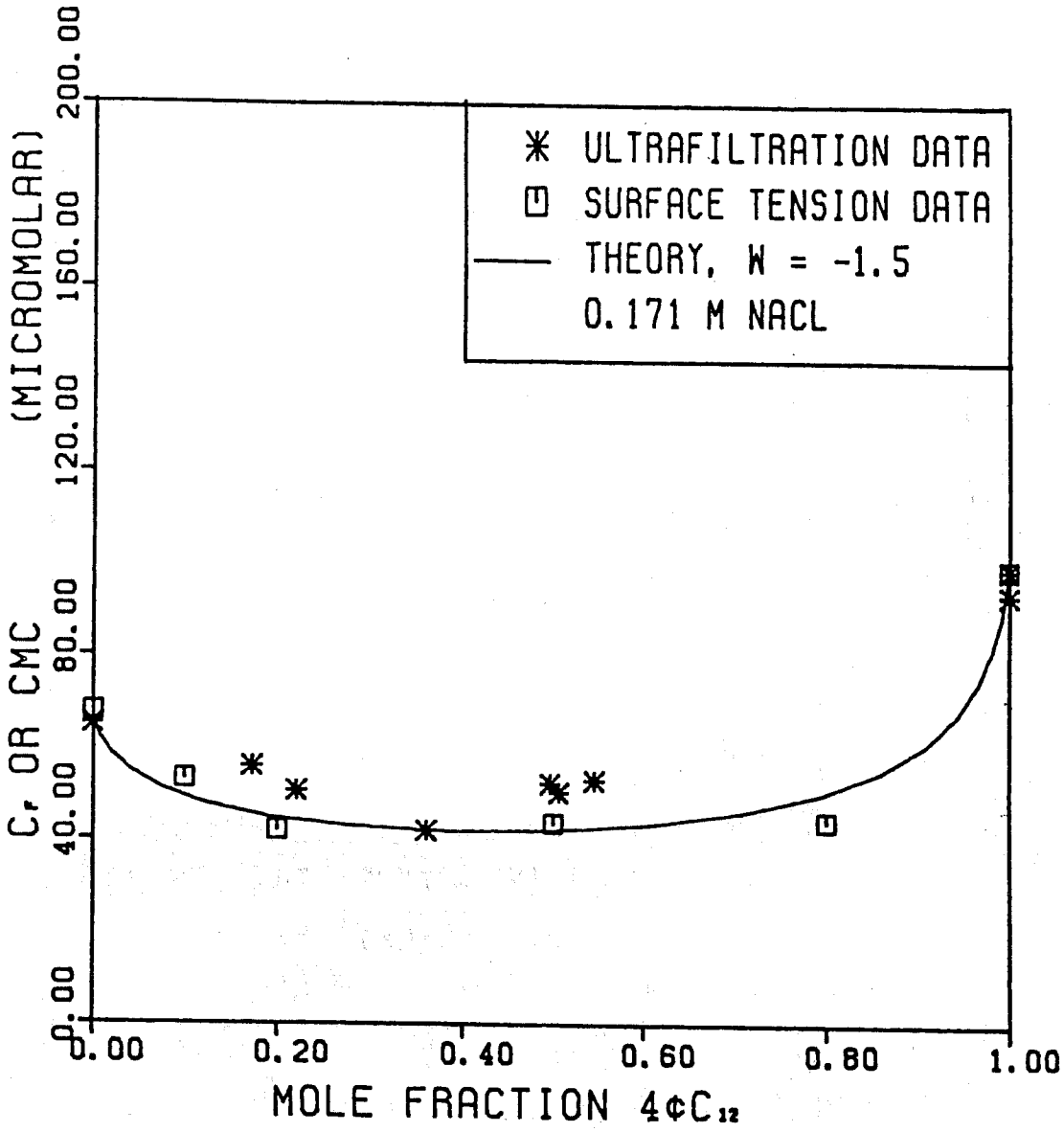

Figure 19. Variation of monomer concentration with phase composition for mixtures of dodecyl benzene sulfonate with IGEPAL CO 660.

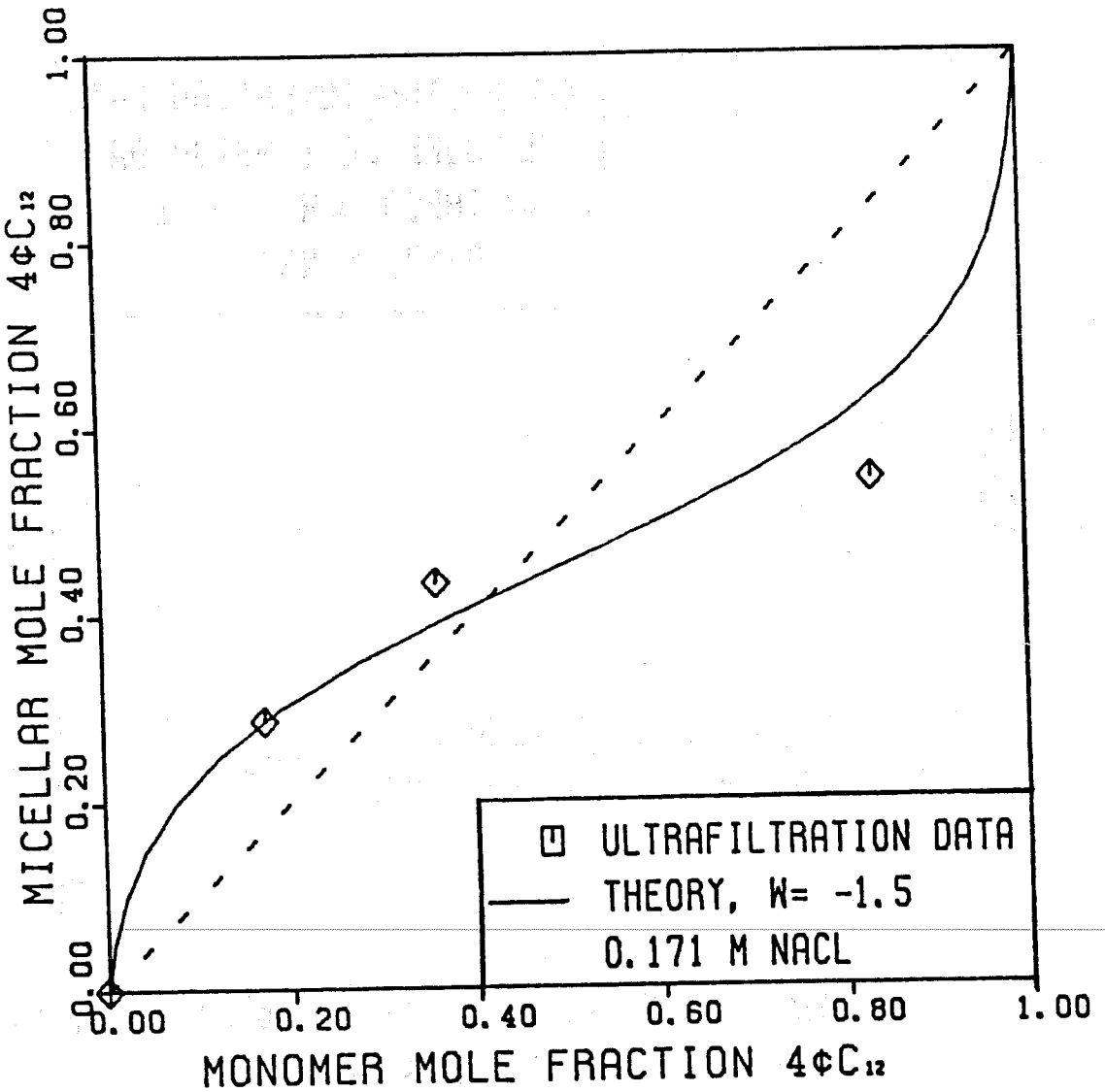

Figure 20. Variation of micellar phase composition with the monomer phase composition for mixtures of dodecyl benzene sulfonate with IGEPAL CO 660.

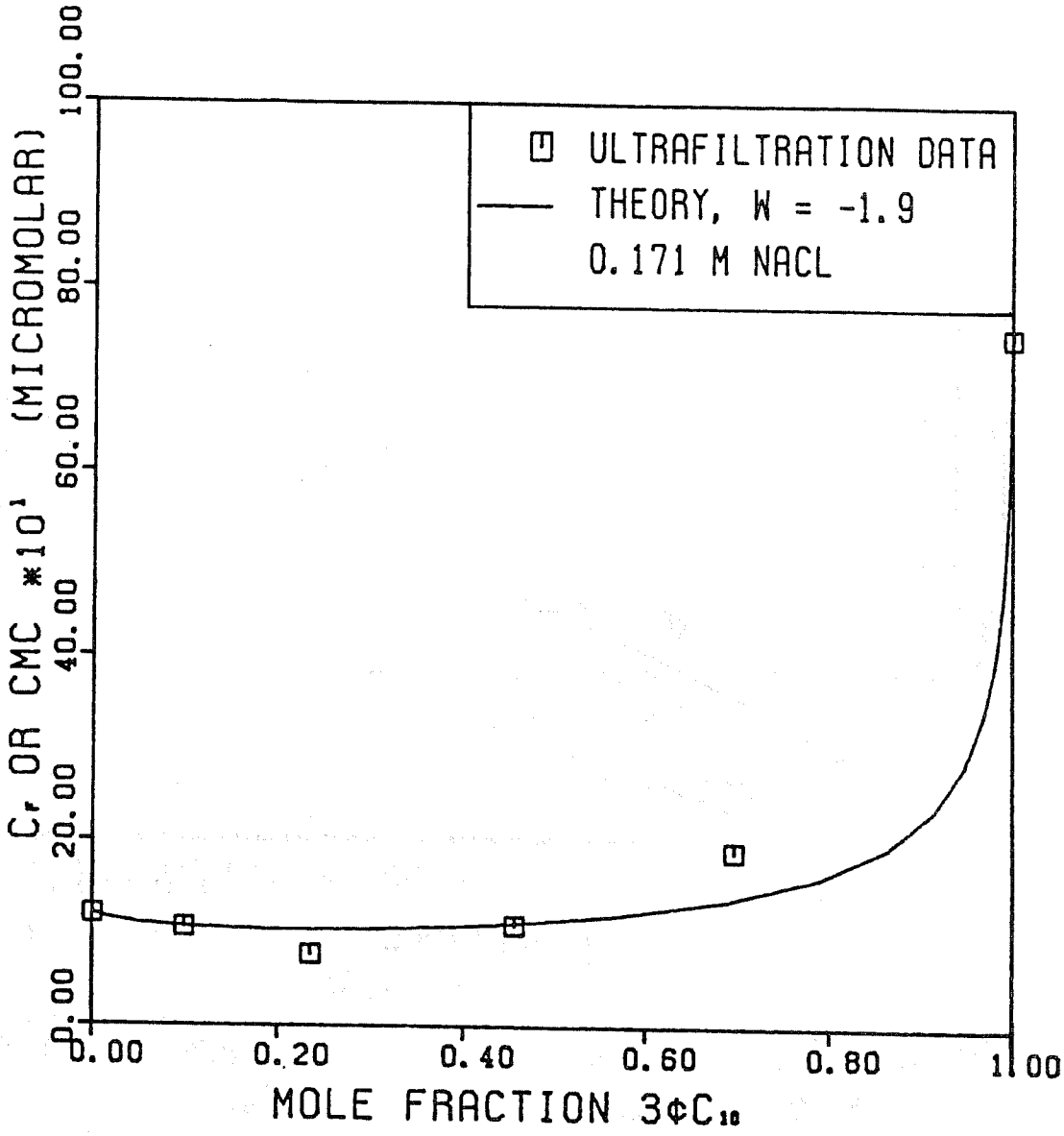

Figure 21. Variation of monomer concentration with phase composition for mixtures of decyl benzene sulfonate with IGEPAL CO 850.

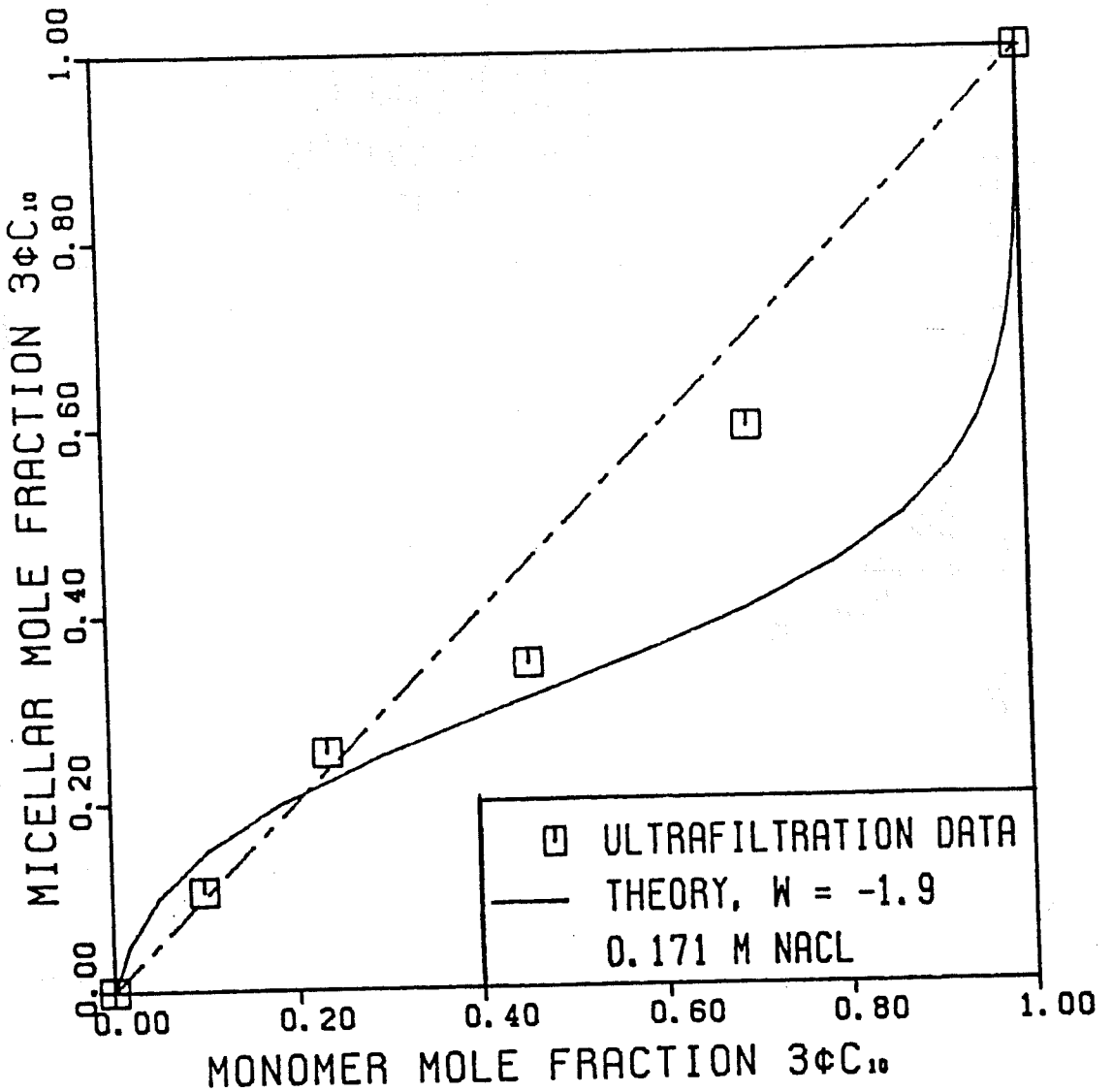

Figure 22. Variation of micellar phase composition with the monomer phase composition for mixtures of decyl benzene sulfonate with IGEPAL CO 850.

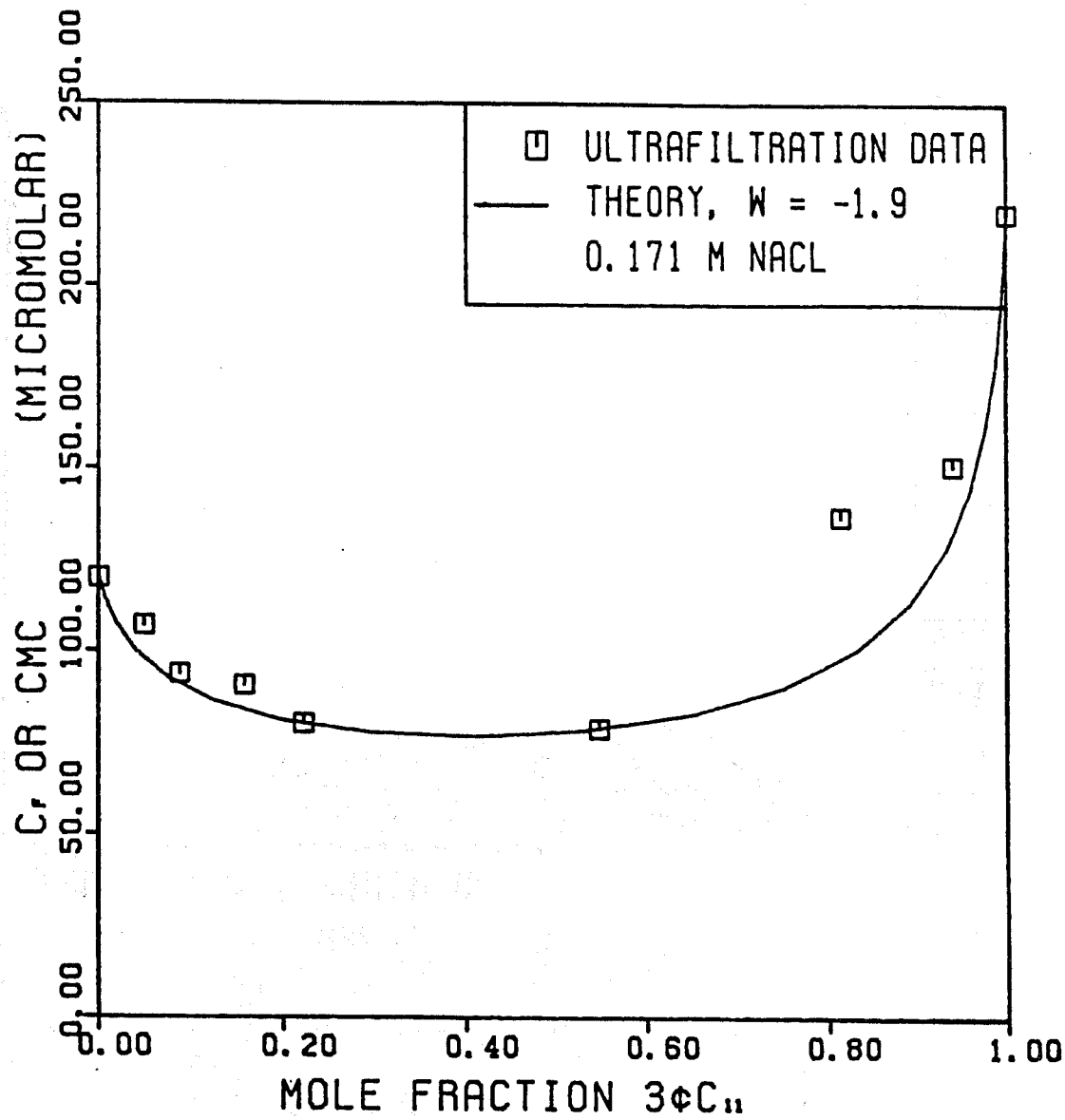

Figure 23. Variation of monomer concentration with phase composition for mixtures of undecyl benzene sulfonate with IGEPAL CO 850.

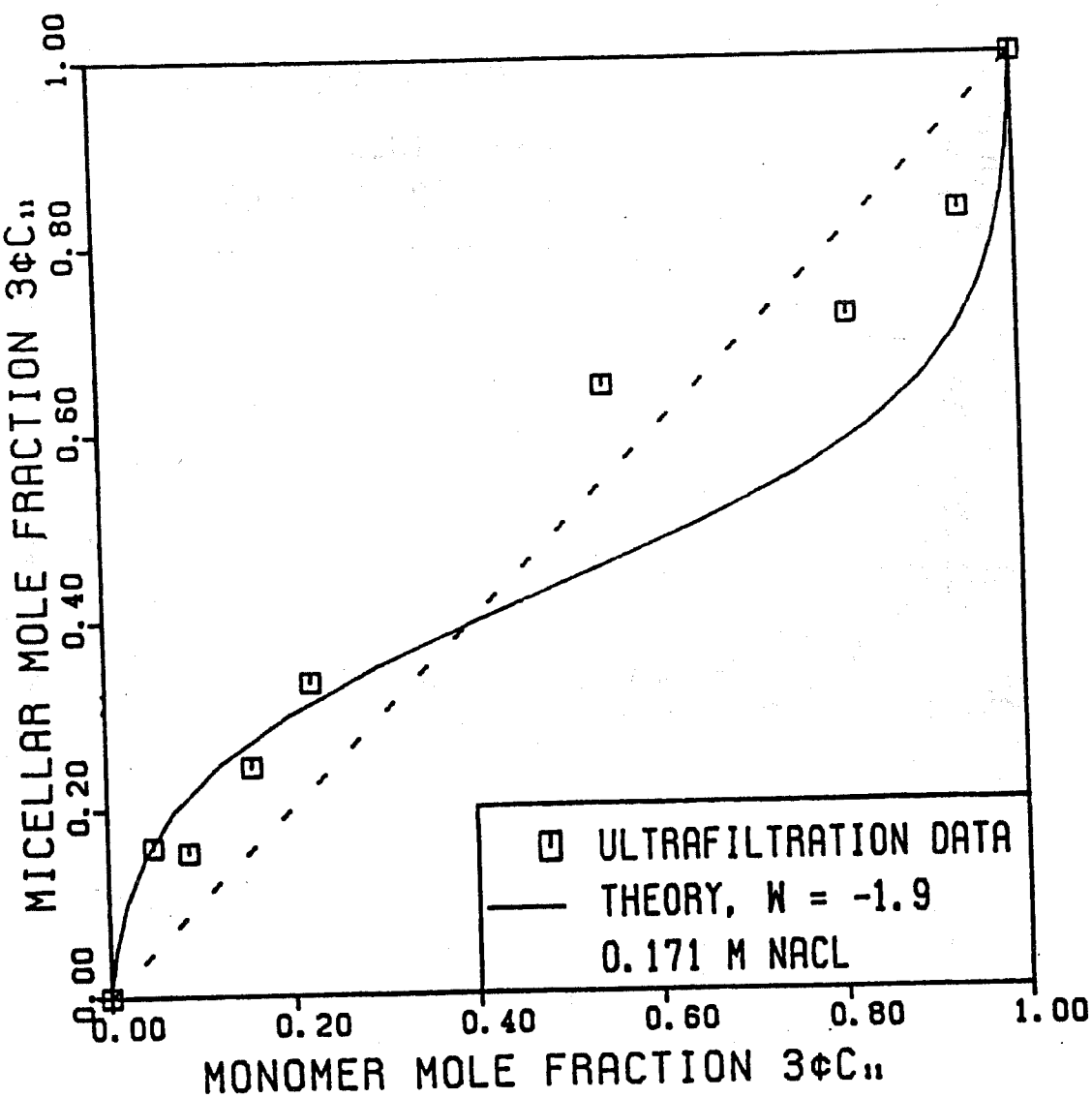

Figure 24. Variation of micellar phase composition with the monomer phase composition for mixtures of undecyl benzene sulfonate with IGEPAL CO 850.

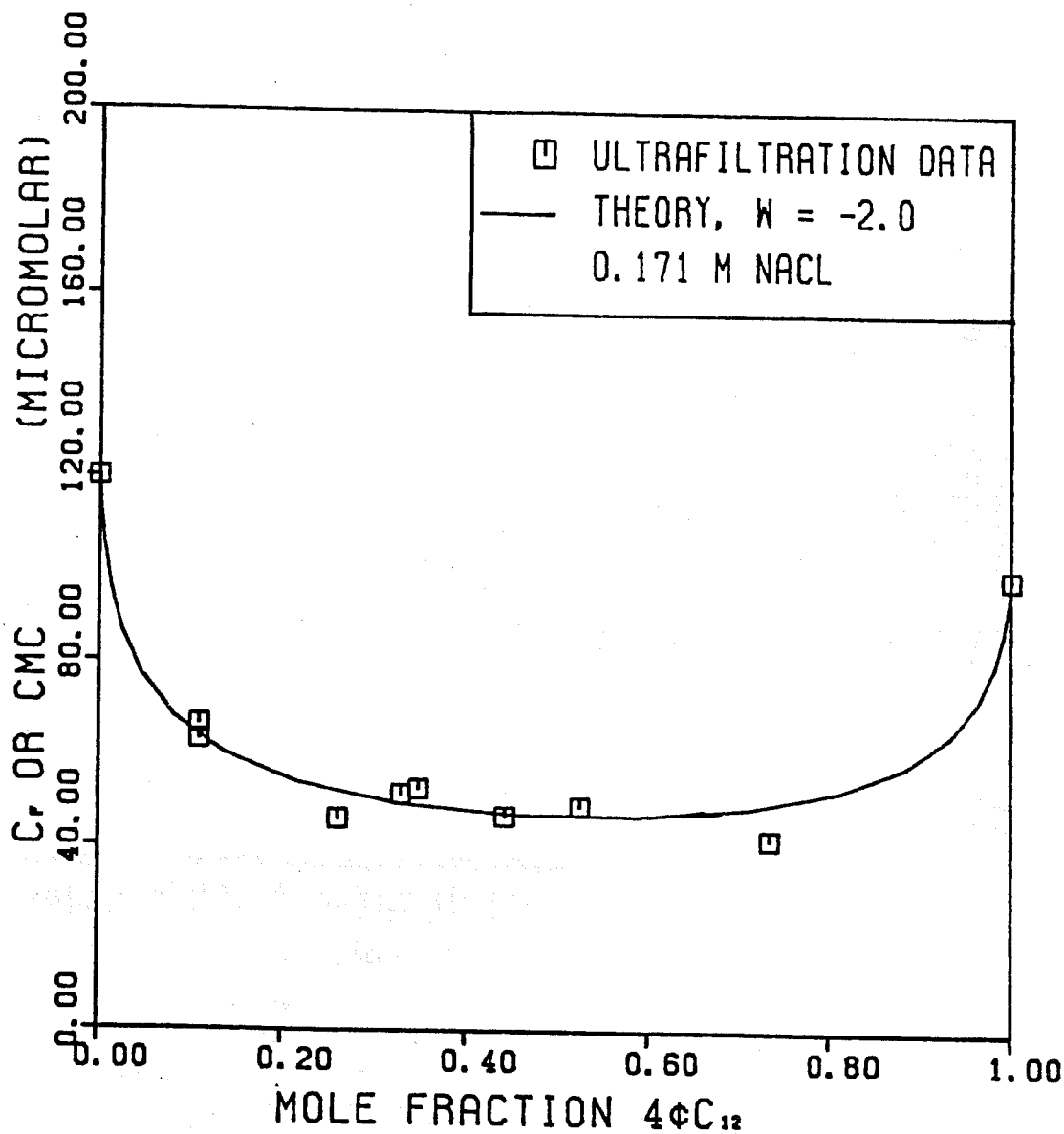

Figure 25. Variation of monomer concentration with phase composition for mixtures of dodecyl benzene sulfonate with IGEPAL CO 850.

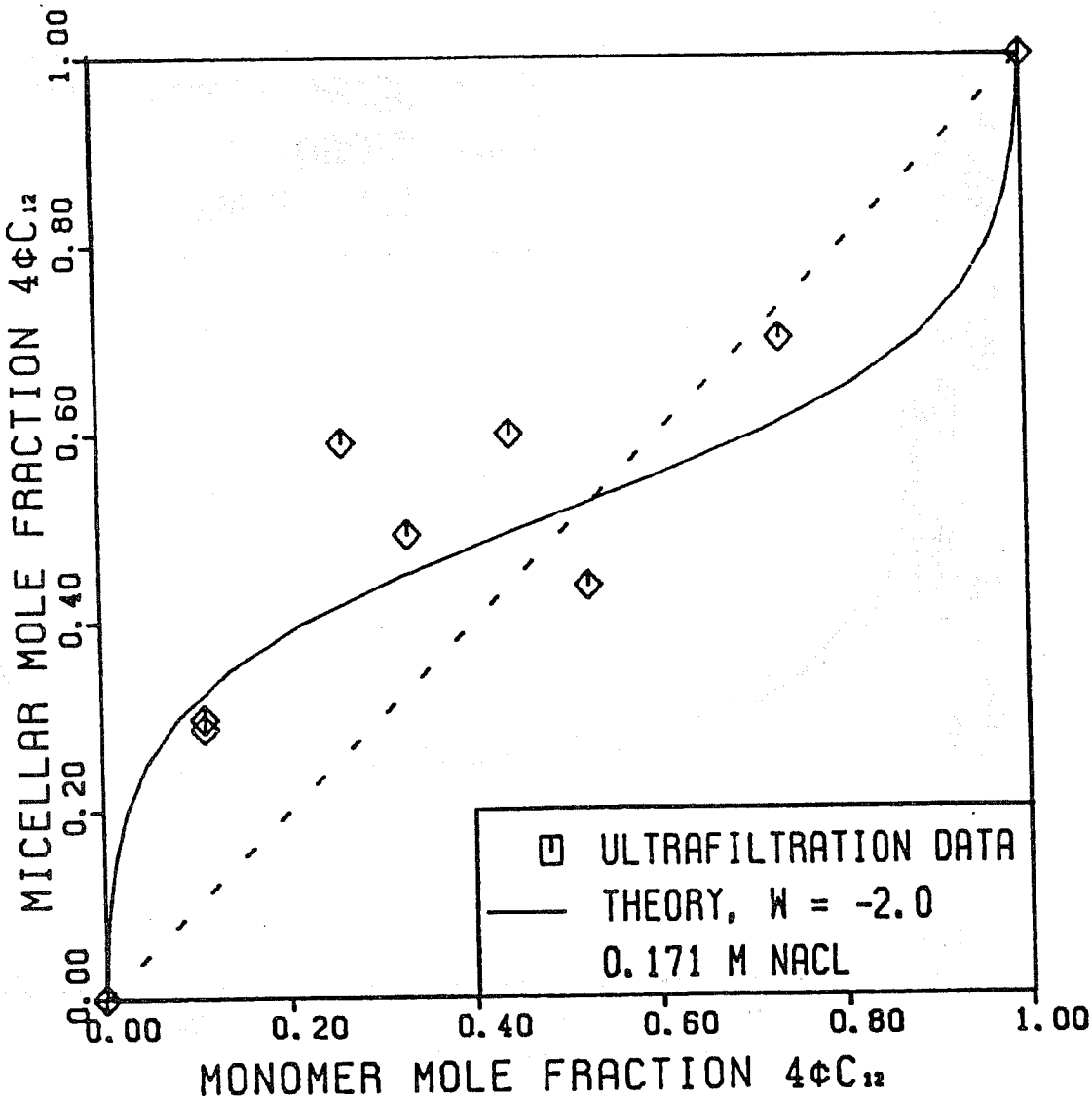

Figure 26. Variation of micellar phase composition with the monomer phase composition for mixtures of dodecyl benzene sulfonate with IGEPAL CO 850.

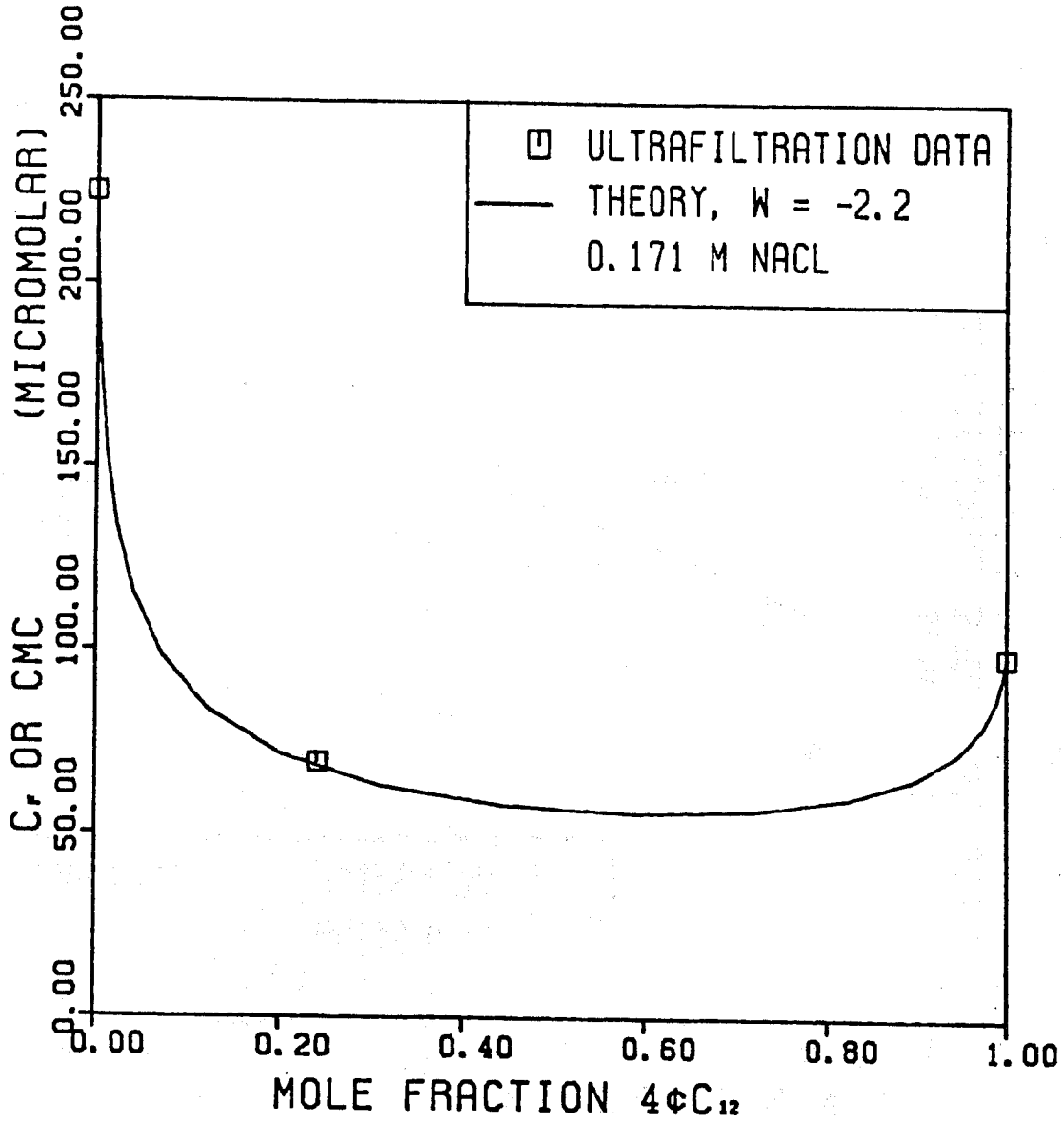

Figure 27. Variation of monomer concentration with phase composition for mixtures of dodecyl benzene sulfonate with IGEPAL CO 970.

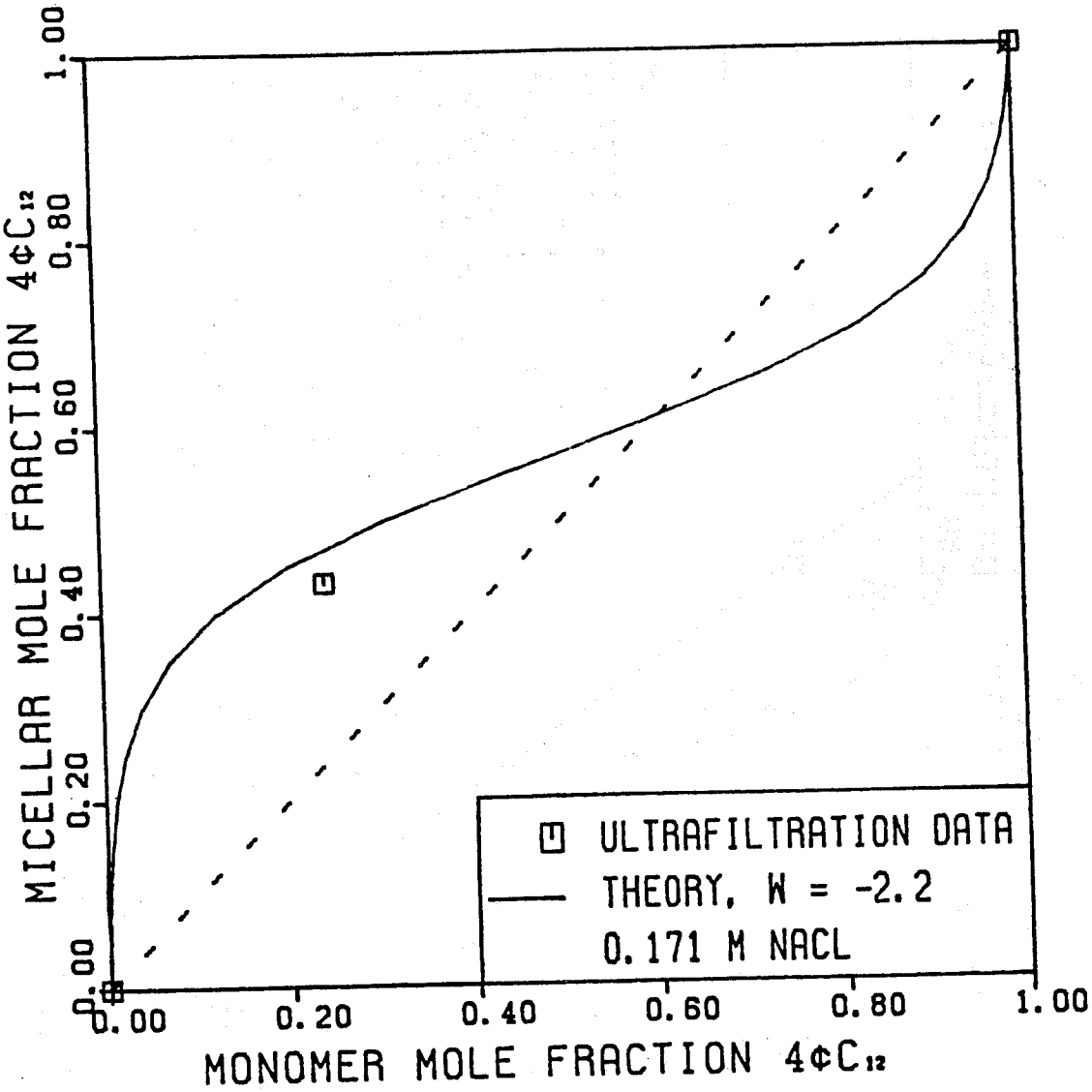

Figure 28. Variation of micellar phase composition with the monomer phase composition for mixtures of dodecyl benzene sulfonate with IGEPAL CO 970.

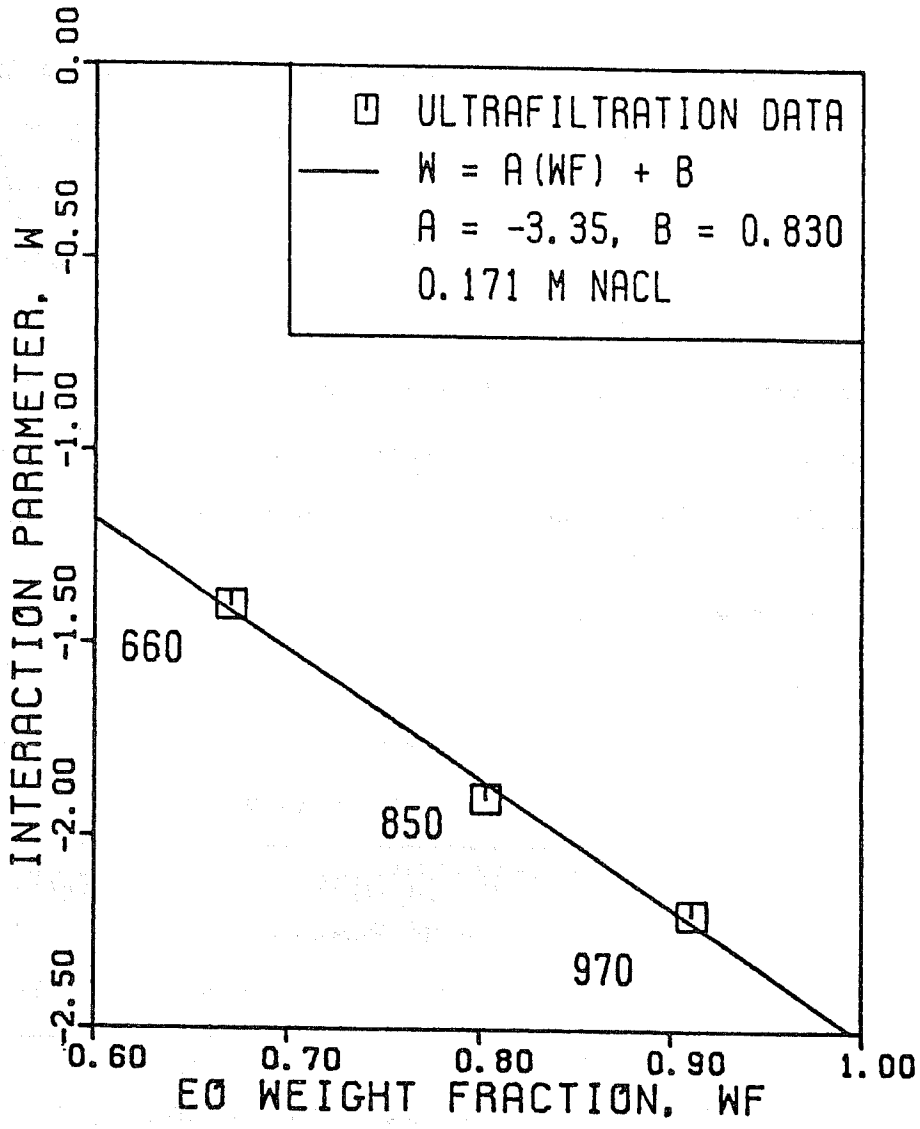

Figure 29. Values obtained for the interaction parameter for different ethylene oxide chain lengths, plotted versus the weight fraction of ethylene oxide in the surfactant molecule.

chains, a consideration which was ignored in the simple model presented here.

E. AN APPARATUS FOR ADSORPTION MEASUREMENTS

E.1. Introduction

It has become clear that surfactant adsorption is dominated by the lateral interactions between adsorbed molecules, and yet there is no systematic study of this important but complex phenomenon. One difficulty is the need to make very precise measurements of small levels of adsorption under controlled conditions of pH and temperature. We have now developed (but not yet perfected) a technique for measuring the adsorption of surfactants with a precision up to an order of magnitude higher than that normally attained. Wide ranges of pH and temperature are accessible.

E.2. Brief Description of the Apparatus

The conventional method of determining isotherms of adsorption from solution[16] involves agitation of the solid with the solution and analysis of the equilibrium liquid. Among the more serious problems which limit the accuracy of this technique[17] are as follows:

(1) The difficulty of separating the liquid from the solid (i.e., the sampling procedure) at the equilibration temperature, especially if this is far from room temperature.

(2) Errors arising from differential evaporation of the liquid and from the dissolution of air (which affects the equilibrium pH) and water vapor in the sample during handling.

(3) Errors arising from the use of different samples of solid for each experiment.

To overcome these problems a sealed apparatus was designed. It consists of a closed circuit (volume $\sim$ 30 cm^3) shown in Figure 30 in which the solution is circulated by a pump, P. A liquid chromatography pump was chosen since it could provide a reasonable flow rate of 8 $cm^3 min^{-1}$ at the pressure drop (200 - 400 psi) across the solid adsorbent bed. The solid adsorbent, A, is contained in a stainless steel column, C, between two fritted disks. The adsorption cell is immersed in a thermostat, TS1, operating to within ± 0.01°K over the temperature range of 303 to 358°K. Solution entering the cell is brought to the thermostat temperature by passage through a heat exchanger coil, HE1. Since the thermostat operates above ambient temperature, the incoming solution is preheated to within ± 1°K of the thermostat temperature by a heater, H, wound on the outside of the capillary tubing and controlled by a RTD controller. The solution leaving the adsorption cell is cooled by a double pipe heat exchanger, HE2, to approximately 303°K before passing through a heat exchanger coil, HE3, located in a thermostat, TS2, operating to within ± 0.01°K at 303°K. The temperature is monitored by thermistors, T1, T2, and T3, via an Omega digital thermometer. The thermostated solution now passes through a spectrophotometer cell where the absorbance is measured by a Beckman 25 spectrophotometer which is followed by glass sample cell, S, where the pH is monitored with a Ross electrode and an Orion research model 601 meter.

The main features of the system are that it is closed to prevent evaporation, the analysis is performed at constant conditions of temperature and pressure independent of the experimental conditions, that the pH and temperature are closely monitored and controlled, that a large surface to volume ratio is used, and that a large range of temperatures can be studied without removing any fluid from the cell. The change in adsorption

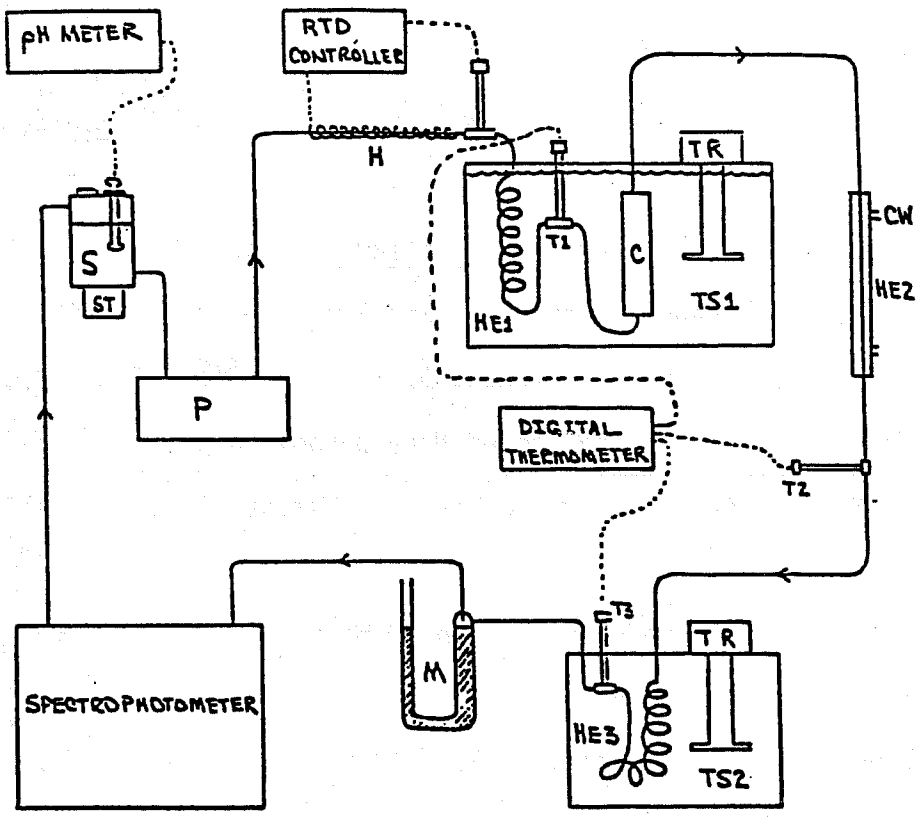

Figure 30. Heat of adsorption apparatus.

with respect to temperature can be accurately obtained. We are especially interested in this aspect.

F. REFERENCES

1. Scamehorn, J. F., Schechter, R. S., and Wade, W. H., J. Colloid Interface Sci., 85, 463 (1982).
2. Scamehorn, J. F., Schechter, R. S., and Wade, W. H., J. Colloid Interface Sci., 85, 479 (1982).
3. Gatta, G. D., Fubini, B., and Sradella, L., J. Chem. Soc., Faraday Trans. 2, 73, 1040 (1977).
4. Tanford, C., The Hydrophobic Effect: Formation of Micelles and Biological Membranes, John Wiley and Sons, New York (1980).
5. Wakamatsu, T. and Fuerstenau, D. W., Adv. Chem. Ser., 79, 161 (1968).
6. Thach, S., "The Mechanism of Nonylphenol Polyoxyethylene Adsorption on Some Mineral Surfaces," Master's Thesis, The University of Texas at Austin (May, 1979).
7. Trogus, F. J., Wade, W. H., and Schechter, R. S., J. Colloid Interface Sci., 70, 293 (1979).
8. Scamehorn, J. F., Wade, W. H., and Schechter, R. S., J. Dispersion Sci., 3, 261 (1982).
9. Yates, D. E., Levine, S., and Healy, T. W., Trans. Far. Soc., 70, 1807 (1974).
10. Mysels, K. J. and Otter, R. J., J. Colloid Sci., 16, 474 (1961).
11. Osborne-Lee, I. W., Wade, W. H., and Schechter, R. S., "Monomer-Micellar Equilibrium of Aqueous Surfactant Solutions by the Use of Ultrafiltration," J. Colloid Interface Sci., In Press.

12. Harwell, J. H., "Surfactant Adsorption and Chromatographic Movement with Application in Enhanced Oil Recovery," Ph.D. Dissertation, The University of Texas at Austin (May, 1983).

13. Rubingh, D. N., 52nd ACS Colloid Surface Science Symposium, 1, 337 (1978).

14. Kurzendorfer, C. P., Schwuger, M. J., and Lange, H., Ber. Bunsenges. Phys. Chem., 82, 962 (1978).

15. Shinoda, K., J. Phys. Chem., 58, 541 (1954).

16. Kipling, J. J., Adsorption from Solution, Academic Press, New York (1965).

17. Parfitt, G. D. and Tompson, P. C., Trans. Far. Soc., 67, 3372 (1971).

II. CHROMATOGRAPHIC MOVEMENT IN REAL SYSTEMS

A. INTRODUCTION

We have previously reported theoretical studies of surfactant chromatographic movement in porous media which were based on the Trogus model of surfactant adsorption.[1] This model is believed to be realistic for concentrations above the CMC and counterintuitive phenomena such as effluent overshoot, the most strongly adsorbed component appearing first in the effluent, inversion curves, and unit velocity waves, are all found to be consequences of mixed micelle formation described by the pseudophase separation model. These phenomena are, therefore, expected to be observed in real systems. However, the Trogus model does not predict the correct isotherm shapes for concentrations less than CMC and this year work has focused on developing the correct composition paths for realistic isotherms and on confirming experimentally the counter intuitive predictions noted above.

B. COMPOSITION PATH GRID

In this section a composition path diagram for a real system will be presented so that its topology may be compared with the topology of the Trogus system composition path diagram previously published.[1] A reasonably accurate mathematical representation of the binary adsorption surface is required, which the model presented in the section on Adsorption provides. The composition path diagram for the $3\phi C_9ABS/3\phi C_{10}ABS$ system fit with this model appears in Figures 1 to 2.

The most striking observation is the great similarity between the Trogus system and the real system. Both contain the discontinuity at the CMC of the system and both have lines of constant adsorption as one family

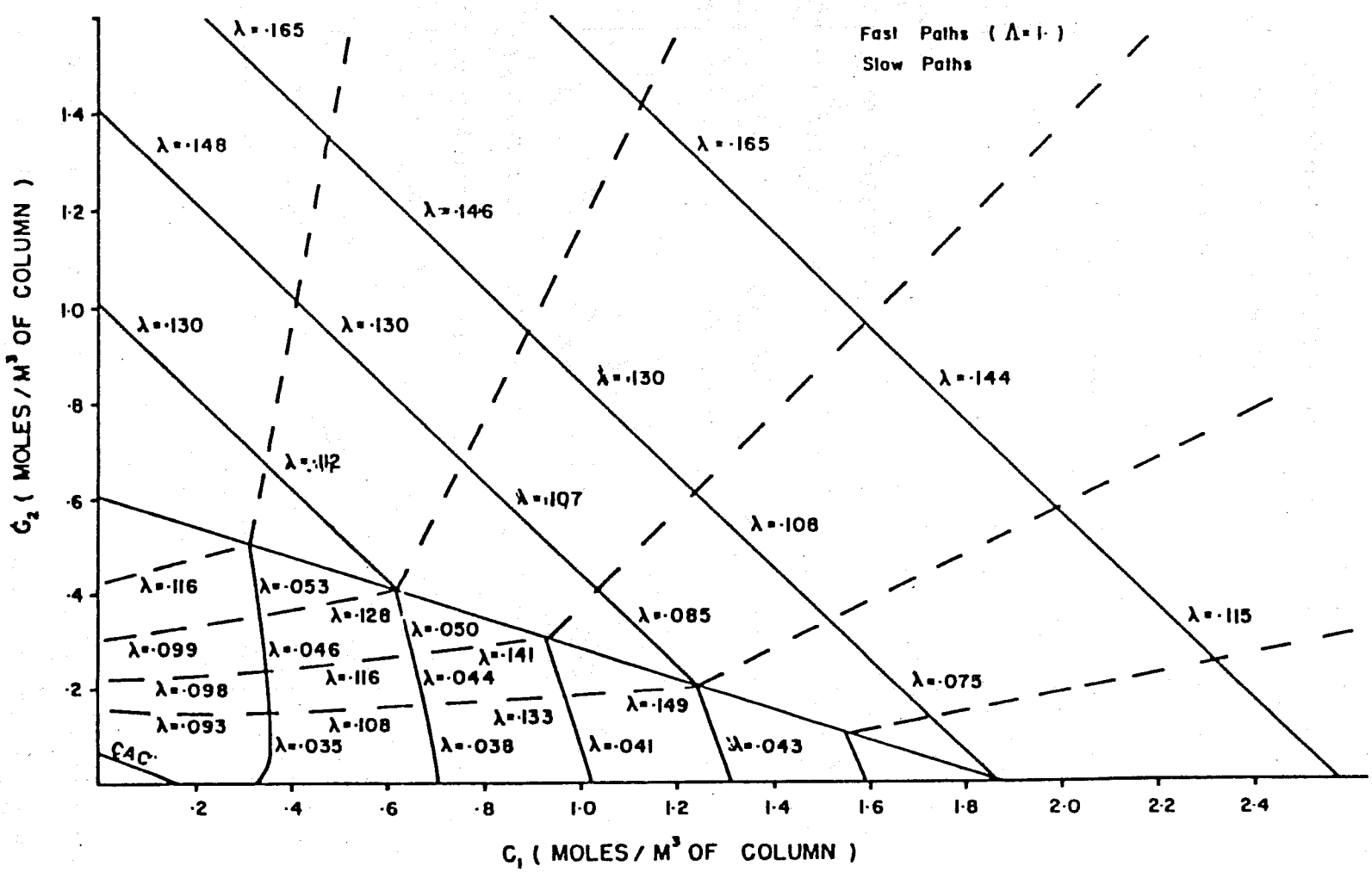

Figure 1. Composition path grid for 3ϕC9ABS/3ϕC10ABS on α-alumina in 0.2 M NaCℓ, pH 8, T = 30°C.

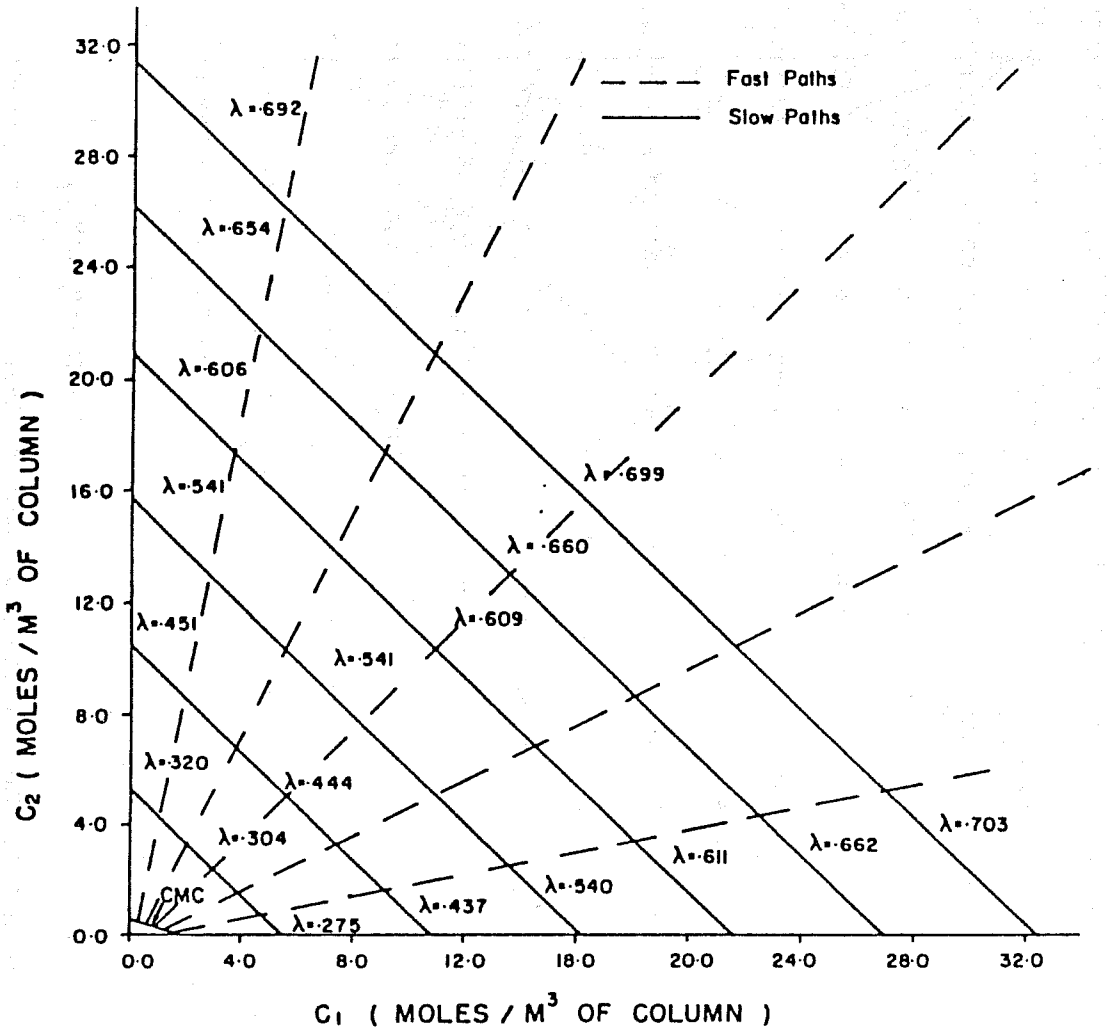

Figure 2. Composition path grid for higher concentrations.

of composition paths above the CMC. These lines of constant adsorption arise as a result of the phase separation model. Since the phase separation of the adsorption in the real system, these lines are again prominent features of the topology. It is worth noting that they are still straight lines, even though the form of the phase separation model used in this section is more general than that used in the Trogus system. The contrasts between the systems are less dramatic. The CMC in the Trogus system is curved; in the real system it is a straight line. This is simply because the Trogus system does not include added electrolyte while the real system is at 0.2 M NaCℓ. For a detailed discussion of this see Harwell.[2] It also appears that the slow paths above the CMC in Figures 1 and 2 are straight lines. No analytical expression has been obtained for these curves, but it seems likely their curvature or lack of curvature is also determined by the counterion.

Another difference between the two systems are the eigenvelocities. Those in the Trogus system are much higher both above and below the CMC than in the real system. This is an insignificant difference. The parameters for the Trogus system were determined from fits of effluent profiles from a Berea sandstone core.[3] Parameter values for the present system are for surfactant adsorption on an α-alumina powder at a system pH below the point of zero charge of the oxide. Surfactant adsorption is much higher on the α-alumina than on the Berea and so the eigenvelocities are much lower in the present system. This has nothing to do with differences in models or with the form of the adsorption isotherms.

Note also that in the real system there is still an inversion curve and that below the inversion curve eigenvelocities decrease along the slow path in the direction of increasing C_1 and above the inversion curve they

increase along the slow paths in the direction of increasing C_1. The exact position of the inversion curve in the real system is more difficult to determine from looking for a slow path with constant eigenvelocities. There are two reasons for this. One is the similarity between the surfactants in the system--$3\phi C_9$ and $3\phi C_{10}$ differ only by one long chain methyl group. The other is that the eigenvelocities are approximated by numerical differentiation. The combination of the very slowly changing eigenvelocities and the numerical approximations makes this an unsatisfactory method for locating the inversion curve with accuracy.

In summary, it must be said that the topology of the real and the Trogus system above the CMC is qualitatively identical. Since the adsorption isotherms differ so drastically, this similarity must be attributed to the phenomenon of mixed micelle formation described by the pseudophase separation model. This serves to illustrate the extent to which mixed micelle formation determines the chromatographic behavior of aqueous surfactant mixtures.

The significant differences in Trogus and real system topologies are below the CMC. Apart from the already discussed trivial observation that the magnitudes of the eigenvelocities are different, the significant observation is that the eigenvelocities are no longer constant along a path and that the paths are curved. In the real system spreading waves and shocks may arise from certain injection sequences; because the composition paths are curved when shocks arise, they may not follow the composition paths. Finally, in the Trogus system wave/wave interactions were all noninterfering because there was no component interaction below the CMC. In the real system complex surface interactions give rise to complex wave/wave interferences and extensive regions of noncoherence. Finally, the real system

contains a discontinuity below the CMC, the mixture CAC. Below the CAC wave behavior is identical to that below the CMC in the Trogus system: all composition paths are orthogonal, all eigenvelocities are constant along the paths, and all waves are noninterfering.

Reported elsewhere[2] are detailed analyses of the behavior of finite and infinite slugs of surfactant. The results emphasize similarities and differences between the Trogus and the real system. These comparisons, while quite interesting, are lengthy and will not be presented here.

C. EXPERIMENTAL RESULTS

The experiments presented in this section were designed to demonstrate the major counterintuitive features of surfactant chromatographic behavior and to provide experimental support for conclusions based on the adsorption model. The theoretical curves in the following examples were not fit to the experimental results by use of an adjustable parameter; they are based entirely on the experimental parameters necessary to fit the isotherm model to the $3\phi C_9/3\phi C_{10}$ adsorption and CMC data presented there and estimates of the column void volume. The experiments were designed to demonstrate the following phenomena:

(1) Formation of micelles enriched in the more strongly adsorbed component.

(2) Formation of micelles enriched in the less strongly adsorbed component.

(3) Existence of waves of unit velocity.

(4) Generation of multiple waves by the discontinuity at the CMC.

(5) Non-Henry's law behavior of the low concentration (below the CMC) region.

(6) Generation of a fast moving low concentration wave by the discontinuity at the CAC.

(7) Effect of dispersion in wiping out any observable chromatographic separation in the present system at concentrations above the inversion curve.

Some of these phenomena will be present in more than one of the examples presented. Several of the phenomena have been shown by comparison of the two theoretical models of this chapter to be a consequence of the pseudophase separation model for monomer/micelle equilibrium and the plateau adsorption model. Hence, observation of unit velocity waves, of overshoot of the more strongly adsorbed component on injection of a higher concentration of the more strongly adsorbed component, and of the generation of an additional chromatographic wave on eluting concentrations above the CMC constitutes dramatic confirmation of both of these models. A detailed description of the procedures is described elsewhere.[2]

C.1. Case 1: Injection of 3ϕC9ABS Enriched Micellar Solution into Column Preequilibrated with a Micellar Solution

The injected composition and the composition with which the chromatographic column had been preequilibrated for this case are shown in Figure 3a, along with the predicted composition route. The original composition in the column is labeled composition O; the injected composition as composition I. The coherent path connecting compositions I and O follows a slow path from I to A, then a fast path from A to O. Eigenvelocities increase along the slow path from I to A (see Figure 1) indicating formation of a spreading wave; however, the velocities change very little. As already discussed, the wave of variation A/O is an indifferent wave of unit velocity. The predicted wave trajectories appear in Figure 3b and the observed

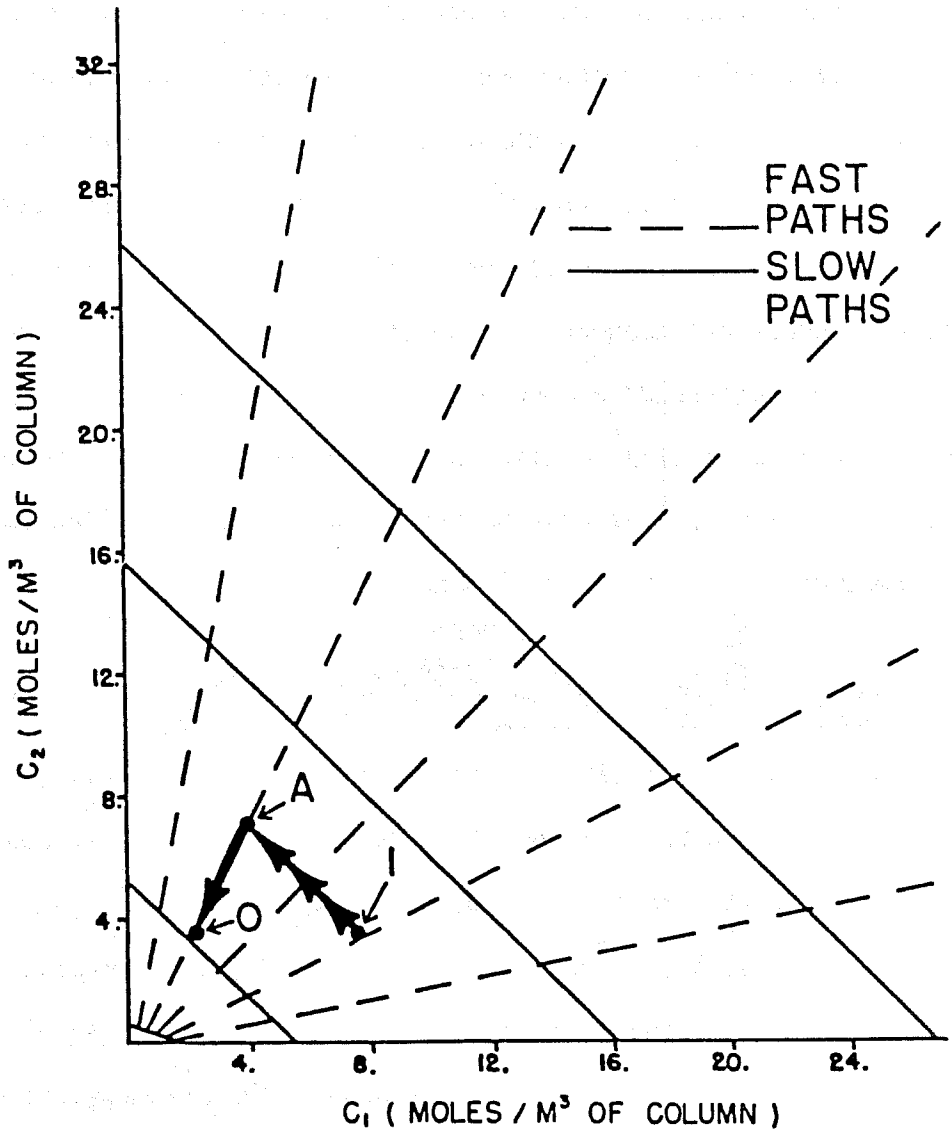

Figure 3a. Composition route for case 1.

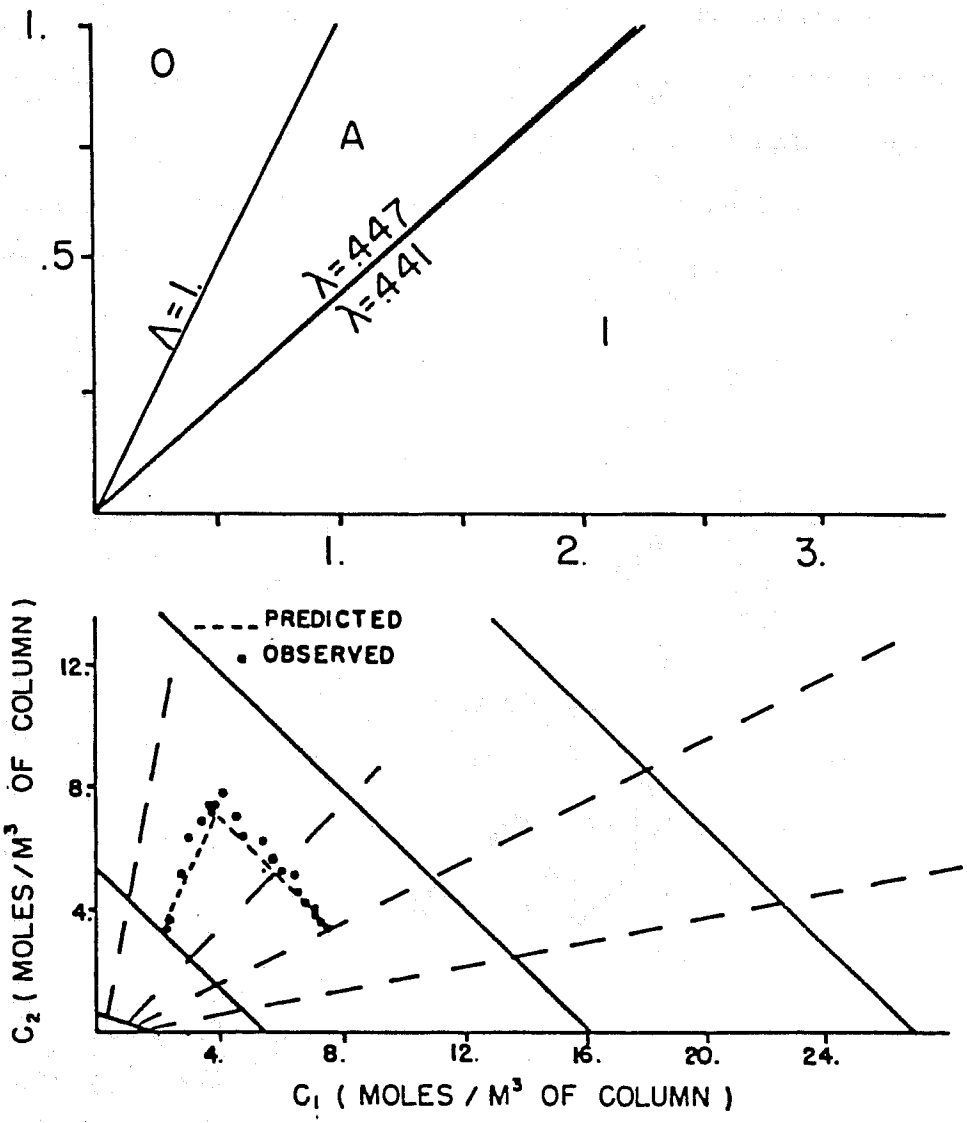

Figure 3b. Distance-time diagram for case 1.

Figure 3c. Observed and predicted composition routes for case 1.

composition route in Figure 3c. Note the close correspondence between the observed and predicted routes. The distance-time diagram of Figure 3b can be translated into an effluent history. The predicted and observed effluent histories are shown in Figure 3d. Taking as the midpoint of the leading wave the arithmetic average of the plateau values on either side of the wave, we arrive at a value of $(3\phi C_{10}ABS) \approx 1.5 * (3\phi C_{10}ABS)|_{injected}$ and so obtain $1/\Lambda_{A/O} = 1.04$ pore volumes, a normalized velocity of 0.96 pore volumes traveled/pore volume injected. Since from a mass balance across the slug front we know that the velocity of the indifferent wave must be close to

$$\Lambda = \frac{1}{\frac{1 + \Delta\overline{C}_{10}}{\Delta C_{10}}}$$

we obtain

$$\Delta\overline{C}_{10} = \Delta C_{10}\left(\frac{1}{\Lambda} - 1\right)$$

Dividing by $\overline{C}_{10}|_0 \approx 9.08$ (moles/m^3 of column) and $\Delta C_{10} = (3.61 - 2.19)$ (moles/m^3 of column) we obtain $\Delta\overline{C}_{10}/\overline{C}_{10\ 0} \times 100\% = .6\%$. Thus, for the wave of variation A/O to have a velocity of approximately 96% of the bulk fluid velocity adsorption of the most strongly adsorbed component must have changed by only about 1/2%. Bear in mind that under the experimental conditions the α-alumina has only about 1/2 of bilayer coverage, while it has been shown that coverage could go up to complete bilayer formation.[4] Thus, adsorption changes from composition A to composition O by less than 1% while total surfactant concentration goes from approximately 11(moles/m^3 of column) at A to 5.6 (moles/m^3 of column) at O. This is dramatic confirmation of the validity of both the phase separation model and the plateau adsorption model for the system being studied.

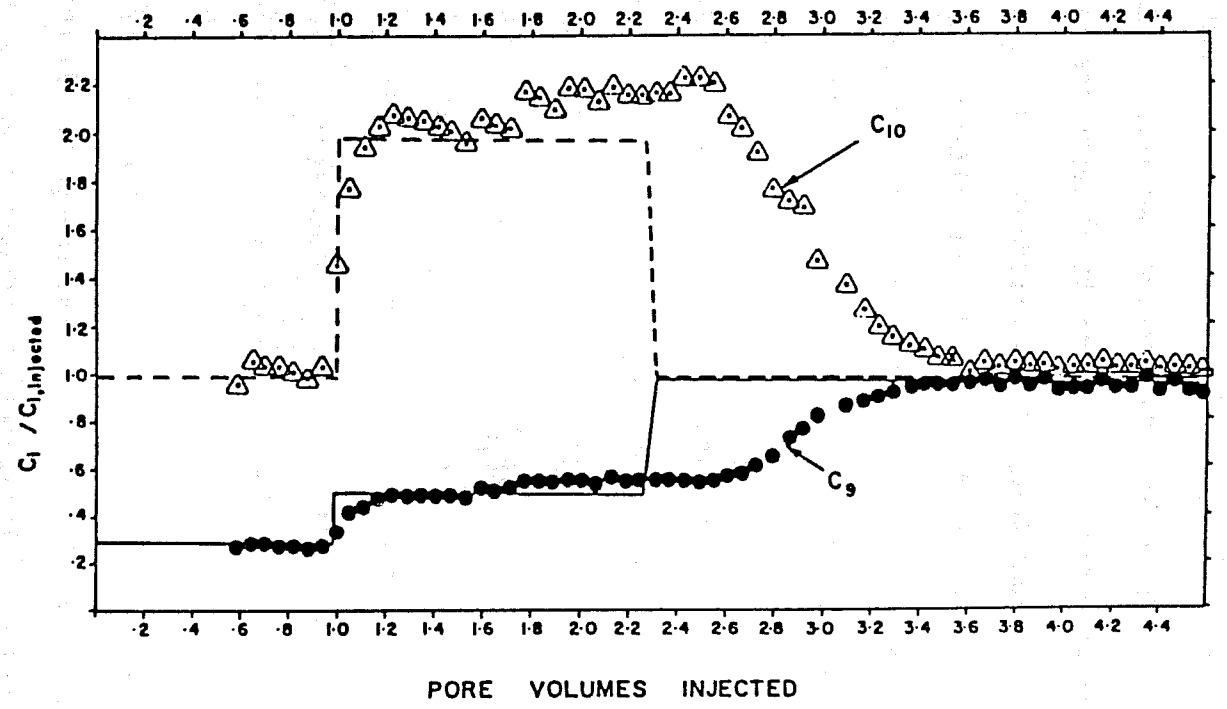

Figure 3d. Observed and predicted effluent profiles for case 1.

It is interesting to consider the counterintuitive behavior of the system observed in the experiments which is predicted by the model. Note that the injected and original concentrations have practically the same concentration of $3\phi C_{10}ABS$ (3.61 moles/m^3 of column orginally in the column and 3.60 moles/m^3 of column injected) whereas the injected concentration of $3\phi C_9ABS$ is over four times the original concentration of $3\phi C_9ABS$ (7.57 moles/m^3 of column compared to 2.19 moles/m^3 of column). Despite the near constancy of the $3\phi C_{10}ABS$ the effluent history shows a pulse of $3\phi C_{10}ABS$ over 2.5 pore volumes in size at nearly twice the injected concentration. This unexpected behavior can be explained in terms of the plateau adsorption and phase separation models. Although the total concentration of $3\phi C_{10}ABS$ is the same in the original and injected fluids, the monomer concentrations are not. The monomer concentration of the $3\phi C_{10}ABS$ is predicted to be 0.407 moles/m^3 of column at composition O and 0.211 moles/m^3 of column at composition I. Correspondingly, composition A, which forms on injection of I against O, has the same monomer concentration and hence the same adsorption as O. But since O has a higher concentration of $3\phi C_{10}ABS$ monomers, the micelles at A are enriched with $3\phi C_{10}ABS$. This is the cause of the otherwise difficult to explain pulse of $3\phi C_{10}ABS$ in the effluent.

The second wave, the wave of variation I/A, arrives somewhat later than predicted. This indicates the change in adsorption from I to A is somewhat higher than predicted $[1/\Lambda = (1/(1 + \Delta\overline{C}/\Delta C)]$ since the values of ΔC correspond fairly well to the predicted values. One possible explanation of this is that the pH in the column differed somewhat from that at which the isotherm points were determined. Only small changes in pH in the area of pH 5 to 8 can result in very large changes in the total adsorption.

Since very few hydrogen ions are needed to change the pH at pH 8, it may be very difficult to control the pH accurately in this region. Nevertheless, the results for this case clearly demonstrate the major conclusions of this study regarding the role of mixed micelle formation and plateau adsorption on surfactant chromatographic movement.

C.2. Case 2: Injection of 3ϕC9ABS Depleted Micellar Solution into a Column Preequilibriated with a Micellar Solution

Figure 4a contains plots of the injected composition I and the composition with which the column was preequilibrated (O) along with the predicted composition route and the composition of the plateau region which arises between compositions I and O. The coherent route from I to O follows a slow path from I to A , then a fast path from A to O. As before, the eigenvelocities along the path from A to O are constant at $\lambda = 1$ and the wave of variation A/O is an indifferent wave. On the other hand, eigenvelocities decrease from I to A, so that the wave of variation I/A is a shock wave. The predicted trajectories of the waves appear in Figure 4b and the observed composition route in Figure 4c. Note again the close correspondence of the observed and predicted composition routes. The observed and predicted effluent histories are presented in Figure 4d. Taking the velocity of the first wave, the wave of variation O/A, as the velocity of the composition which is the arithmetic average of the plateaus on either side of the wave, we obtain $1/\Lambda_{A/O} = 1.02$ which corresponds to a velocity of $\Lambda = 0.98$ pore volumes traveled/pore volume injected. This tells us that the adsorption of $3\phi C_9ABS$ changes by less than 0.2% from composition A to composition O, although the total fluid phase concentration changes from 4.09 to 7.57 moles/m^3 of column. This again is a dramatic demonstration of the validity of the phase separation and plateau adsorption models

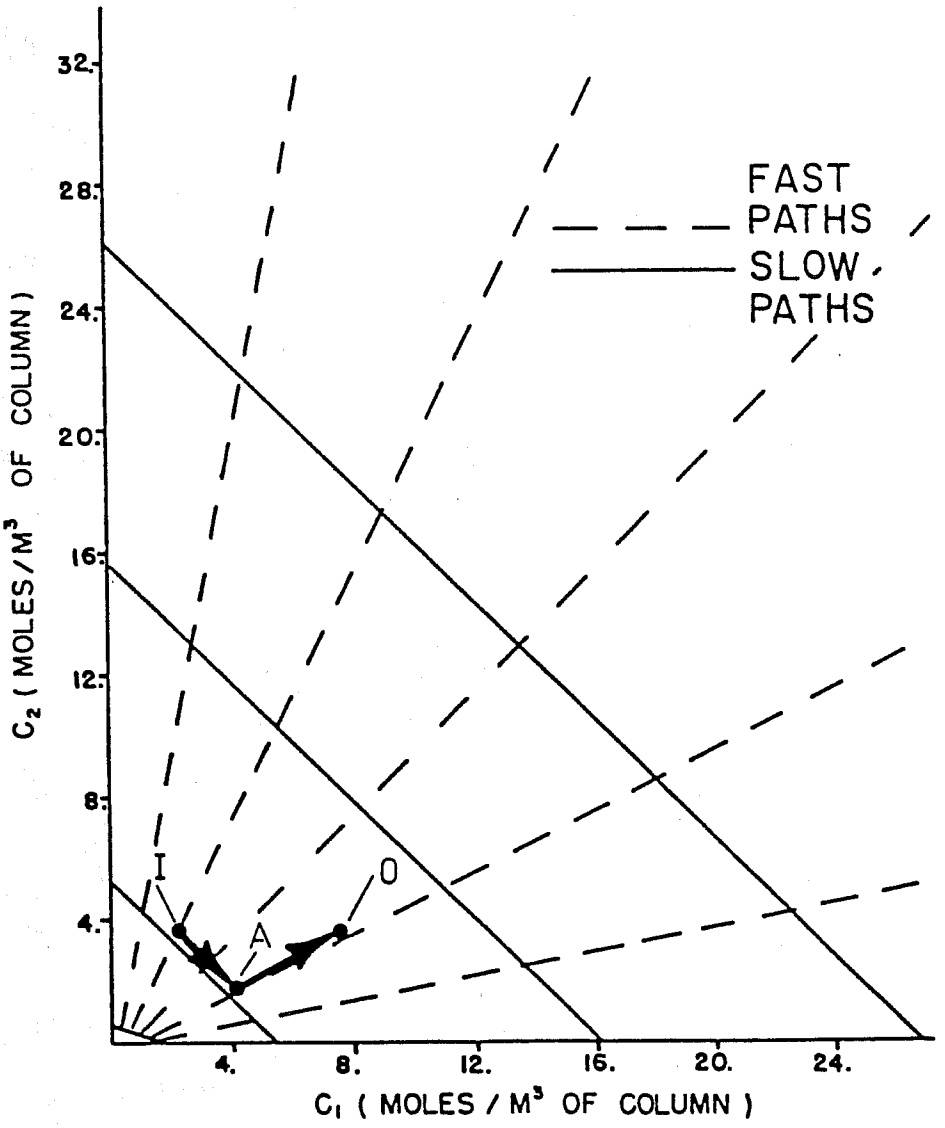

Figure 4a. Composition route for case 2.

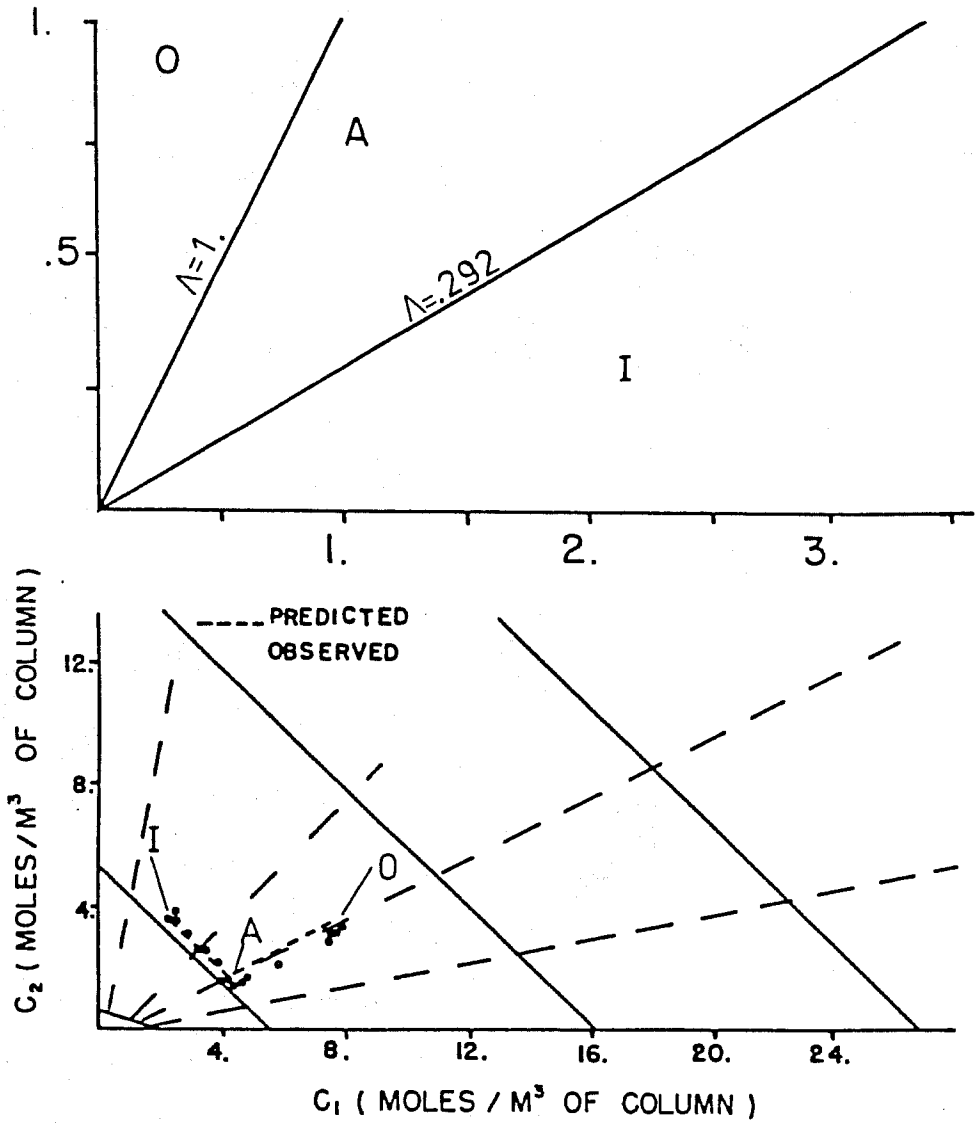

Figure 4b. Distance-time diagram for case 2.

Figure 4c. Composition route for case 2.

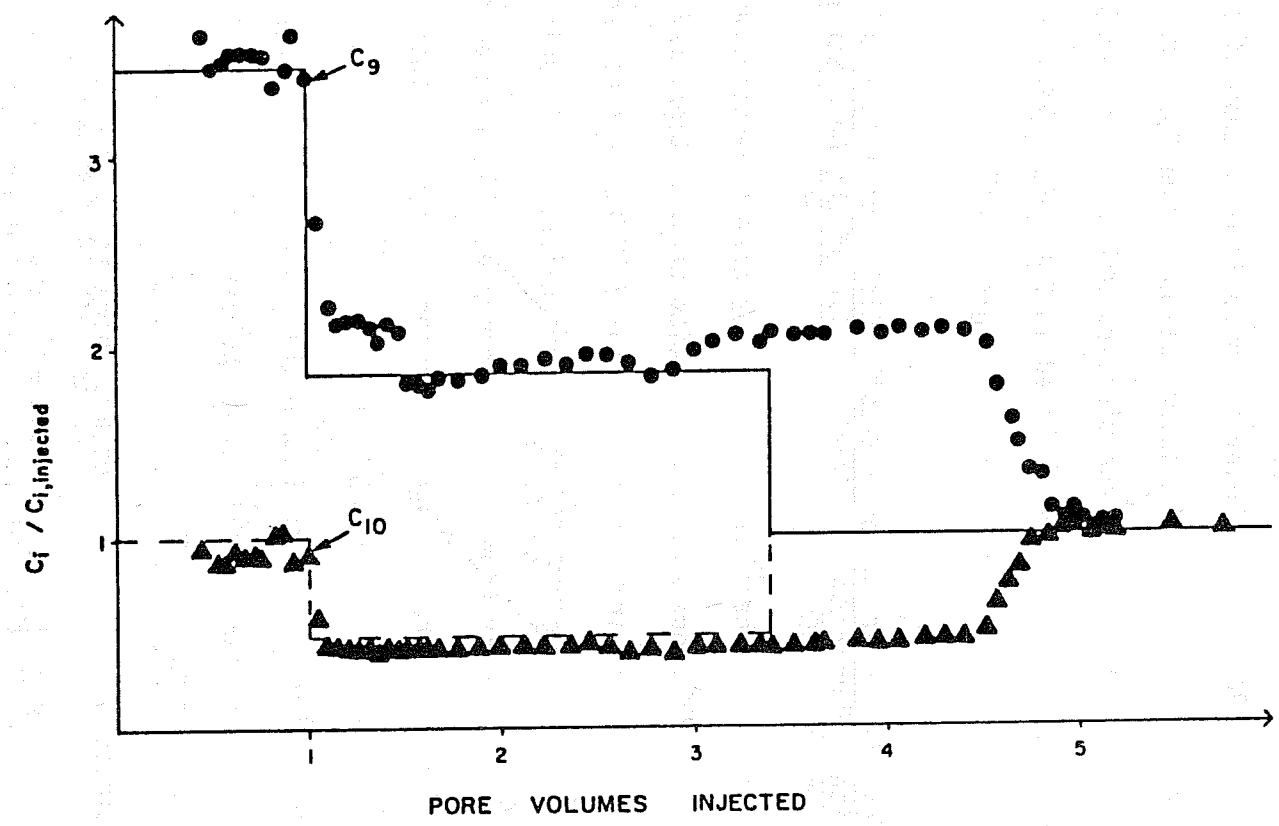

Figure 4d. Observed and predicted effluent profiles for case 2.

for this system and an illustration of the predicted effects of mixed micelle formation on the chromatographic behavior of these systems.

Note that in contrast to case 1, where we observed a large increase in the concentration of $3\phi C_{10}ABS$ in the effluent, we now observe and predict a large decrease in $3\phi C_{10}ABS$ concentration. Since the monomer concentration of $3\phi C_{10}ABS$ is lower at composition O than at composition I because of the preferential incorporation of the $3\phi C_{10}ABS$ into the larger micellar pseudophase at O, the micelles which form in equilibrium with the downstream monomers are depleted in $3\phi C_{10}ABS$. Thus, we observe a dip in $3\phi C_{10}ABS$ concentration in the effluent.

C.3. Case 3: Injection of a Micelle Rich Slug into a Column Equilibrated with a Higher Monomer Concentration of the More Strongly Adsorbed Component ($3\phi C_{10}ABS$)

In Figure 5a the alumina column has been preequilibrated as determined by liquid chromatographic analysis, with the solution indicated at point O. The solution to be injected is at point I. The original solution, O, is very near the CMC so that it has few micelles. While solution I is at a much higher concentration of $3\phi C_{10}$ (component 2), much of this $3\phi C_{10}$ is in micelles, so that the C_{10}-monomer concentration is actually lower in solution I than in solution O. The predicted composition route in Figure 5a follows a slow path from I to A, then a unit velocity path from A to O. The eigenvelocities increase along the path from I to A, indicating formation of a spreading wave. The unit velocity wave is an indifferent wave. The predicted wave trajectories are shown in Figure 5b. The unit velocity wave quickly appears in the column effluent, followed nearly five pore volumes later by the spreading wave. The intermediate plateau region (where no waves are present) is at composition A from Figure 5a. The

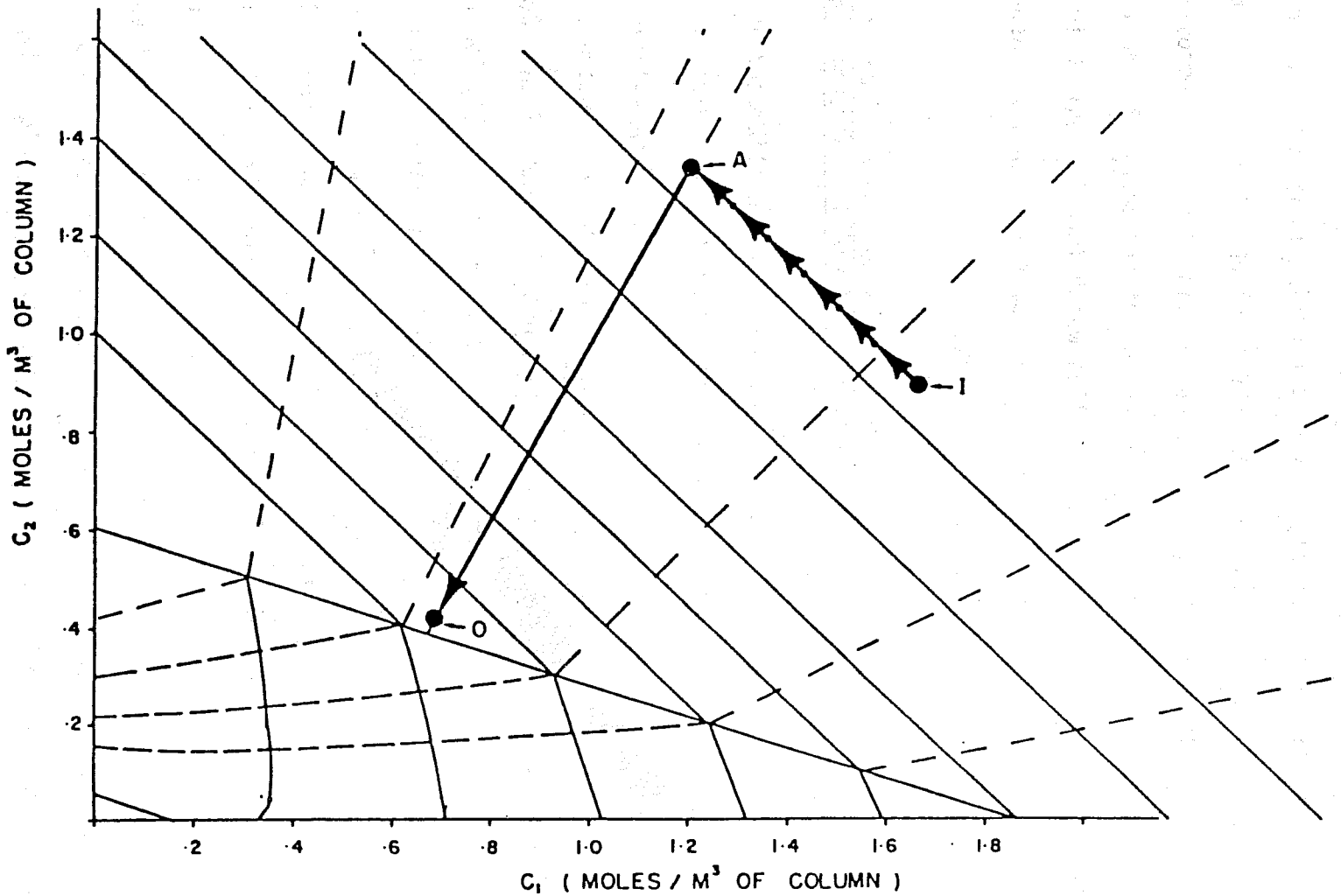

Figure 5a. Schematic of composition route for case 3.

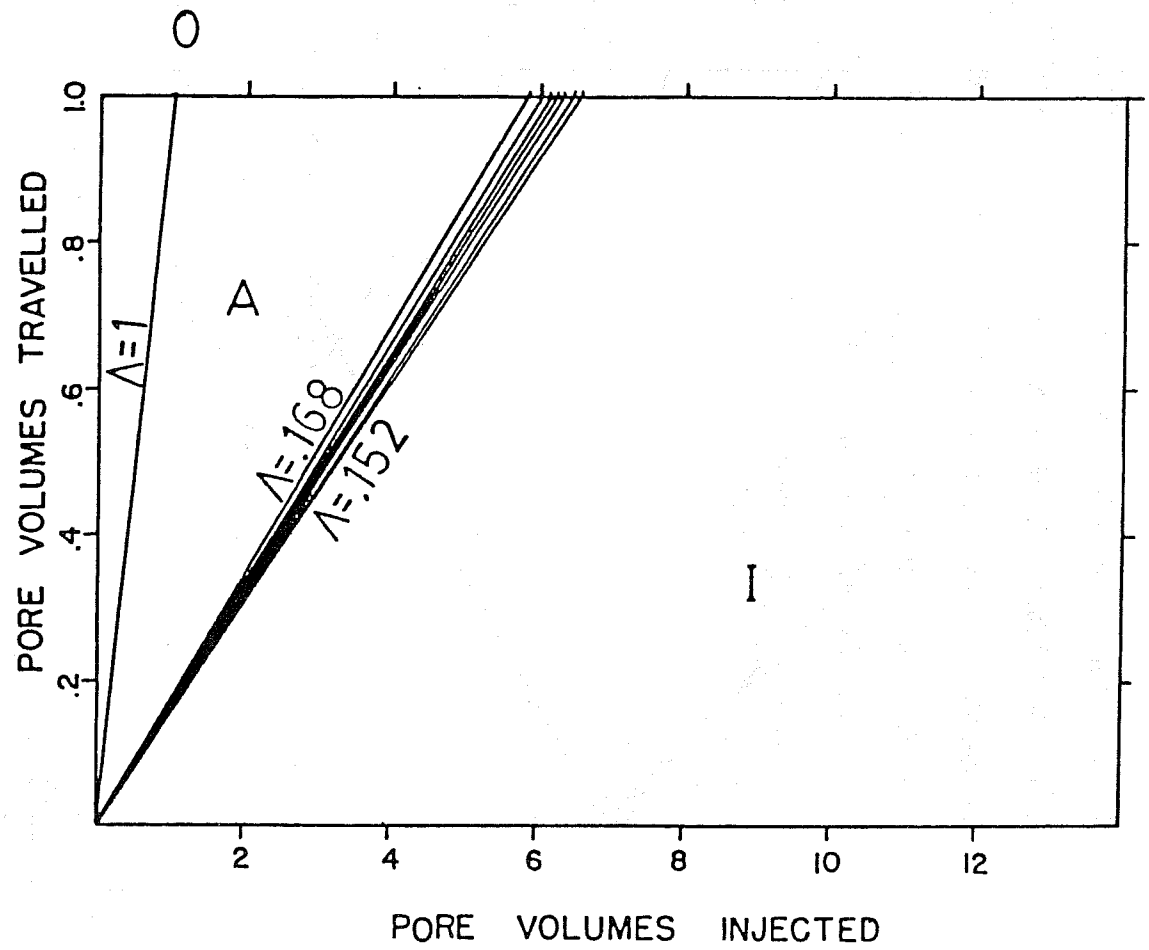

Figure 5b. Distance-time diagram for case 3.

predicted and observed effluent profiles are presented in Figure 5c and the observed composition route in Figure 5d. From Figure 5d it can be seen that the observed composition route followed very closely the predicted route. Composition A corresponds to an increase in C_{10} enriched micelles which are in equilibrium with the monomer ahead in the preflooded sections of the column. This is a consequence of both the phase separation and plateau adsorption models. In calculating the velocity of the leading wave (Figure 5c) take as the midpoint of the wave the point at which the concentration has reached the arithmetic average of the plateau regions behind and before the wave. This point is ($C_2/C_{2,inj}$ = 0.998), which appears at 1.19 pore volumes, a normalized velocity of 0.84. Applying a mass balance across the wave front produces

$$\Lambda = \frac{1}{\dfrac{1 + \Delta\bar{C}_2}{\Delta C_2}}$$

or

$$\Delta\bar{C}_2 = \Delta C_2 \frac{k}{\Lambda - 1}$$

$$= 0.176 \text{ moles/m}^3 \text{ of column}$$

The amount of component 2 ($3\phi C_{10}ABS$) actually adsorbed is given by the theoretical isotherm as 8.7 moles/m^3 of column; thus, the adsorption in going from 0.415 moles of $3\phi C_{10}/m^3$ of column to 1.34 moles/m^3 of column is seen to change by only 2%:

$$\Delta\bar{C}_2 = \frac{0.176}{8.7} \times 100\% = 2\%$$

which is in excellent accordance with the plateau adsorption model.

The chromatographic behavior indicated in Figures 5c and 5d has possibly significant practical implications. Note that a very dilute surfactant

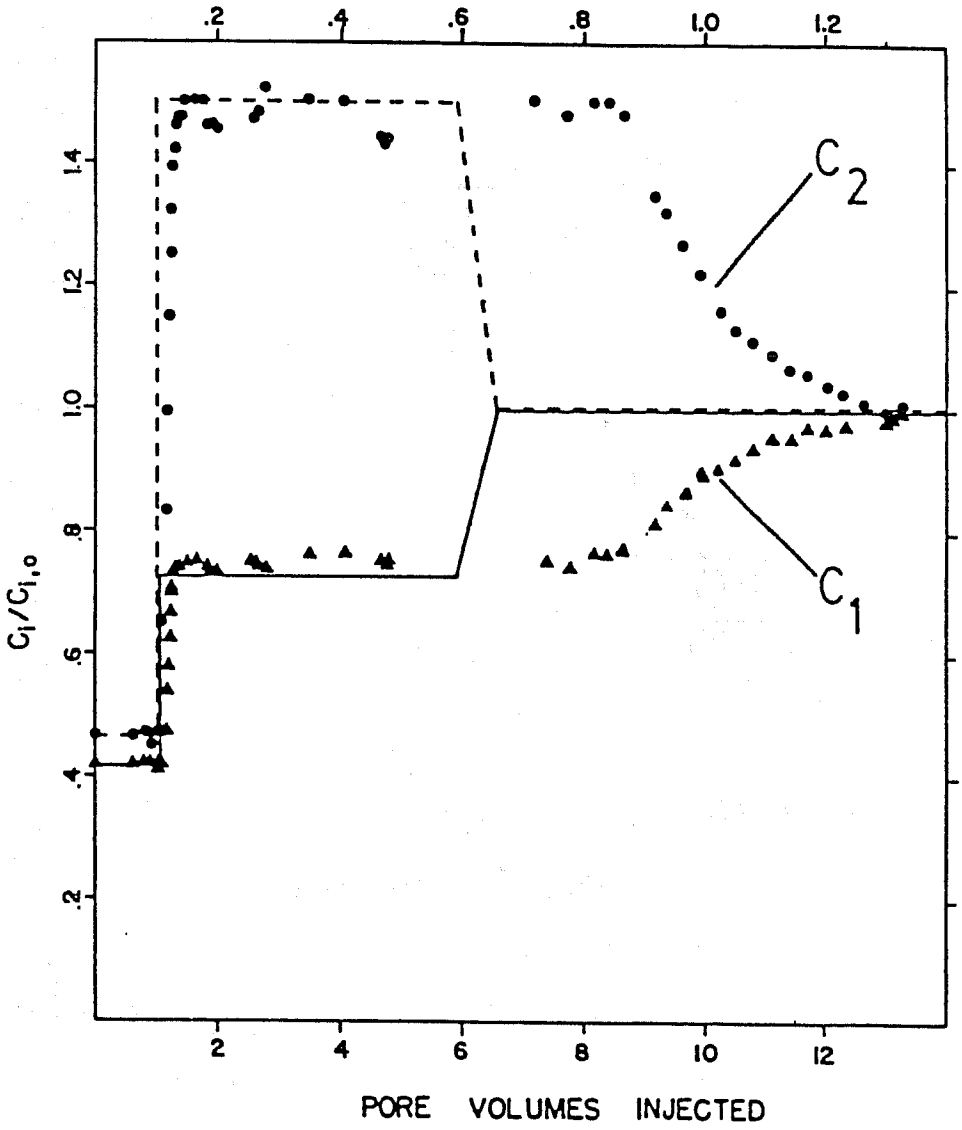

Figure 5c. Observed and predicted effluent histories for case 3.

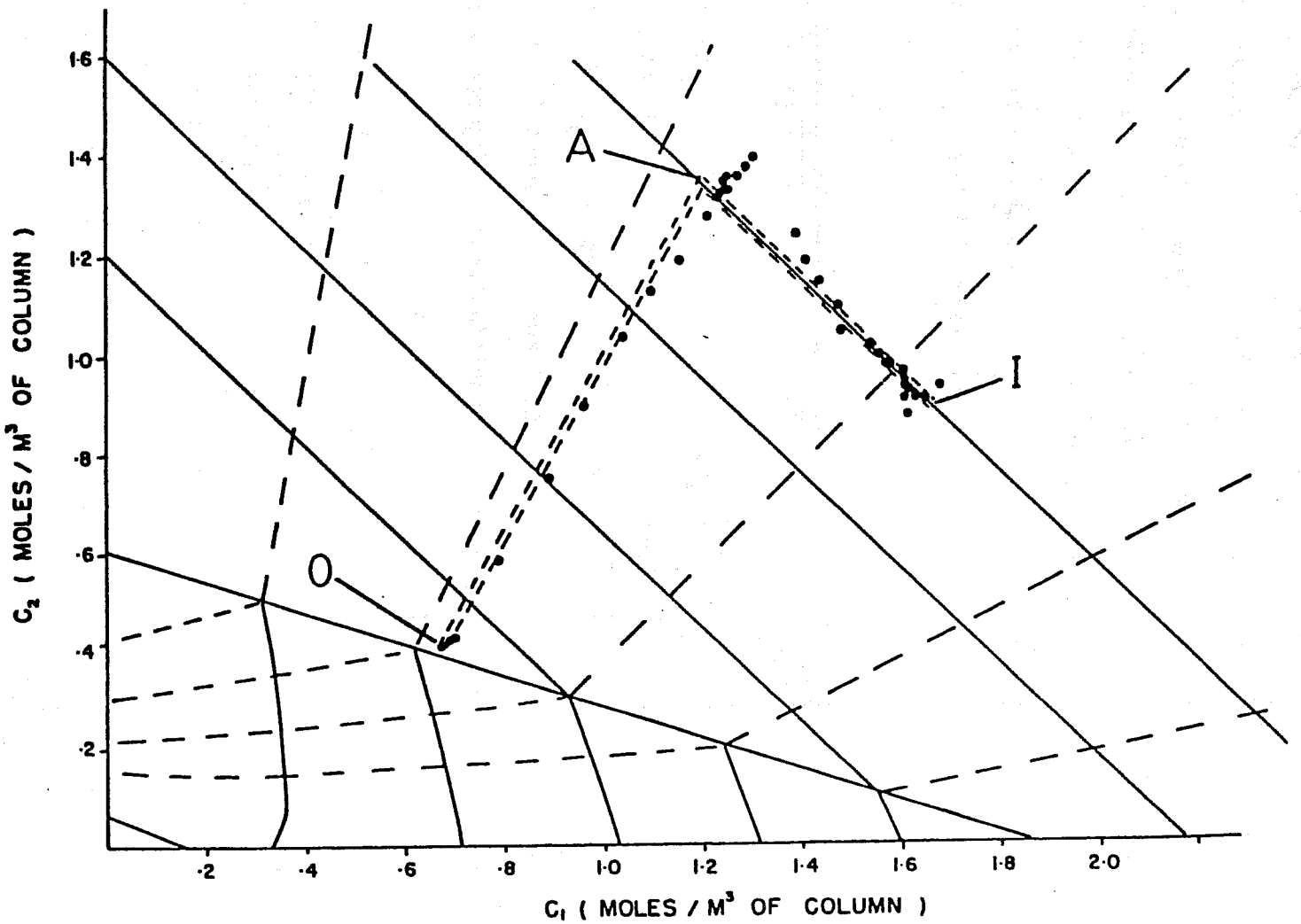

Figure 5d. Observed and predicted composition routes for case 3.

preflood, just at the mixture CMC, at a higher concentration of monomers of the more surface active compound, results in overshoot of the more strongly surface active compound. A very large plateau zone is produced which is at a composition enriched in the more surface active compound. This presents the possibility of using the chromatographic behavior of surfactant mixtures to improve the oil recovery efficency rather than reduce it. This possibility would, of course, have to be examined in light of the cost of equilibrating the reservoir or part of the reservoir with even a very dilute concentration of surfactant.

C.4. Case 4: Injection of a Micelle Rich Slug into a Column Equilibrated with a Lower Monomer Concentration of the More Strongly Adsorbed Component

In Figure 6a the preflood mixture has a lower $3\phi C_{10}$ monomer concentration than the injected mixture. The micelles which form in equilibrium with the downstream composition are then enriched in $3\phi C_9$. Now, however, the eigenvelocities decrease from I to A and a slow shock is formed. Comparing the observed and predicted composition routes (Figures 6a and 6b) it is evident the agreement is not as good as it was for case 1. There seems to be no simple explanation for why this route differs so much from the predicted route while the previous case differed so little. One possible explanation arises from comparing the predicted and observed velocities of the leading wave. In Figure 6c composition O is below the CMC. The predicted solution is for formation of a shock from A to O, with velocity of $\Lambda = 0.68$. However, from the experimental profile in Figure 6d, the leading wave reaches half its total height gain (C_1/C_1 injected = $(1.2 + .67)/2 = 0.935$) at 1.09 pore volumes or $\Lambda_{A\to O} = 0.92$. This means that, in fact, very little change in adsorption occurs across. The

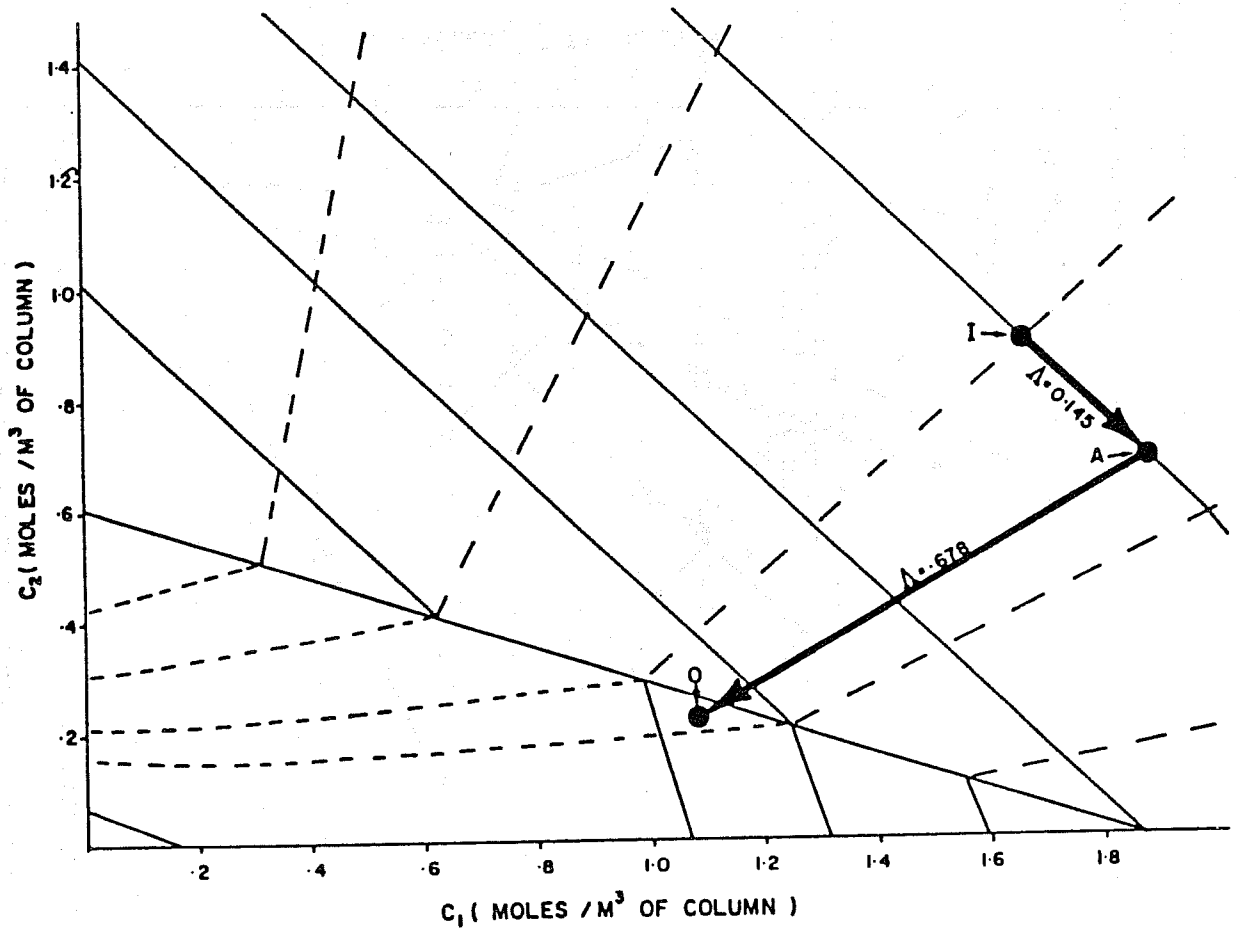

Figure 6a. Schematic of composition route for case 4.

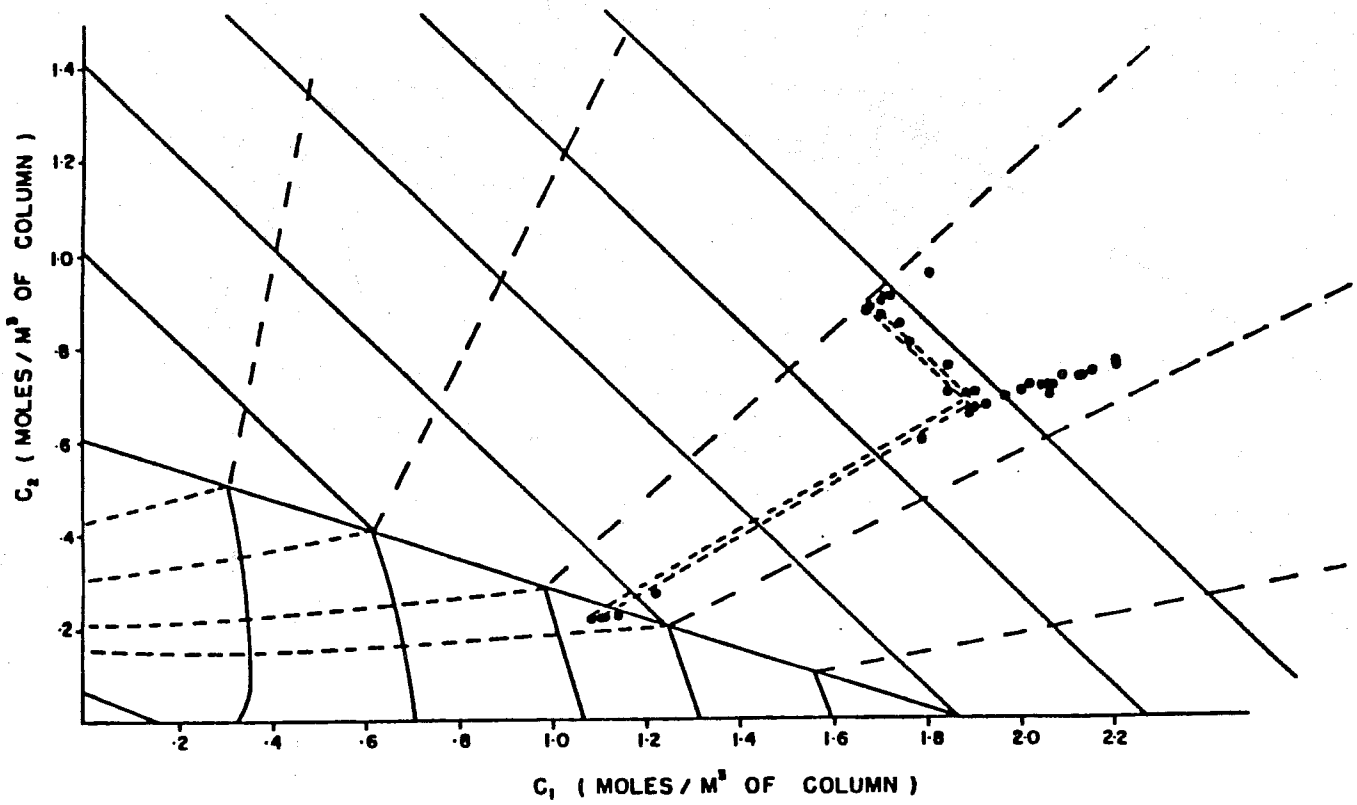

Figure 6b. Observed and predicted composition routes for case 4.

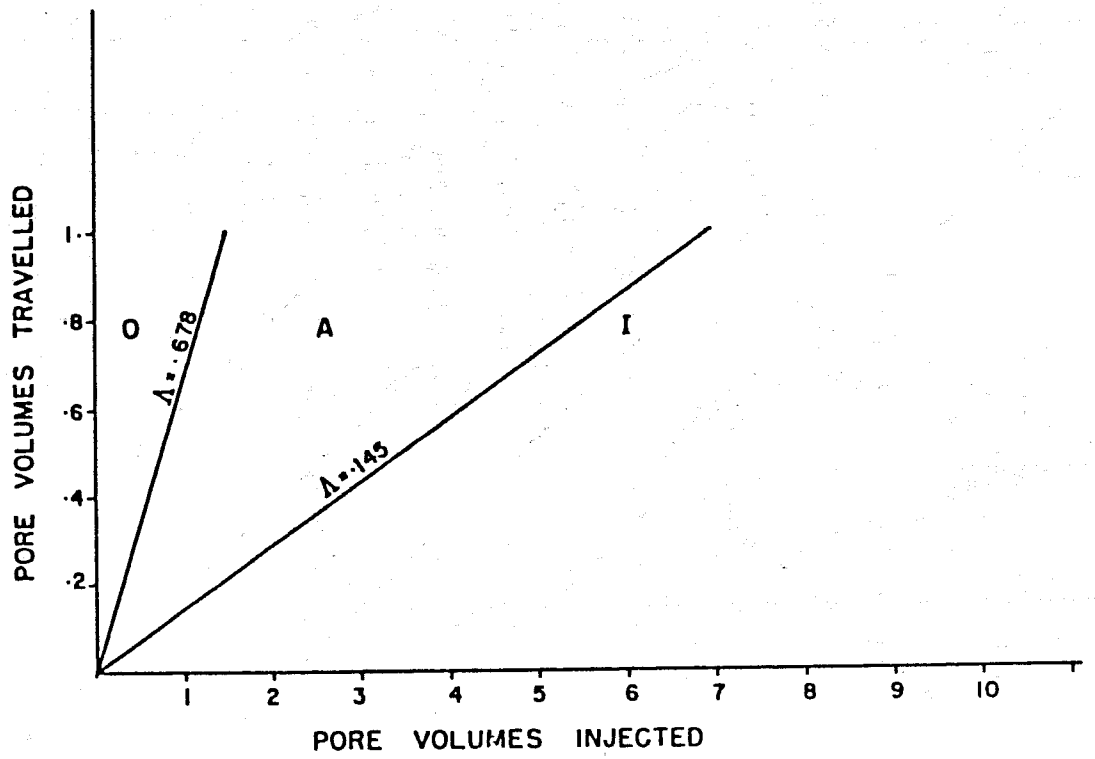

Figure 6c. Distance-time diagram for case 4.

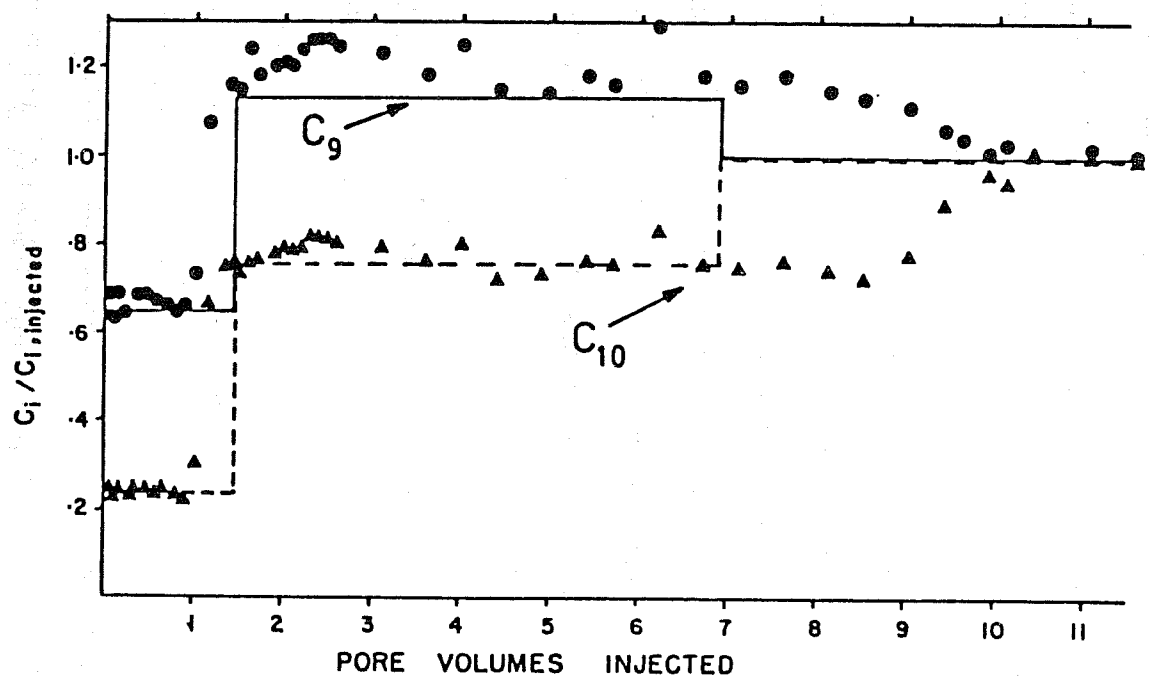

Figure 6d. Observed and predicted effluent history for case 4.

apparent explanation is that the model value for the $3\phi C_9$ABS CMC is off enough so that while point O appears to be below the CMC it is actually on or above it. If this is so, then the line of constant adsorption is also off and, thus, so also is the composition route. The error is not so large in case 1 because this part of the composition path grid is further from the pure component C_9-CMC. The problem with this explanation is that too much of the observed composition route does lie on the predicted route. All in all, there is no obvious answer for why the points to the right of the route arise here but not in case 1.

It should be noted that in case 4 preflooding has produced overshoot of the less strongly adsorbed component. Preflooding alone is not sufficient to produce overshoot of the more surface active compound. In case 4 the preflooding has a higher concentration of $3\phi C_9$ABS, so the micelles that form in equilibrium with the downstream monomer concentrations are enriched in $3\phi C_9$ABS.

C.5. Case 5: Elution of a Micelle Containing Composition

The observed and predicted composition routes for elution of a micelle containing composition can be seen in Figures 7a and 7b, respectively. The predicted route takes a slow shock from I to A, $\Lambda = 0.035$, a spreading wave from A to B ($.094 \leq \lambda \leq .148$), then a unit velocity path from B to I. Note that in the distance-time diagram (see Figure 7c) a plateau region at B is predicted to be precisely on the mixture CMC and that this plateau composition is observed. This suggest the possibility of using such a technique for determining mixture CMC's. The predicted route is followed very closely from B to A, an illustration of the validity of the phase separation and plateau adsorption models upon which prediction of this part of the route

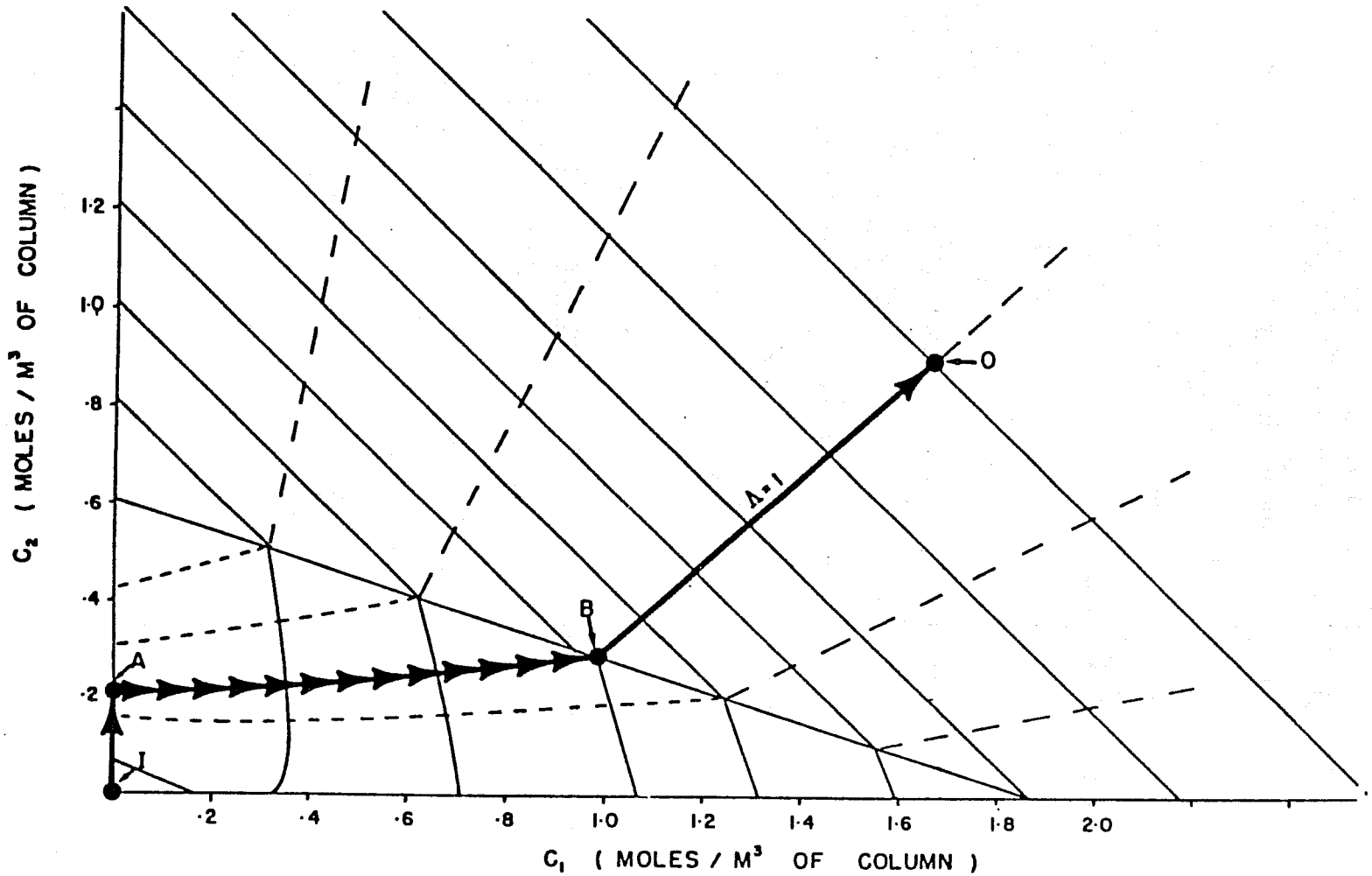

Figure 7a. Schematic of composition route for case 5.

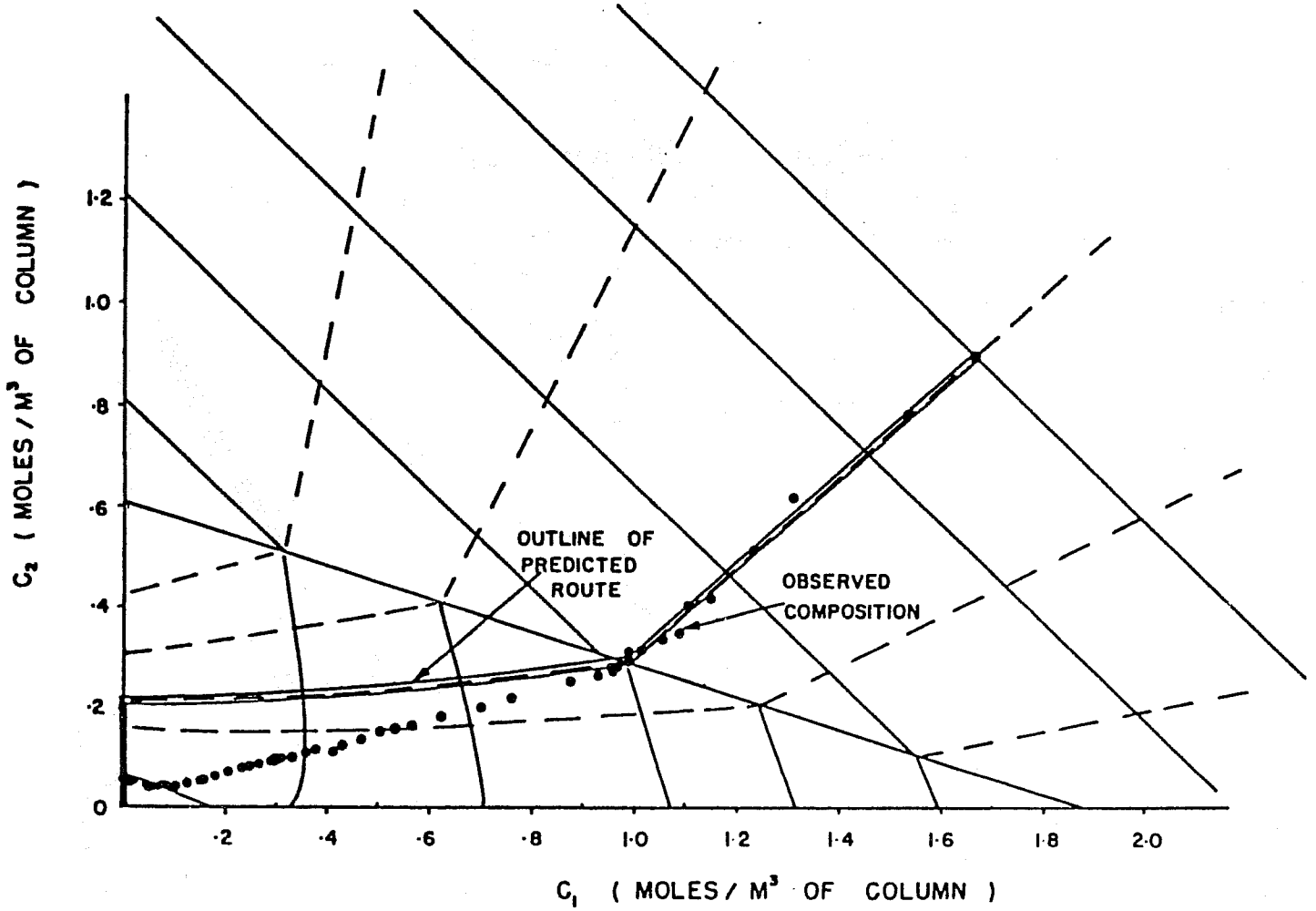

Figure 7b. Observed and predicted composition routes for case 5.

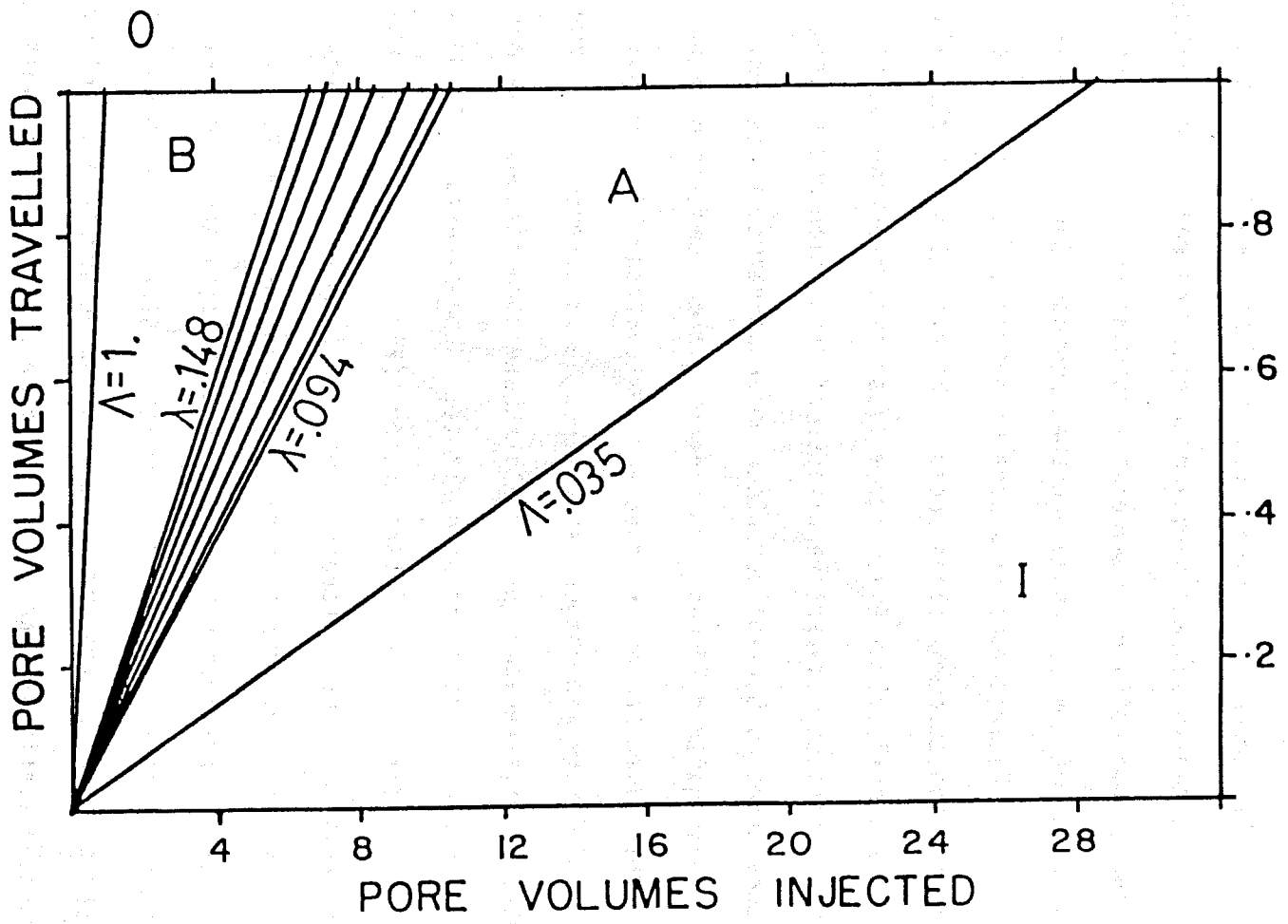

Figure 7c. Distance-time diagram for case 5.

relys. The midpoint of wave O/B appeared at approximately 0.98 pore volumes, indicating a normalized velocity $\Lambda = 1.02$, which corresponds within experimental error to a unit velocity wave.

In this case the departure of the second wave from the predicted route is more easily understood. Since the wave from I to A is very slow ($\Lambda = 0.035$), the system is subject to mixing across the rear waves. Thus, dispersion produces compositions intermediate to O and B by mixing fluid from volume elements of the column having these compositions, as illustrated in Figure 8. These compositions are noncoherent and tend to be resolved along the system composition routes. However, these routes also have very small eigenvelocities (see Figure 1) so that when the system finally reaches a balance between the effects of dispersion and the tendency of noncoherences to be resolved along coherent paths, the system is locked into a route quite different from the predicted composition route. Note, though, the deflection in the observed route at the CMC. Compositions below the CAC have much higher velocities because there are no surface aggregates in this region. As a result these compositions move more strongly in the direction of the coherent route. The effects of the dispersion are also evident in the elution history (Figure 7d). Though the first wave from B to O is very apparent, the wave from A to B has been extended by the combined effects of spreading and dispersion until it covers over fifteen pore volumes of the elution history. Nevertheless, the general shape has been maintained, the wave crest which was predicted to occur at approximately seven pore volumes has been advanced to two pore volumes, and the deflection at approximately nine pore volumes appears at fifteen volumes. This large degree of dispersion is not surprising when

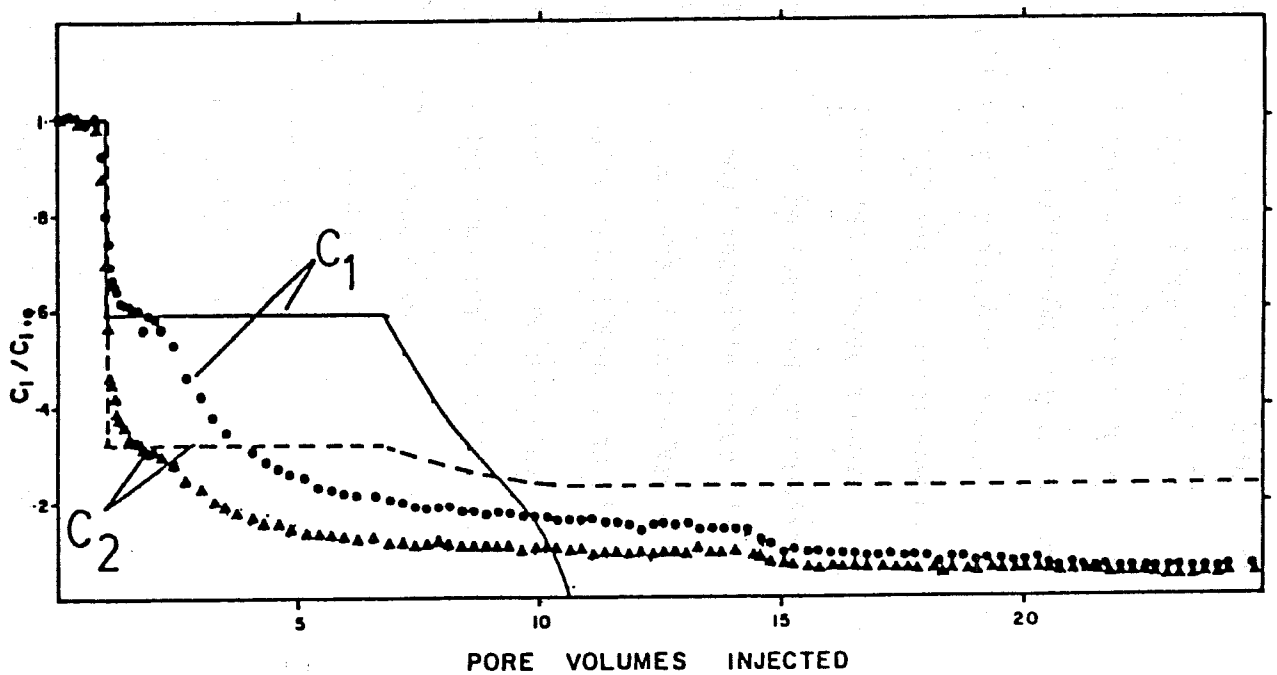

Figure 7d. Observed and predicted effluent profiles for case 5.

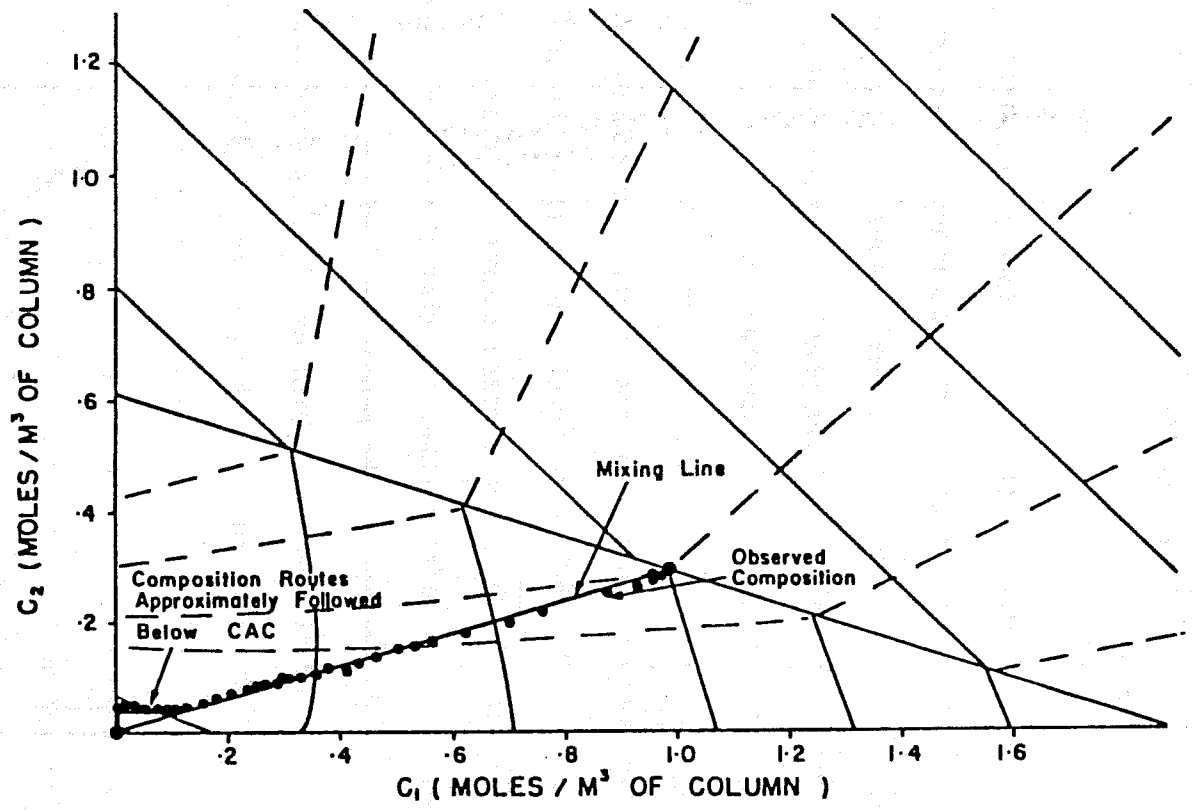

Figure 8. Effect of dispersion on observed compositions.

one considers that the alumina particles were seen to be shaped as flakes and to pack very poorly. One can imagine these flakes form chambers in the column almost like card houses. These chambers act as mixing chambers, resulting in very large dispersion coefficients.

D. SUMMARY AND CONCLUSIONS

In this section the effect of the interactions of adsorption, mixed micelle formation, and dispersion on the chromatographic movement of surfactant mixtures has been discussed. It has been demonstrated conclusively that the plateau adsorption model and the phase separation model are, if not exact, very powerful concepts for understanding surfactant adsorption and chromatographic movement. The results presented here are dramatic evidence that multicomponent surfactant adsorption with complex bulk and surface interactions can be dealt with successfully using the concept of a pseudophase separation for bulk and surface aggregate formation and the concept that micelles do not adsorb--that is, that the chemical potential of the surfactants is determined by the monomer concentrations.

From a more immediately practical point of view, several aspects of surfactant chromatographic movement which have potentially significant implications for enhanced oil recovery chemical flooding have been pointed out. The experimental results have borne out the predictions which we have made in the past regarding the existence of a unit velocity wave which form at the rear of the surfactant slug. This fast moving wave will tend to overtake the front of the slug reducing its oil recovery effectiveness.

E. REFERENCES

1. Harwell, J. H., Helfferich, F. G., and Schechter, R. S., AIChE J., 28, 448 (1982).
2. Harwell, J. H., "Surfactant Adsorption and Chromatographic Movement with Application in Enhanced Oil Recovery," Ph.D. Dissertation, The University of Texas at Austin (May, 1983).
3. Trogus, F. J., Schechter, R. S., Wade, W. H., and Pope, G. A., J. Pet. Tech., 31, 769 (1979).
4. Scamehorn, J. F., Schechter, R. S., and Wade, W. H., J. Colloid Interface Sci., 85, 463 (1982).

III. Surfactant Synthesis and Phase Behavior

During the past year studies have continued to define the role of hydrophobe tail structure in reducing interfacial tension, increasing solubilization parameters, reducing sensitivity to system variables, and, most recently, to minimization of cosolvent requirements.

These studies have necessitated the development of new synthesis schemes which have resulted in two manuscripts, copies of which follow as Sections IIA and IIB. Of particular interest is the facile carbon-sulfur bond formation adding thioacetic acid to double bonds. The yield is good and the process simple.

The phase behavior of α-olefin sulfonates and their components, the alkene and hydroxy species, have been studied with regard to phase behavior. This class of sulfonates seem to have inherently high salinity tolerance and give inherently low interfacial tensions.

This latter observation seems to be characteristic of straight tailed hydrophobes. The results of this study, in manuscript form, appear in Section IIIC.

Studies have been completed on monoisomeric oleyl sulfonates with 1, 2, and 3 moles of ethylene oxide added. These species are straight tailed and thus have properties similar to the alpha-olefin sulfonates mentioned previously. However the addition of ethylene oxide significantly reduces phase transition temperatures and hence cosolvent requirements as is seen from the results presented in Section IID.

Precisely branched alkane sulfonates have also been studied. Their behavior parallels the alkyl benzene sulfonates with the added observation that their calcium tolerance is much higher. Results are presented in Section IIE.

In summary all the above studies support the importance of the role of tail structure in designing synthetic surfactants for enhanced oil recovery.

Synthesis and Performance of Isomer-free Secondary Alkane Sulfonate Surfactants

by

R.S. Schechter, W.H. Wade, U. Weerasooriya
V. Weerasooriya, and S. Yiv

Departments of Chemistry and Petroleum Engineering
University of Texas
Austin, Texas 78712

ABSTRACT

Isomer-free secondary alkane sulfonates were synthesized from a series of pure secondary alcohols. The C-S bond was formed by thioesterification of the alcohol. A subsequent mild oxidation followed by neutralization generated the monoisomeric sodium sulfonates in good yield. These surfactants were prepared as alternatives to alkane sulfates, which do not have the requisite thermal stability for many high temperature studies and applications.

INTRODUCTION

Commercially available secondary alkane sulfonates are mixtures of isomers. This is a direct consequence of the method by which they are produced, namely photochemically induced sulfoxidation of alkanes (1), which leads to little or no control over their isomeric composition (eq.1).

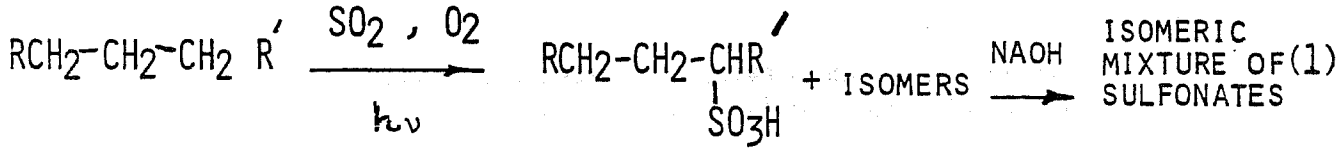

As part of our research program aimed at understanding the physi chemical behavior of each component isomer in these mixtures, a methodology for synthesizing isomer-free secondary alkane sulfonates was developed.

A most convenient method for synthesizing primary alkane sulfonates would appear to be by way of the well known Strecker reaction (2) in which a primary alkyl halide is reacted with an aqueous sodium sulfite solution at 180° for 12-16 h under pressure (eq.2). Hence to realize our objective of synthesizing secondary alkanesulfonates, an extension

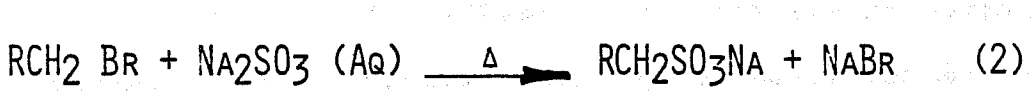

of this methodology was attempted on isomer-free secondary alkyl halides. However, it turned out that the favored reaction between secondary alkyl bromides (3a,b) and sodium sulfite under the above reaction conditions was one of elimination (E^2) rather than substitution (S_N2) (Scheme 1).

SCHEME 1

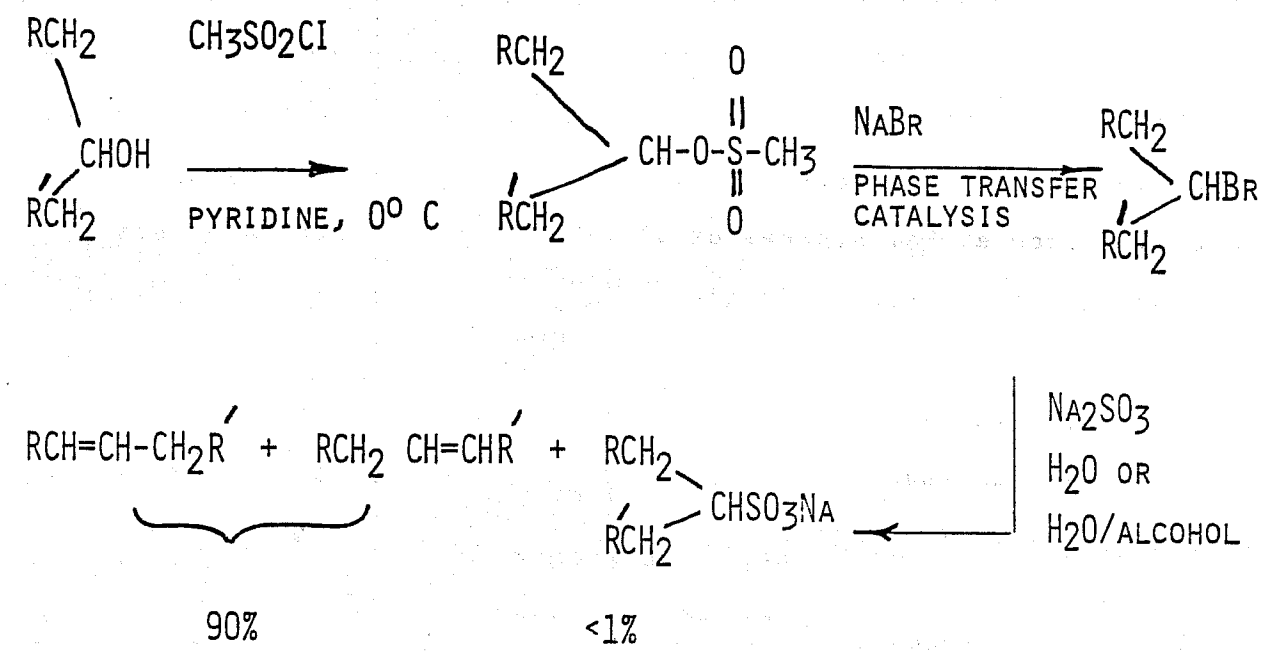

These extremely poor yields of secondary alkanesulfonates in this reaction compelled us to explore other avenues for synthesizing our target molecules.

A convenient precursor to sulfonic acid is the corresponding thiolacetate 1. The latter can be easily oxidized to the former with 30% hydrogen peroxide and acetic acid (eq. 3).

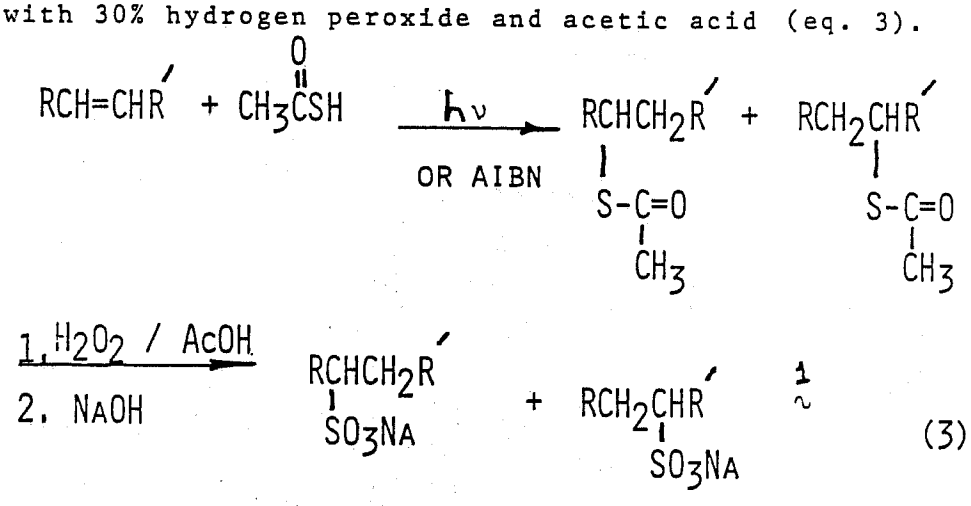

(3)

Thus, thiolacetates 1 were utilized as a key intermediate in this process. Several methods are available for synthesizing thiolacetates from either alkenes or alcohols. The former processes involve the free radical addition of thiolacetic acid to an alkene (4,5).

The main drawback in this otherwise simple procedure is the formation of two isomers, except in the case of symmetrical alkenes. Terminal alkenes (α-olefins) give only 1-thiolacetates.

The latter processes (6,7) involve the activation of the hydroxyl functionality followed by displacement with a suitable thio-nucleophile. The mildest and shortest route to thiolacetates involves the treatment of a preformed adduct of triphenyl phosphine and diisopropyl azodicarboxylate with a mixture of the alcohol and thiolacetic acid (eq.4). (7) A possible mechanism for this transformation is given below. (8) (Scheme 2)

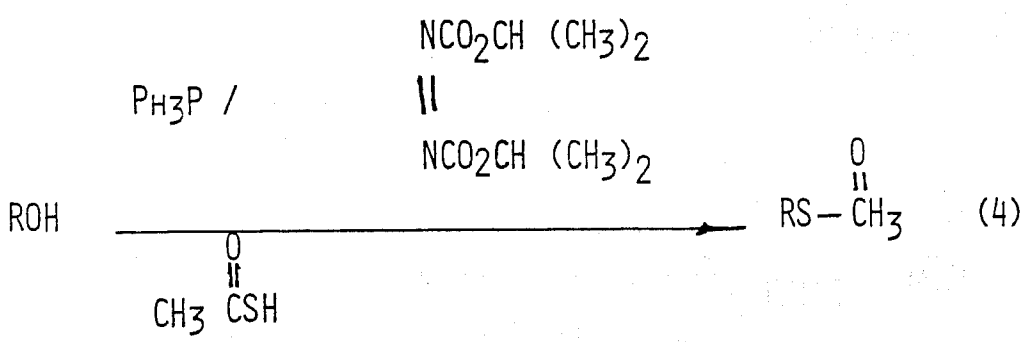

(4)

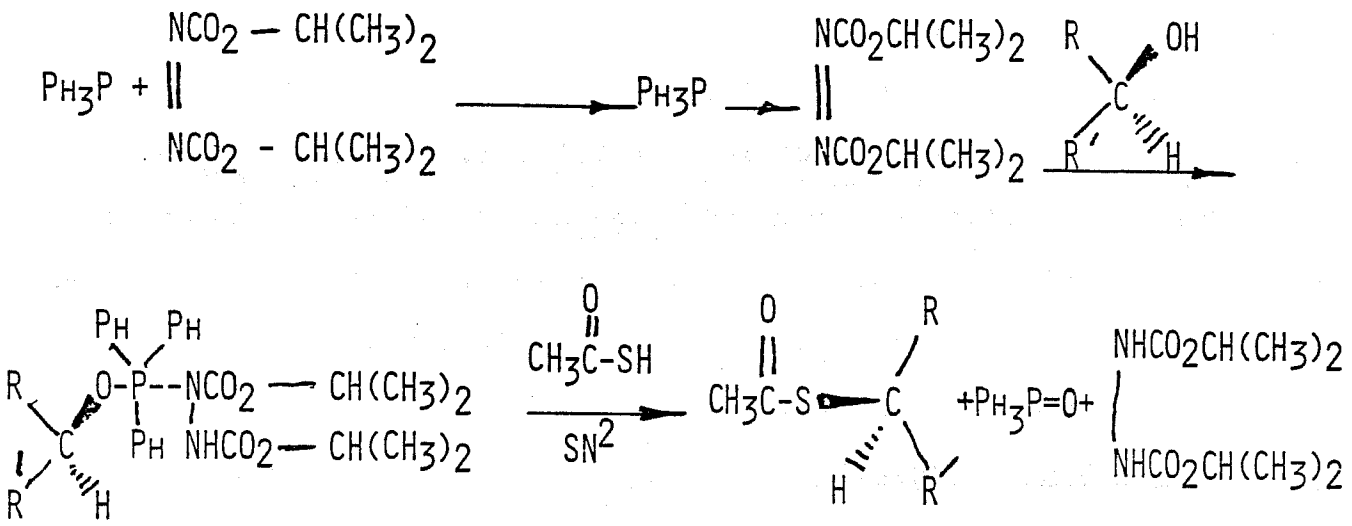

Scheme 2

The high regiochemical integrity of this reaction was shown by the conversion of 2-octanol to 2-octylthiolacetate in 98% yield. It was also shown that this reaction goes with complete inversion of configuration.

This reaction sequence of converting an alcohol to a thiolacetate (eqn. 4) and its subsequent oxidation (eqn. 3) followed by neutralization was applied to several secondary hexadecanols and octadecanols.

EXPERIMENTAL:

I. Product Analysis

Proton magnetic resonance (^{1}H NMR) spectra were obtained by using a Varian EM 390 spectrometer. Chemical shifts were reported in parts per million relative to tetramethyl silane or chloroform as internal references at 0.00 and 7.25 ppm, respectively. Unless otherwise noted, ^{1}H NMR data are for solutions in $CDCl_3$ or $CDCl_3$ and CF_3CO_2H, and are reported in the following manner: parts per million downfield from Me_4Si or upfield from $CHCl_3$, multiplicity and the number of protons.

Carbon magnetic resonance (^{13}C NMR) spectra were obtained using a Varian FT 80-A instrument.

All infrared (IR) spectra were recorded in units of reciprocal centimeters and are designated as s(strong), m(medium) and w(weak). IR analysis of liquids were performed on neat samples held as films between salt plates and those of solids as KBr pellets. Determination of accurate mass was made on a duPont (CEC) 21-210 high-resolution mass spectrometer, operating at 70eV.

II. Synthesis Procedure

Secondary alcohols:

These were prepared by way of a Grignard reaction (9) between an aldehyde and an alkyl magnesium bromide. After the subsequent acidic work up, secondary alcohols were obtained in 80% yield.

Secondary thiolacetates:

The secondary alcohols were converted to their corresponsing thiolacetates according to a published procedure. (7) Thus, diisopropyl azodicarboxylate (41.7g, 0.20 mole) was added with stirring to a solution of triphenylphosphine (52.5g, 0.20 mole) in 500 mL of tetrahydrofuran (THF) at $0^{o}c$. There was an immediate formation of a white slurry. After 30 min. of stirring at $0^{o}c$, this complex was treated with a solution of the alcohol (0.10 mole) and thiolacetic acid (15.2g, 0.20 mole) in 250 mL of THF added dropwise over 15 min. Stirring was continued and the reaction mixture was kept at $0^{o}c$ for 1 h. and at room temperature for 2 h. By this time a clear solution formed. The solvent (THF) was stripped off and the residue was extracted three times with pentane. The combined pentane fractions were washed twice with water and dried (Na_2SO_4). Solvent was removed to yield the crude

thiolacetate, ^1H NMR analysis of which showed the conversion to be greater than 60%. Purification was effected by passing the crude through an activated silica gel column and eluting with hexane.

Spectral data:

9-octadecyl thiolacetate

^1H NMR (CCl_4): δ0.85 (2t,6H), 1.25-1.65 (m,30H), 2.25 (s,3H), 3.40 (m,1H)

^{13}C NMR ($CDCl_3$): δ14.09 (2C), 22.70 (2C), 26.83 (2C), 29.34-29.54 (7C), 30.69 (1C), 31.93 (2C), 34.91 (2C), 44.75 (1C), 195.70 (1C)

IR (neat): 1685 cm^{-1} (-C(O)S-)

HRMS: molecular ion, m/e 328.2811 (calcd. for $C_{20}H_{40}OS$ 328.2800)

2-Octadecyl thiolacetate

^1H NMR (CCl_4): δ0.80 (t,3H), 1.20-1.60 (m,30H), 1.25 (d,3H), 2.20 (s,3H), 3.45 (m,1H)

IR (neat): 1685 cm^{-1} (-C(O)S-)

2-Hexadecyl thiolacetate

^1H NMR (CCl_4): δ0.85 (t,3H), 1.20-1.60 (m,26H), 1.25 (d,3H), 2.20 (s,3H), 3.45 (m,1H)

IR (neat): 1685 cm^{-1} (-C(O)S-)

4-Hexadecyl thiolaceate

^1H NMR (CCl_4): δ0.85 (t,3H), 0.90 (t,3H), 1.20-1.70 (m,26H), 2.25 (s,3H), 3.40 (m,1H)

IR (neat): 1685 cm^{-1} (-C(O)S-)

Sodium secondary alkane sulfonates:

A secondary thiolacetate (0.022 mole) in 10 mL of acetic acid was warmed to 50°c. A drop of concentrated sulfuric acid was added

as a catalyst and the well stirred reaction mixture was treated with a 30% hydrogen peroxide solution (7.8 mL, 0.068 mole) added slowly and the temperature was maintained at 60°. An exothermic reaction was usually observed after an induction period of 30 min. Heating and stirring was continued for an additional 1h. Excess oxidant was destroyed by treating with a 20% sodium sulfite solution (checked for absence of oxidizing agent with acidic potassium iodide solution when no liberation of iodine takes place). This sulfonic acid solution was dissolved in a mixture of 2-propanol (IPA)-water (300mL each) and neutralized with a 50% solution of sodium hydroxide. The sulfonate solution was heated to 50°C and saturated with sodium carbonate. The IPA fraction containing the surfactant was isolated, diluted with 250 mL of water and washed with 300 mL of Skelly B. The IPA layer was separated, diluted with water and treated with sodium carbonate. This IPA-water-sodium carbonate work up prcedure[10] was repeated a fourth time to remove virtually all the sodium acetate that was formed as a by-product. The final IPA fraction was volatilized using a rotary evaporator followed by a vaccum oven to isolate the sulfonate in a near quantitative yield.

Spectral data

Sodium 2-octadecanesulfonate (11a)

^1H NMR (CCl_4/CF_3CO_2H): δ0.85 (t, 3H), 1.10-2.20 (m, 30H), 1.45 (d, 3H), 3.15 (m, 1H)

^{13}C NMR ($CDCl_3/CF_3CO_2H$): δ15.62, 24.76, 28.73, 31.36-31.85 (12C) 32.77, 34.12, 58.47

IR (KBr pellet): 2920 (s), 2850 (s), 1470 (m)

HRMS (as sulfonic acid): molecular ion, m/e334.2527(calcd. for $C_{18}H_{38}O_3S$ 334.2542)

Anal. Calcd. for $C_{18}H_{37}O_3SNa$: C, 60.64; H, 10.46: found: C,60.44;H, 10.40

Sodium 9-octadecanesulfonate (11b)

^1H NMR ($CDCl_3$): δ 0.85 (2t, 6H), 1.10-2.10 (m, 30H), 2.70 (m,1H)

^{13}C NMR ($CDCl_3$): δ 14.14 (2C), 22.89 (2C), 27.58, 29.20-31.72 (10C), 32.22 (2C), 59.96

HRMS (as sulfonic acid): molecular ion, m/e 334.2550 (calcd. for $C_{18}H_{38}O_3S$ 334.2542)

Sodium 2-hexadecanesulfonate (11a)

^1H NMR (CF_3CO_2H): δ 0.85 (t, 3H), 1.15-2.20 (m, 26H), 1.45 (d, 3H) 3.15 (m, 1H)

^{13}C NMR (CF_3CO_2H/D_2O): δ 15.24, 24.19, 28.39, 30.98-31.29 (10C), 32.60, 33.56, 58.07

HRMS (as sulfonic acid): molecular ion, m/e 306.2241 (calcd. for $C_{16}H_{34}O_3S$ 306.2299)

Sodium 4-hexadecanesulfonate (11c)

^1H NMR ($CDCl_3$): δ 0.80 (t, 3H), 0.85 (t, 3H), 1.10-2.20 (m, 26H), 2.70 (m, 1H)

^{13}C NMR (CF_3CO_2H/D_2O): δ 14.76, 15.04, 21.59, 24.08, 28.60, 30.86-31.17 (8C), 33.22, 33.43, 62.18

HRMS (as sulfonic acid): molecular ions, m/e 306.2235 (calcd. for $C_{16}H_{34}O_3S$ 306.2299)

The secondary alkane sulfonates thus prepared showed satisfactory spectroscopic purity. The regiochemical integrity of this process was ascertained in the case of sodium 2-hexadecanesulfonate 3 and sodium 2-octadecanesulfonate 2. The proton NMR spectra of both these compounds

showed a distinct doublet at δ1.45 accounting for three protons. The carbon NMR spectral analysis of 2 and 3 showed the chemical shift of the carbon bearing the sulfonate functionality to be δ58. Both these results indicate that the sulfonate group is attached to the second carbon of the alkane chain. Attempts to convert tertiary alcohol to tertiary alkane sulfonates were unsuccessful mainly due to the failure in the transformation of the alcohol to the thiolacetate. This result substantiates further the stereochemical integrity of this displacement reaction (eqn. 5 and Scheme 2).

III. Performance

The spectrum of molecules thus prepared can be utilized to produce microemulsion formulations at various electrolyte concentrations usable for enhanced oil recovery processes. As such they are designed to be model surfactants to meet a variety of ionic environments of oil reservoirs. These sulfonates were evaluated for interfacial properties in system compositions where there is equipartitioning of surfactant between hydrocarbon and water. The sulfonate attachment point to the hydrocarbon tail has been found to be a key variable governing the ionic strength sensitivity as well as the alcohol requirement for microemulsion formation. Figure 1. shows the minimal secondary butyl alcohol concentrations in grams per deciliter (gpdl) required to get into the microemulsion regime at 40°C with n-decane as oil phase for the C_{18} species. The salt concentration in gpdl to form an optimum system* is shown near each data point. The cosolvent requirement, being the greatest for lowest isomer number (IN) species, falls off to zero as IN increases, then increases slightly at IN=9. Figure 1. thus highlights a trade-off between surfactant tail branching and cosurfactant content as an alternative to the temperature - cosurfactant trade-off (8). The optimum phase behavior in oil phase

equivalent alkane carbon number/NaCl space are displayed in Figure 2. at either constant or variable temperature as noted. Salt concentrations at optimum underwent an increase in excess of tenfold as the sulfonate attachment position to C_{18} species was displaced from 9 to 2. The optimum system microemulsions thus formulated exhibited desirable solubilizing performance as shown in Figure 3, where optimum solubilization, σ*, is seen to vary from 10 to 50cc of oil or water in the middle phase per cc of neat surfactant. From previous studies (8) this translates to interfacial tensions between 4×10^{-3} and 1.5×10^{-4} dyne/cm which is sufficient to mobilize residual oil in porous formations.

* An optimal system is a Winsor III composition with a surfactant middle phase microemulsion in equilibrium with excess alkane and electrolyte phases which further has equal volumes of oil and water in the middle phase.

FIGURES:

FIGURE 1. Minimal sec butanol concentration for microemulsion formation as a function of attachment point of sulfonate to a linear octadecane chain (I.N.)

FIGURE 2. Optimum Phase Behavior lines in salinity/EACN space.

FIGURE 3. Optimum Solubilization Parameters taken on the lines in Figure 2.

ACKNOWLEDMENTS

The authors wish to express their appreciation to Dr. Kaye Motz for helpful suggestions. Assistance from the following organizations is gratefully acknowledged. The U.S. Department of Energy, The Robert A. Welch Foundation, Amoco, Arco, British Petroleum, Chevron, Conoco, Elf-Aquitane, Exxon, TOTAL-CFP, Dowell, GAF Corp, Getty, Gulf, Mobil, Shell, Sun, Tenneco, Texaco, Union, Witco, Petrole, and Rhone Poulenc Petrole.

REFERENCES AND NOTES

1. Quack, von J.M.; Reng, A.K. Fette. Seifen. Anstrichmittel, 1976, 78 (5), 200.

2. Reed, R.M.; Tarter, H.V. J. Am. Chem. Soc. 1935, 57, 570.

3. a) Weiner, H.; Sneen, R. A. J. Am. Chem. Soc. 1965, 87 (2), 287; b) Landini, D.; Quici, S.; Rolla, F. Synthesis, 1975, 430.

4. Showell, J.S.; Russell, J.R.; Swern, D. J. Org. Chem. 1962, 27, 2853.

5. Yoshihara, M.; Fujihara, H.; Yoneda, A.; Maeshima, T. Chem. Lett. 1980, 39.

6. a) Beretta, E.; Cinquini, H.; Colonna, S.; Fornasier, R. Synthesis, 1974, 425; b) Hojo, K.; Yoshino, H.; Mukaiyama, T. Chem. Lett. 1977, 133; c) ibid, 437.

7. Volante, R.P. Tetrahedron Lett. 1981, 22 (33), 3119.

8. Y. Barakat, L.N. Fortney, R.S. Schechter, W.H. Wade and S.H.Yiv, "Alpha Olefin Sulfonates for Enhanced Oil Recovery", 2nd European Symposium, Enhanced Oil Recovery, Nov. 1982 (Editions Technip, Paris) p.11.

9. For a recent review see Eicher, T. in Patai, "The Chemistry of the Carbonyl Group", Vol. 1., pp621-693, Interscience Publishers, New York, 1966.

10. Turbak, A.F.; Livingston, J.R. Ind. Eng Chem. Prod. Res. Develop 1963, 2, 229.

11. a) recrystallized from water; b) recrystallized from acetone; c) recrystallized from ethanol-acetone mixture.

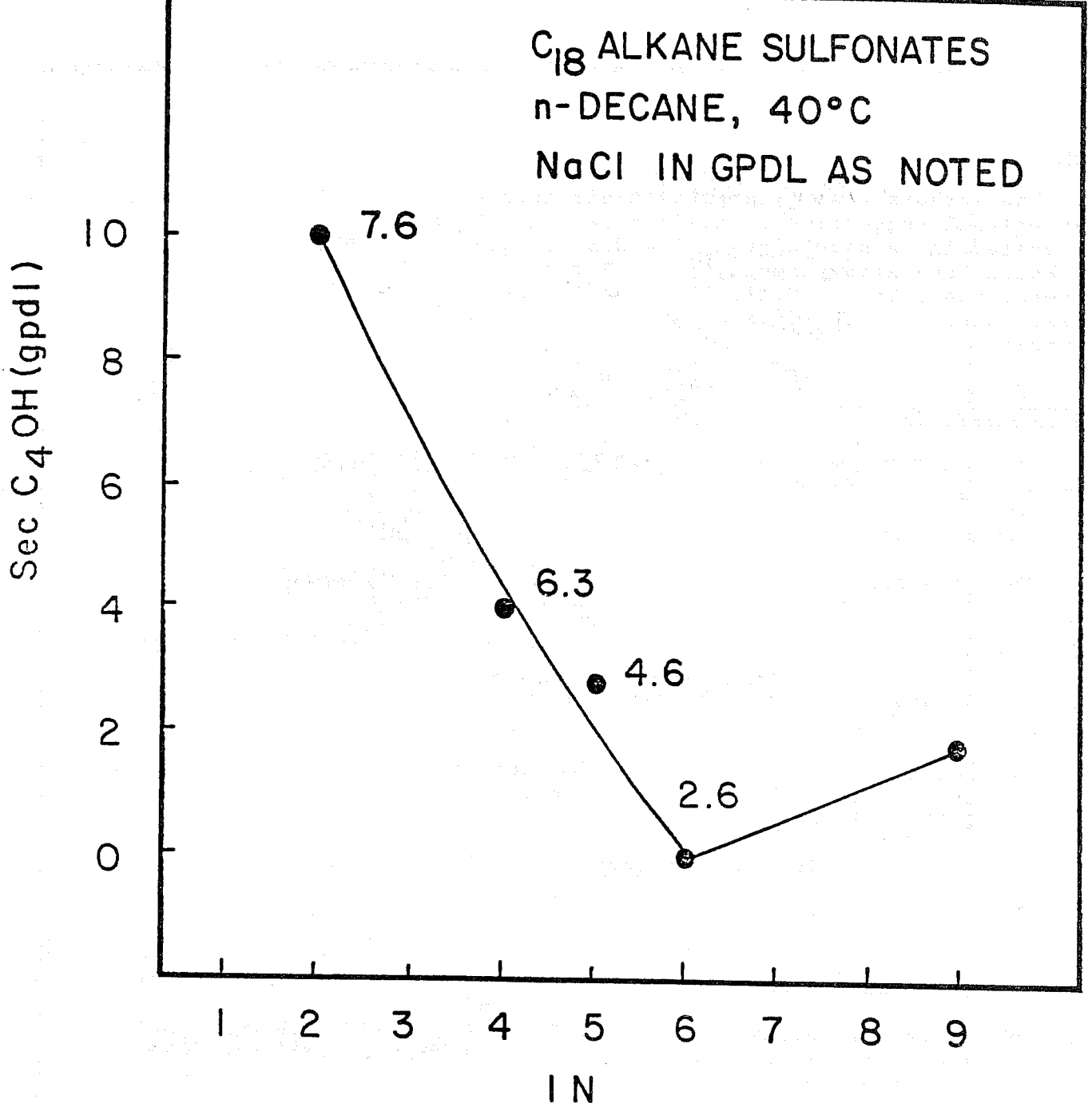
C_{18} ALKANE SULFONATES
n-DECANE, 40°C
NaCl IN GPDL AS NOTED
Sec C_4OH (gpdl)
10
8
6
4
2
0
7.6
6.3
4.6
2.6
1
2
3
4
5
6
7
8
9
I N

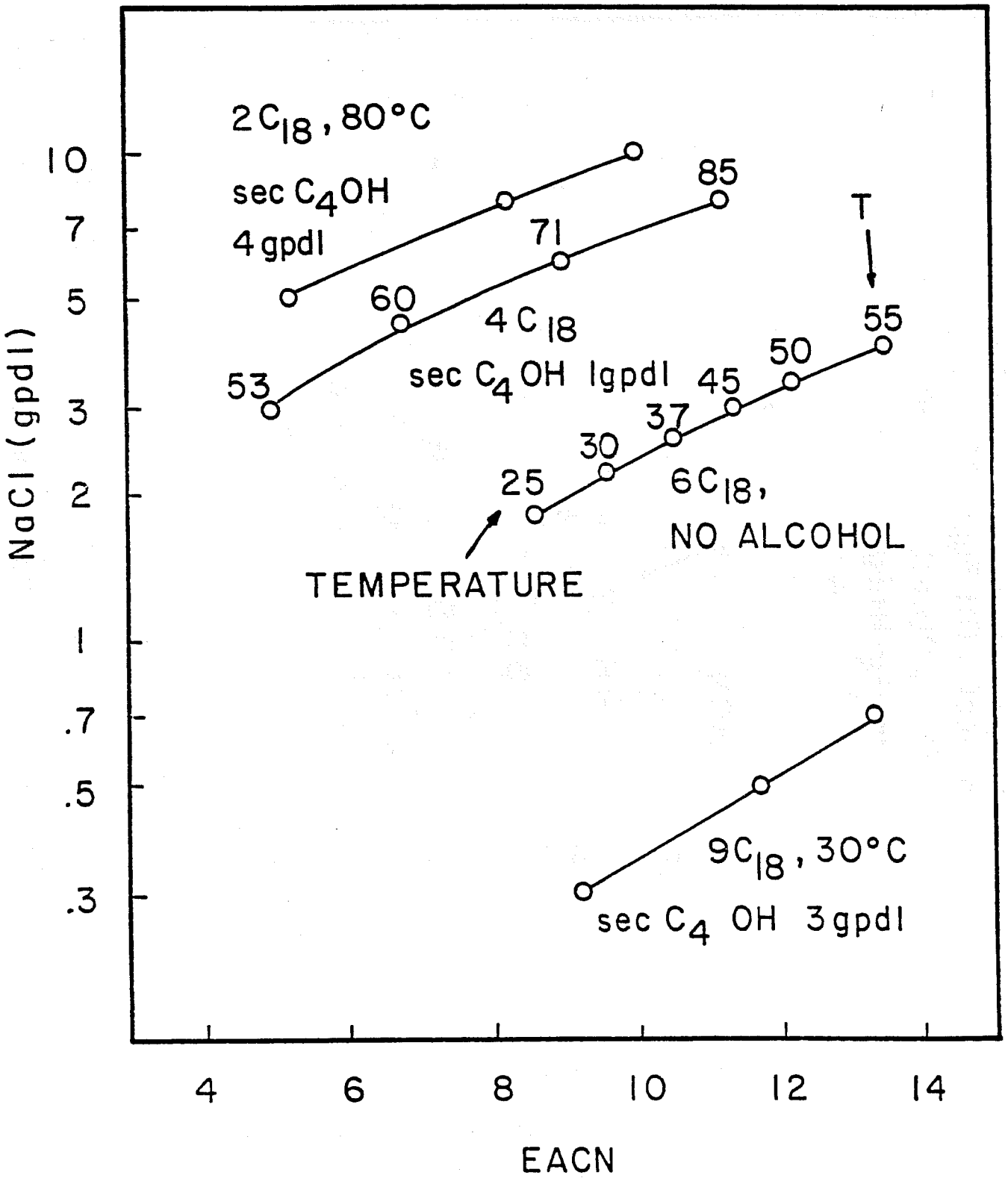
2C18, 80°C
sec C4OH
4 gpdl
85
71
60
53
4 C18
sec C4 OH 1gpdl
T
55
50
45
37
30
25
6C18,
NO ALCOHOL
TEMPERATURE
9C18, 30°C
sec C4 OH 3gpdl
NaCl (gpdl)
10
7
5
3
2
1
.7
.5
.3
4
6
8
10
12
14
EACN

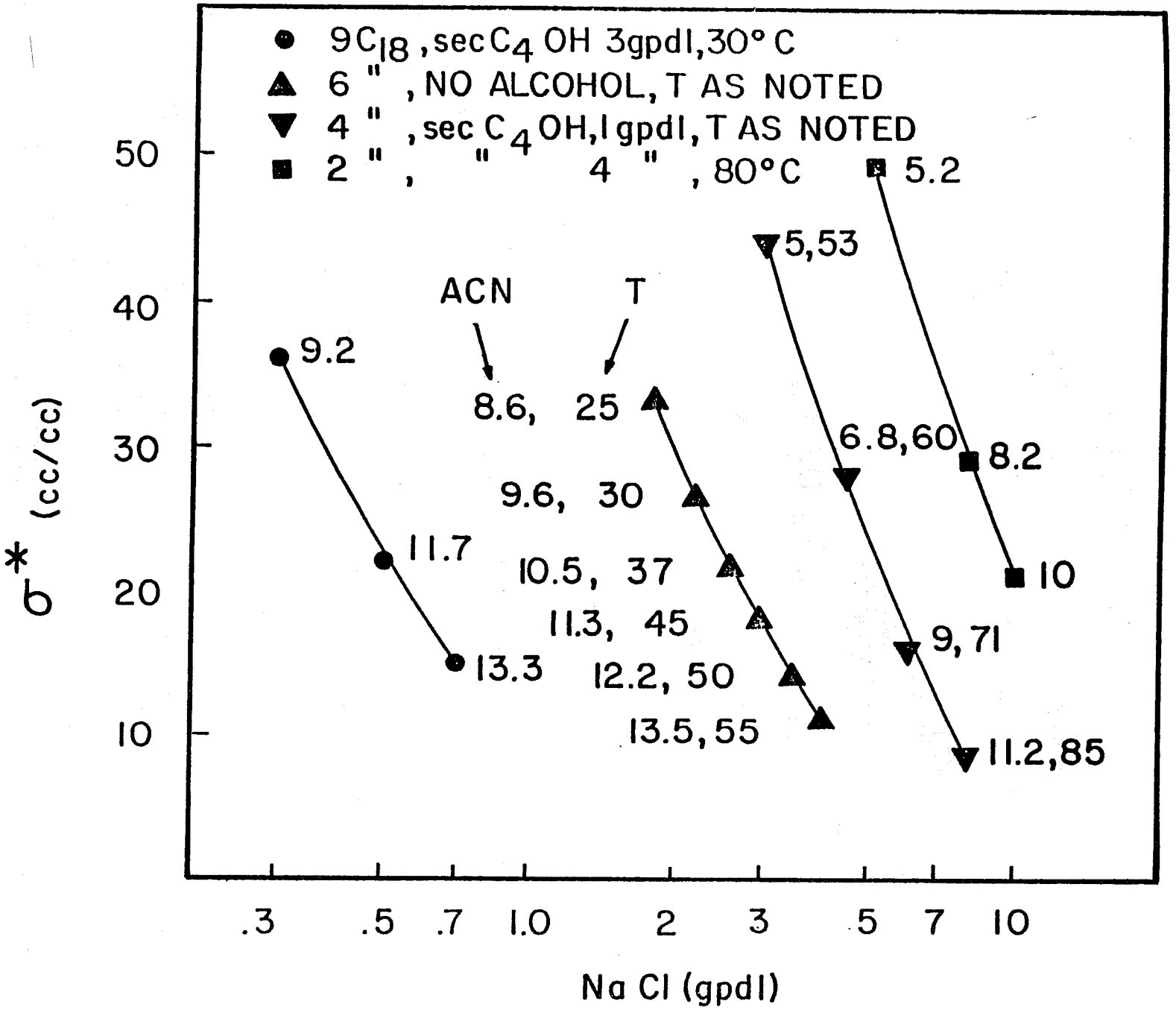
9 C_{18}, sec C_4 OH 3gpdl, 30° C
6 " , NO ALCOHOL, T AS NOTED
4 " , sec C_4 OH, 1 gpdl, T AS NOTED
2 " , " 4 " , 80°C
ACN
T
9.2
11.7
13.3
8.6, 25
9.6, 30
10.5, 37
11.3, 45
12.2, 50
13.5, 55
5,53
6.8,60
9, 71
11.2,85
5.2
8.2
10
σ^* (cc/cc)
50
40
30
20
10
.3
.5
.7
1.0
2
3
5
7
10
Na Cl (gpdl)

Synthesis and Performance of Linear Monoisomeric Ethylene Oxide Sulfonate Surfactants

by

I.Carmona, R.S. Schechter, W.H. Wade, U.Weerasooriya, and V. Weerasooriya

Departments of Chemistry and Petroleum Engineering

University of Texas

Austin, Texas 78712

ABSTRACT

Reaction of sodium bromoethanesulfonate with sodium alkoxides of several linear alcohols produced linear ethylene oxide sulfonates in good yield. These sulfonates were constructed with hydrophobe tails of eighteen and twenty carbons and precisely one, two and three moles of ethylene oxide. All species could be made to produce Winsor III systems with suitable alkane oil phases and the appropriate salt and cosolvent concentrations.

INTRODUCTION

As part of our studies aimed at elucidating the effect on surface properties of ethylene oxide units implanted in sulfonate surfactant molecules, the compounds listed below were synthesized.

$$C_{18}H_{37}OCH_2SO_3NA \qquad (1)$$

Sodium octadecyloxyethanesulfonate 1

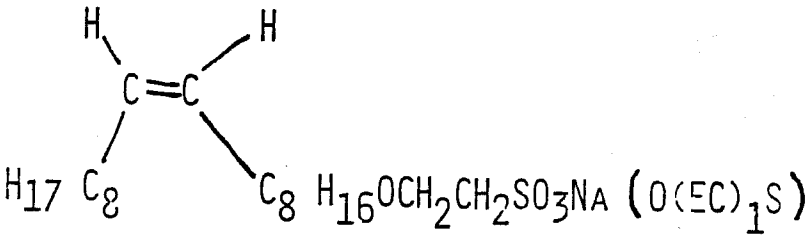

(2)

Sodium (9-octadecenyloxy) ethane sulfonate 2

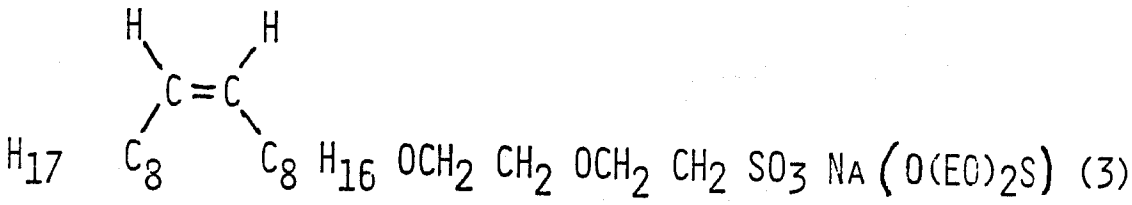

(3)

Sodium (9-octadecenyloxythoxy) ethane sulfonate 3

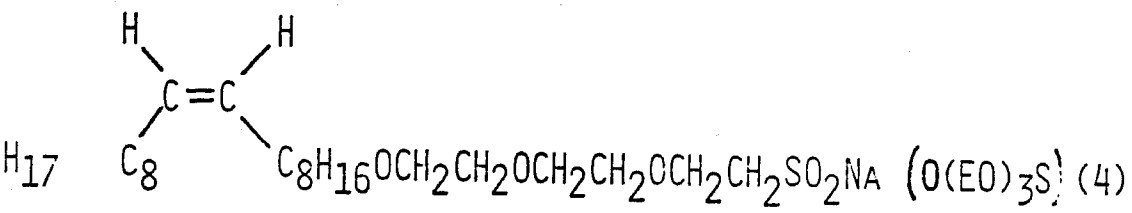

(4)

Sodium((9-octadecenyloxyethoxy) ethoxy) ethane sulfonate 4

$$H_{41}C_{20}OCH_2CH_2SO_3NA \qquad (5)$$

Sodium eicosyloxyethanesulfonate 5

Synthesis

The key transformation in these syntheses involved the sulfoethylation of an alcohol with sodium bromoethanesulfonate (eqn. 1).

$$RO^{\ominus}Na^{\oplus} + BrCH_2CH_2SO_3Na \xrightarrow{SN^2} ROCH_2CH_2SO_3Na + NaBr \qquad (1)$$

R = $C_{18}H_{37}$–,

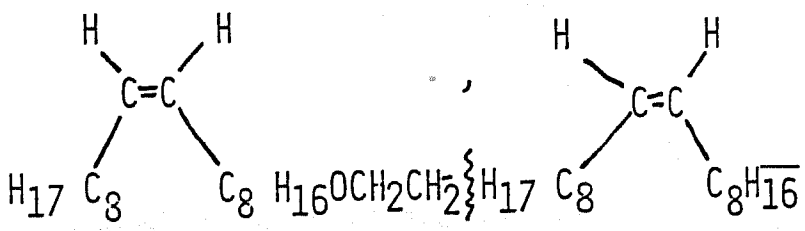

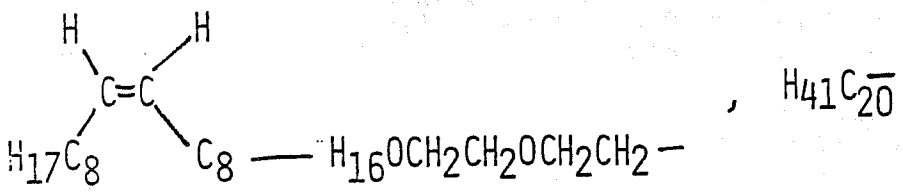

The sulfonates 1, 2 and 5 were prepared directly from the commercially available octadecyl alcohol, 9-octadecenyl alcohol and eicosyl alcohol respectively, by sulfoethylation as shown in eqn. (1). The precursor alcohol for the synthesis of 3 was 9-octadecenyloxyethanol 6. [1] This was prepared from 9-octadecenyl alcohol (oleyl alcohol) according to a published procedure [2] (eqn.2). The alcohol, (9-octadecenyloxy) ethoxyethanol, 7, [1] required for synthesizing the sulfonate 4 was prepared in an analogous manner (eqn.3).

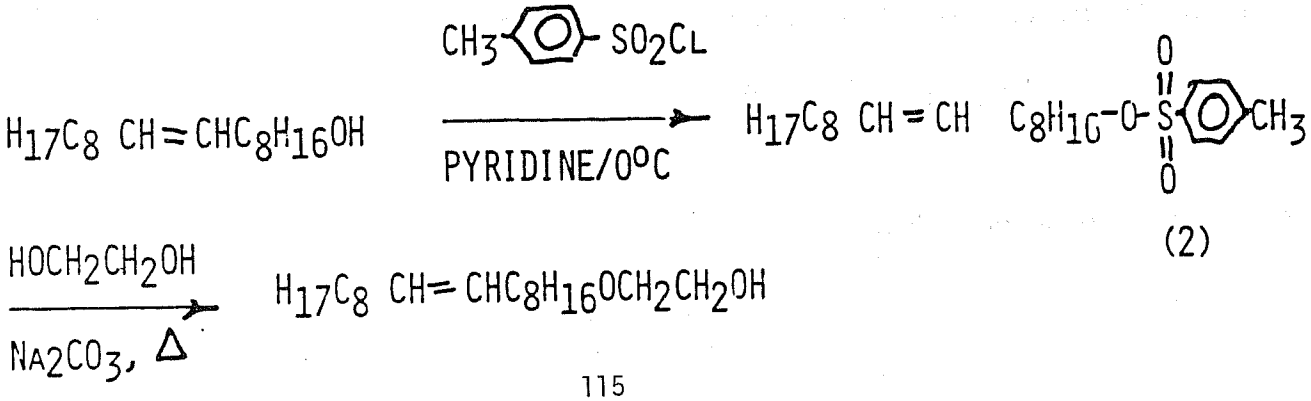

(2)

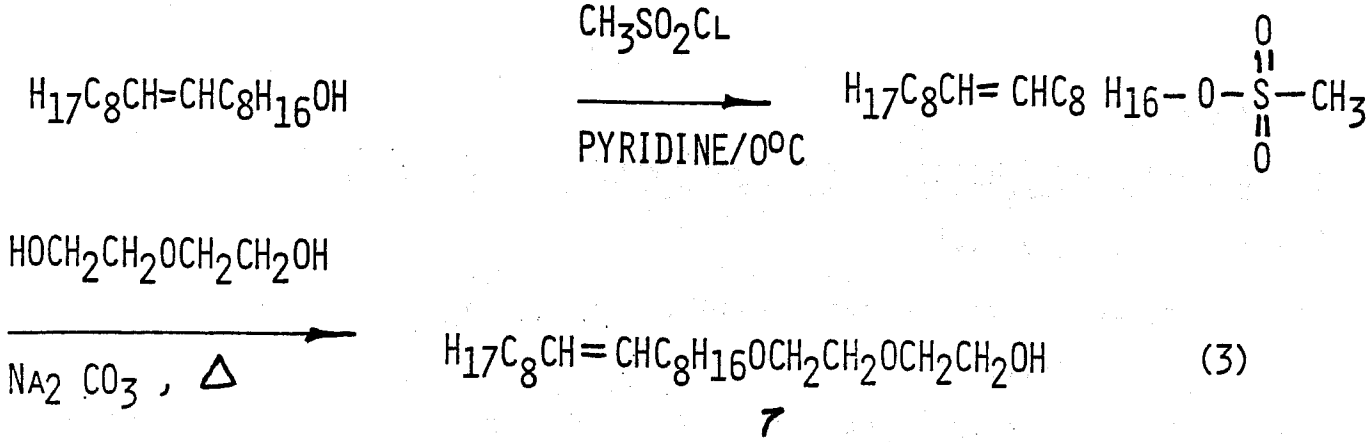

A typical experimental procedure is as follows. In a 3-necked, 1L round bottomed flask equipped with a reflux condenser, a nitrogen inlet, and a magnetic stirring bar, was dispersed sodium hydride (2.64 g, o.11 mole) in 400 ml of tetrahydrofuran (THF) at room temperature under an atmosphere of dry nitrogen. A solution of octadecyl alcohol (27.0g, 0.10 mole) in 50 ml of THF was added slowly over a period of 3 minutes, and the resulting mixture was heated at reflux using an oil bath and kept stirring overnight. Subsequently, sodium bromoethane sulfonate (21.1g., o.10 mole) was added with stirring. The reaction mixture was stirred with heating for a further 16 hours. Next, the solvent (THF) was removed by rotary evaporation and the residue was dissolved in a 1:1 mixture of water and 2-propanol (1200 ml each).[3,4] This solution, after being washed twice with Skelly B[5], was saturated with anhydrous sodium carbonate at 55°C. The alcoholic fraction (upper layer) was retained and the alcohol volatilized to yield the surfactant which was further dried under high vacuum overnight. This compound was recrystallized twice from hot water to obtain an analytically pure sample.

Isolated yield: 30 g,70%

Spectral data:

Sodium octadecyloxyethanesulfonate 1

^1H NMR ($CDCl_3/CF_3CO_2H$): δ 0.80(t,3H), 1.20(m,32H), 3.30(t,2H), 3.55(t,2H), 3.95(t,2H)

^{13}C NMR ($CDCl_3/CF_3CO_2H$): δ 16.06,24.83,27.63, 30.64,31.21-32.15,34.11, 52.76,67.07,74.49

Molecular ion (as the solfonic acid), m/e 378.2813 (calculated for $C_{20}H_{42}O_4S$ 378.2804)

Anal. Calcd. for $C_{20}H_{41}O_4SNa$: C,59.97; H, 10.32. Found C,60.12;H,10.36

This same experimental procedure[6] was followed in the synthesis of sodium (9-octadecenyloxy) ethanesulfonate 2, sodium (9-octadecenyloxyethoxy) ethanesulfonate 3, sodium ((9-octadecenyloxyethoxy)ethoxy) ethanesulfonate 4, and sodium eicosyloxyethanesulfonate 5. Spectral data for these compounds are given below.

Spectral Data

Sodium (9-octadecenyloxy) ethane sulfonate, 2

^1H NMR (D_2O): δ 0.80(t,3H), 1.20(m,24H), 1.95(m,4H), 3.05(t,2H), 3.35(t,2H), 3.75(t,2H), 5.30(m,2H)

^{13}C NMR (D_2O): δ 14.53,23.31,26.76,27.86,30.07-30.46,32.61,51.27,66.30, 71.82,130.22 (2 c's)

Sodium (9-octadecenyloxyethoxy) ethane sulfonate,3

^1H NMR (D_2O): δ 0.80(t,3H), 1.20(m,24H), 1.95(m,4H), 2.95-3.95(m,10H), 5.30(m,2H)

^{13}C NMR (D_2O): δ 14.09,22.80,26.34,27.46,27.51-31.04,32.19,50.87,66.32, 69.76,69.90,71.49,129.70,129.93

Sodium (9-octadecenyloxyethoxy) ethoxy ethane sulfonate, 4

^1H NMR (D_2O): δ 0.80(t,3H), 1.20(m,24H), 1.95(m,4H), 3.15(t,2H),3.30-3.75 (m,10H), 3.85(t,2H), 5.30(m,2H)

^{13}C NMR (D_2O): δ 14.11,22.86,26.37,27.45,27.55,29.23-30.47,32.18,50.84, 66.28,69.89-70.06 (4c's), 71.37,129.67,129.98

Sodium eicosyloxcyethane sulfonate, 5.

^{1}H NMR ($CDCl_3/CF_3CO_2H$): δ 0.80(t,3H), 1.20(m,30H), 3.30(t,2H), 3.55(t,2H), 3.95(t,2H)

^{13}C NMR ($CDCl_3/CF_3CO_2H$): δ 14.08,22.79,25.61,28.61,28.96-29.82,32.06, 50.74,65.05,72.39

Performance

The phase behavior of the oleyl species with 1,2,and3 moles of ethylene oxide were determined experimentally and the behavior of the octadecanol and eicosanol species was only inferred based on structural considerations.

All oleyl species, whether with 1,2,or 3 moles of EO are examples of straight tailed, quite hydrophylic surfactants, similar in behavior to C_{18} α-olefin sulfonates (7). In this vein when one attempts to make classical Winsor type microemulsions (8) one finds instead complex gel and/or liquid crystal formation. As noted earlier (7, 9) there is a sharp phase transition temperature above which the Winsor type behavior is attained. These temperatures are noted in Figure 1. for the three species for, what we have come to consider in this laboratory, the most logical reference state. This reference state is a surfactant system formulated to give firstly a Winsor III middle phase microemulsion in equilibrium with excess oil and water and secondary, more precisely formulated so that equal volumes of oil and water are incorporated in the middle phase. This is alternately often referred to as an optimum system (10,11).

With specific regard to the data of Figure 1., for the constant system conditions noted in the legend the $O(EO)_1S$ species requires an equivalent alkane carbon number for the oil phase of 10.3*; where as the $O(EO)_3^S$ a required EACN=8.5 and $O(EO)_3^S$ requires 4.1. This is synonymous with increased EO requiring a better and better hydrocarbon solvent to attain the reference state (11).

One also notes from Figure 1. that the phase transition temperature significantly and non-linearly decreases as EO is added. Since it has been shown (7,9) that the phase transition temperature is inversely related to cosolvent requirements, addition of ethylene oxide inherently reduces cosolvent requirements.

Whereas the salinity was held constant for the data of Figure 1., one can alternately maintain the reference state with a fixed oil phase alkane, fixed cosolvent concentration, and fixed system temperature. Then the influence of EON on optimum salinity can be evaluated. This is shown in Figure 2. with all systems at 40°c, a temperature sufficiently high for microemulsion formation in all three systems. One notes that there is a quite non-linear dependence in optimum salinity of the aqueous phase on EON, and with EON = 3, that salinity is ∿15 gpdl and the microemulsion is stable.

In addition to salinity tolerance one ultimately must address the quality of middle phase microemulsion formed. The crucial criterion to establish quality in this laboratory is the interfacial tension one obtains for optimum systems, and the specifically required value is

* Alkanes have been shown to average their oil phase properties on phase properties on a mole fraction basis (12).

$\gamma < 10^{-3}$ dynes/cm. From studies involving a variety of surfactants it has been established that interfacial tension at optimum, γ^*, is related to solubilization parameter at optimum, σ^*, by

$$\sigma^{*2} \quad \gamma^* \simeq 0.3 \text{ dyne/cm} \qquad (A)$$

where solubilization parameter is defined as the volume of oil or water in the middle phase per unit volume of surfactant. At optimum

$$\sigma^* = \frac{V^o}{V_s} = \frac{Vw}{V_s} \qquad (B)$$

σ^* is plotted as a function of EON in Figure 3. for the system conditions as displayed in the leger. One can see that 1) all values of σ^* are greater than 30cc/cc and 2) σ^* increases as more EO is incorporated in the surfactant. By the application of equation (A) one can see that γ^* is well below 10^{-3} dynes/cm. for all species. Thus all these system formulations have the requisite low interfacial tensions. However it should be noted that at 8 gpdl NaCl and 40°c there is a considerable alcohol cosolvent requirement.

ACKNOWLEDGEMENT

The authors wish to thank the Robert A. Welch Foundation, the Department of Energy and the following companies for their continued interest and support: Amoco, Arco, British Petroleum, Chevron, Conoco, Elf-Aquitane, Exxon, TOTAL-CFP, Dowell, GAF Corp, Getty, Gulf, Mobil, Shell, Sun, Tenneco, Texaco, Union, Witco, Petrole, and Rhone Poulenc Petrole.

REFERENCES AND FOOTNOTES

1. Abe, Y., and Watanabe, S., Kogyo Kagaku Zasshi 66, 1842 (1963).

2. Shirley, D.A., Zietz, J.R. and Reedy, W.H., J. Am. Chem. Soc. 75, 378 (1953).

3. Turbak, A.F., and Livingston, J.R., Ind. Eng. Chem. Prod. Res. Develop. 2, 229 (1963).

4. This workup procedure was found to be a very powerful, simple method of isolating a variety of sulfonates, among which are various alkylbenzene sulfonates, alkene sulfonates, and alkane sulfonates.

5. This step removes any unreacted starting alcohol, if present.

6. It is intersting to note that this method works equally well for the synthesis of branched chain ethylene oxide sulfonate surfactants. Thus, the alcohol, 2-octadecanol, when allowed to react with sodium-bromoethanesulfonate, resulted in sodium (2-octadecyloxy) ethanesulfonate.

7. Barakat, Y., Fortney, L.N., Schechter, R.S., Wade, W.H., and Yiv, S., "Alpha Olefin Sulfonates for Enhanced Oil Recovery", 2nd European Symposium, Enchanced Oil Recovery, Nov. 1982 (Editions Technip, Paris) p.11.

8. Winsor, P.A.: Solvent Properties of Ampiphillic Compounds, Butterworth's Scientific Publications, London (1954).

9. Carmona, I., Schechter, R.S., Wade, W.H., and Weerasooriya, V., "Ethoxylated Oleyl Sulfonates as Model Compounds for Enhanced Oil Recovery, " Soc. Petrol. Eng. Reprint 11771.

10. Healy, R.N. and Reed, R.L.: "Physico-chemical Aspects of Microemulsion Flooding" Soc. Petrol. Eng. (Oct.1974) 491-501; TRANS.,AIME, Vol.257.

11. Salager, J.L. Vasquez, E., Morgan, J.C., Schechter, R.S.,and Wade, W.H.; "Optimum Formulation of Surfactant Oil-Water Systems for Minimum Interfacial Tension or Phase Behavior," Soc. Petrol. Eng., 19, 107 (1979).

12. Cash, L., Cayias, J.L., Fournier, G., McAllister, D., Shares, T., Schechter, R.S., and Wade, W.H., "The Application of Low Interfacial Tension Scaling Rules to Binary Hydrocarbon Mixtures," J. Coll. and Interface Sci., 59, 39(1977).

9. Carmona, I., Schechter, R.S., Wade, W.H., Weerasooriya, U., and Weerasooriya, V., "Ethoxylated Oleyl Sulfonates as Model Compounds for Enhanced Oil Recovery," Soc. Petrol. Eng. Reprint 11771.

10. Healy, R.N. and Reed, R.L.: "Physico-chemical Aspects of Microemulsion Flooding" Soc. Petrol. Eng. (Oct.1974) 491-501; TRANS.,AIME, Vol.257.

11. Salager, J.L. Vasquez, E., Morgan, J.C., Schechter, R.S., and Wade, W.H.; "Optimum Formulation of Surfactant Oil-Water Systems for Minimum Interfacial Tension or Phase Behavior," Soc. Petrol. Eng. 19, 107 (1979).

12. Cash, L., Cayias, J.L., Fournier, G., McAllister, D., Shares, T., Schechter, R.S., and Wade, W.H., "The Application of Low Interfacial Tension Scaling Rules to Brinary Hydrocarbon Mixtures," J.Coll. and Interface Sci. 59, 39(1977).

Figure 1

LQXTAL/μE transition temperatures as a function of EON for system conditions as noted.

Figure 2

Electrolyte concentration requirements for optimum for conditions as noted.

Figure 3

Solubilization parameters versus EON for conditions as noted.

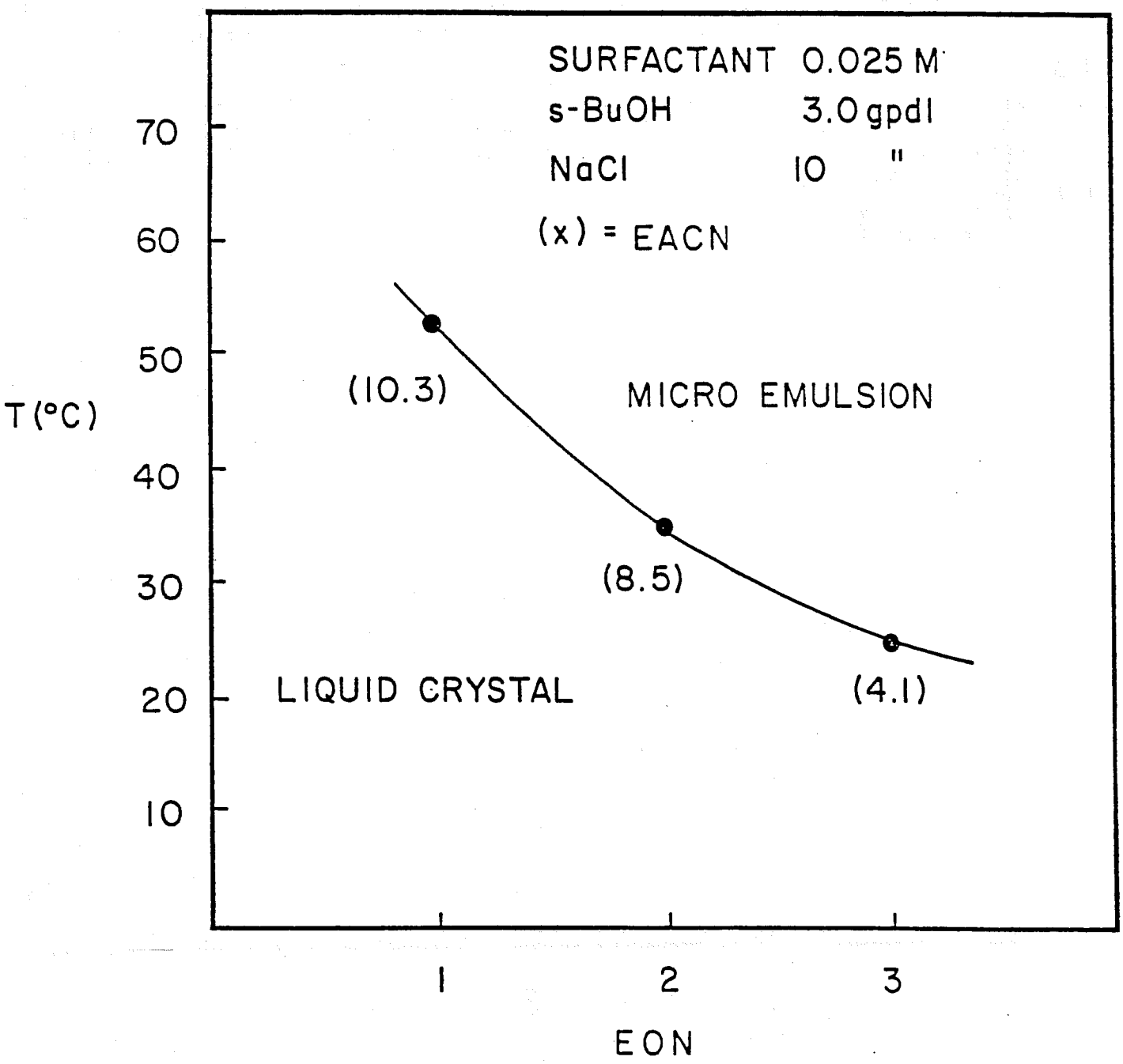
SURFACTANT 0.025 M
s-BuOH 3.0 gpdl
NaCl 10 "
(x) = EACN
70
60
50
40
30
20
10
T (°C)
(10.3)
(8.5)
(4.1)
MICRO EMULSION
LIQUID CRYSTAL
1
2
3
EON

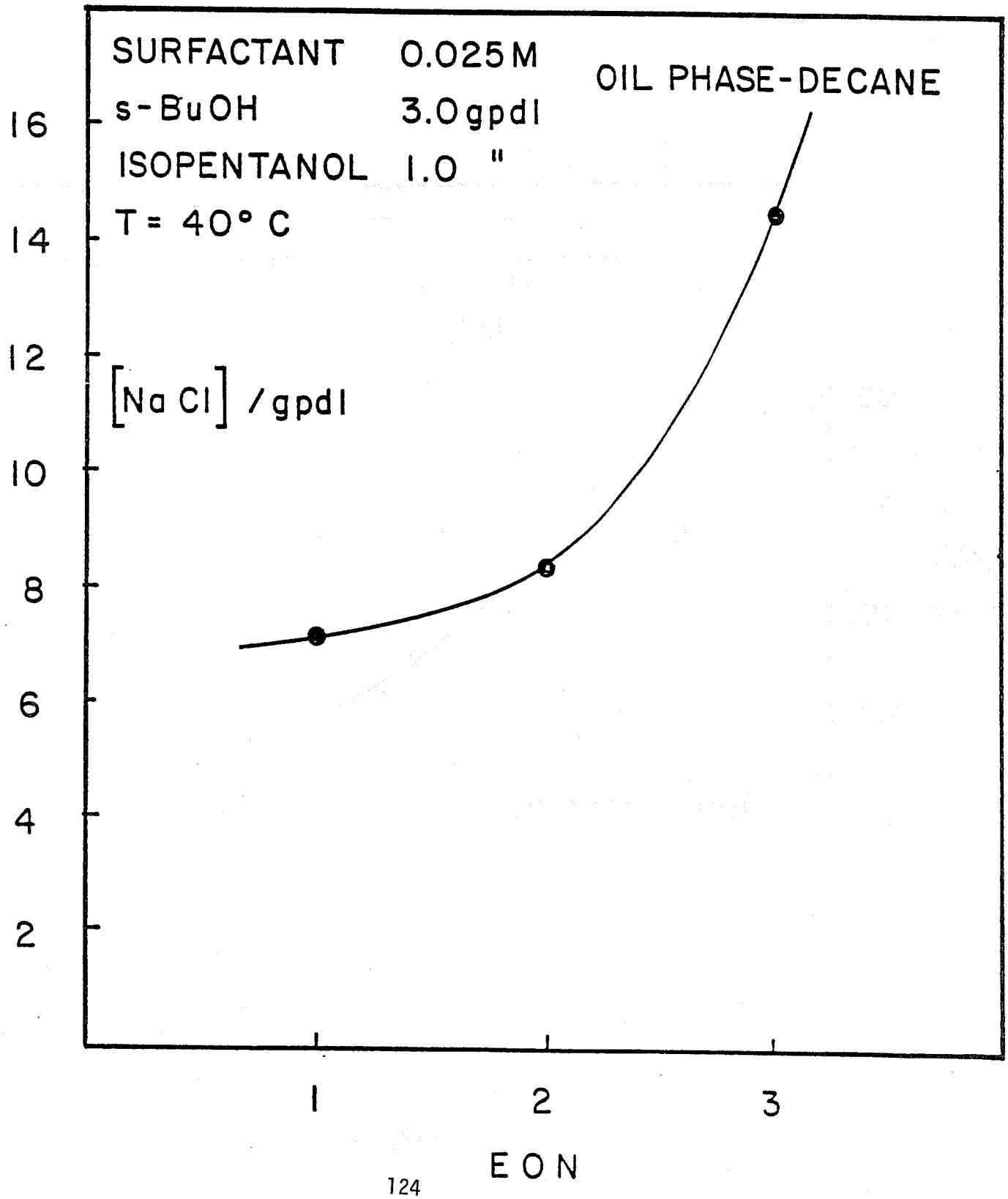
SURFACTANT 0.025 M
s-BuOH 3.0 gpdl
ISOPENTANOL 1.0 "
T = 40° C
OIL PHASE-DECANE
[Na Cl] /gpdl
16
14
12
10
8
6
4
2
1
2
3
EON

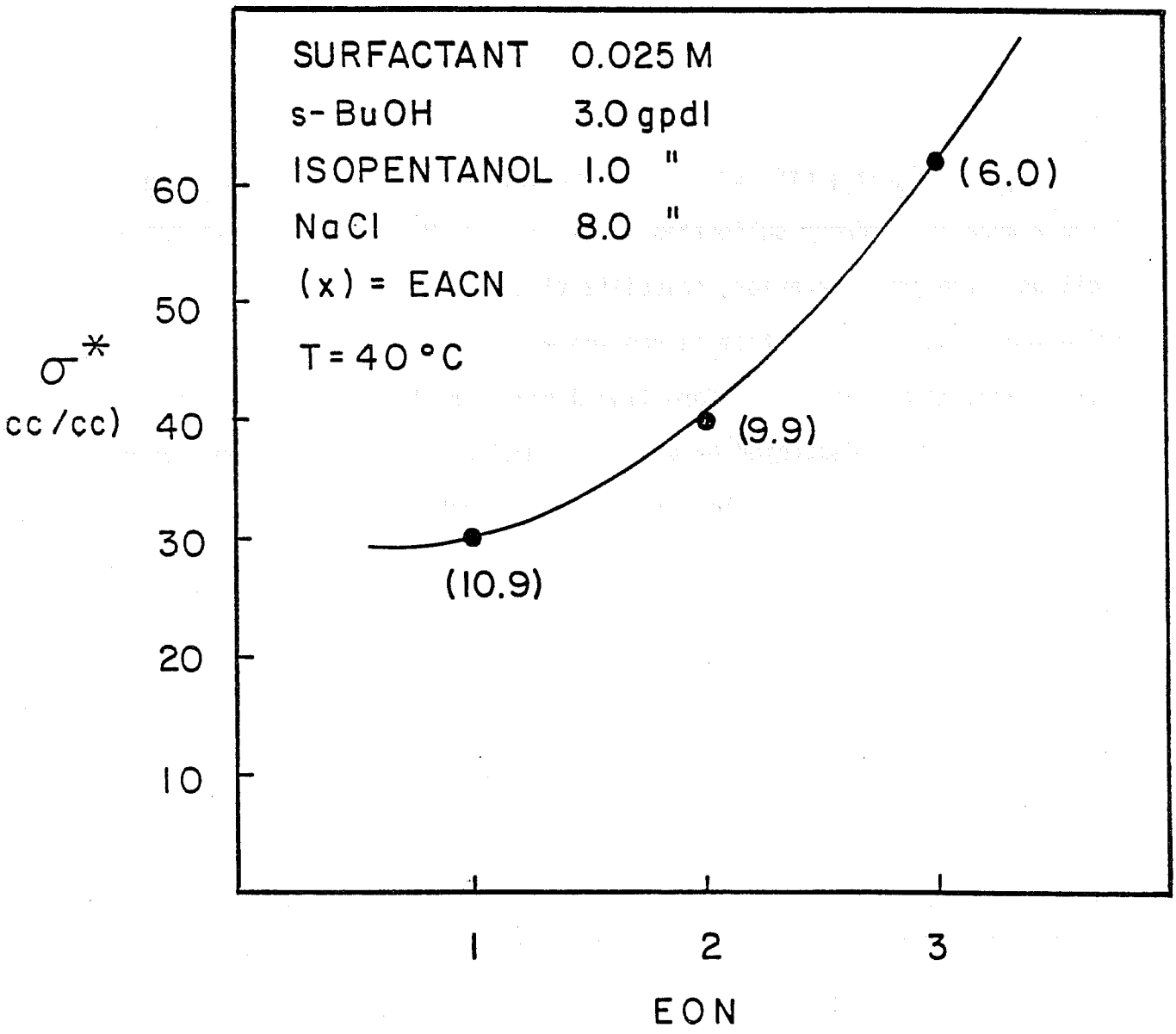
SURFACTANT 0.025 M
s-BuOH 3.0 gpdl
ISOPENTANOL 1.0 "
NaCl 8.0 "
(x) = EACN
T = 40 °C
σ*
cc/cc)
60
50
40
30
20
10
(6.0)
(9.9)
(10.9)
1
2
3
EON

ALPHA-OLEFIN SULFONATES FOR ENHANCED OIL RECOVERY

by
Y. Barakat, L. N. Fortney, R. S. Schechter,
W. H. Wade, S. H. Yiv

The University of Texas at Austin
Austin, Texas, USA

ABSTRACT

C_{18} and C_{20} α-olefin sulfonates and the components of the C_{18} species, the alkene and hydroxy sulfonates, have been studied for potential EOR application. The phase behavior, solubilization parameters, and interfacial tensions augur well for them as candidates. Their only bad feature thus far discovered is a tendency to form liquid crystals; however, these extended structures can be destroyed by alcohol or melted at elevated temperatures in order to obtain classical microemulsion phase behavior.

INTRODUCTION

From its inception, surfactant assisted enhanced oil recovery processes have placed stringent requirements on the surfactant of choice. To the present time, sulfonation of aromatic effluents from refineries have been widely used, with the alkyl xylene, benzene or toluene sulfonate synthetics also receiving attention. Both classes can generate the required phase behavior and the low interfacial tensions which are nearly universally perceived as requisites for successful mobilization of trapped oil. However, both suffer from the deficiency of being very sensitive to the presence of multivalent ions, e.g., Ca^{++}, Mg^{++}, Al^{+++}, etc. Even though this difficulty has been appreciated for some time, no simple solution has yet been reported.

It has been well documented that the sensitivity of nonionic surfactants to multivalent ions is about the same as to mono-species. But the perception remains that adsorption loss of these species is greater than with anionics, because of the inherent negative charge on many mineral surfaces. Additionally, there is some indication[1] that the most suitable nonionic structures are not commercially available. These problems are somewhat alleviated by using mixtures of nonionics and anionics to attain a moderate tolerance; however, this does generate additional problems. There is the possibility of chromatographic separation of the differently charged molecules, and there can be fractionation of the nonionic itself, between the various phases generated when surfactants, oil and water are mixed.[2]

The former of the above two problems has been attacked. A number of recent patents[3] have detailed the building of both the nonionic and anionic moieties into the same molecular structure. The most complicated of these species are alkyl phenols, which have variable ratios and amounts of propylene and ethylene oxide added, terminated by a capping with sulfonate.

Such structures probably offer the needed flexibility to obtain acceptable performance; yet one cannot help but question their cost effectiveness.

Our research has as one of its primary objectives the development of fundamental principles which govern the design of good surfactant molecules. Some evidence[4] strongly suggests that straight-tailed surfactants maximize interfacial tension, the trade-off for "straightness" being a reduction in optimal salinity - often an undesirable feature, considering that many brines have high electrolyte concentrations. Nevertheless, it has focussed out attention on species which can be made easily with straight-tailed configurations.

α-olefins are a common chemical of commerce, being routinely produced with from 12 to 24 carbons in a linear array with the double bond in the terminal position. The sulfonation of these species has also been reduced to commercial practice. A mixture of three species is produced during sulfonation. They are the corresponding alkene sulfonate,

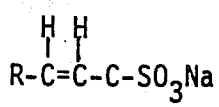

hydroxy sulfonate (see later),

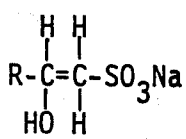

and some disulfonates, such as

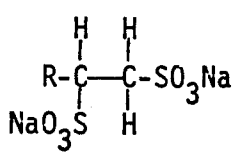

One notes that all these species have straight tails and this, along with with their simplicity, was what first attracted us to them. In a preliminary study, they were found to be promising candidates and in the report

which follows it will be seen that they do have the ability to promote good solubilization and interfacial tension, but in addition, they can easily tolerate both high electrolyte concentrations and multivalent ions.

EXPERIMENTAL

C_{18} and C_{20} α-olefin sulfonates were prepared by reacting SO_3 (complexed with tributyl phosphate) with the appropriate α-olefin and purified using a 2-propanol/water extraction procedure according to the method of Turbak and Livingston.[5] The α-olefin sulfonate obtained after purification is a mixture of alkene sulfonate and 3- and 4-hydroxy sulfonate. A few percent of disulfonate was presumed to be fractionated away during the purification process. The analysis by proton NMR and bromide-bromate titration have shown that the C_{18} and C_{20} α-olefin sulfonates contain approximately 50% and 60%, respectively, of the alkene species. We have not separately quantified the hydroxy species but have assumed that only the two species are present.

In addition to the α-olefin sulfonates, C_{18} alkene sulfonate and 3-hydroxy C_{18} sulfonates were kindly provided by Ethyl Corporation, and were used as received.

All systems were equilibrated in sealed 10cc graduated pipettes. In general, three days were required for phase volumes to reach their ultimate values, but systems exhibiting high solubilization needed more than a week of equilibration. The water/oil ratio was always 1, and all surfactant concentrations were kept constant at .6 gpdl. 96% purity alkanes, C.P. salts and alcohols were used.

Because of a large number of variables needed to define system experimental conditions and in order to abbreviate the presentation, sec

C_4OH, iso C_5OH and NaCl concentrations are given in the figures and text respectively by three consecutive numbers. For instance "3 2 x" means that the system scan was made at 3 gpdl of sec C_4OH, 2 gpdl of iso C_5OH and at variable salt concentration as indicated on the co-ordinate axis.

Interfacial tensions were measured by the spinning drop technique. All values reported here were taken at optimum conditions. Occasionally, gas chromatography with a thermal conductivity detector was used to analyze water, oil and alcohol in different phases.

RESULTS AND DISCUSSION

1. Phase behavior.

Figure 1 shows the phase behavior for C_{18} α-olefin sulfonate and its two major components, C_{18} alkene sulfonate and C_{18} 3-hydroxy sulfonate. The α-olefin sulfonate exhibits phase behavior intermediate between alkene and hydroxy sulfonate, as one would expect. All species show what might be called classical phase behavior in that, at low salinities, surfactant is partitioned into water, therefore forming an oil-in-water microemulsion, whereas at intermediate and high salinities partitioning is such that middle phase and oil phase microemulsions are formed, respectively.

All three surfactants are seen in Figure 1 to be very electrolyte tolerant. The salt tolerance is greatest for the hydroxy sulfonate, followed by the α-olefin and, finally, the alkene sulfonate. Moreover, it is significant to note that the optimum salinities for alkene and hydroxy sulfonates are very different. At ACN 10, for example, optimum salinities are 7.2 gpdl and 16.5 gpdl for the alkene and hydroxy species, respectively. This difference in optimum salinity could alternately be attained by adding approximately 5 methylene groups to the hydrophobic chain of the hydroxy

species,[6] or, more generally, by an increase of 2.3 units of the surfactant HLB. Alternately, if one assumes that the effect of the unsaturated group on alkene sulfonates is small,[7] and therefore that the shift in optimum salinities in going from alkene to hydroxy sulfonate is due solely to an addition of the hydroxy group to the surfactant, one finds good agreement between the results obtained here and one based on group HLB values of Davies,[8] wherein he assigns a value of 4 methylene groups as the equivalent of a single hydroxy group.

An examination of Figure 1 shows also that the optimum salinity is linearly related to the EACN in the range of salinities studied. The slopes $\Delta S/\Delta EACN$ for the optimum lines are 0.8, 0.97 and 1.08 gpdl/methylene group for alkene, α-olefin and 3-hydroxy sulfonates respectively.

Additional optimum phase behavior under different conditions is shown in Figure 2 for the previous three surfactants as well as for a C_{20} α-olefin sulfonate. The linear relationship still holds and $\Delta S/\Delta EACN$ ranges from 0.8 at low salinities to 1.36 at higher salinities.

Earlier investigations on anionic surfactants, namely alkylbenzene sulfonates, alkyl orthoxylene sulfonates and petroleum sulfonates,[9] have shown linearity between EACN and log S. However, those studies were seldom performed at NaCl concentrations greater than 5 gpdl. We have good reason to believe that if an α-olefin sulfonate were chosen so that a study below 5 gpdl were feasible (for example, the C_{22} or C_{24} series), one would obtain a linear relationship between EACN and log S similar to previous results on other anionic surfactants.[9] However, linearity between optimum salinity and EACN for a wide range of salinities has been reported for nonionic surfactants,[10] the slope $\Delta S/\Delta EACN$ being 1.15 gpdl per methylene group for ethoxylated alkylphenols.

The data in Figure 2 do show that the optimum phase behavior covers a wide range of salinity. Therefore one is able to select the surfactant mixture needed to match a particular salt concentration between 5 and 20 gpdl NaCl by (1) changing the ratio alkene/hydroxy in the α-olefin sulfonate mixture, (2) changing the surfactant molecular weight, or (3) changing the alcohol concentration. The effect of molecular weight can be seen by comparing optimum line #1 for C_{20} α-olefin sulfonate and #5 for C_{18} α-olefin sulfonate. One estimates a preferred ACN increase of about 2.2 per unit increase in the number of methylene groups, and this is quite close to that found for increasing the tail of an alkylbenzene sulfonate.[6]

Finally, it is possible to evaluate the influence of sec C_4OH and iso C_5OH concentration on the optimum phase behavior using the data in Figure 2. Since the slope, $\Delta S/\Delta EACN$, varies, the value calculated will depend on the salt concentration and EACN considered. In order to simplify, one neglects, as a first approximation, the temperature effect on optimum phase behavior and calculates the mean value centered on n-decane. One thus obtains a shift of 2.2 and 0.5 in EACN for 1 gpdl of iso C_5OH and sec C_4OH added, respectively. The shift due to an addition of sec C_4OH is similar to a previous value of 0.4 for other anionic surfactants.[9] As for the effect of the iso C_5OH, it is smaller than a previously obtained value of 3.5 for anionic surfactants,[9] but in good agreement with a value of 2.1 obtained for nonionic surfactants.[10]

2. <u>Liquid crystal/microemulsion equilibrium</u>.

Winsor type phase behavior[11] yielding classical middle phase microemulsion as shown in Figures 1 and 2 can not always be obtained at low temperature and at low alcohol concentration. Gels and liquid crystals were found to form in systems containing small quantities of alcohol and

at low temperature. Such complex phases are often purposely suppressed by an addition of alcohol and by elevated temperature.

The data in Figure 3 display a typical phase map showing the liquid crystal regime, the microemulsion regime and the phase boundary separating the two. The numbers near the experimental data points are the salt concentrations, which required adjustment along the phase boundaries to keep the system at optimum.

At a given alcohol concentration, the system having a composition corresponding to the three phase region often underwent the following change when the temperature was increased: At low temperature, precipitates or gels were observed, followed, at intermediate values, by the formation of birefringent liquid crystals. These can be identified using cross polarizers. With further temperature increase, liquid crystals are converted into a non-birefringent microemulsion. Liquid crystals and microemulsions were found to coexist within a few °C below the phase boundary or the transition temperature, T*. At the transition temperature, T*, liquid crystals disappear completely from the system and thereafter only the classical middle phase microemulsion exists. The liquid crystals observed here solubilize a variable amount of oil but always very small quantities of water. In addition, the total amount of oil and water solubilized in the liquid crystals is always smaller than that solubilized in the corresponding middle phase microemulsion at T*.

It can be seen in Figure 3 that, upon a decrease in the sec C_4OH concentration, the transition temperature, T*, between the liquid crystal and microemulsion regimes increases rapidly with little change in optimum salinity.

Phase maps similar to the one in Figure 3 have also been observed for systems at different ACN and salt concentrations. The influence of NaCl concentration on T* was found to be small compared with the influence of the alcohol concentration. T* passes through a shallow maximum somewhere between 10 and 15 gpdl NaCl for most of the systems studied.

The influence of the surfactant structure on T* has not yet been completely defined; but qualitatively, C_{18} α-olefin sulfonate and C_{20} α-olefin sulfonate have approximately the same T* at a given salt and alcohol concentration. However, T* for C_{18} 3-hydroxy sulfonate is about 50°C higher than other surfactants at low alcohol concentration.

3. Optimum solubilization.

The results reported in this section are at temperatures greater than or equal to the transition temperature. The solubilization parameter at optimum, σ*, is defined as the volume of oil (or water) in the middle phase microemulsion per unit volume of surfactant. σ* for the three surfactants of Figure 1 and for the C_{20} α-olefin sulfonate in Figure 2 are plotted in Figure 4 for the same system conditions. The numbers near the data points are the oil phase ACNs.

One notes immediately that σ* is exceptionally high even at the high salinities studied. For instance, σ* of greater than 30 was obtained at 4, 6, 8 and 16 gpdl NaCl for C_{18} alkene sulfonate, C_{20} and C_{18} α-olefin sulfonates, and C_{18} 3-hydroxy sulfonate, respectively. For 4.5 gpdl and 12 gpdl NaCl, a σ* even greater than 50 was observed for C_{20} α-olefin and C_{18} 3-hydroxy sulfonates. In previous studies on alkylbenzene sulfonates,[4] it has been established that decreased tail branching enhanced σ*. The α-olefin sulfonates and their components which seem to have inherently high values of σ* are not branched, and thus we might expect this to be an important factor.

The solubilization parameter has also been found to increase upon an increase in the molecular weight of the surfactant for alkylbenzene sulfonate[4] and ethoxylated nonylphenols.[1] In this study, we would expect a similar result for α-olefin sulfonates. Unfortunately, the results in Figure 4 for C_{18} and C_{20} α-olefin sulfonates are insufficient to draw definite conclusions.

Pursuing the influence of surfactant structure on σ*, Figure 4 data shows also the importance of adding an -OH group (e.g., a 3-hydroxy group) to the surfactant. For the three C_{18} species all at the same given salinity, σ* increases in the order alkene, α-olefin, hydroxy sulfonates. Furthermore, σ* still increases in the same order even at constant ACN, although in this case the optimum salinity increases by 9 gpdl in going from the alkene to the hydroxy sulfonate. Nevertheless, one should remember that the hydroxy sulfonate exhibits higher transition temperatures as indicated in the previous section. Note that the 3-hydroxy and 4-hydroxy are fortunately the predominate hydroxy species in the α-olefin sulfonate by the snythesis scheme here employed. The 2-hydroxy sulfonate is known to be water insoluble[5] even at high temperature[12]; the large separation between the polar groups, sulfonate and hydroxy, among the hydrophobic moiety of the ≥5-hydroxy species may cause a loss of their amphipathic properties.

σ* at the phase boundary in Figure 3 and at the same system conditions are displayed in Figure 5. The numbers near the data points are the salt concentration and temperature. There is a marked increase in σ* at high temperature and at low sec C_4OH concentration. This increase of σ* is evidently ascribable to a decrease in the alcohol concentration and, in fact, the elevated temperature generally has a minor influence on σ*.

On the other hand, a small change in optimum salinity has a rather slight effect of σ^* regardless of the alcohol concentration.

If the alcohol concentration is decreased and compensated by an increased temperature, one expects an upward shift of the σ^* shown in Figure 4 for all salinities and surfactants. This anticipated trend is shown in Figure 6 for C_{18} α-olefin sulfonate for salinities varying from 5 to 18 gpdl and sec C_4OH concentrations varying from 1 to 4 gpdl. The oil phase ACNs are shown at each data point. The results at 1 and 2 gpdl of sec C_4OH were approximately at the microemulsion/liquid crystal phase boundary. The similar influence of iso C_5OH concentration is displayed in Figure 7 data also. From data in Figures 5, 6 and 7, it is obvious that in oder to achieve the highest possible σ^*, one should keep the quantity of alcohol in the system at the lowest possible level for a given temperature.

Experimental observation shows that the solubilization parameter and the horizontal width of the three phase regime EACN are inversely related. Figure 8 shows a plot of σ^* as a function of a reciprocal EACN taken from the boundaries of Winsor region III in Figure III. One can see that a linear relationship exists. The equation of the line is given by

$$\sigma^* = 24.7(\Delta EACN)^{-1} \qquad (1)$$

An earlier sutdy on alkylbenzene sulfonates[4] has shown the slope to be 5.5 rather than the 24.7 in equation (1). On the other hand, data points from ethoxylated nonylphenols have also been found to fall on the line in Figure 8, within experimental error. This is a further indication of the generality of a functional form similar to equation (1).

4. Tolerance to divalent ions.

Almost universally, one finds that surfactants such as petroleum sulfonates or alkylbenzene (or xylene) sulfonates precipitate out of aqueous solution or lose their activity in the presence of divalent ions. α-olefin sulfonates show a greatly reduced sensitivity to divalent ions. The data in Figure 9 display the influence of calcium ion on solubilization, transition temperature, and shift in EACN comparatively of C_{18} alkene, α-olefin and 3-hydroxy sulfonates. Precipitation has not been observed over the salinity range reported provided that the temperature is sufficiently elevated. The oil phase EACNs and corresponding T* are shown at each data point.

An addition of calcium chloride shifts EACN and T* upward and decreases σ*. Variations in EACN, T* and σ* for C_{18} α-olefin sulfonate are nearly comparable to those for 3-hydroxy sulfonate. Approximately 1 gpdl of $CaCl_2$ shifts the EACN by 2 to 3 units, which is equivalent to adding 2 to 3 gpdl of NaCl. At the same time, T* increases by 30°C. However, Figure 9 shows a much stronger effect on EACN, T* and σ* of C_{18} alkene sulfonate.

Also, it is seen in the data of Figure 9 that all the σ* values obtained are still useful in the presence of calcium ions. Note the extreme case for 3-hydroxy sulfonate where σ* of 25 was obtained at EACN ≈ 11 and 110°C in the presence of 17.5 gpdl of NaCl and 1 gpdl of $CaCl_2$.

5. Interfacial tension.

Interfacial tensions reported in Figures 10 and 11 have been measured at optimum phase behavior and therefore the interfacial tensions of the oil/microemulsion interface and the water/microemulsion interface are equal. These tensions are denoted as γ* by analogy with solubilization at optimum σ*. Figure 10 data display γ* versus NaCl concentration for C_{18} alkene sulfonate under system conditions similar to those of Figure 1. The numbers

at each data point are the oil phase ACNs. Figure 11 data show γ^* versus sec C_4OH concentration for C_{18} α-olefin sulfonate under the same conditions given in Figure 3. The numbers near the data points are optimum saltinities and temperature. By comparing the data of Figures 10 and 4, and also the data of Figures 11 and 5, one notes immediately that α^* and γ^* are inversely related. Huh[13] has recently predicted that for a particular microemulsion

$$\frac{\gamma^*\alpha^{*2}}{\cos \pi/4} = \text{constant} \qquad (2)$$

middle phase model. This theory has been experimentally verified for alkylbenzene sulfonates[4] and ethoxylated alkylphenols.[1] The constants were found to be 0.48 ± 0.06, respectively. When the results on α^* and γ^* for α-olefin sulfonates are combined, one finds a constant of 0.4 ± 0.15, in good agreement with previous results. Nevertheless, the values of the constants are moderately scattered, and this was expected because most of the interfacial tensions reported here were obtained at temperatures greater than ambient, which greatly complicates measurement of γ^*. For instance, interfacial tension measurements have not been performed on C_{18} 3-hydroxy sulfonate because of the large experimental uncertainties at high temperature. But one would predict quite small values for γ^* if the measured σ^*s were used in equation (2).

In summary, the results of this study together with earlier results on alkylbenzene sulfonates and ethoxylated alkylphenols provide solid evidence for the generality of the Huh relationship between γ^* and α^*.

CONCLUSIONS

1) The C_{18} and C_{20} α-olefin sulfonates, as well as their components, the alkene and hydroxy sulfonates, all appear to be potential candidates for oil recovery.

2) The hydroxy, at least the 3- or 4- species, is more water soluble than the alkene species with the α-olefin sulfonate being intermediate between the two.

3) The hydroxy sulfonate has a greater tendency to form liquid crystals, therefore requiring a higher temperature to give a phase transition to microemulsion.

4) As previously found, the width of the three phase regime is inversely related to solubilization parameter at optimum.

5) Also as previously found, alcohol can destroy liquid crystals at sufficiently high temperature.

6) Optimum ACN is linearly related to optimum salinity as found for nonionic surfactants.

7) Large optimum solubilization parameters and low interfacial tensions can be obtained with all species.

8) The tolerance to electrolyte and especially Ca^{++} is very good, being in the order hydroxy (best), then α-olefin, and finally alkene sulfonate.

9) σ^{*2} and γ^* bear the same relationship as for the alkylbenzene sulfonates and the ethoxylated alkylphenols.

FIGURES

Figure 1. Phase behavior for the systems as noted. Lines with data points are the optimum lines and the other lines are the extrem of the three phase regions.

Figure 2. Optimum phase behavior lines for the systems as noted.

Figure 3. Phase map showing transition line between liquid crystal state (below line) and microemulsion state (above line). Numbers by data points are the optimum ACNs for the system conditions as noted.

Figure 4. Phase map showing transition lines between liquid crystal state (below lines) and microemulsion state (above lines). Numbers by data points are the optimum ACNs for the system conditions as noted.

Figure 5. Solubilization parameter as a function of alcohol concentration for system conditions as noted.

Figure 6. Optimum solubilization parameter versus concentration of NaCl for a variety of sec butanol concentrations.

Figure 7. Optimum solubilization paramenter versus NaCl concentration for two isopentanol concentrations.

Figure 8. Solubilization parameter versus reciprocal width of the three phase regime for various salinities.

Figure 9. Solubilization parameter versus $CaCl_2$ concentration for the C_{18} α-olefin sulfonate and its components for the conditions as noted.

Figure 10. Optimum interfacial tension versus salinity for C_{18} alkene sulfonate for the conditions noted.

Figure 11. Optimum interfacial tension versus concentration of alcohol for C_{18} α-olefin sulfonate for the conditions as noted.

REFERENCES

1. A. Graciaa, L. N. Fortney, R. S. Schechter, W. H. Wade, and S. Yiv, "Criteria for Structuring Surfactants to Maximize Solubilization of Oil and Water I: Commercial Nonionics", SPE 9815.

2. A. Graciaa, J. Lachaise, J. G. Sayous, P. Grenier, W. H. Wade, R. S. Schechter and S. Yiv, "The Partitioning of Complex Surfactant Mixtures Between Oil/Water/Microemulsion Phases at High Surfactant Concentration", J. Coll. and Interface Sci., 93, 474 (1983).

3. a) D. W. Dycus, E. W. Malmberg and H. L. Winchester, U.S. Patents 3827497 and 3890239.

   b) W. W. Gale, R. K. Saunders and T. L. Ashcraft, Jr., U.S. Patent 3977471.

   c) K. H. Fluornoy, R. L. Gardenas, G. L. Haferkampf and R. D. Shupe, U.S. Patent 3811505.

   d) K. H. Fluornoy and R. D. Shupe, U.S. Patent 3811507.

   e) J. Reisberg, J. B. Dawson and G. Smith, U.S. Patent 3508612.

   f) K. H. Fluornoy, K. Maddox, Jr. and J. F. Pate, U.S. Patent 3858656.

   g) K. Maddox, Jr. and R. D. Shupe, U.S. Patent 4077471.

   h) V. H. Schievelbein, U.S. Patent 4307782.

4. Y. Barakat, L. N. Fortney, R. S. Schechter, W. H. Wade, S. H. Yiv and A. Graciaa, "Criteria for Structuring Surfactants to Maximize Solubilization of Oil and Water II: Alkylbenzene Sodium Sulfonates", J. Coll. -d Interface Sci., 92, 561 (1983).

5. A. F. Turbak and J. R. Livingston, "Reaction of Phosphate-Complexed Sulfur Trioxide with Alpha-Olefins", Ind. Eng. Chem. Prod. Res Dev. 2 (1963)229.

6. A. Graciaa, Y. Barakat, M. El-Emary, L. N. Fortney, R. S. Schechter, S. Yiv and W. H. Wade, "HLB, CMC and Phase Behavior as Related to Hydrophobe Branching", J. Colloid Int. Sci., J. Coll. and Interface Sci., 89, 209 (1982).

7. Preliminary results show that C_{18} alkene sulfonates and primary C_{18} alkane sulfonates exhibit nearly the same optimum salinity, suggesting therefore a small effect of double bond on optimum salinity.

8. J. T. Davies, "A Quantitative Kinetic Theory of Emusion Type, I. Physical Chemistry of the Emulsifying Agent", Proc. 2nd Intern. Congr. Surface Activity Vol. I (London, 1957) 426.

9. J. L. Salager, J. C. Morgan, R. S. Schechter, E. Vasquez and W. H. Wade, "Optimum Formulation of Surfactant-Oil-Water Systems for Minimum Interfacial Tension or Phase Behavior", Soc. Petr. Eng. J. 19(1979)107.

10. M. Bourrel, J. L. Salager, R. S. Schechter and W. H. Wade, "A Correlation for Phase Behavior of Nonionic Surfactants", J. Colloid Int. Sci. 75 (1980).

11. P. A. Winsor, "Solvent Properties of Amphiphilic Compounds". Butterworths, London (1954).

12. U. Weerasooriya, Department of Chemistry, University of Texas at Austin, private communication.

13. C. Huh, "Interfacial Tensions and Solubilizing Ability of a Microemulsion Phase that Coexists with Oil and Brine", J. Colloid Int. Sci. 71 (1979)408.

ACKNOWLEDGMENTS

This research has received financial support from the following organizations and companies: The Robert A. Welch Foundation, the Department of Energy, the National Science Foundation Chevron, Gulf, Tenneco, Arco, Witco, Shell, Mobil, Elf-Aquitane, Conoco, Union Oil, Texaco, Exxon, Sun, Amoco, Dowell, British Petroleum, TOTAL CFP, Getty and GAF.

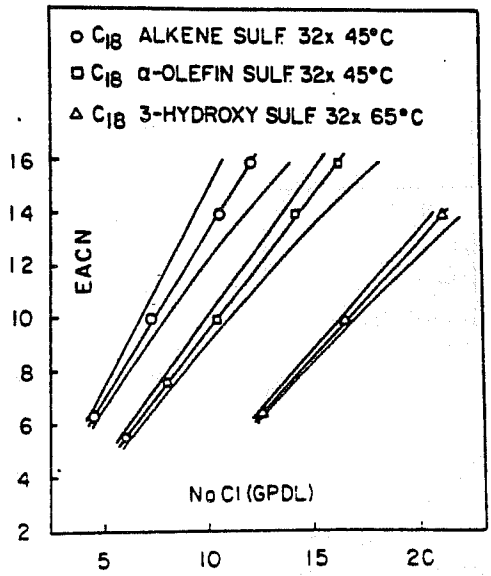

Figure 1. Phase behavior for the systems as noted. Lines with data points are the optimum lines and the other lines are the extrema of the three phase regions.

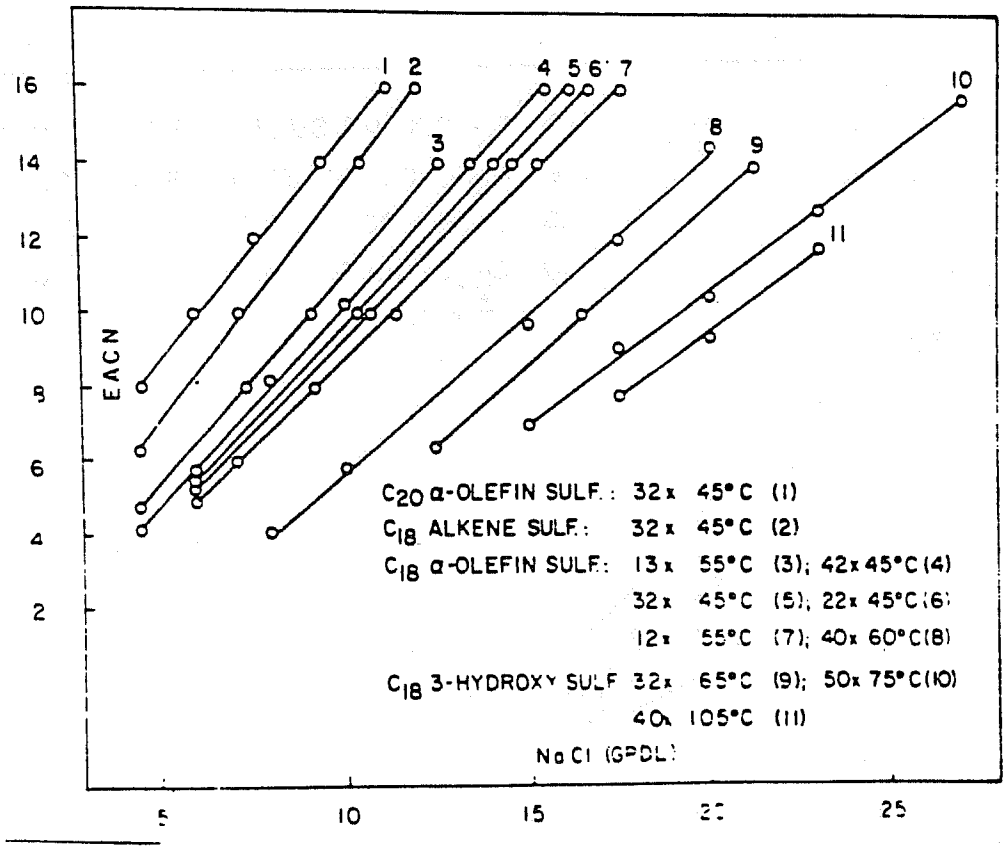

Figure 2. Optimum phase behavior lines for the systems as noted.

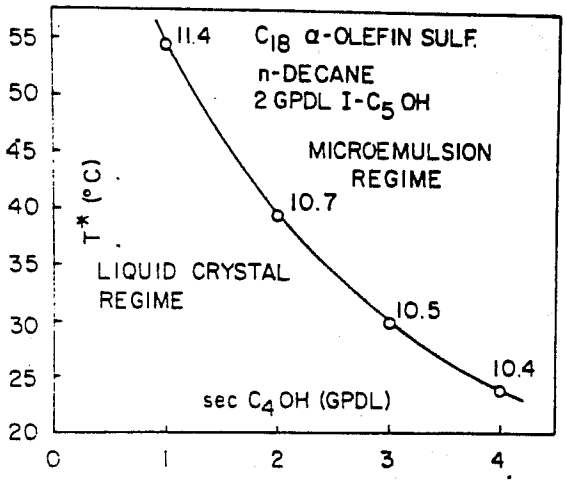

Figure 3. Phase map showing transition line between liquid crystal state (below line) and microemulsion state (above line). Numbers by data points are the optimum ACNs for the system conditions as noted.

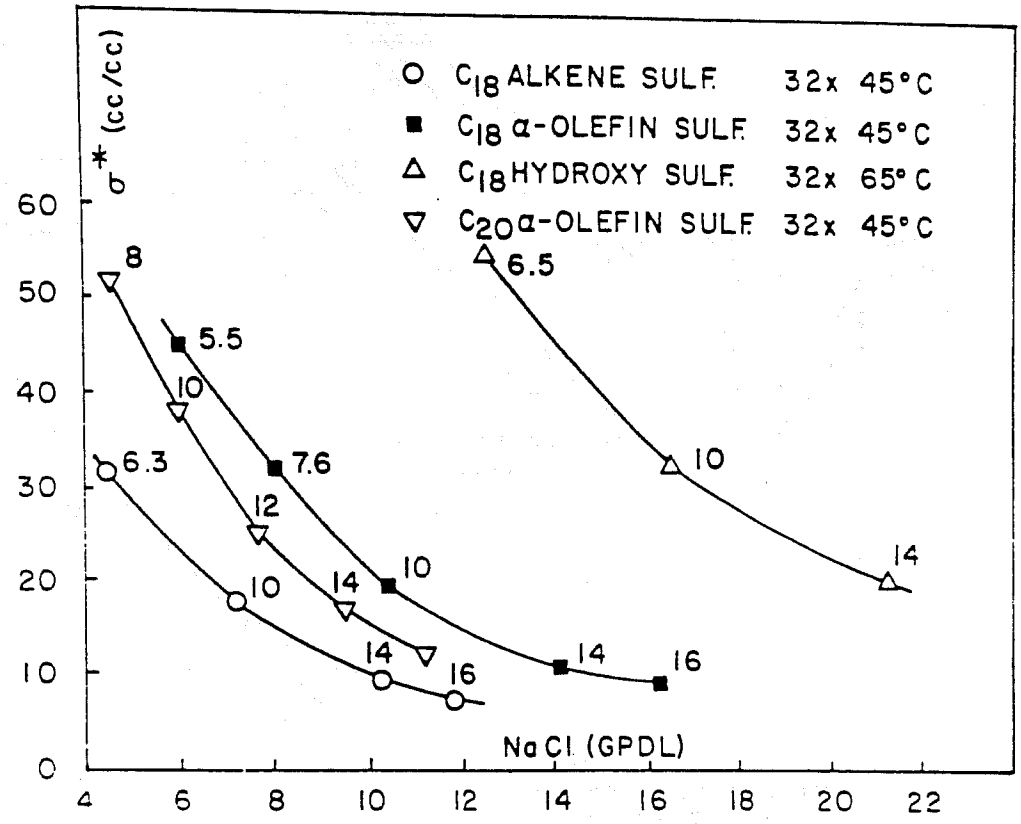

Figure 4. Phase map showing transition lines between liquid crystal state (below lines) and microemulsion state (above lines). Numbers by data points are the optimum ACNs for the system conditions as noted.

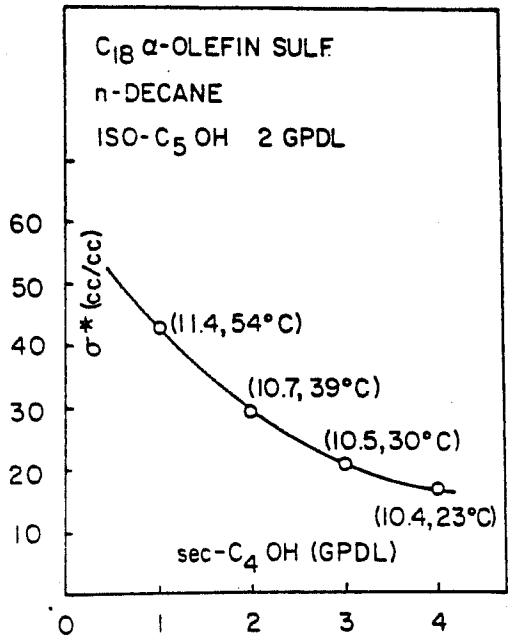

Figure 5. Solubilization parameter as a function of alcohol concentration for system conditions as noted.

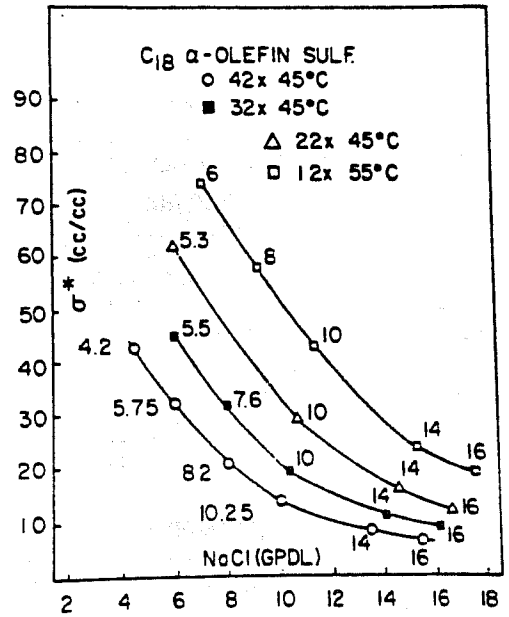

Figure 6. Optimum solubilization parameter versus concentration of NaCl for a variety of sec butanol concentrations.

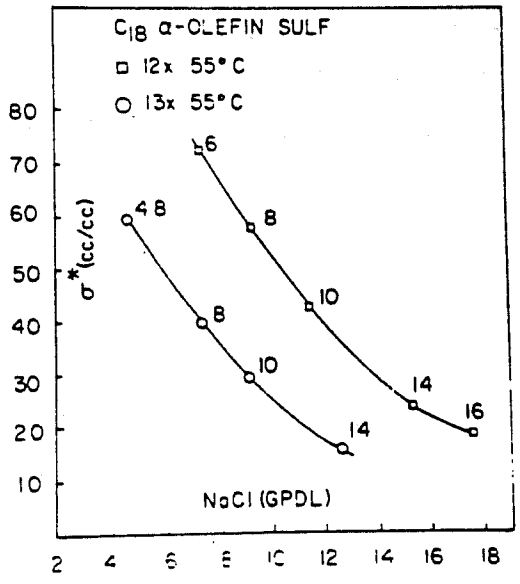

Figure 7. Optimum solubilization parameter versus NaCl concentration for two isopentanol concentrations.

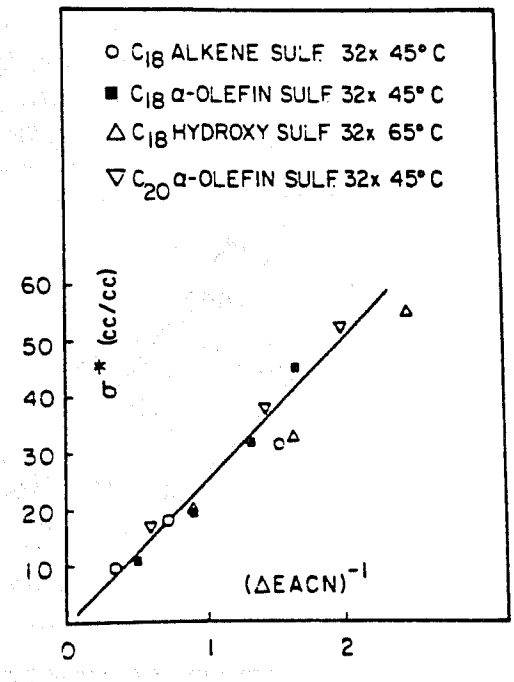

Figure 8. Solubilization parameter versus reciprocal width of the three phase regime for various salinities.

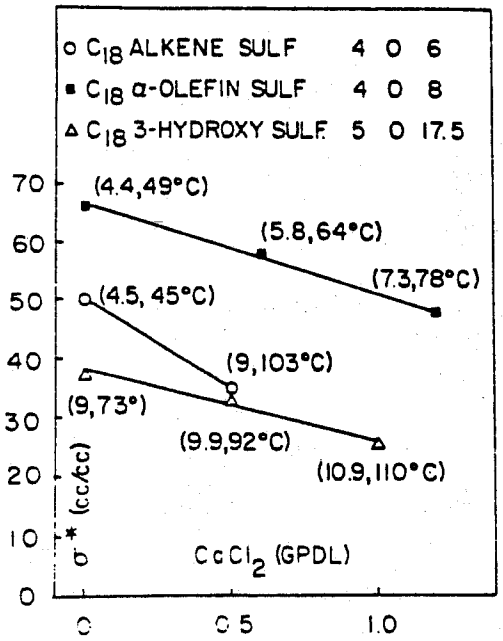

Figure 9. Solubilization parameter versus $CaCl_2$ concentration for the C_{18} α-olefin sulfonate and its components for the conditions as noted.

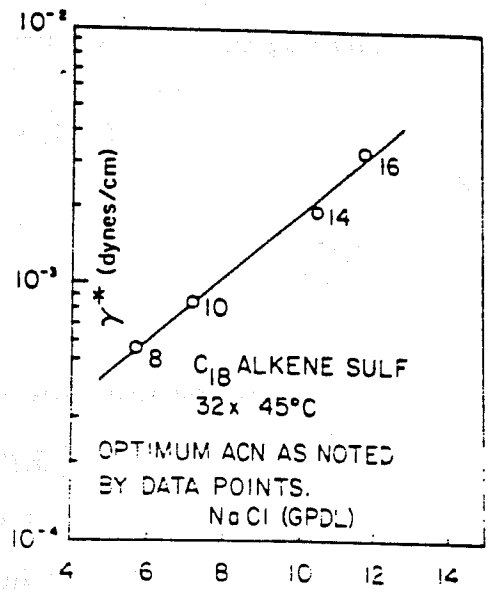

Figure 10. Optimum interfacial tension versus salinity for C_{18} alkene sulfonate for the conditions noted.

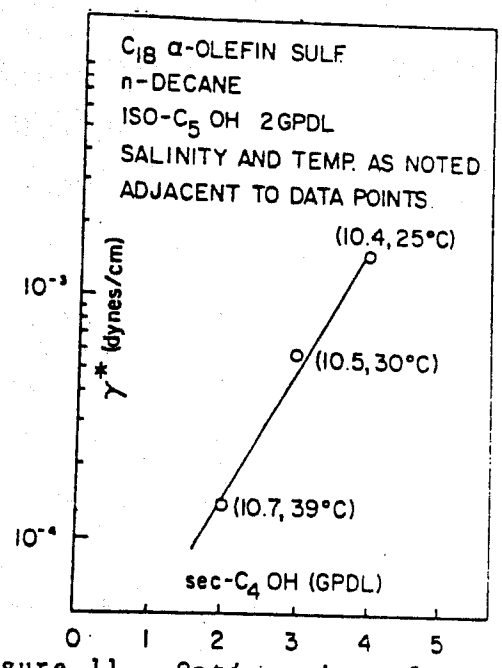

Figure 11. Optimum interfacial tension versus concentration of alcohol for C_{18} α-olefin sulfonate for the conditions as noted.

ETHOXYLATED OLEYL SULFONATES AS MODEL COMPOUNDS FOR ENHANCED OIL RECOVERY

by

I. Carmona, R. S. Schechter, W. H. Wade, and U. Weerasooriya

Department of Chemistry

University of Texas

Austin, Texas 78712

ABSTRACT

Precisely ethoxylated oleyl sulfonates were prepared and studied as model surfactant candidates for enhanced oil recovery. They were found to yield low interfacial tensions, give high solubilization parameters, and have high electrolyte tolerance. Unfortunately, as a class of compounds they have a tendency to form liquid crystals (rather than microemulsions) which must be overcome by addition of cosolvents, elevated temperatures, or restriction to the maximally ethoxylated species.

INTRODUCTION

The primary requirement for any surfactant to be considered as a possible candidate in enhanced oil recovery processes is its ability to form systems with ultra low interfacial tensions between immiscible phases.[1,2] To this requirement others must be added: minimal alcohol concentrations, good electrolyte tolerance (especially including multivalent cations such as Ca^{++} and Mg^{++}), and finally, maximal values of solubilization parameter.[3]

Many ethoxylated species which satisfy the required tolerance to electrolyte have been studied in this laboratory; however, the species investigated have not been found to give interfacial tensions or solubilization parameters of as good quality as those found for many sulfonates.

The commercially available species similar to the ones reported here have several disadvantages: (1) they exist only as sulfates, and these species hydrolyze at elevated temperatures; (2) there is a Gaussian distribution of ethylene oxide numbers (EON) which causes partitioning complications;[6] and (3) there is less than perfect knowledge of the structure of the hydrophobic tail. The purpose of this study is to remove the three above-mentioned complications through the use of a monoisomeric ethoxylated sulfonate species, in particular 1-oleyl sulfonate with 1, 2 or 3 moles of ethylene oxide (EO) added between the oleyl and sulfonate groups. The species were chosen for two additional reasons. First, earlier results on alkylbenzene sulfonates indicated that straight tailed hydrophobes maximized solubilization parameter,[11] and second, there is little information available on the effect of the benzene rings in the molecule on its enhanced oil recovery properties. In our report a shorthand notation will be used for the structure

$$C_8H_{17}\text{-}CH=CH\text{-}C_8H_{16}\text{-}(OCH_2CH_2)nSO_3Na$$

where n = 1,2,3. The molecules will simply be referred to as n = 1, n = 2, n = 3.

EXPERIMENTAL

The synthesis of these species will be described elsewhere,[12] but a brief description follows. The appropriate alcohol was converted to the sodium salt, which in turn was reacted with 2-bromoethane sodium sulfonate

$$ROH + NaH \xrightarrow[\text{THF},\Delta]{} R\bar{O}Na^{+} + H_2 \uparrow$$

$$R\bar{O}Na^{+} + BrCH_2CH_2SO_3.Na \xrightarrow[\Delta]{-NaBr} ROCH_2CH_2SO_3Na \qquad (1)$$

and the sulfonate was isolated and purified by an extraction procedure using $IPA/H_2O/Na_2CO_3$ with a final yield of approximately 70%. For the n = 1 species, the starting alcohol was oleyl alcohol; for both the n = 2 and n = 3 species, oleyl alcohol was first converted to the tosylate and then reacted with dihydroxy alcohols prior to sulfoethoxylation.

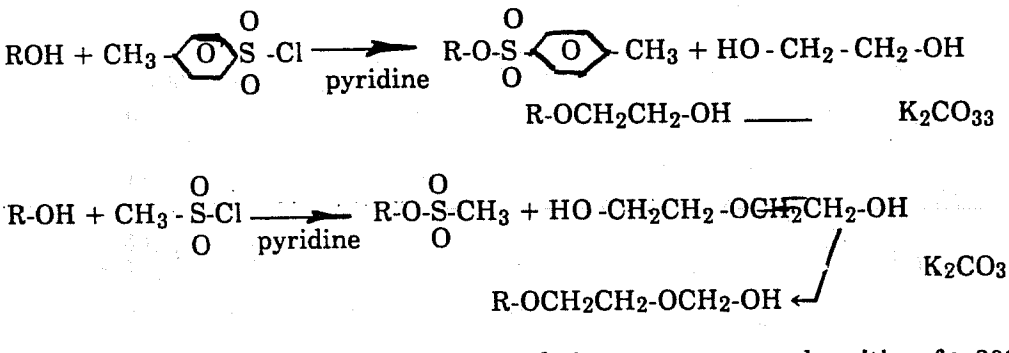

(2)

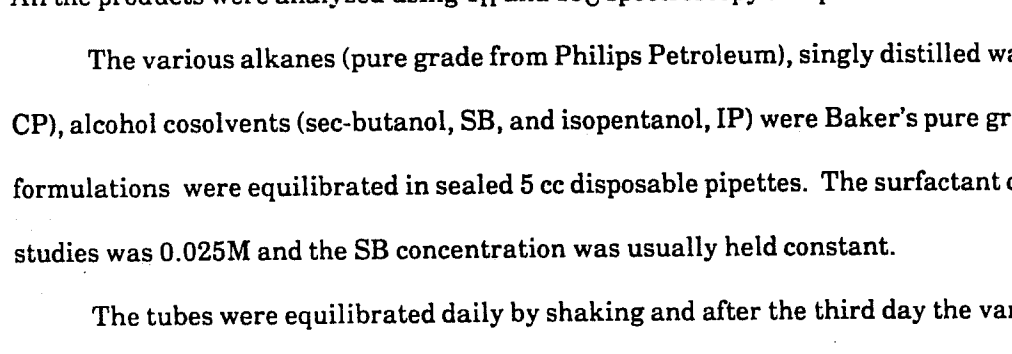

(3)

All the products were analyzed using 1_H and 13_C spectroscopy and purities of >90% were determined.

The various alkanes (pure grade from Philips Petroleum), singly distilled water, NaCl (Baker's CP), alcohol cosolvents (sec-butanol, SB, and isopentanol, IP) were Baker's pure grade. Surfactant formulations were equilibrated in sealed 5 cc disposable pipettes. The surfactant concentration in all studies was 0.025M and the SB concentration was usually held constant.

The tubes were equilibrated daily by shaking and after the third day the various phase volumes were found to no longer change with time. All the solubilization parameters reported here are for optimal systems (equal water and oil solubilized) and were calculated assuming that all the surfactant but none of the alcohol was in the middle phase. Furthermore, in this study the concentrations of surfactant, NaCl, $CaCl_2$ and alcohol are based on the initial aqueous phase volume

and the water/oil ratio was always one. As found earlier,[5,13] optimal formulations had minimal phase equilibration times and this was often used to preliminarily identify such systems.

RESULTS AND DISCUSSION

1. Effect of Temperature on Phase Behavior

Two standard methods have previously been employed to examine the effect of temperature on phase behavior: (1) studying its effect on optimal salinity , and (2) studying its effect on optimal ACN. We have chosen to do the latter. The alcohol concentration chosen for this study was sufficiently high to destroy any liquid crystal or surfactant aggregations over the entire ACN/temperature range studied.

In Figure 1, the optimal ACN is reported for all three species over the temperature interval 24-70°C with the system conditions as noted. All three surfactant species show an increase in optimal ACN with increased temperature. The n=2 and n=3 species have approximately the same temperature coefficient, ACN/T = 0.06 and the n=1 species is significantly smaller at 0.02. The positive value of this coefficient is that expected for nonionic surfactants and is synonymous with increased temperature favoring partitioning into the oil phase. Data from an earlier study[8] are reproduced for an ethoxylated alkylphenol which has a thermal coefficient of 0.47, illustrating this latter point. The magnitude of these coefficients indicates that the ethoxylated sulfonates are intermediate in character between the pure nonionics and the pure sulfonates, for which the temperature coefficient is small and often negative in sign.

Unfortunately, these studies could not be performed under the same system conditions because of the large variation in head group polarity, but one notes from the figure that for the n=2 species, salinity has no effect on thermal coefficient. Moreover, it is worthwhile to note that the n=1 species does have a very small temperature coefficient; this might be of some practical importance.

2. Precipitation and Liquid Crystal Formation

As noted earlier, the most desirable systems for EOR would have minimum alcohol requirements. Unfortunately, the removal of alcohol routinely leads to either surfactant precipitation, liquid crystal formation, or generally complex phase behavior. Thus it is generally

considered necessary for surfactants to form microemulstions, and it was therefore necessary to map the phase boundary separating the liquid crystal and microemulsion regimes.

Data are given in Figure 2 for the n=1 species and in Figure 3 for the n=3 species. In both figures, one sees the behavior noted earlier[14] for alpha olefin sulfonates, namely the diminished alcohol requirement with higher equilibration temperature. For the n=1 species, the concentration of isopentanol was varied, causing a dramatic shift in optimal ACN. This is less than desirable since the alkane itself can affect liquid crystal formation.

The study presented in Figure 3 for n=3 eliminates this complication since the alcohol, whose concentration was varied, was secondary butanol. As noted earlier,[15] this alcohol has little influence on optimum formulation. One sees that the preferred alkane changes by only 0.5 unit over the temperature interval studied. Nevertheless, the trend is the same for both studies.

The phase transition temperatures, although not obvious from intercomparing Figures 2 and 3 because of system differences, are significantly less for the n=3 species than for the n=1 species. This is buttressed by the data in Table 1, wherein transition temperatures are reported at constant salinity with a variation only in ACN. There one clearly sees the lowering of alcohol requirements as more EO is added to produce the n=2 and n=3 species. As a preview of results which will appear in more detail later, it is possible to obtain solubilization parameters of 75 cc/cc for the n=3 species with a salinity of 15 gpdl and 1.25% sec butanol with hexane as the oil phase at 100°C.

It was observed that the phase transition lines were not a strong function of salinity. However, the uniform trend is that increased salinity leads to increased phase transition temperatures, the extent being approximately 10°C over the range of salinities studied.

All of the above are consistent with the system variables of temperature, alcohol concentration, salinity, and ethylene oxide content affecting lateral interactions between surfactant molecules, as recently discussed.[14,16] Liquid crystals or "condensed structures" are inherently more ordered than microemulsion droplets and thus exist at temperatures below the phase transition line, i.e., the conversion is always more ordered to less ordered with increased temperature. The addition of alcohol or bulky EO groups physically separates the molecules and reduces van der Waals

interactions between molecules. Reduced electrolyte concentration increases the half thickness of the electric field around the polar heads and thereby increases the electrostatic repulsion between surfactant molecules. All three of the modifications would reduce phase transition temperature akin to the freezing point depression of a solvent by added solute. This is in fact the observed behavior for these system variables.

One final observation in regard to the n = 3 species is that it would probably function at salinities too high for many applications. The salinity requirements can be lowered by addition of methylene groups to the hydrophobe tail. Unfortunately, this by itself would probably raise the phase transition temperature, which is already high for many applications if minimal alcohol concentrations are desired.

3. Phase Behavior and Solubilization Parameters

Figure 4 shows the optimum phase behavior for n = 1 at four alcohol concentrations. In general agreement with earlier reported results on anionics,[15] the salinity requirements are approximately doubled when 3 gpdl of IP are removed. Although the surfactant has only one EO, it tolerates very high salinities, ranging up to 16 gpdl. Temperatures in the plat refer to the transition one in each case. To span the alcohol concentration range shown and yet remain in the microemulsion regime required elevated temperatures as noted for the two lowest IP concentrations. A general linear relationship bestween ACN and lnS* was found and the slope $\Delta \ln S / \Delta$ ACN = 0.12 was observed at > 5 gpdl and was found to be independent of alcohol concentration. The slope value is somewhat lower than the 0.16 reported for the anionic surfactants.[15] The optimal solubilization parameters are presented in Figure 5 with the exception of the 0 gpdl IP. This was done so that the systems shown in Figure 5 could be compared at the constant temperature of 40°C. The dotted lines represent approximate paths of constant ACN. On these lines one can see the amount of salt needed to compensate for alcohol in the middle phase formation, as one could similarly observe for moving vertically in Figure 4. However, more information is contained in Figure 5, wherein one sees that adding salt to replace alcohol yields systems with higher solubilization parameters, the effect being more profound at lower salinities or lower ACNs.

The data presented in Figures 4 and 5 were for the n=1 species; Figure 6 compares the phase behavior of all three surfactant species at two different alcohol concentrations. One notes that at constant ACN, optimal salinity is not linearly dependent on EON. Secondly, the effect of IP on optimal salinity is quantitatively the same for all three species. Thirdly, the n=2 and n=3 species do not obey the Salager equation [15] predicting that optimal ACN will be logarithmically related to optimal salinity

$$\ln S^* = K(ACN) + f(A) - KN_{min} \tag{4}$$

where f(A) is a near-linear function of alcohol concentration and N_{min} is characteristic of the surfactant. Rather, the phase behavior of the two species can be better represented by the Bourrel equation[8]

$$a - EON = K'ACN + \beta T + \lambda S + \ldots\ldots\ldots\ldots \tag{5}$$

as though these species were nonionics. The linear plot of s*/ACN in Figure 7 confirms this. From this plot the contribution of EO groups to the optimum formulation can be evaluated. This data is summarized in Table II. The slope $\Delta S^*/\Delta$ ACN taken at decane (because of the nonlinearity for the n=1 species) is seen here to vary from approximately 0.625 to 1.09. The value obtained for the ethoxylated alkyl phenols[8] was 1.15. At both alcohol concentrations, the addition of the second EO produces a 1.1 gpdl added NaCl requirement. Adding the third EO requires an additional 3.7 to 7.0 gpdl.

It is worth noting that the three surfactant species studied here can be used to span a salinity range of 2 to 20%. This wide range is largely due to the ability to combine the sulfonate head group with from 1 to 3 ethylene oxides. An additional advantage to these molecules, when compared with the alpha olefin sulfonates,[14] is that for chemically similar system compositions the transition from liquid crystals to microemulsion occurs at a lower temperature. Optimum solubilization parameters comparing the three different surfactant species at two different alcohol concentrations are displayed in Figure 8. These data were obtained at 40°C. The conclusions are the same as those arrived at for the data of Figure 5. One notes that very large values of solubilization parameter can be obtained at sufficiently low salinities.

During the course of the study, it was noted that phase transition temperature was sufficiently low for the n = 3 species to permit studies over a wide range of chemical compositions at 25°C. Solubilization parameters obtained in such studies are shown in Figure 9. The conclusions are the same as before.

In previous publications,[11,14] it was noted that there exists an inverse relation between solubilization parameters and width of the three phase region, width being defined as the range of ACN over which three-phase systems may be attained. To avoid confusion, the phase boundaries separating the Winsor I, II, and III systems have not been plotted for this study, but the relationship between the width, EACN, and solubilization parameter, σ^*, is shown in Figure 10. The relationship survives variations in both IP concentration and EO number. The equation of the line drawn is

$$\sigma^* = 40.3\,(\Delta EACN)^{-1} \tag{6}$$

with the slope value of 40.3 being considerably greater than the 5.5 found for alkylbenzene sulfonates and 24.7 for alpha olefin sulfonates. For a given solubilization parameter, ethoxylated oleyl sulfonates are clearly more tolerant to variations in system composition than are the alpha olefin sulfonates and especially the alkylbenzene sulfonates.

4. Divalent Ion Tolerance

For this study, the NaCl concentration was kept constant at 5 gpdl and the reported amount of $[CaCl_2]$ was that required for optimum formulation while other compositional variations were carried out. The influence of $CaCl_2$ on solubilization parameter for the n = 1 species is shown in Figure 11. Qualitatively, $CaCl_2$ has the same effect of NaCl. Increasing the $[Ca^{++}]$ shifts the alkane preference to higher values, decreasing the solubilization parameter at constant alcohol concentration. The difference is that Ca^{++} concentrations comparable to those of sodium ions have a higher phase transition temperature. From the data of Figure 11, one can see that 1 gpdl of $CaCl_2$ shifts the optimum ACN by 5 units, independent of the alcohol concentration, whereas the reported value for the alpha olefin sulfonatesis 2-3 units.[14]

Figure 12 reports a study of the influence of $CaCl_2$ concentration on optimum ACN for the three species studied. The data were taken at room temperature and the alcohol concentration was

sufficiently high to span reasonable variations in Ca^{++}. One notes the linear dependence for all three species. In addition, as expected, one observes a nonlinear tradeoff between EO number and calcium ion at constant alkane.

Finally, it is worth noting that with the n = 3 species, acceptable values for the solubilization parameter were obtained with 3 gpdl $CaCl_2$ in the system formulation.

5. Interfacial Tension

Interfacial tension measurements using the spining drop technique[17] were performed for several systems at temperatures lower than 50°C. The main purpose was to check the Chun Huh relationship[18] at optimum

$$\frac{\gamma^* \sigma^{*2}}{\cos \pi/4} = \text{constant} \qquad (7)$$

which predicts an inverse relationship between solubilization parameter, σ^*, and interfacial tension (γ^*) at optimum. The relationship was verified experimentally for systems having solubilization parameters > 40. Systems with higher values of σ^* were too delicate (temperature-wise) to successfully extract from the pipettes and load in the tensiometer. The value of the constant obtained for (7) was 0.35 +/- 0.05 for alkylbenzene sulfonates[11] and 0.34 +/- 0.06 for ethoxylated alkylphenols.[7] From eq. (7), one predicts that σ^*s of 25 and 50 cc/cc would correspond to tensions of 4 x 10^{-4} and 1 x 10^{-4} dynes/cm, respectively.

6. Summary

The molecules studied here would seem to be good model compounds for the development of commercially attractive surfactants which would function under extreme reservoir conditions. They will produce systems with good solubilization parameters at elevated temperatures and high salinity and divalent ion concentration for a variety of alkanes. On the other hand, these molecules have two deficiencies. First, if anything, the species studied are too hydrophilic for the average reservoir. Second, they have an inherently high alcohol cosurfactant requirement. From the data, it is obvious that the alcohol requirements are minimized by elevated temperatures, addition of EO, low salinity and low ACN.

7. Conclusions

1. Ethoxylanted oleyl sulfonates have many desirable features as model compounds for EOR.

2. These species are strongly hydrophilic and have very high electrolyte tolerance, even with divalent ions present.

3. The incorporation of ethylene oxide reduces alcohol requirements.

4. The n = 1 species behaves more like an anionic surfactant, where as the n = 2 and n = 3 species behave more like nonionic surfactants.

5. The liquid crystal-to-microemulsion phase transition temperature is inversely related to alcohol concentration.

6. High solubilization parameters are reciprocally related to interfacial tension via the Chun Huh relationship.

ACKNOWLEDGEMENTS

This research has been supported by the following organizations and companies: The U.S. Department of Energy, the Robert A. Welch Foundation, Amoco, Arco, British Petroleum, Chevron, Conoco, Elf-Aquitane, Exxon, Getty, Gulf, Mobil, Shell, Sun, Tenneco, Texaco, TOTAL-CFP, Union Oil, and Witco. We are grateful for their continued interest in our work.

REFERENCES

1. J. J. Taber, "Dynamic and Static Forces Required to Remove a Discontinuous Oil Phase from Porous Media Containing both Oil and Water," Soc. Petrol. Eng. J., 3, March 1969.

2. J. C. Melrose and C. F. Brander, "Role of Capillary Forces in Determining Microscope Displacement Efficiency for Oil Recovery by Waterflooding," Canadian J. Petrol. Tech. 13, 54 (1974).

3. R. L. Reed and R. N. Healy, "Some Physico-chemical Aspects of Microemulsion: A Review," in Improved Oil Recovery, D. O. Shah and R. S. Schechter, eds., Academic Press (1977).

4. A. Graciaa, Y. Barakat, M. El-Emary, L. N. Fortney, R. S. Schechter, S. Yiv and W. H. Wade, "HLB, OMC and Phase Behavior as Related to Hydrophobe Branching," J. Colloid Interface Sci. 89, 209 (1982).

5. (a) A. Graciaa, Y. Barakat, R. S. Schechter, W. H. Wade, and S. Yiv, "Emulsion Stability and Phase Behavior for Ethoxylated Nonyphenol Surfactants," J. Colloid Interface Sci. 89, 217 (1982).

   (b) H. Shinoda, H. Saito and H. Arai, "The Effect of the Size and the Distribution of the Oxyethylene Chain Lengths of Nonionic Emulsifiers on the Stability of Emulsions," J. Colloid Interface Sci. 35, 624 (1971).

6. A. Graciaa, J. Lachaise, J.-G. Sayous, M. Bourrel, R. S. Schechter and W. H. Wade, "Partage d'un Tensioactif Non-Ionique Polydistribue entre les Phases des Systemes de Winsor," ARTEP 2nd European Symposium on Enhanced Oil Recovery, Paris (November 1982). Editions Technip (Paris) p. 61.

7. A. Graciaa, L. N. Fortney, R. S. Schechter, W. H. Wade and S. H. Yiv, "Criteria for Structuring Surfactants to Maximize Solubilization of Oil and Water I: Commercial Nonionics," Soc. Petrol. Eng. J. (Octobser 1982) p. 743.

8. M. Bourrel, J. L. Salager, R. S. Schechter, and W. H. Wade, "A Correlation for Phase Behavior of Nonionic Surfactants," J. Colloid Interface Sci. 75, 451 (1982).

9. M. Bourrel, C. Koukounis, R. S. Schechter, and W. H. Wade, "Phase and Interfacial Tension Behavior of Nonionic Surfactants," J. Dispersion Sci. Tech. 1,13 (1980).

10. V. K. Bansal and D. O. Shah, "The Effect of Ethoxylated Sulfonates on Salt Tolerance and Optimal Salinity of Surfactant Formulations for Tertiary Oil Recovery," Soc. Petrol. Eng. J., 167 (June 1978).

11. A. Graciaa, L. N. Fortney, R. S. Schechter, W. H. Wade, and S. H. Yiv, "Criteria for Structuring Surfactants to Maximize Solubilization of Oil and Water. II.," J. Colloid Interface Sci. (in press).

12. W. H. Wade, U. Weerasooriya and V. Weerasooriya, manuscript in preparation.

13. M. Bourrel, A. Graciaa, R. S. Schechter, and W. H. Wade"The Relation of Emulsion Stability to Phase Behavior and Interfacial Tension of Surfactant Systems," J. Colloid Interface Sci. 72. 161 (1979).

14. Y. Barakat, L. N. Fortney, R. S. Schechter, W. H. Wade and S. H. Yiv, "Alpha Olefin Sulfonates for Enhanced Oil Recovery," ARTEP 2nd European Symposium on Enhanced Oil Recovery, Paris (November 1982). Editions Technip (Paris) p. 11.

15. J. L. Salager, E. Vasquez, J. C. Morgan, R. S. Schechter and W. H. Wade, "Optimum Formulation of Surfactant-Oil-Water Systems for Minimum Interfacial Tension or Phase Behavior," Soc. Petrol Eng. J. 19, 107 (1979).

16. M. C. Puerto and R. L. Reed, "A Three-Parameter Representation of Surfactant-Oil-Brine Interaction," SPE Preprint 10678 (1982).

17. J. L. Cayias, R. S. Schechter and W. H. Wade, "The Measurement of Interfacial Tension via the Spinning Drop Technique" ACS Symposium Series 8, Adsorption at Interfaces, 234 (1975).

18. Chun Huh, "Interfacial Tensions and Solubilizing Ability of a Microemulsion Phase that Coexists with Oil and Brine," J. Colloid Interface Sci. 71, 408 (1979).

FIGURE CAPTIONS

Figure 1. Temperature coefficient of optimum ACN for the three ethoxylated species. For comparison, data is also reproduced for an ethoxylated nonyl phenol.

Figure 2. Phase boundary separating the liquid crystal and microemulsion regimes for the n = 1 species.

Figure 3. Phase boundary separating the liquid crystal and microemulsion regimes for the n = 3 species.

Figure 4. Optimum phase behavior lines for the n = 1 species in S*/ACN* spaces for four isopentanol concentrations.

Figure 5. Optimum solubilization parameters vs. S* for the n = 1 species at three isopentanol concentrations. Dashed lines indicate constant ACN.

Figure 6. LnS*/ACN* for the n = 1, 2, and 3 species at two isopentanol concentrations.

Figure 7. The linear S* plot of Figure 6.

Figure 8. Optimum solubilization parameters for the data presented in Figure 7.

Figure 9. Additional solubilization parameters for the n = 3 species for conditions as noted.

Figure 10. The relationship between optimum solubilization parameter and reciprocal width of the 3-phase regime (ΔACN) for the n = 1 and n = 2 species.

Figure 11. The influence of $CaCl_2$ on optimum solubilization parameter for the n = 1 species at 3 alcohol concentrations.

Figure 12. Optimum ACN with concentration of $CaCL_2$ as the variable .

TABLE I

Transition Temperatures

Secbutanol 3 gpdl

NaCl 10 gpdl

EON	%IP	ACN*	Transition Temperature (°C)
1	2	15.2	<25
	1	13.1	38
	0	10.3	63
2	2	13.5	<25
	1	11.4	30
	0	8.5	35
3	2	6.3	<25
	1	4.6	<25
	0	4.1	25

TABLE II

NaCl Increment Related to EON

Under Decsane and n = 1 Basis

Isopentanol	EON	ΔS*/ΔACN	NaCl (gpdl) Increment
3	1	0.625	0
	2	0.625	1.1
	3	0.83	3.7
1	1	0.82	0
	2	0.83	1.1
	3	1.09	7.0

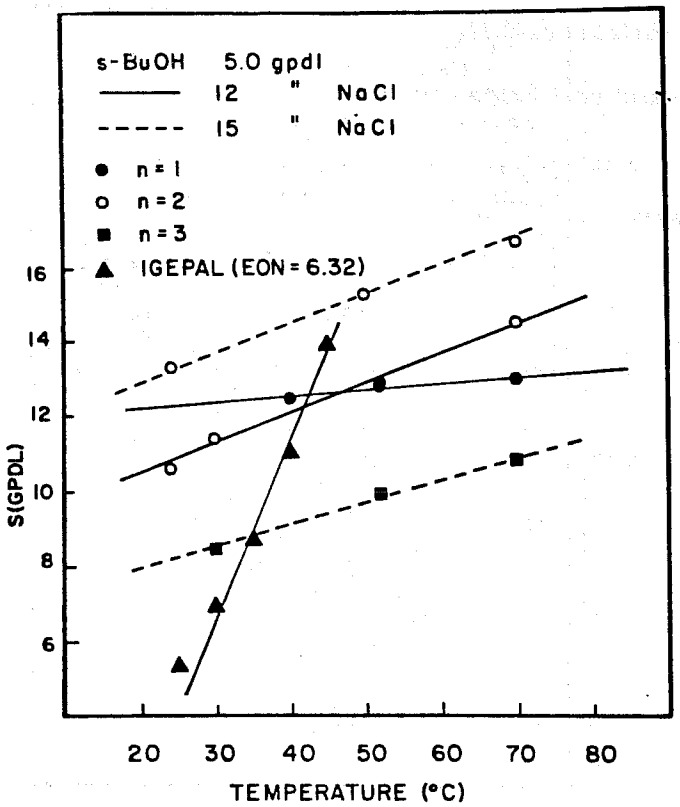
s-BuOH 5.0 gpdl
12 " NaCl
15 " NaCl
n = 1
n = 2
n = 3
IGEPAL (EON = 6.32)
S(GPDL)
TEMPERATURE (°C)

1

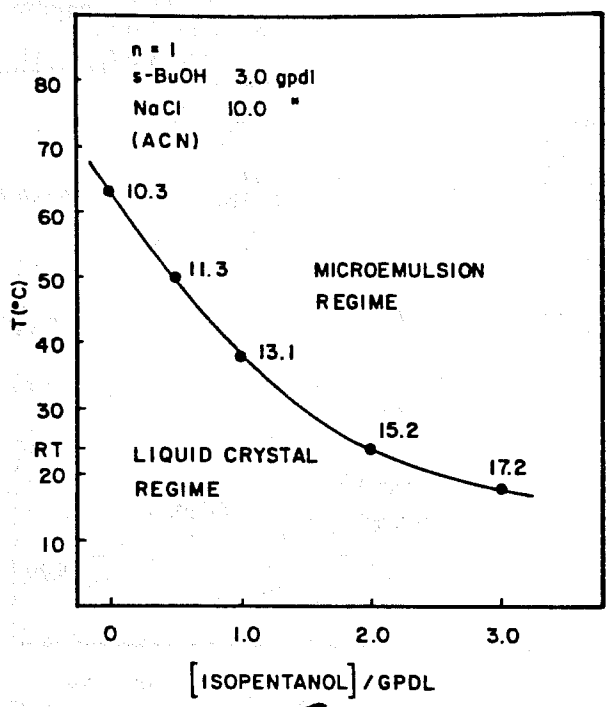
n = 1
s-BuOH 3.0 gpdl
NaCl 10.0 "
(ACN)
10.3
11.3
13.1
15.2
17.2
MICROEMULSION REGIME
LIQUID CRYSTAL REGIME
T(°C)
RT
[ISOPENTANOL] / GPDL

2

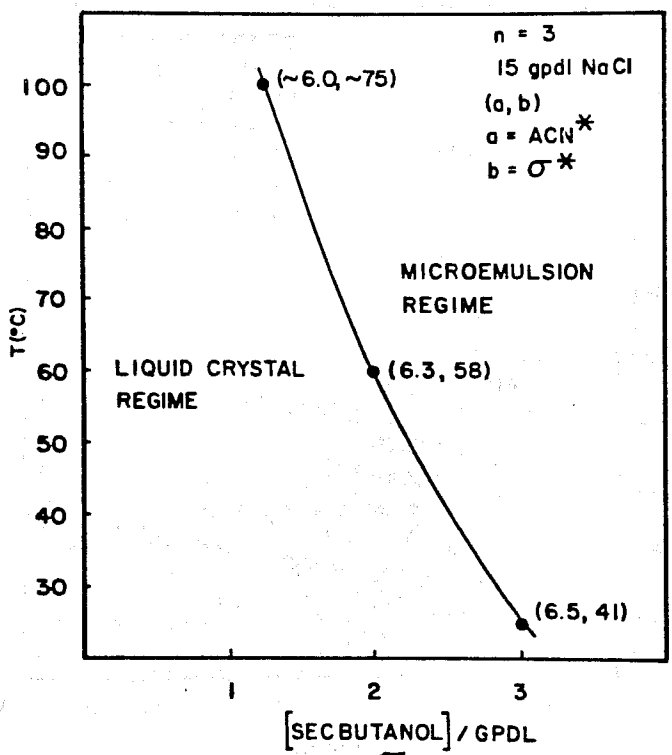
n = 3
15 gpdl NaCl
(a, b)
a = ACN*
b = σ*
(~6.0, ~75)
(6.3, 58)
(6.5, 41)
MICROEMULSION REGIME
LIQUID CRYSTAL REGIME
T(°C)
[SEC BUTANOL] / GPDL

3

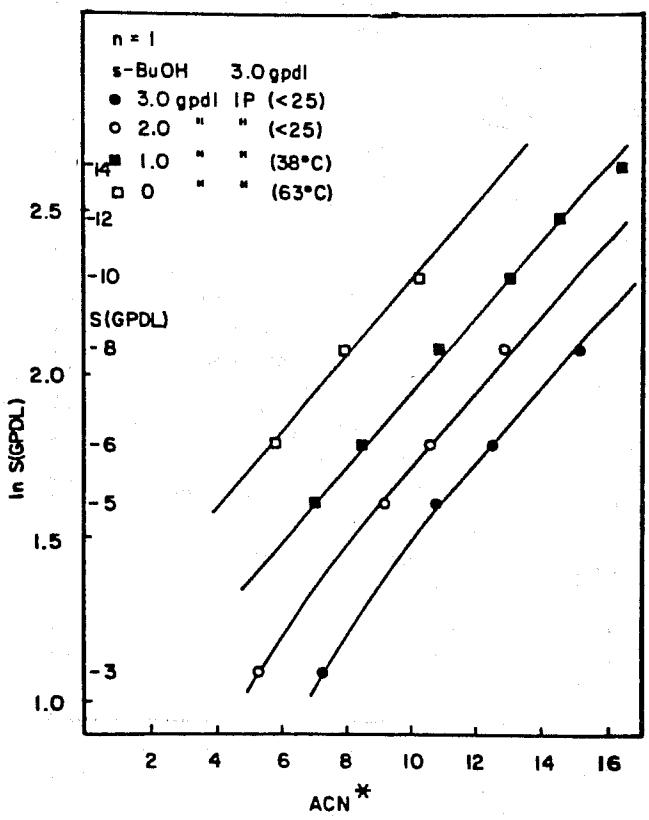
n = 1
s-BuOH 3.0 gpdl
3.0 gpdl IP (<25)
2.0 " " (<25)
1.0 " " (38°C)
0 " " (63°C)
S(GPDL)
ln S(GPDL)
ACN*

4

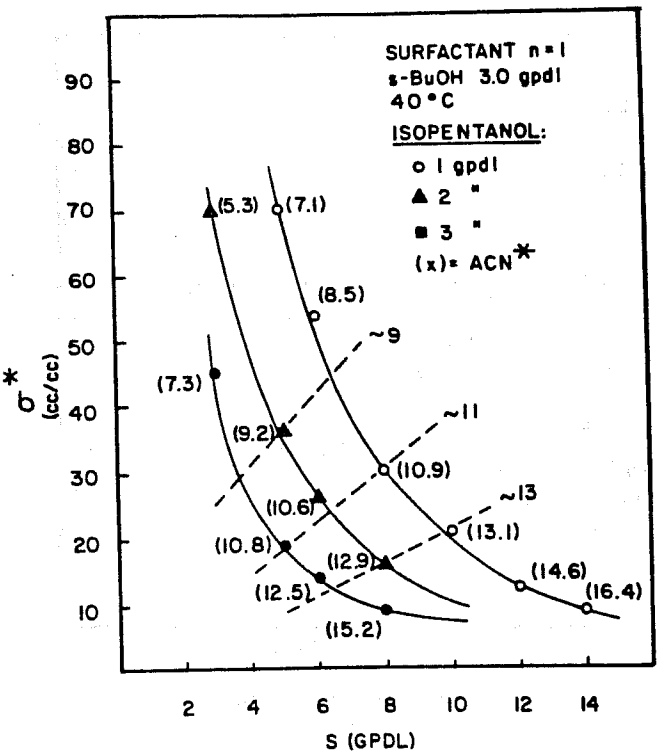
SURFACTANT n = 1
s-BuOH 3.0 gpdl
40 °C
ISOPENTANOL:
o 1 gpdl
▲ 2 "
■ 3 "
(x) = ACN*
σ* (cc/cc)
S (GPDL)
~9
~11
~13
(5.3)
(7.1)
(8.5)
(7.3)
(9.2)
(10.9)
(10.6)
(13.1)
(10.8)
(12.9)
(14.6)
(16.4)
(12.5)
(15.2)

5

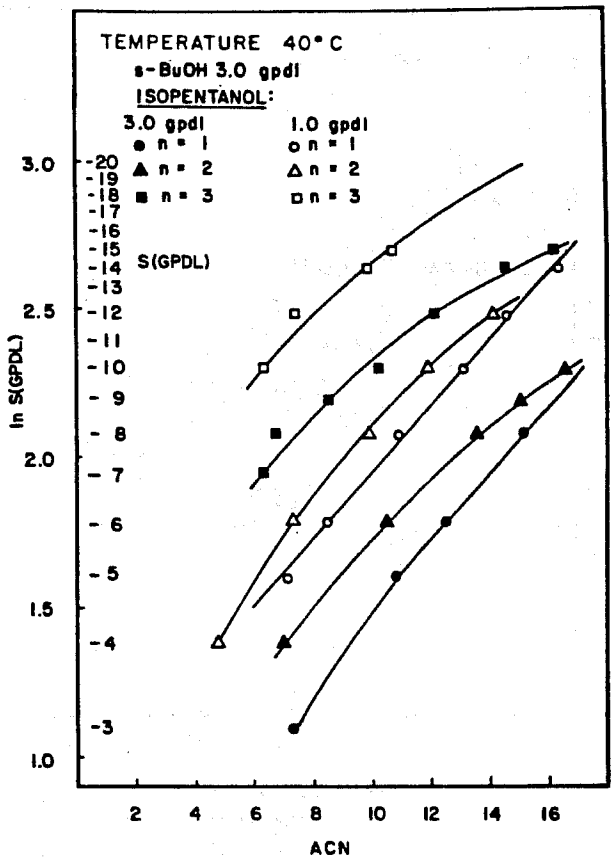
TEMPERATURE 40° C
s-BuOH 3.0 gpdl
ISOPENTANOL:
3.0 gpdl
● n = 1
▲ n = 2
■ n = 3
1.0 gpdl
o n = 1
△ n = 2
□ n = 3
S(GPDL)
ln S(GPDL)
ACN

6

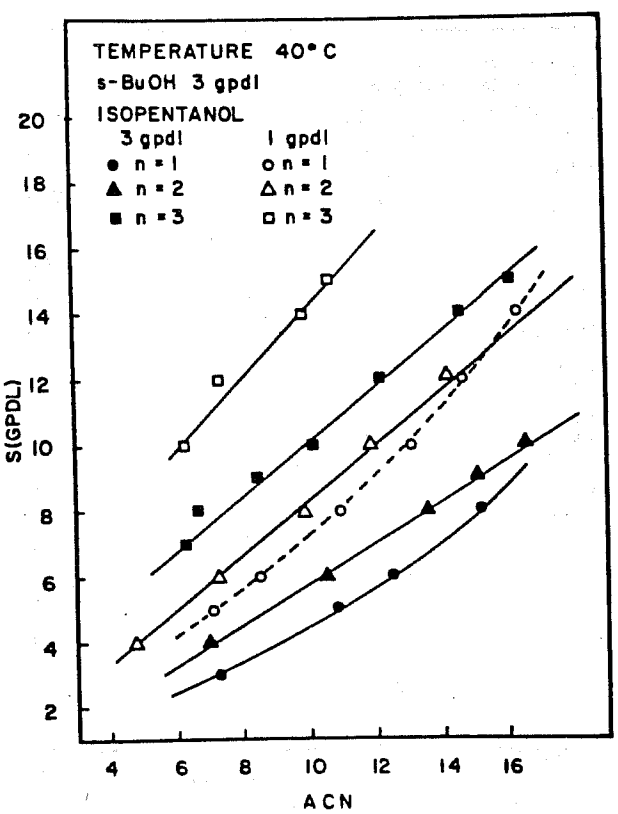
TEMPERATURE 40° C
s-BuOH 3 gpdl
ISOPENTANOL
3 gpdl
● n = 1
▲ n = 2
■ n = 3
1 gpdl
o n = 1
△ n = 2
□ n = 3
S(GPDL)
ACN

7

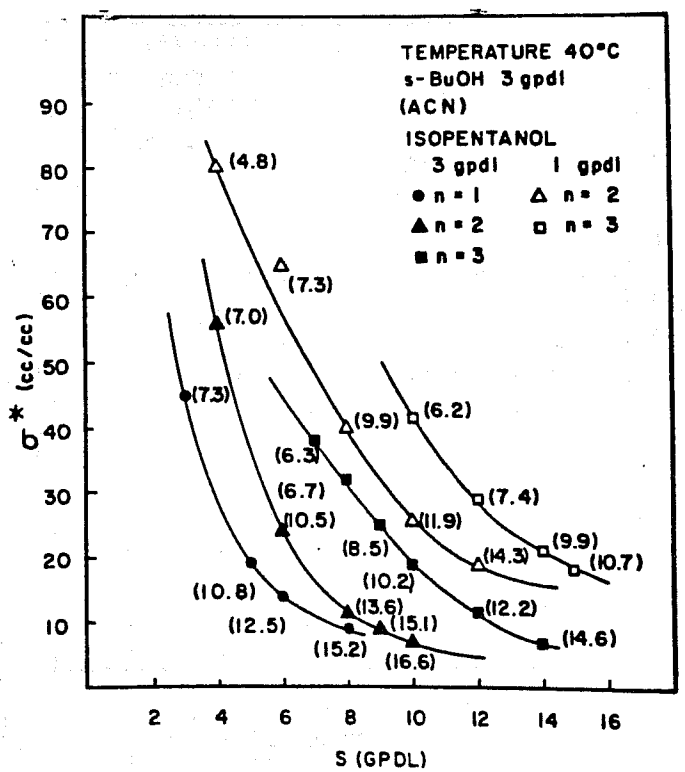
TEMPERATURE 40°C
s-BuOH 3 gpdl
(ACN)
ISOPENTANOL
3 gpdl
● n = 1
▲ n = 2
■ n = 3
1 gpdl
△ n = 2
□ n = 3
σ* (cc/cc)
S (GPDL)
(4.8)
(7.3)
(7.0)
(7.3)
(9.9)
(6.2)
(6.3)
(6.7)
(7.4)
(10.5)
(11.9)
(8.5)
(9.9)
(14.3)
(10.7)
(10.2)
(10.8)
(13.6)
(12.2)
(12.5)
(15.1)
(14.6)
(15.2)
(16.6)

8

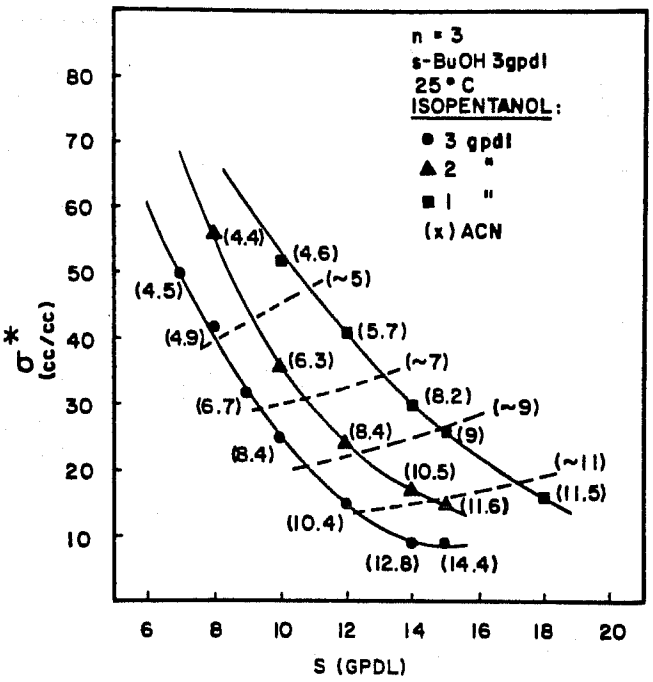
n = 3
s-BuOH 3gpdl
25°C
ISOPENTANOL:
● 3 gpdl
▲ 2 "
■ 1 "
(x) ACN
σ* (cc/cc)
S (GPDL)

9

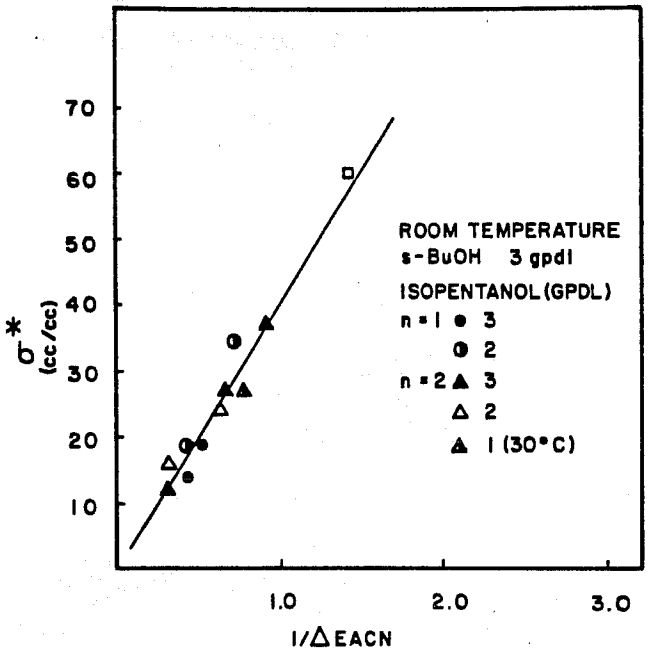
ROOM TEMPERATURE
s-BuOH 3 gpdl
ISOPENTANOL (GPDL)
n = 1 ● 3
● 2
n = 2 ▲ 3
△ 2
▲ 1 (30°C)
σ* (cc/cc)
1/ΔEACN

10

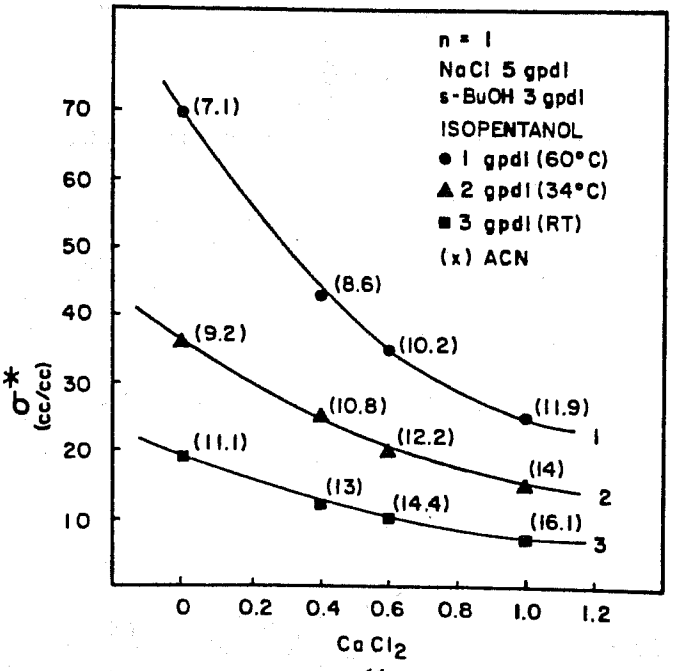
n = 1
NaCl 5 gpdl
s-BuOH 3 gpdl
ISOPENTANOL
● 1 gpdl (60°C)
▲ 2 gpdl (34°C)
■ 3 gpdl (RT)
(x) ACN
σ* (cc/cc)
CaCl2

11

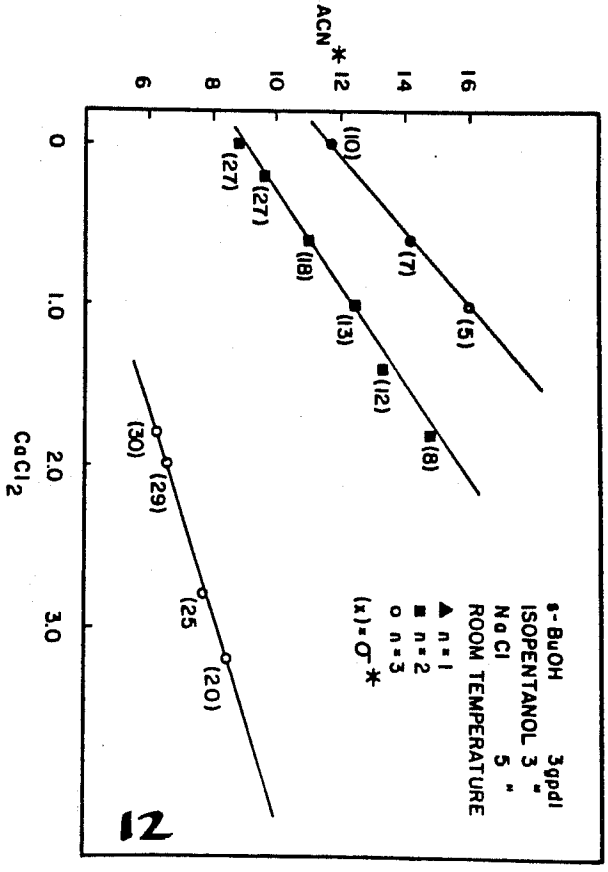
s-BuOH 3gpdl
ISOPENTANOL 3 "
NaCl 5 "
ROOM TEMPERATURE
▲ n = 1
■ n = 2
○ n = 3
(x) = σ*
ACN σ*
CaCl2

12

"The Phase Behavior of Simple Salt Tolerant Sulfonates"

by

Y. Barakat, L.N. Fortney, C. LaLanne-Cassou, R.S. Schecter
W.H. Wade, U. Weerasooriya, V. Weerasooriya and S. Yiv
The University of Texas at Austin
Austin, Texas 78712

ABSTRACT

Alkane and α-olefin sulfonates can be utilized to produce optimal microemulsion formulations having very high salinity (including divalent ion) tolerance while maintaining large solubilization parameters and low interfacial tensions. Such molecules require elevated temperatures or higher alcohol concentrations to suppress liquid crystal formation. As found for other species, solubilization is inversely related to width of the three phase regime, and interfacial tension and solubilization are strongly coupled.

INTRODUCTION

Because of their availability in commercial quantities, their ease of manufacture and their relative low cost, sulfonates, either petroleum or synthetic, were the surfactants first selected for extensive evaluation and study in polymer/micellar flooding. As the apparent surfactants of choice, they have been studied extensively in our laboratory in the past years (1-7) recently culminating in correlations which interrelate the width of the three phase region, the solubilization parameter (σ^*) and the interfacial tension (γ^*), both at optimum, for specific alkyl benzene sulfonate structures (8). In this latter study, it was found that branching in the surfactant's hydrocarbon tail influenced both σ^* and γ^* -specifically, decreasing the branching tended to increase σ^* and decrease γ^*. In other words, surfactants which have linear tails perform better if minimal interfacial tension is the prime consideration.

Other potential serious problems remain in the utilization of either petroleum or synthetic sulfonates. In particular, they will seldom tolerate salinities greater than 5% and calcium ion concentrations greater than 0.05%. This, of course, would remove many fields from consideration for surfactant flooding. One method for reducing the sensitivity of sulfonates to increased ionic strengths is to blend nonionic surfactants with the sulfonates. For this reason we have examined the relationship which exist between the structural features of polyethyleneoxide alkyl phenols and the performance of these nonionic surfactants (9-12). Although it is possible to achieve a high level of tolerance to cations, another potential problem is introduced,

namely the possible chromatographic separation of the sulfonates and nonionics (13) as well as fractionation within the nonionic species itself (14) between oil and aqueous phases. This problem has been recognized and recently a number of patents have been issued wherein the nonionic and anionic polar groups are built into the same molecule (15-22). As a specific example, octadecyl phenol first has ethylene oxide added, followed by sulfonation. Such molecules represent a new level of sophistication.

Thus the ideal surfactant system would be one which, if possible, consists of a single molecular species or of structures which are very similar so that chromatographic effects can be avoided, which will function at high ionic strength, which will tolerate divalent ions and which will exhibit reasonable, if not outstanding, performance. Such a system has not yet been reported. In this paper we shall report some results for the simplest possible surfactant structure, alkane sulfonates, and show that, unexpectedly, they give values of solubilization which are much larger than those found for alkyl benzene sulfonates, and they also function well at both high ionic strengths and in the presence of large concentrations of divalent ion. In addition results will be presented to demonstrate that α-olefin sulfonates exhibit similar performance to the pure monoisomeric surfactants studied here.

EXPERIMENTAL

Secondary alkane sulfonates were prepared using the synthesis route shown in Figure 1. The appropriate Grinard reagent was condensed with an aldehyde to produce a secondary alcohol, followed by a procedure recently introduced by Volante (23), which converts the

alcohol to a thiol acetate without isomerization. Ten such species were prepared with the sulfonates attached to the seventh carbon in linear tetradecane ($7C_{14}$), the second ($2C_{16}$), the fourth ($4C_{16}$), the sixth ($6C_{16}$), or the eigth ($8C_{16}$) carbon in linear hexadecane, the second ($2C_{18}$), the fourth ($4C_{18}$), the fifth ($5C_{18}$), the sixth ($6C_{18}$) or the ninth ($9C_{18}$) carbon in linear octadecane. Primary alkane sulfonates ($1C_{14}$, $1C_{16}$, $1C_{18}$) were prepared using the Strecker reaction (24). After purification using an i-propanol/water extraction prodedure (25), all compounds were analyzed from their ^{1}H and ^{13}C nmr spectra.

C_{18} α-olefin sulfonate ($C_{18}AOS$) was prepared by reacting SO_3 (complexed with tributyl phosphate) with the C_{18} α-olefin and purified using the same i-propanol/water extraction procedure (25). The α-olefin sulfonate obtained is a mixture of alkene sulfonate and 3- and 4-hydroxy sulfonate. The analyses both by proton NMR and bromide/bromate titration have shown that approximately 50% of the alkene species were present in all syntheses. A few percent of disulfonate was presumed to be fractionated away during the purification process. In addition, the fractionated C_{18} alkene and C_{18} 3-hydroxy sulfonate components were kindly provided by Ethyl corporation and used as received.

Phase behavior studies with the above surfactants were done in sealed 10cc pipettes using C.P. salts and alcohols as well as 96 mole% purity alkane or mixtures thereof. The water/oil ratio was always 1 and alcohol concentrations are expressed in grams per deciliter (gpdl). All surfactant concentrations were kept constant at .6 gpdl.

In order to simplify the notation in the figures, sec-C_4OH, iso-C_5OH, and NaCl concentrations are given by three consecutive numbers. For

example "5 0 x" means that the system scan was made at 5gpdl of sec C_4OH, no iso-C_5OH and at variable salt concentration as noted on the co-ordinate axis.

Interfacial tensions were measured by the spinning drop technique. All values reported here were taken at optimum as were the reported solubilization parameters.

RESULTS AND DISCUSSIONS

Phase Behavior

The phase behavior in NaCl/EACN space is mapped in Figure 2. for the primary alkane sulfonates, C_{18} α-olefin sulfonate and C_{18} 3-hydroxy sulfonate and in Figure 3. for the various secondary alkane sulfonates.

The phase behavior particularly for straight tail molecules at low temperature with small quantities of added alcohol is complex. Gels and liquid crystals were found to form and occasionally several different surfactant-rich phases were observed and under some experimental conditions a bifrigent liquid crystalline phases were found to coexist with a middle phase microemulsion. Such complex behavior was found to be obviated by the addition of sufficient alcohol as cosolvent and/or by elevated temperatures.

Figures 2. and 3. show phase behavior under experimental conditions yielding classical microemulsion middle phases. For a given EACN, surfactant is partitioned in water at low salinity, into middle phase microemulsion at intermediate salinities, and into oil at high salinities. The optimum formulation was usually found midway between the bounds of the three phase regime.

Increased hydrophobe branching in the secondary sulfonates considerably favors partitioning into the oil phase as evidenced by reduced optimum salinities. For example, optimum salinities with decane were decreased from 8 gpdl to 0.35 gpdl by varying the sulfonate attachment point from the end to the mid position of the C_{18} alkane sulfonates. In terms of ACN, moving the sulfonate attachment from one carbon to the next shifts optimum ACN roughly by 2.1 units. This result is in good agreement with that previously found for alkylbenzene sulfonates (8).

Increased surfactant chain length at constant hydrophobe branching also favors partitioning into the oil phase as once again evidenced by the salt requirement at optimum, as one would expect. Figures 2. and 3. show that an addition of one methylene group shifts the ACN upward approximatively by 1.6 units, and this result also agrees with that reported for alkylbenzene sulfonates (8).

Figure 2. further indicates that high optimum salinities were obtainted for all straight tail surfactants studied. Salt tolerances are greater for the C_{18} alpha olefin and C_{18}3-hydroxy sulfonates than the $1C_{18}$. This enhanced salt tolerance is obviously caused by the hydroxy group and probably to a small extent by the double bond and any undectable residual disulfonate present in the α-olefin sulfonates.

It is possible to estimate the influence of the benzene ring on phase behavior by comparing the results in Figures 2. and 3. and that previously published for alkylbenzene sulfonates (8). Using group additivity values, Davies (26) assessed an equivalent of 3.5 methylene

groups for the benzene ring. In the present work, the benzene ring shows to have an equivalent of 2 to 4 methylene groups depending on hydrophobe branching.

Earlier studies on alkylbenzene sulfonates and petroleum sulfonates (6) have shown linearity between EACN and lnS and that the slope lnS/EACN for optimum phase behavior was always equal to 0.16. In Figures 2. and 3. one sees that lnS versus EACN are not always linear and, moreover, the slope, lnS/EACN, varies. It is equal to 0.2 at low salinities for branched surfactants, and it decreases gradually as the electrolyte concentration increases. At high salt concentration, it is nearly 0.1 for straight tail surfactants. Nonlinearlity between lnS and EACN and slope variations have recently been observed for ethoxylated alkyl sulfonates (27). Rather, for these surfactants EACN is linearly dependent on S .

The phase map showing the liquid crystal (LC) regime, the microemulsion (μE) regime and the phase boundary separating the two were constructed for $1C_{18}$ and C_{18}AOS (Figure 4). These maps show the LC/μE transition temperature for a variety of sec C_4OH concentrations. As noted above, straight tail surfactants require considerable alcohol to convert liquid crystals into microemulsion as the thermodynamically stable phase. An alternate approach is to reduce the alcohol concentration and increase the temperature sufficiently to melt the crystals. An additional constraint was placed on the transition temperature in that the systems were kept at optimum. This constraint required that the oil or salinity be changed as the alcohol concentration changed, and the values of the EACN and NaCl concentrations are noted by each

data point. As expected from earlier studies, variations in sec C_4OH concentration have a minor influence on EACN (or optimum salinity). One notes, however, that sec C_4OH has a marked influence on the transition temperature.

As seen in Figures 2. and 3., hydrophobe branching causes considerable change in alcohol requirement and transition temperature. Straight tail sulfonates needed the combined effect of elevated temperature and alcohol to get into the microemulsion regime. The level of alcohol and temperature were less for all other isomers. Near room temperature midchain isomers required approximately 2-3 gpdl of sec C_4OH to form middle phase microemulsion whereas no alcohol was needed for 5 and 6 isomers. These results show clearly that alcohol requirement can be minimized by selecting the appropriate hydrophobe branching.

OPTIMUM SOLUBILIZATIONS

The solubilization parameter at optimum (equal volumes of oil and water in the middle phase microemulsion) is defined as the volume of oil (or water) per unit volume of surfactant and is denoted as σ^*.

σ^* was determined for primary alkane sulfonates, α-olefin sulfonates and 3-hydroxy sulfonate of Figure 2. for the same system conditions and are displayed in Figure 5. The numbers by the individual data points are the experimental oil phase EACN'S.

As expected from earlier studies, σ^* decreases with increased electroyte concentration or EACN for all species. Figure 5. shows that improved solubilization obtained by increasing surfactant chain length. In addition, $1C_{18}$, C_{18} AOS and C_{18} 3-hydroxy sulfonates all

exhibit high solubilization although optimum salinities are very different. This result is a good example where minor structure modification near the head group can considerably change the salt tolerance without significantly compromising solubilization.

Figure 6. reproduces σ^* for secondary alkane sulfonates. The number near the experimental points are the oil phase EACN's and temperature. Salinities have arbitrary been plotted on a logarithmic scale in order to expand the results at low salinities. In Figure 6., one sees that increasing molecular weight also enhances solubilization for branched as it does for the primary species. Figure 6. also shows that good solubilization parameters were obtained for all isomers within their appropriate range of electrolyte concentrations.

Figure 7. shows the optimum solubilization recorded along the phase boundaries in Figure 4. One notes considerable improvement in σ^* at low alcohol concentrations and elevated temperature. This increase in σ^* is obviously due to the decrease in alcohol concentration. In fact, a small change in optimum salinity or EACN as noted near each data point as well as the elevated temperatures have a rather small effect on σ^*.

Figure 8. shows the effect of sec C_4OH and isoC_5OH on σ^* for C_{18}AOS at a variety of electrolyte concentrations. The oil phase ACNs are shown at each data point. Figures 7. and 8., therefore, reaffirm that elevated temperature and minimal alcohol favor high solubilization parameter regardless of salt concentration.

When solubilization parameters are plotted against reciprocal of the width of the three phase regime in ΔEACN units, it was found that a linear relationship exists with the exception of two data points at low salinities for $8C_{16}$ and $9C_{18}$. These data are shown in Figure 9. and the equation of the line as drawn is

$$\sigma^* = 22.5\ (\Delta EACN)^{-1} \qquad \{1\}$$

A similar study of alkylbenzene sulfonates (8) has shown the slope to be 5.6, rather than 22.5 in Eqn. {1}. This is a further indication of a potential advantage of the alkane sulfonates as compared to alkylbenzene sulfonates. It should be noted that such a reciprocal relationship appears to be quite general; for instance non-ionic ethoxylated nonylphenols have also been found to obey a similar relationship (12).

INTERFACIAL TENSIONS

Interfacial tensions for a number of systems have been measured under optimum condtions where the interfacial tension of the oil microemulsion interface of a three phase system is the same as the interfacial tension of the water-microemulsion interface. It was found that the tensions are extremely low in correspondence with large solubilizations. Huh (28) has predicted on theorical grounds that the following relationships exists between solubilization and interfacial tension:

$$\frac{\sigma^{*2} \cdot \gamma^*}{\cos \frac{\Pi}{2}} = \text{constant} \qquad \{2\}$$

Equation {2}has been experimentally verified for alkylbenzene sulfonates and ethoxylated alkylphenols (12). The constant were found to be 0.48 $\pm$.05 and 0.34 $\pm$.06 dynes/cm, respectively. In this study, the constant was found to be 0.40$\pm$.15, in good agreement with previous results. The values of the constants are moderately scattered, and this was expected because most of the interfacial tension reported here were obtained at elevated temperatures which greatly complicates measurement of γ. The present result, therefore, supports the universality of the constant in the Huh relationship, and reaffirms the strong coupling between σ^* and γ^*.

TOLERANCE TO DIVALENT IONS

The data in Figure 10. show the influence of calcium ion on solubilization. The numbers near data points represent either optimum EACN or optimum EACN and temperature. One sees that the calcium tolerance depends on surfactant structure and especially on hydrophobe branching. C_{18} AOS tolerates more than 1% calcium chloride while branched species like $6C_{18}$ can only tolerate 0.05% $CaCl_2$. The shift in EACN and the rate at which σ^* falls off upon addition of $CaCl_2$ are also greatly affected by the surfactant structure, being in the order: $6C_{18}$ (greatest variation) > $1C_{16}$, $1C_{18}$ > C_{18} AOS.

In all cases, it was observed that adding $CaCl_2$ beyond a critical concentration favored liquid crystal formation which, as it was found with NaCl, can be melted by adding alcohol and/or elevating the temperature.

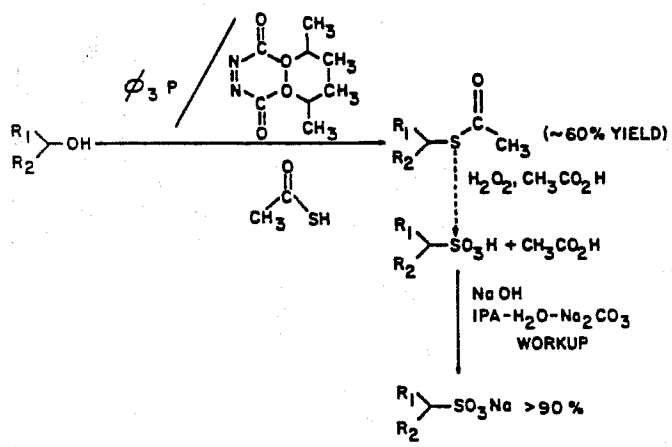
(~60% YIELD)
H_2O_2, CH_3CO_2H
NaOH
IPA-H_2O-Na_2CO_3
WORKUP
>90 %

1 A

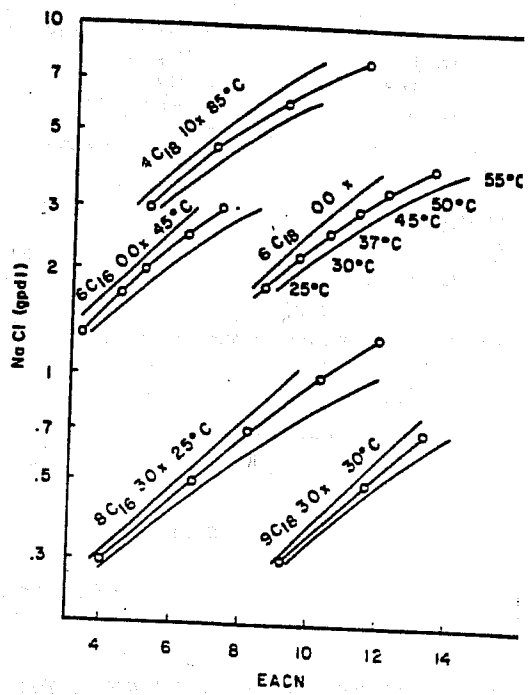
NaCl (gpdl)
EACN
4 C_{18} 10x 85°C
6 C_{16} 00x 45°C
6 C_{18} 00 x
55°C
50°C
45°C
37°C
30°C
25°C
8 C_{16} 30x 25°C
9 C_{18} 30x 30°C

1 B

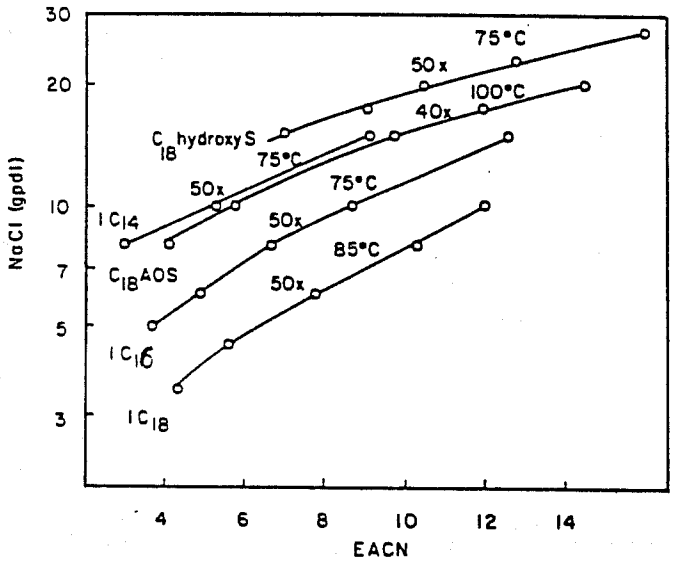
NaCl (gpdl)
EACN
75°C
50x
100°C
40x
C_{18} hydroxy S
75°C
50x
1 C_{14}
75°C
50x
C_{18} AOS
85°C
50x
1 C_{16}
1 C_{18}

1 C

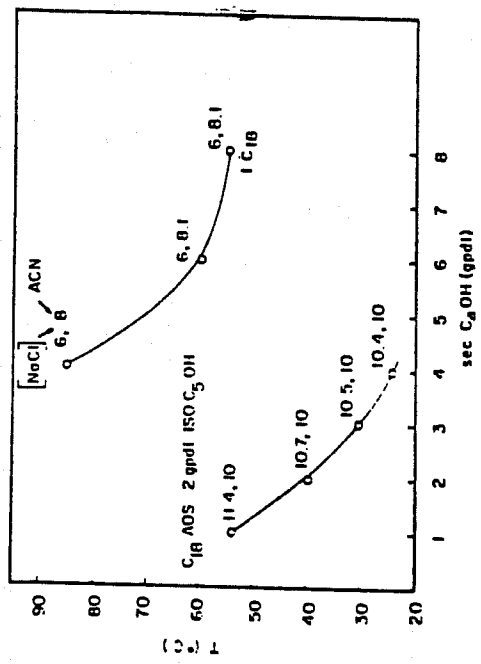
[NaCl]
ACN
6, 8
6, 8.1
6, 8.1
1 C_{18}
C_{18} AOS 2 gpdl ISO C_5 OH
11.4, 10
10.7, 10
10.5, 10
10.4, 10
sec C_8OH (gpdl)
T (°C)

1 D

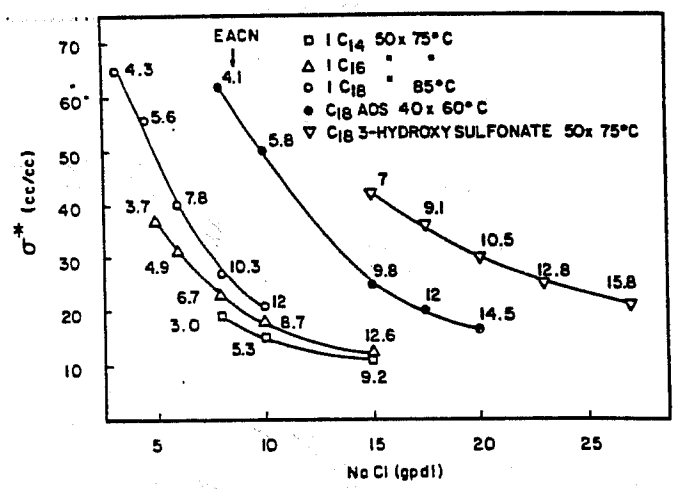
EACN
I C14 50x 75°C
I C16 " "
I C18 " 85°C
C18 AOS 40x 60°C
C18 3-HYDROXY SULFONATE 50x 75°C
σ* (cc/cc)
NaCl (gpdl)

5↑

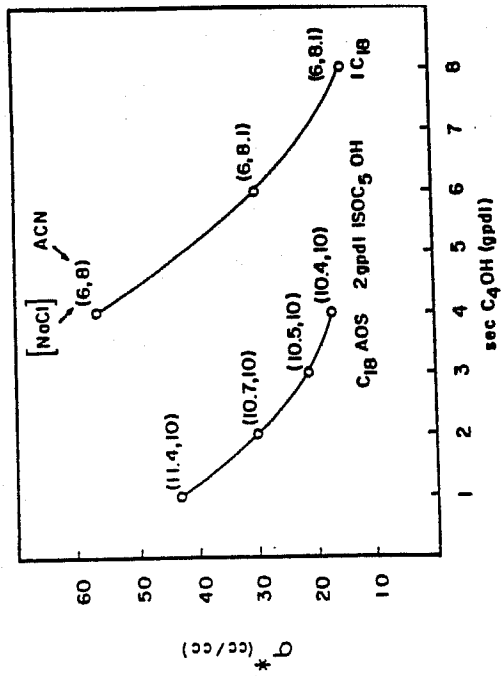
ACN
[NaCl]
I C18
C18 AOS 2gpdl ISOC5 OH
sec C4OH (gpdl)
σ* (cc/cc)

7↑

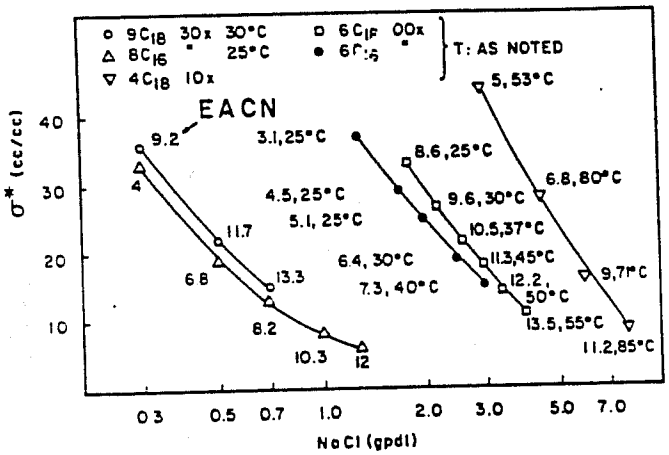
9C18 30x 30°C
8C16 " 25°C
4C18 10x
6C18 00x
T: AS NOTED
EACN
σ* (cc/cc)
NaCl (gpdl)

6↑

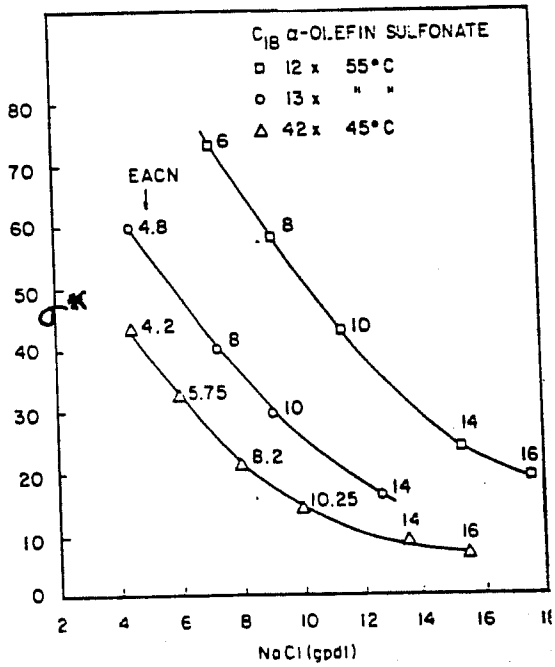
C18 α-OLEFIN SULFONATE
12 x 55°C
13 x " "
42 x 45°C
EACN
σ*
NaCl (gpdl)

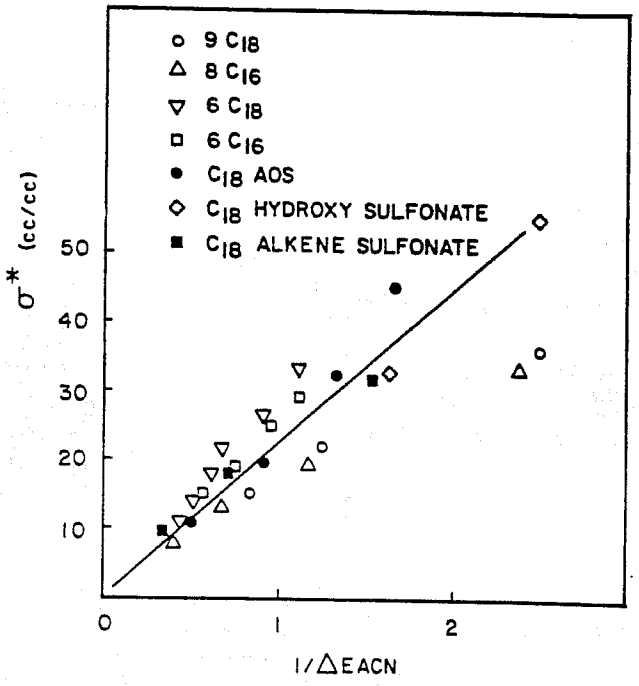
9 C18
8 C16
6 C18
6 C16
C18 AOS
C18 HYDROXY SULFONATE
C18 ALKENE SULFONATE
σ* (cc/cc)
50
40
30
20
10
0
1
2
1/ΔEACN

91

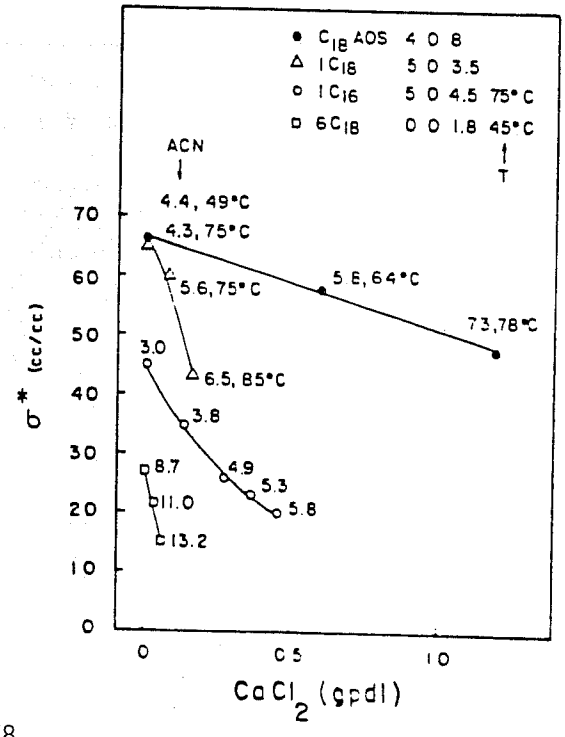
C18 AOS 4 0 8
1C18 5 0 3.5
1C16 5 0 4.5 75°C
6C18 0 0 1.8 45°C
T
ACN
4.4, 49°C
4.3, 75°C
5.6, 75°C
5.6, 64°C
7.3, 78°C
6.5, 85°C
3.0
3.8
4.9
5.3
5.8
8.7
11.0
13.2
σ* (cc/cc)
70
60
50
40
30
20
10
0
0
0.5
1.0
CaCl2 (gpdl)

CONCLUSIONS

1. Alkane and α-olefin sulfonates have been tested for their potential as surfactants for enhanced oil recovery and the preliminary results are encouraging.

2. The tolerance to either ionic strength or to the presence of divalent ions is very good for primary alkane sulfonates, α-olefin and hydroxy sulfonates. These species tend to form liquid crystals rather than homogenous, isotropic microemulsion phase when the alcohol concentration and the temperature are low. Increasing either of these variables does give rise to microemulsions and the boundaries separating these two phases have been determined.

3. The electrolyte tolerance decreases as tail branching increases. Optimum salinities go from 5-20 gpdl NaCl for straight tail surfactants to 1-6 gpdl NaCl for intermediate branched surfactants then to <1gpdl NaCl for symetrically branched tailed surfactants.

4. Alcohol concentrations needed to give a phase transition from condensed to microemulsion phases also depends on hydrophobe branching. Primary alkane and α-olefin sulfonates require the most alcohol followed by midattachment isomers. Surfactants with sulfonates attached to 5th, 6th, and 7th carbon, on the other hand, were found to form middle phase microemulsion with no alcohol added.

5. Large solubilization parameters and low interfacial tensions at optimum can be obtained with all species under appropriate conditions.

6. The benzene ring was found to be the equivalent of 2-4 methylene groups based on comparison of corresponding alkane and alkylbenzene sulfonates.

7. As previously found, the width of the three phase regime is inversely related to solubilization parameter at optimum.

8. Also as previously found, the product of σ^{*2} and γ^* is constant as predicted by theory.

ACKNOWLEDGMENTS

The authors wish to thank the following for their support of this research: The Department of Energy, The Robert A. Welch Foundation, and the following companies: Amoco, Arco, British Petroleum, Chevron, Elf-Quitane, Exxon, Getty, Gulf, Shell, Sun, Tenneco, Union Oil, Witco, Mobil R&D, GAF Corp, Dowell, Conoco, TOTAL-CFP, and Rhone Roulenc Petrole.

REFERENCES

1. J.L. Cayias, R.S. Schechter, and W.H. Wade, Soc. of Petr. Eng. J. 16 (1976) 351.

2. J.L. Cayias, R.S. Schechter, and W.H. Wade, J. Coll. Int. Sci. 59 (1977) 31.

3. J.C. Morgan, R.S. Schechter, and W.H. Wade, "Recent Advances in the Study of Low Interfacial Tensions", Improved Oil Recovery by Surfactant and Polymer Flooding, Academic Press (New York, 1977).

4. J.K. Jacobson, J.C. Morgan, R.S. Schechter, and W.H. Wade, Soc. of Petr. Eng. J. 17 (1977) 122.

5. J.C. Morgan, R.S. Schechter, J.K. Jacobson, and J.L. Salager, and W.H. Wade, Soc.of Petr. Eng. J. 18(1978) 242.

6. J.L. Salager, E. Vasquez, J.C. Morgan, R.S. Schechter, and W.H. Wade, Soc. of Petr. Eng. J. 19(1979) 107.

7. E. Vasquez, J.L. Salager, M. El-Emary, C. Koukounis, R.S. Schechter and W.H. Wade, "Interfacial Tension and Phase Behavior of Pure Surfactant Systems", Solution Chemistry of Surfactants, Vol. 2, Plenum Press (New York, 1979).

8. Y. Barakat, L.N. Fortney, R.S. Schechter, S.H. Yiv, W.H. Wade, and A. Graciaa, "Criteria for Structuring Surfactants to Maximize Solubilization of Oil and Water II." J. Coll. Int. Sci. 92(1983) 561.

9. M. Hayes, M. Bourrel, M. El-mary, R.S. Schechter, and W.H. Wade. SPE 7581 (1978).

10. M. Bourrel, J.L. Salager, R.S. Schechter, and W.H. Wade, J. Dispersion Sci. Tech. 1(1980) 13.

11. M. Bourrel, J.L. Salager, R.S. Schechter, and W.H. Wade, J. Coll. Int. Sci. 75(1980) 451.

12. A. Graciaa, R.S. Schechter, W.H. Wade, and S.H. Yiv, "Criteria for Structuring Surfactants to Maximize Solubilization of Oil and Water I: Commercial Nonionics", SPE 9815.

13. S. Thach, and S.J. Salter, "Characterization of Broad Equivalent Weight Petroleum Sulfonates Used in a Field Test," SPE 10721.

14. A. Graciaa, J. Lachaise, J.G. Sayous, M. Bourrel, R.S. Schechter, W.H. Wade, "Partage d'um tensioactif non-ionique polydistribue entre les phases des systemes de Winsor", Presented at the 2nd European Symposium on Ehanced Oil Recovery, Paris (Nov.1982). Editions Technip (Paris) p.61.

15. D.W. Dycus, E.W. Malmberg, and H.L. Wilchester, "Oil Recovery Using Aqueous Surfactant Compositions", U.S. Patent. 3827497.

16. D.W. Dycus, E.W. Malmberg, and H.L. Wilchester, "Surfactant Compositions Useful in Oil Recovery Processes". U.S. Patent. 3890239.

17. W.W. Gale, R.K. Saunders, and T.L. Ashcraft, Jr., "Oil Recovery Using a Surfactant", U.S. Patent. 3977471.

18. K.H. Fluornoy, R.L. Cardenas, G.L. Haferkampf, and R.D. Shupe, "Surfactant Oil Recovery Process Usable in Formations Containing Water Having High Concentrations of Polyvalent Ions Such As Calcium α Magnesium", U.S. Patent. 3811505.

19. K.H. Fluornoy, and R.D. Shupe, "Sufactant Oil Recovery Process Usable in Formations Containing Water Having High Concentrations of Polyvalent Ions Such As Calcium α Magnesium", U.S. Patent. 3811507.

20. K.H. Fluornoy, K. Maddox, Jr., and J.F. Pate, "Oil Recovery Processes Usable In Formations Containing Water Having High Concentrations Of Polyvalent Ions", U.S. Patent. 3858656.

21. K. Maddox, Jr., and R.D. Shupe, "Surfactant Oil Recovery Processes Usable in High Temperature, High Salinity Formations", U.S. Patent 4077471.

22. V.H. Schievelbein, "Surfactant Water Flooding Oil Recovery Method", U.S. Patent. 6307782.

23. R.P. Volante, Tetrahedron Lett 22(1981) 3119.

24. R.M. Reed, and H.V. Tartar. J. Am. Chem. Soc. 57(1935) 570.

25. A.F. Turbak, and J.R. Livingston, J.R. Ind. Eng. Chem. Prod. Res. Dev. 2(1963) 229.

26. J.T. Davies, "A Quantitative Kinetic Theory of Emulsion Type, I. Physical Chemistry of the Emulsifying Agent", Proc. 2nd Interm. Cong. Surface Activity Vol. I(London, 1957) 426.

27. I. Carmona, R.S. Schechter, W.H. Wade, and U. Weerasooriya "Ethoxylated Oleyl Sulfonates as Model Compounds for Enhanced Oil Recovery", SPE 11771.

28. C.Huh, "Interfacial Tensions and Solubilizing Ability of A Microemulsion Phase That Coexists with Oil and Brine." J. Coll. Int. Sci. 71(1979) 408.

Figure Captions

Figure 1. Synthesis scheme for alkane sulfonates.

Figure 2. Optimum phase behavior for primary sulfonates.

Figure 3. Phase maps for secondary alkane sulfonates.

Figure 4. Phase boundary separating the liquid crystal and microemulsion regimes for two species.

Figure 5. Solubilization parameters for the systems of Figure 2.

Figure 6. Solubilization parameters for the systems of Figure 3 at a function of NaCl concentration.

Figure 7. σ^* vs ($2-C_4OH$) for conditions as noted by the data points.

Figure 8. σ^* vs (NaCl) for different alcohol concentrations.

Figure 9. Solubilization parameter, σ^* vs reciprocal ΔEACN.

Figure 10. Influence of ($CaCl_2$) on σ^* for surfactants as shown.

Publications of last year's work

M.Baviere, R.S. Schechter, and W.H. Wade, "The Effect of Salt, Alcohol and Surfactant on Optimum Middle Phase Composition", Surface Phenomena in Enhanced Oil Recovery, D.O. Shah, ed., (New York, 1981) p.117.

J.F. Scamehorn, R.S. Schechter, and W.H. Wade, "Adsorption of Surfactants on Mineral Oxide Surfaces from Aqueous Solutions I: Isomerically Pure Anionic Surfactants", J.Colloid Interface Sci. 85, 479 (1982).

J.F. Scamehorn, R.S. Schechter, and W.H. Wade, "Adsorption of Surfactants on Mineral Oxide Surfaces from Aqueous Solutions II: Binary Mixtures of Anionic Surfactants", J.Colloid Interface Sci. 85, 479 (1982).

J.F. Scamehorn, R.S. Schechter, and W.H. Wade, "Adsorption of Surfactants on Mineral Oxide Surfaces from Aqueous Solutions III: Binary Mixtures of Anionic and Nonionic Surfactants", J.Colloid Interface Sci. 85, 494 (1982).

J.F. Scamehorn, R.S. Schechter and W.H. Wade, "Micelle Formation in Mixtures of Anionic and Nonionic Surfactants", J. Dispersion Sci. Tech. 3, 261 (1982).

M.Bourrel, C.Chambu, R.S. Schechter, and W.H. Wade, "The Topology of Phase Boundaries for Oil/Brine and Surfactant Systems", J.Soc. Petrol. Eng. 22, 28 (Feb. 1982).

A. Graciaa, Y.Barakat, M.El-Emary, L.Fortney, R.S. Schechter, W.H. Wade, and S. Yiv, "HLB, CMC and Phase Behavior as Related to Hydrophobe Branching", J. Colloid Interface Sci. 89, 209 (1982).

A.Graciaa, R.S. Schechter, W.H. Wade, and S.H. Yiv, "Emulsion Stability and Phase Behavior for Ethoxylated Nonyl Phenol Surfactants", J.Colloid Interface Sci. 89, 217 (1982).

Y.Barakat, L.N.Fortney, C.Lalanne-Cassou, R.S.Schechter, W.H. Wade and S.Yiv, "The Phase Behavior of Simple Salt-Tolerant Sulfonates", SPE 1067 (1982).

L.M. Baldauf, R.S.Schechter, and W.H. Wade, "The Relationship Between Surfactant Phase Behavior and the Creaming and Coalescence of Macroemulsions", J. Colloid Interface Sci. 85, 187 (1982).

R.S. Schechter, J.Harwell, and F.G. Helferich, "Effect of Micelle Formation on Chromatographic Movement of Surfactant", AIChe J., 28(3), 448 (1982).

A.Graciaa, Y.Barakat, M.El-Emary, L.Fortney, R.S. Schechter, S.Yiv, and W.H. Wade, "HLB,CMC, and Phase Behavior as Related to Hydrophobe Branching", J.Colloid Interface Sci.,89(1), 217(1982).

C.C.Nunn, R.S. Schechter, W.H. Wade, "Visual Evidence Regarding the Nature of Hemimicelles Through Surface Solubilization of Pnacyanol Chloride," J.Phys.Chem.,86, 3271 (1982).

Invited lectures, papers and speeches

by William H. Wade

"Surfactant Architecture for Enhanced Oil Recovery", Dallas, Texas, October 1981.

"Criteria for Structuring Alkyl Benzene Sulfonates for Enhanced Oil Recovery" INTEVEP, S.A. Centro de Investigacion y Desarrollo Filial de Petroleos de Venezuela, S.A., Caracus, Venezuela, December 1981.

"The Phase Behavior of Simple Salt-Tolerant Sulfonates", Tulsa, Oklahoma, April 1982.

"Synthetic Surfactants for Enhanced Oil Recovery and the Rules Governing Their Behavior", Morristown, New Jersey, April 1982.

"Structural Variations in Alkyl Benzene Sulfonates for Enhanced Oil Recovery", Irvine, California, May 1982.

"International Symposium on Surfactants in Solution", Lund, Sweden June-July 1982.

"Criteria for Structuring Surfactants to Maximize Solubilization of Oil and Water:II", Kansas City, Missouri, September 1982.

Invited lectures, papers and speeches

by Robert S. Schechter

"Unexpected Characteristics of Surfactant Solutions and Some Practical Consequences", Seminar given at the Illinois Institute of Technology, Chicago, Illinois, October 1981 and at Rice University, Houston, Texas, December 1981.

"Critical Behavior in Surfactant Oil/Water Systems", Seminar given at the University of Houston, Houston, Texas, January 1982.

"Compositional Effects on the Adsorption of Surfactant from Aqueous Phases in Equilibrium with a Middle Phase Microemulsion," SPE paper 11212 presented at the 57th Annual Technical Conference and Exhibition, New Orleans, Louisiana, September 26-29, 1982 (with Marc Vernet, Remy Truchetet, and W.H. Wade).

☆U.S. GOVERNMENT PRINTING OFFICE:1985 -544 -063/ 10537 REGION NO. 4